

Table 10.1 Electronic polarizabilities α_e of some selected ions and rare gas atoms^a, in 10^{-24} cm^3

Ions	α_e	Ions	α_e	Rare gas atoms	α_e
Li^+	0.03	F^-	1.2	He	0.2
Na^+	0.2	Cl^-	3	Ne	0.4
K^+	0.9	Br^-	4.5	Ar	1.6
Rb^+	1.7	O^{2-}	3.88	Kr	2.5
Cs^+	2.5	S^{2-}	10.2	Xe	4.0

^aFrom: A. Dalgarno, *Adv. Phys.*, **11**, 281 (1962).

L. Pauling, *Proc. R. Soc. London, A* **114**, 181 (1927).

Now, equating the value of α_e from (10.42) to the one obtained from the Clausius–Mossotti relation (10.38) and solving for $\epsilon(\omega)$, we get

$$\epsilon(\omega) = 1 + \frac{\frac{N_e e^2}{m \epsilon_0 (\omega_0^2 - \omega^2 + i\gamma\omega) - \frac{1}{3} N_e e^2}}{(10.45)}$$

where N_e denotes the density of polarizable electrons. So, the dielectric constant turns out to be a complex function when examined in the presence of an alternating electric field. When $\omega = 0$, from (10.45), we have

$$\epsilon_s = 1 + \frac{\frac{N_e e^2}{m \epsilon_0 \omega_0^2 - \frac{1}{3} N_e e^2}}{(10.46)}$$

which is real and known as the *static dielectric constant*.

We can separate the RHS of (10.45) into real (ϵ') and imaginary (ϵ'') parts and rewrite it as

$$\epsilon(\omega) = \epsilon'(\omega) + i\epsilon''(\omega) \quad (10.47)$$

This gives

$$\epsilon'(\omega) = 1 + \frac{\frac{N_e e^2}{m \epsilon_0} \left[\left(\omega_0^2 - \frac{N_e e^2}{3 m \epsilon_0} \right) - \omega^2 \right]}{\left[\left(\omega_0^2 - \frac{N_e e^2}{3 m \epsilon_0} \right) - \omega^2 \right]^2 + \gamma^2 \omega^2} \quad (10.48)$$

and

$$\epsilon''(\omega) = \frac{\frac{N_e e^2}{m \epsilon_0} \gamma \omega}{\left[\left(\omega_0^2 - \frac{N_e e^2}{3 m \epsilon_0} \right) - \omega^2 \right]^2 + \gamma^2 \omega^2} \quad (10.49)$$

Relations (10.48) and (10.49) show that there occurs a resonance at frequency,

$$\omega_r = \left(\omega_0^2 - \frac{N_e e^2}{3 m \epsilon_0} \right)^{1/2} \quad (10.50)$$

The resonance frequency is shifted away from the natural frequency, obviously because of the presence of a large density of polarizable electrons N_e . We say that a resonant absorption occurs at this frequency of the optical radiation. Later, when we describe the variation of the polarizability as a function of frequency, it will be clear that this absorption occurs in the ultraviolet region.

In the situation described above each electron behaves as a harmonic oscillator, possessing an induced dipole moment. Therefore, the oscillating collective electron shell may be viewed as a dipole harmonic oscillator. The terms $\epsilon'(\omega)$ and $\epsilon''(\omega)$ for such a dipole oscillator are plotted as functions of frequency in Fig. 10.4. For finite damping, we get only the approximate values of ω_r and the frequency of the active longitudinal mode ω_L , as obtainable from the zero crossings of $\epsilon'(\omega)$. The dissipation constant γ is alternatively identified as the damping factor. It is shown as a measure of the width at half the maximum of the absorption line appearing in the $\epsilon''(\omega)$ curve. If there were no damping, no absorption of radiation would take place. Such an absorption is termed *resonance absorption*. When the dielectric constant is a complex function, we will show, as a general case, in Section 10.6 that the energy absorbed per unit volume is proportional to $\epsilon''(\omega)$. The constant $\epsilon'(\omega)$ depends on frequency in the absorption region and accounts for the dispersion.

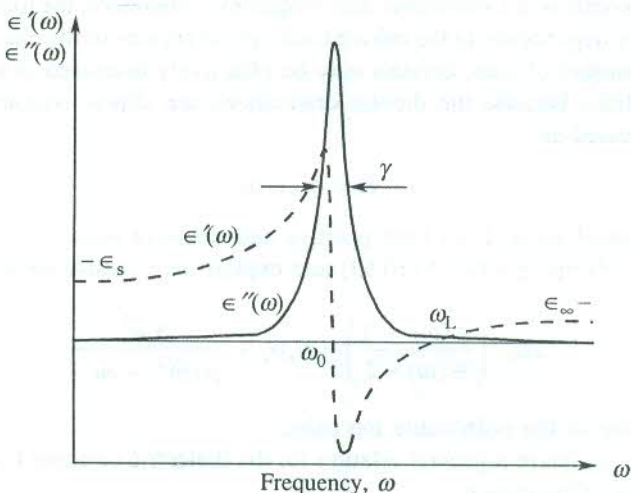


FIG. 10.4 The behaviour of $\epsilon'(\omega)$ and $\epsilon''(\omega)$ for a dipole oscillator. In the presence of damping, the zeros of $\epsilon'(\omega)$ correspond to the approximate values of ω_0 and ω_L (the frequency of the longitudinal mode).

10.5.2 Ionic Polarization

The polarizability of ionic crystals cannot be accounted for without appreciating the contribution from induced ionic dipoles created by the displacement of ions under the action of an electric field. The ionic polarizability α_i on account of having its origin in the displacement of ions is also referred to as the *displacement polarizability*. The problem is treated in the same fashion as for the electronic

polarization. Let us consider an ionic crystal with masses of cations and anions being denoted by M^+ and M^- . The applied electric field produces a relative displacement of ions in an ion pair. If this displacement is $\mathbf{x}(t)$ at any time t , the equation of motion of the ion pair in terms of its reduced mass $\left(\mu = \frac{M^+ M^-}{M^+ + M^-}\right)$ can be written in the form

$$\mu \left[\frac{d^2 \mathbf{x}}{dt^2} + \gamma \frac{d\mathbf{x}}{dt} + \bar{\omega}^2 \mathbf{x} \right] = e \mathbf{E}_{\text{loc}} \quad (10.51)$$

Here γ stands for the damping constant and $\bar{\omega}$ is the natural frequency obtained with the knowledge of force constant $f (= \mu \bar{\omega}^2)$.

Similar to the electronic response, the solution to (10.51) is found to be a complex function at frequencies of the order of $\bar{\omega}$. Accordingly, the ionic polarizability is

$$\alpha_i(\omega) = \frac{e^2}{\mu(\bar{\omega}^2 - \omega^2 + i\gamma\omega)} \quad (10.52)$$

Since the frequency $\bar{\omega}$ is characteristic of lattice vibrations, in the long wavelength limit, $\hbar\bar{\omega} \approx \hbar\omega_D$ which may lie in the range of 0.01 to 0.1 eV. This leads to a frequency that may be 10^2 to 10^3 times smaller than ω_0 (the atomic or the electronic shell frequency). Therefore, the ionic polarizability shows a significant frequency dependence in the infrared and optical regions of the electromagnetic spectrum.

The dielectric constant of ionic crystals may be effectively discussed in terms of the ionic and electronic polarizabilities because the dipolar orientations are almost remote. Therefore, the total polarizability is expressed as

$$\alpha = \alpha_e + \alpha_i$$

where α_i includes contributions from both positive and negative ions.

If we neglect the damping term in (10.52) and exploit the Clausius–Mossotti relation, we get

$$3\epsilon_0 \left(\frac{\epsilon(\omega) - 1}{\epsilon(\omega) + 2} \right) = N_e \alpha_e + \frac{N_i e^2}{\mu(\bar{\omega}^2 - \omega^2)} \quad (10.53)$$

where N_i is the density of the polarizable ion pairs.

Now, we attempt to derive a general relation for the dielectric constant by evaluating (10.53) in the two limiting cases of frequency.

When $\omega \rightarrow 0$ or $\omega \ll \bar{\omega}$, we get

$$3\epsilon_0 \left(\frac{\epsilon_s - 1}{\epsilon_s + 2} \right) = N_e \alpha_e + \frac{N_i e^2}{\mu \bar{\omega}^2} \quad (10.54)$$

When ω approaches the optical frequencies, i.e. $\omega \gg \bar{\omega}$, we have

$$3\epsilon_0 \left(\frac{\epsilon_\infty - 1}{\epsilon_\infty + 2} \right) = N_e \alpha_e \quad (10.55)$$

From (10.54) and (10.55), we obtain

$$\frac{N_i e^2}{\mu \bar{\omega}^2} = 3 \epsilon_0 \left[\frac{\epsilon_s - 1}{\epsilon_s + 2} - \frac{\epsilon_\infty - 1}{\epsilon_\infty + 2} \right] \quad (10.56)$$

Making use of (10.55) and (10.56) in (10.53), we get

$$\frac{\epsilon(\omega) - 1}{\epsilon(\omega) + 2} = \frac{\epsilon_\infty - 1}{\epsilon_\infty + 2} + \frac{1}{\left(1 - \frac{\omega^2}{\bar{\omega}^2} \right)} \left[\frac{\epsilon_s - 1}{\epsilon_s + 2} - \frac{\epsilon_\infty - 1}{\epsilon_\infty + 2} \right] \quad (10.57)$$

Solving (10.57) for $\epsilon(\omega)$, we get

$$\epsilon(\omega) = \epsilon_\infty + \frac{(\epsilon_s - \epsilon_\infty) \omega_T^2}{\omega_T^2 - \omega^2} \quad (10.58)$$

where

$$\omega_T^2 = \bar{\omega}^2 \left(\frac{\epsilon_\infty + 2}{\epsilon_s + 2} \right) = \bar{\omega}^2 \left(1 - \frac{\epsilon_s - \epsilon_\infty}{\epsilon_s + 2} \right) \quad (10.59)$$

with ω_T as the natural resonant frequency defined by the pole of $\epsilon(\omega)$ [$\epsilon(\omega) = \infty$]. It is the long wave limiting frequency of transverse optical modes of the crystal. Relation (10.58) is an extremely useful one and exploited for describing optical dispersion in ionic crystals which is the subject of discussion in Section 10.9.

10.5.3 Polarization from Dipole Orientation

As already mentioned, an asymmetrical molecule composed of atoms with a difference of electronegativity is characterized by a permanent dipole moment. Under the action of an electric field the permanent dipoles tend to align themselves with the field. The process of orientation is partially frustrated by thermal agitations in solids. The rotation of permanent dipoles contributes to the polarization and, therefore, to the polarizability of the solid. The concept of rotatory motion is, however, more pertinent to the cases of gases and liquids. In solids, the polar molecules are generally not completely free to rotate when acted upon by an electric field. For molecules like HCl and H₂O, several stable orientations are known to exist for each molecule in the solid at high temperatures. Therefore, it is appropriate to describe the orientational motion in a polar solid as a jump in the angular displacement of molecules from one stable set of orientations to another stable set in which the dipoles are expected to be aligned more nearly along the field direction. A set of orientations of polar molecules in a crystal is stable only if allowed by the crystal symmetry.

Notwithstanding the free rotation of polar molecules in solids being scarce, the polarization contributed by the free rotation has been calculated. Such a calculation was made initially for the unhindered rotation of magnetic dipoles while developing the theory of paramagnetic susceptibility. We are giving below the results for permanent electric dipoles in paraelectric materials. For details, the reader should consult Chapter 13. This would enable him to obtain the relations given below without much ado.

The polarization contributed by the unhindered rotation of permanent dipoles measures as

$$P_{\text{dip}} = \frac{Np^2 E}{3k_B T} \quad (10.60)$$

where N denotes the number of dipoles per unit volume at temperature T .

The resulting relation for the susceptibility is

$$\chi_{\text{dip}} = \frac{P_{\text{dip}}}{\epsilon_0 E} = \frac{Np^2}{3\epsilon_0 k_B T} \quad (10.61)$$

At low frequencies ($\omega \rightarrow 0$), where the contribution from the induced ionic dipoles is meaningful, the paraelectric properties are discussed in terms of the static dielectric constant expressed as

$$\epsilon_s = 1 + \chi_E \quad [\text{using (10.13)}] \quad (10.62)$$

Here

$$\chi_E = \chi_{\text{dip}} + \chi_i + \chi_e \quad (10.63)$$

From the last three relations it is obvious that the dipole moment p can be determined by measuring the static dielectric constant as a function of temperature making use of the fact that χ_i and χ_e are temperature independent.

The behaviour of low frequency (5 kHz) dielectric constant of H_2S crystal from just above the melting point to well below the melting point is depicted in Fig. 10.5. It describes the practical picture within a polar solid. On cooling, the part of the dielectric constant having its origin in the dipole orientation increases significantly in an irregular way. The irregularity is the reflection of a limited freedom available for the free orientation of dipoles. The dipoles, however, jump from one set of orientations to another as may be permitted by the crystal symmetry. An almost constant level below 100 K demonstrates that the jumps are frozen on cooling below this temperature.

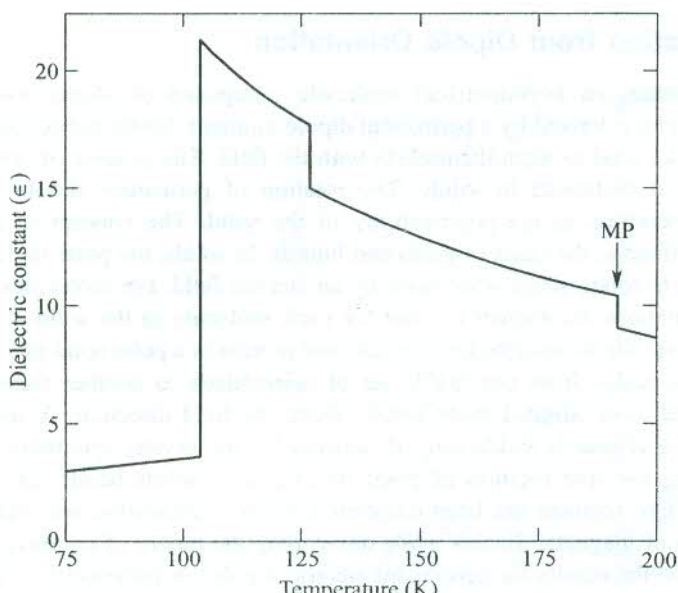


FIG. 10.5 Variation of the dielectric constant of H_2S with change in temperature, as measured at 5 kHz. [After C.P. Smyth and C.S. Hitchcock, *J. Am. Chem. Soc.*, **56**, 1084 (1934).]

The case of a real polar crystal is treated adequately in terms of the major jump of the angular displacement of molecules in going from one stable set of orientations to the other. The rate, at which the jump occurs, is characterized by the relaxation time τ . Using the Boltzmann distribution function, the ratio of occupation number densities in (1) parallel and (2) antiparallel to the field orientations is

$$\frac{N_1}{N_2} = \exp\left(\frac{2Ep}{k_B T}\right) \quad (10.64)$$

The fraction of excess dipoles that align parallel to the field is then given by

$$\frac{N_1 - N_2}{N_1 + N_2} = \frac{e^x - e^{-x}}{e^x + e^{-x}} = \tanh x \approx x \quad (10.65)$$

in the limit, $x = \frac{Ep}{k_B T} \ll 1$.

In this approximation, the bulk polarization is expressed as

$$P_{\text{dip}} = Npx = \frac{Np^2 E}{k_B T} \quad (10.66)$$

Apart from a factor, (10.66) is identically the same as (10.60) derived from the freely rotating dipoles.

A short while ago we discussed the case of low frequencies. If we consider the higher limit of frequencies at which the jumping response of permanent dipoles may be endangered but the induced ionic and electronic polarizations may still be able to catch up with the time dependence of the electric field, Debye showed for the first time (1929) that the dielectric constant describing the properties in this situation is a complex function such that its real part $\epsilon'(\omega)$ and imaginary that $\epsilon''(\omega)$ are given by

$$\epsilon'(\omega) = A + \frac{B}{1 + \omega^2 \tau^2} \quad (10.67)$$

$$\epsilon''(\omega) = \frac{\omega \tau B}{1 + \omega^2 \tau^2} \quad (10.68)$$

where A and B are some constants, and τ the relaxation time.

Relations (10.67) and (10.68) are named as the Debye equations. The real part is related to the polarization which is in phase with the applied field. The imaginary part represents the dielectric loss inherent in a mechanism that lags behind in phase relative to that of the applied field. The dielectric loss occurs for frequencies at which the dispersion occurs. The real and imaginary parts of the dielectric constant of a medium are related to each other by an extremely important pair of integral equations known as the Kramers-Kronig dispersion relations.*

* H.A. Kramers, *Collected Scientific Papers* (North-Holland, 1956).

It might surprise the reader as to why no attempt has been made in this section to obtain an expression for the polarization as is usually done by invoking the Clausius–Mossotti relation. The answer to this question follows from the fact that the Lorentz method of calculating E_{loc} applies only to the induced dipoles which align themselves completely with the applied field. Since the permanent dipoles in a polar crystal are oriented along a number of directions, the usual method of calculation becomes irrelevant in the case of orientational polarization.

Within solids, that contain permanent dipoles, all three sources of polarization discussed in this section contribute to the polarizability. The general behaviour of the real part of the total polarizability over the frequency range from microwave to ultraviolet region is shown in Fig. 10.6. It shows that the contributions from α_e , α_i and α_{dip} fall in different frequency ranges of the electromagnetic radiation.

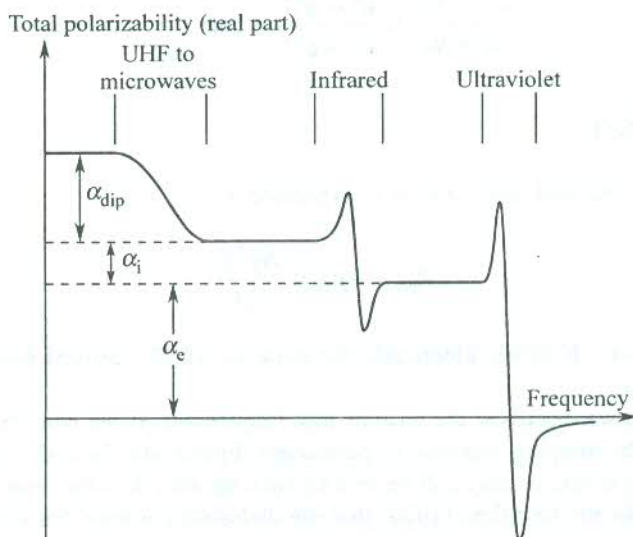


FIG. 10.6 Effectiveness of different sources of polarizability. The specific frequency range in which a certain source contributes in a major way can be identified.

10.6 DIELECTRIC LOSSES

In this section we show that the energy absorbed per second per unit volume (or the energy loss) in a dielectric medium is proportional to the imaginary part $\epsilon''(\omega)$ of the dielectric constant. The relationship among vectors E , P and D clearly indicates that on the application of an alternating electric field in a dielectric, vectors P and D would both vary periodically. They may generally be lagging behind in phase relative to that of E . Defining vectors' magnitudes as

$$E(t) = E_0 \exp(-i\omega t) \quad (10.69)$$

$$D(t) = D_0 \exp[-i(\omega t - \delta)] \quad (10.70)$$

where δ is the phase angle, giving the measure of phase lag.

In view of (10.14) and (10.15) we express the dielectric function in the following form, being aware that it is a complex quantity in the present situation:

$$\epsilon(\omega) = \epsilon'(\omega) + i\epsilon''(\omega) = \frac{D(t)}{\epsilon_0 E(t)} \quad (10.71)$$

On substituting E and D from (10.69) and (10.70), respectively, in (10.71) and then rationalizing the obtained relation for $\epsilon(\omega)$, we get

$$\epsilon'(\omega) = \frac{D_0 \cos \delta}{\epsilon_0 E_0} \quad (10.72)$$

$$\epsilon''(\omega) = \frac{D_0 \sin \delta}{\epsilon_0 E_0} \quad (10.73)$$

or

$$\tan \delta = \frac{\epsilon''(\omega)}{\epsilon'(\omega)} \quad (10.74)$$

Relation (10.74) establishes the frequency dependence of the phase angle.

Let us now take the example of a parallel plate capacitor filled with a dielectric material and bearing a surface charge density $\sigma(t)$ on its plates at any time t . Then the current density in the capacitor at that moment of time is

$$\begin{aligned} j(t) &= \frac{d\sigma(t)}{dt} = \frac{dD(t)}{dt} \\ &= \omega(-D_0 \cos \delta \sin \omega t + D_0 \sin \delta \cos \omega t) \end{aligned} \quad (10.75)$$

Since $j(t)$ is a real physical quantity, only the real part of $D(t)$ is considered in (10.75).

The energy dissipated per unit time in one cubic metre of the dielectric is equal to

$$W = \frac{\omega}{2\pi} \int_0^{2\pi/\omega} j(t) E(t) dt \quad (10.76)$$

Using (10.75) and (10.69) (taking the real part as W is real), we obtain

$$W = \frac{1}{2} \omega \epsilon_0 E_0^2 \epsilon''(\omega) \quad (10.77)$$

showing thereby that the energy losses in the dielectric are proportional to $\epsilon''(\omega)$.

Relation (10.77) can also be put in the form

$$W = \frac{1}{2} \omega E_0 D_0 \sin \delta \quad (10.78)$$

The $\tan \delta$, given by (10.74), is often referred to as the *loss factor*. But this terminology is relevant only when δ is small, so that $\tan \delta \approx \sin \delta \approx \delta$, and the usage may thus be held justified.

10.7 OPTICAL PHENOMENA

We know that some solids are transparent and some opaque to the light. Also, some solid surfaces are known to be highly reflecting whilst others bend the electromagnetic waves incident on them.

These properties are investigated by measuring certain physical quantities that have a close relationship with the dielectric constant ($\epsilon(\omega)$) of the solid. This dielectric constant represents the behaviour of all electrons, those in filled and those in unfilled bands. It must be distinguished from the electrical conductivity ($\sigma(\omega)$) that takes the effect of electrons in the partially filled bands (conduction band) only. Mathematical relations applied for the study of optical properties of solids follow from the theory of propagation of electromagnetic waves. An account of the same is summarized below.

The electric field associated with the electromagnetic waves travelling along z -direction in a medium is expressed as

$$E = E_0 \exp[-i\omega(t - \bar{n}(\omega)z/c)] \quad (10.79)$$

where $\bar{n}(\omega)$ is the complex index of refraction, described as

$$\bar{n}(\omega) = n + ik = \sqrt{\epsilon(\omega)} \quad (10.80)$$

with the usual definition

$$\bar{n}(\omega) = \frac{c}{v} \quad (10.81)$$

where v is the velocity in the medium.

According to (10.71), complex dielectric constant is written as

$$\epsilon(\omega) = \epsilon'(\omega) + i\epsilon''(\omega)$$

Then using (10.80) we get

$$\epsilon'(\omega) = n^2 - k^2$$

and

$$\epsilon''(\omega) = 2nk \quad (10.82)$$

Here k is called the extinction coefficient, while n and k are the two optical constants which one generally quotes.

Determination of Optical Constants

The optical constants, n and k (and hence the dielectric constant, $\epsilon(\omega)$) are estimated by exploiting their relationship with the reflectance and the absorption coefficient, measured independently. The exercise involving the measurements at normal incidence is simple. Suppose a plane wave of light from vacuum falls on a crystal at normal incidence. The intensities of the reflected and incident light waves are measured to obtain the reflectance (R) which is defined as the ratio of the former to the latter. The reflectance corresponds with another quantity called reflectivity (r) that is written as

$$r = \frac{E_{\text{refl}}}{E_{\text{inc}}} \quad (10.83)$$

where E stands for the electric field.

By requiring the components of the electric field vector (\mathbf{E}) and the magnetic field vector (\mathbf{B}) parallel to the crystal surface to be continuous, it can be shown that

$$r = \frac{n + ik - 1}{n + ik + 1} \quad (10.84)$$

By its definition, the reflectance is given by

$$R = \frac{E_{\text{refl}}^* E_{\text{refl}}}{E_{\text{inc}}^* E_{\text{inc}}} = r^* \cdot r = \frac{(n - 1)^2 + k^2}{(n + 1)^2 + k^2} \quad (10.85)$$

One can follow either of the following two approaches to extract the values of the two optical constants:

1. In one approach, relation (10.85) is generalized to non-normal angles of incidence (say, θ) and a second expression for reflectance is obtained at angle of incidence θ , in terms of θ , $n(\omega)$, $k(\omega)$, and the polarization of the incident radiation. When one compares this with the measured reflectance at angle θ , another equation containing $n(\omega)$ and $k(\omega)$ is formed and two constants can be readily estimated.
2. In the other approach, one makes use of the Kramers–Kronig relations through which $n(\omega)$ and $k(\omega)$ are connected:

$$\begin{aligned} n(\omega) &= 1 + P \int_{-\infty}^{\infty} \frac{d\omega'}{\pi} \frac{k(\omega')}{\omega' - \omega} \\ k(\omega) &= -P \int_{-\infty}^{\infty} \frac{d\omega'}{\pi} \frac{n(\omega') - 1}{\omega' - \omega} \end{aligned} \quad (10.86)$$

where P stands for a principal value integral.

The required input for the numerical analysis, employing these equations, is the knowledge of $r(\omega)$ at all frequencies. Thus the method is practically disadvantaged by the need of making measurements over a vast range of frequencies so as to have reliable extrapolations over the full range of frequencies on the demand of (10.86). The procedure, though fraught with complications, is ideal in principle. It is in fact preferred because of the high accuracy achieved in the estimation of the optical constants.

10.8 APPLICATION TO PLASMA

In this section we apply the theory developed so far to study the properties of a plasma.

10.8.1 Plasma Oscillations

A medium of equal concentrations of positive and negative charges, with at least one charge type being mobile, is known as a *plasma*. A metallic crystal may be described as an assembly of immediate positive ion cores (atomic nuclei) and conduction electrons that are nearly free to move over the whole of the crystal. The condition of charge neutrality is maintained because of the balance struck between the negative charge on conduction electrons and an equal concentration of positive charge on ion cores. Thus a metal serves as a good example of plasma.

An idealized plasma in which both particles carrying positive and negative charges, respectively, are motionless is referred to as *cold plasma*. But every real plasma at temperatures of interest is characterized by thermal agitations which at times are random in nature. A random motion may be a momentary fluctuation in the equilibrium position of an electron, caused by the average electrostatic field of all other electrons. The position fluctuation would create a charge imbalance in the region of that electron, as a result of which other electrons would rush into that region in order to restore the condition of charge neutrality. At any finite temperature, electrons being very light particles, move with fairly large speed relative to ions which we consider to be at rest. The electrons rushing into the region of the electron that suffered a fluctuation in its equilibrium position are unable to stop at the desired positions and overshoot their mark on account of the large kinetic energy which by the way represents the total energy there. As soon as the energy goes totally electrostatic, electrons turn around and attempt again to approach the wanted locations in the region of the misbehaving electron. The repetition of this process constitutes the collective oscillatory motion. These collective oscillations are called *plasma oscillations*.

The plasma oscillations, in principle, need to be interpreted in terms of the collective modes of the electron gas. For a proper theoretical treatment, extra degrees of freedom associated with the collective motion of the electron gas must be identified in addition to those associated with the motion of individual electrons. In this description, the electrons beyond a certain distance (the screening radius) from a given electron act cooperatively on that electron. Only for distances shorter than this, are the independent-particle aspects important. Therefore, an accurate description of plasma oscillations can be found only in the framework of many body theory which is too an advanced subject to find place in this book. Nevertheless, we present below a rather simple picture of the screening mechanism as given for the first time by Debye and Hückle.*

Consider a metal plasma in which a negative charge is introduced at a point chosen as the origin. Let the volume charge density at the point be denoted by ρ . If the charge imbalance because of a momentary fluctuation in charge density lowers the electron concentration at that point by δN , then the resulting charge density at the point is $(\rho - e\delta N)$. The effective electrostatic potential ϕ is related to this charge density by the Poisson equation

$$\nabla^2 \phi = \frac{1}{\epsilon_0} (\rho - e\delta N) \quad (10.87)$$

When the excitation energy $e\phi$ is very much smaller than $k_B T$ and the electron concentration N is so low as to permit the use of classical statistics, the decrease in electron concentration can be written as

$$\begin{aligned} \delta N &= N_0 \left[\exp \left(\frac{e\phi}{k_B T} \right) - 1 \right] \\ &\approx N_0 \left(\frac{e\phi}{k_B T} \right) \end{aligned} \quad (10.88)$$

where N_0 is the equilibrium electron concentration (in the absence of fluctuation in the equilibrium position). Putting the value δN from (10.88) in (10.87), we have

* P.P. Debye and E. Hückel, Z. Physik, 24, 185 (1923).

$$\left(\nabla^2 + \frac{N_0 e^2}{\epsilon_0 k_B T} \right) \phi = \frac{\rho}{\epsilon_0} \quad (10.89)$$

which has the solution,

$$\phi = \frac{\rho}{r} \exp \left(- \frac{r}{\lambda_D} \right) \quad (10.90)$$

with

$$\lambda_D = \left(\frac{\epsilon_0 k_B T}{N_0 e^2} \right)^{\frac{1}{2}} \quad (10.91)$$

Relation (10.90) explains the screening of a given electron from other electrons via the fluctuation of the electron charge density. λ_D is known as the Debye length. The effect of screening is such that when other electrons are at a distance λ_D from the given electron, the normal Coulomb potential is suppressed by the factor (1/e). The screening effect closely controls the behaviour of the dielectric constant* which is exploited to explain many interesting phenomena involving electron-electron, electron-photon and electron-phonon interactions.

We follow a classical approach to calculate the dielectric constant of a plasma in the absence of an external source of perturbation. Let us consider the two-dimensional model of a metal plasma as shown in Fig. 10.7(a). It is assumed that the configuration of the plasma particles does not depend on their position on the third spatial axis. In view of this fact, we suppress this direction in our calculations. On account of a random fluctuation in the equilibrium positions of electrons, two adjoining regions of positive and negative charge densities are created, meaning thereby that the charge neutrality condition is destroyed in these regions. In order to calculate the frequency of a given plasma electron, we work with a picture that is alternative to the one used earlier for describing the plasma oscillations.

Let a small volume element enclosed by surface S in the negatively charged region have a charge q . The electric field in this small volume is given by Gauss' theorem:

$$\int_S \mathbf{E} \cdot d\mathbf{S} = \frac{q}{\epsilon_0} \quad (10.92)$$

And suppressing the third spatial axis, we have

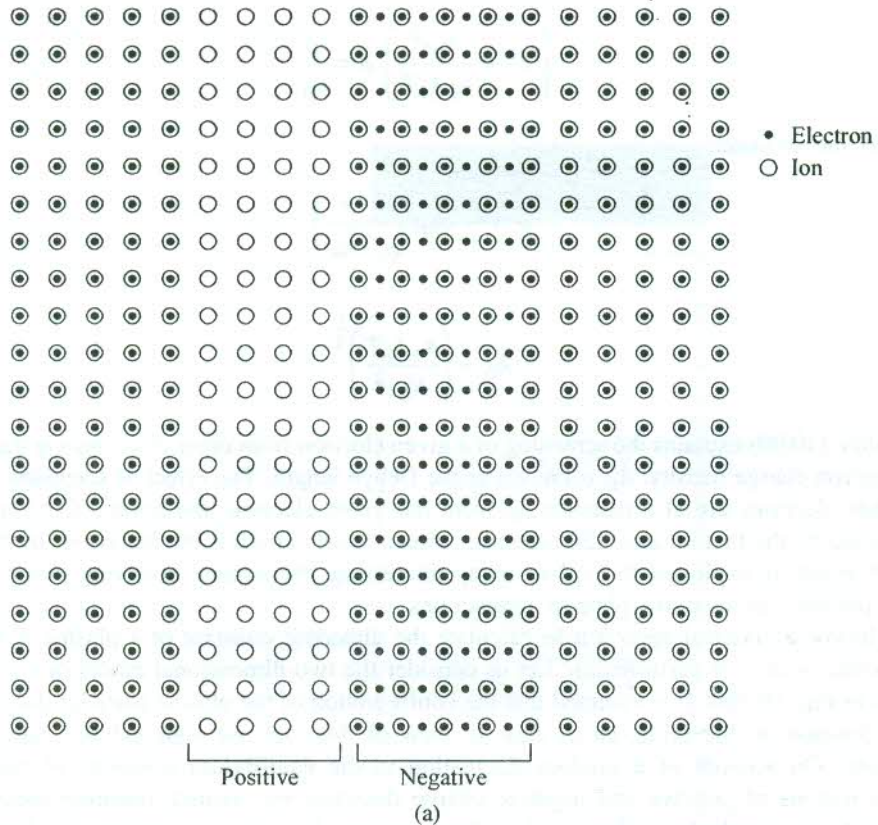
$$\int_S \mathbf{E} \cdot d\mathbf{S} = - lE \quad [\text{see Fig. 10.7(b)}] \quad (10.93)$$

Also,

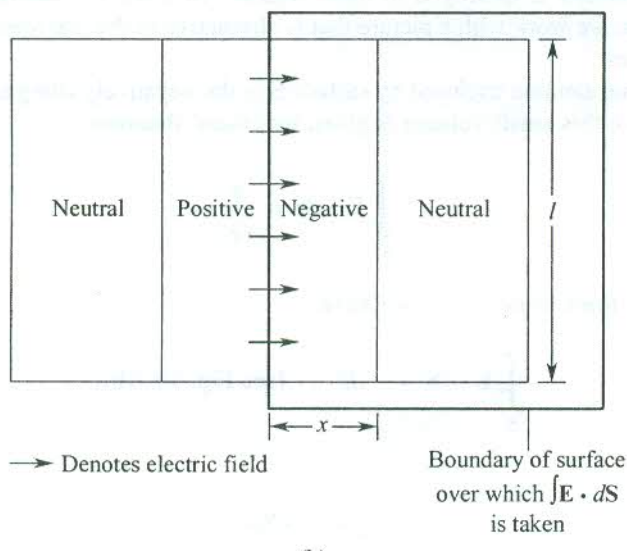
$$q = - lx N_0 e \quad (10.94)$$

where x denotes the displacement or the overshoot in the direction of E .

* J.M. Ziman, *Principles of the Theory of Solids*, Chap. 5 (Cambridge Univ. Press, 1972).



(a)



(b)

FIG. 10.7 (a) Displacement of electrons in a two-dimensional plasma. (b) Electric field in a two-dimensional plasma stands for the electric field. The dark line shows the boundary of surface over which $\int \mathbf{E} \cdot d\mathbf{S}$ is evaluated.

From the preceding three relations, we have

$$\mathbf{E} = \frac{N_0 e \mathbf{x}}{\epsilon_0} \quad (10.95)$$

The electric field \mathbf{E} serves as a perturbation and drives an electron into oscillatory motion. The equation of motion has the form

$$m\ddot{\mathbf{x}} = -e\mathbf{E} \quad (10.96)$$

Making use of (10.95), we get

$$\ddot{\mathbf{x}} = - \left(\frac{N_0 e^2}{\epsilon_0 m} \right) \mathbf{x} \quad (10.97)$$

This relation describes a simple harmonic motion of the characteristic frequency

$$\omega_p = \left(\frac{N_0 e^2}{\epsilon_0 m} \right)^{1/2} \quad (10.98)$$

where ω_p is known as the *plasma frequency*.

In the presence of an external field, both \mathbf{E} and \mathbf{x} are bound to a common oscillatory character represented by the time-dependent perturbation $\sim \exp(-i\omega t)$, where ω denotes the angular frequency of the perturbation force. We may now easily calculate the dielectric constant of the plasma in which the positive ion cores are at rest. Under the influence of \mathbf{E} , an electron has a dipole moment and the bulk polarization of the plasma is

$$P(\omega) = -N_0 e x \quad (10.99a)$$

with

$$m\ddot{x} = -m\omega^2 x = -e E(\omega) \quad (10.99b)$$

But,

$$\epsilon(\omega) = \frac{D(\omega)}{\epsilon_0 E(\omega)} = 1 + \frac{P(\omega)}{\epsilon_0 E(\omega)} \quad (10.100)$$

Using (10.99a) and (10.99b), we have

$$\epsilon(\omega) = 1 - \frac{N_0 e^2}{\epsilon_0 m \omega^2} \quad (10.101)$$

or

$$\epsilon(\omega) = 1 - \frac{\omega_p^2}{\omega^2} \quad [\text{using (10.98)}] \quad (10.102)$$

Relation (10.102) obviously expresses the dielectric constant of the free electron gas. When the frequency of the position fluctuation ω matches the plasma frequency ω_p , the dielectric constant $\epsilon(\omega) = 0$. This condition refers to the longitudinal plasma oscillations whose wavevector is taken as very nearly zero. The energy quanta $\hbar\omega_p$ are commonly known as *plasmons*. By the geometry of a

longitudinal polarization wave, a depolarization field $E = -P/\epsilon_0$ is created. This leads to $D = \epsilon_0 E + P = 0$ and $\epsilon(\omega) = 0$. During a longitudinal plasma oscillation, the electron gas is moved as a whole relative to the positive ion background. Figure 10.8 shows how the regions of negative charge and positive charge emerge out of a neutral charge distribution within a thin metal slab.

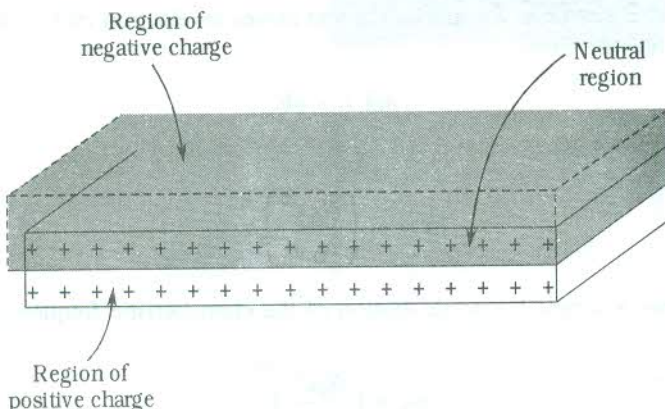


FIG. 10.8 The negative charges (electrons) against the background of positive ions in the thin slab of a metal.

Typical values of plasmon energy lie between 3 and 20 eV. They can be calculated if the electron number density and an appropriate value for the effective mass of electrons are known. The calculated values are found to be in good agreement with the observed ones in several metals and dielectrics. For example, they are 5.71 and 5.95 eV respectively in sodium. The plasmons may be excited by passing electrons through a thin metal film. The reflection of electrons or photons is also used for the purpose. During the process the charge of an electron couples with the electrostatic field fluctuations of plasma oscillations and the reflected or transmitted electron shows a loss of energy that equals an integral multiple of $\hbar\omega_p$. Figure 10.9 shows the energy loss spectrum for a 20 keV electron beam, incident on an aluminium foil. In this case, the characteristic energy loss peaks are all due to the excitation of one or more plasmons by the electrons passing through the foil.

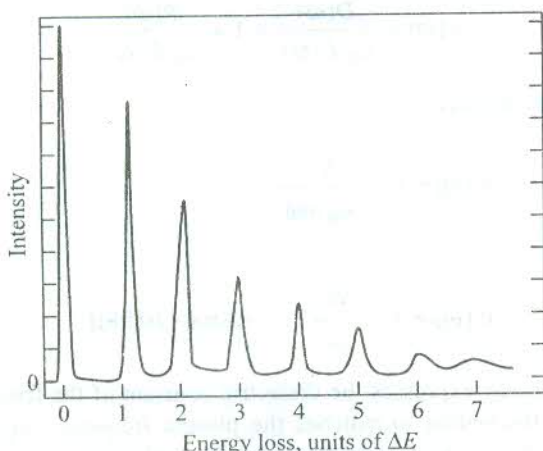


FIG. 10.9 Energy loss spectrum for a beam of 20 keV primary electrons passing through an aluminium foil of thickness 2580 Å. The unit of energy loss, ΔE , is about 1.5 eV, the plasmon excitation energy in aluminium. [After L. Marton, J.A. Simpson, H.A. Fowler and N. Swanson, *Phys. Rev.*, **126**, 182 (1962).]

If we treated ionic motion independently, we would get a much smaller frequency of oscillation for ions due to their heavier mass. The dielectric constant of the positive ion core background may be defined by (10.102) with the frequency of ion cores coming in for ω_p . It remains practically constant (a little below unity) up to the frequencies of perturbation ω well above ω_p . On account of its correspondence with high frequencies, it is denoted by ϵ_{∞} . Accordingly, we rewrite (10.102) as

$$\epsilon(\omega) = \epsilon_{\infty} - \frac{\omega_p^2}{\omega^2} = \epsilon_{\infty} \left[1 - \frac{\omega_p^2 / \epsilon_{\infty}}{\omega^2} \right]$$

or

$$\epsilon(\omega) = \epsilon_{\infty} \left(1 - \frac{\Omega_p^2}{\omega^2} \right) \quad (10.103)$$

with

$$\Omega_p = \frac{\omega_p}{\sqrt{\epsilon_{\infty}}} \quad (10.104)$$

The frequency Ω_p expresses the uniform collective longitudinal oscillation of the electron gas against a background of the fixed positive ions. It also denotes the low cutoff for the propagation of transverse electromagnetic waves in plasma because at this frequency $\epsilon(\omega) = 0$ (defining the longitudinal waves).

10.8.2 Transverse Optical Modes in Plasma

We first derive the dispersion relation for the electromagnetic waves, taken as model transverse waves. Then, using the theory developed above we obtain a relation for the positive real values of the dielectric constant. This relation when compared with the dispersion relation for the electromagnetic waves will be found to describe the electromagnetic waves that propagate through the plasma, establishing thereby the excitation of the transverse optical modes of the plasma oscillation.

The electromagnetic wave equation in a non-magnetic isotropic medium is given by

$$\mu_0 \epsilon_0 \epsilon(\omega, \mathbf{k}) \frac{\partial^2 \mathbf{E}}{\partial t^2} = \nabla^2 \mathbf{E} \quad (10.105)$$

where \mathbf{k} is the wavevector of the electromagnetic wave. With the electric field vector \mathbf{E} varying as $\sim \exp(i\mathbf{k} \cdot \mathbf{r}) \exp(-i\omega t)$, we get the following dispersion relation:

$$\epsilon(\omega, \mathbf{k}) \mu_0 \epsilon_0 \omega^2 = \mathbf{k}^2 \quad (10.106)$$

Substituting the value of the dielectric constant from (10.103) into (10.106), we obtain

$$\epsilon(\omega) \omega^2 = \epsilon_{\infty} \omega^2 \left(1 - \frac{\Omega_p^2}{\omega^2} \right) = \frac{\mathbf{k}^2}{\mu_0 \epsilon_0} \quad (10.107)$$

For $\omega < \Omega_p$, the above relation gives a negative value of the dielectric constant and an imaginary value of the wavevector. It gives the k -dependence of waves, say along the x -direction as $\exp(-|k_x|x)$

in the frequency range $0 < \omega \leq \Omega_p$. These waves cannot propagate through the medium and suffer complete reflection.

But at frequencies such that $\omega > \Omega_p$, (10.107) gives a positive real value of the dielectric constant and real k -values. Thus the medium is transparent to these waves. We rewrite (10.107) as

$$\omega^2 = \Omega_p^2 + \frac{k^2}{\mu_0 \epsilon_0 \epsilon_\infty} \quad (10.108)$$

This relation is similar to (10.106) and it represents the dispersion relation of the transverse electromagnetic modes in plasma. The dispersion curve is drawn in Fig. 10.10.

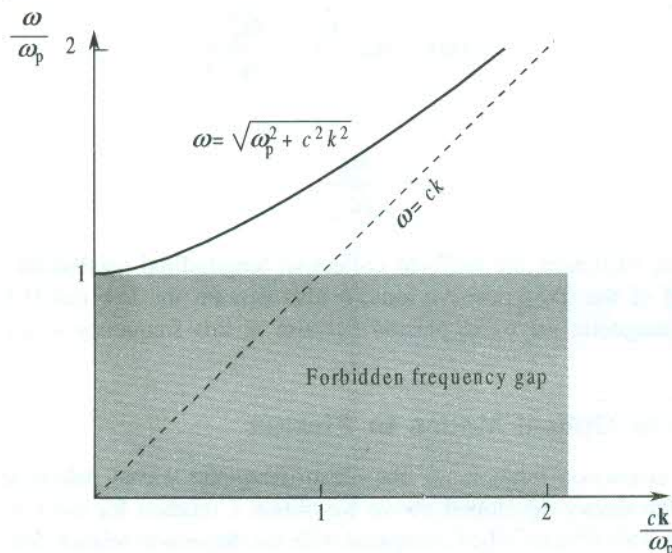


FIG. 10.10 The dispersion curve for transverse electromagnetic waves in a plasma.

The significance of the transverse optical modes in plasma is underlined by their close involvement in controlling the optical properties of crystals, especially metals. For example, the metallic lustre is attributed to the total reflection of visible light to which metals are not transparent. The reason being that the frequency of visible radiation is less than Ω_p . The transparency of alkali metals in the ultraviolet region strongly vindicates the theory that requires an electromagnetic radiation to have a certain minimum frequency or a wavelength not longer than a certain value to be able to pass through a plasma. The limit is defined in terms of ω_p or the corresponding wavelength in vacuum $\lambda_p (= 2\pi c/\omega_p)$. The theoretical and observed values of λ_p in alkali metals are given in Table 10.2. The two sets of values are within a reasonable limit of agreement.

Table 10.2 Longest electromagnetic waves λ_p , allowed for transmission in alkali metals (in Å)

P	Li	Na	K	Rb	Cs
Observed	1550	2100	3150	3400	—
Calculated	1550	2090	2870	3220	3620

It is equally interesting to apply our free electron gas model to semiconductors. The practice of doping facilitates the variation of the free electron concentration over a wide range. This is extremely helpful in varying the plasma edge of reflectivity. For example, Sn-doped In_2O_3 layers are almost totally transparent to the visible light but serve as effective barrier to the propagation of infrared radiation. Figure 10.11 shows the reflectivity and the transmissivity of one such layer. The coatings of Sn-doped In_2O_3 are applied in sodium vapour lamps and used as heat reflecting windows.

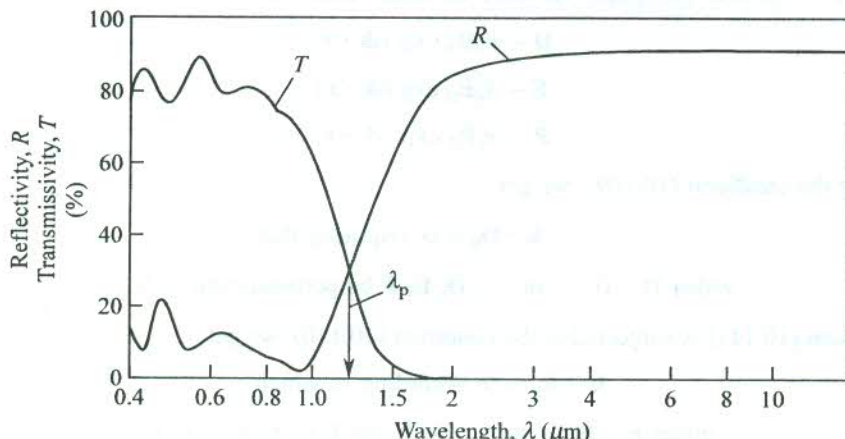


FIG. 10.11 Variations of reflectivity R and transmissivity T with change in the wavelength for a Sn-doped In_2O_3 layer. Thickness of the layer = $0.3 \mu\text{m}$ and the electron concentration is $1.3 \times 10^{21} \text{ cm}^{-3}$. [After G. Frank, E. Kauer, H. Köstlin, *Phys. Blätter*, **34**, 106 (1978).]

10.9 APPLICATION TO OPTICAL PHONON MODES IN IONIC CRYSTALS

The dispersion relations for the normal modes of an ionic crystal were treated in Chapter 4. The general technique is, however, fraught with difficulties in dealing with the long ranging interior electrostatic interactions. If we limit our attention to long wavelength optical modes we can avoid the use of complicated methods, developed for the purpose and work in an electrostatic approximation where the Maxwell's equation for $\text{curl } \mathbf{E}$ is relaxed to ignore the effect of $-\partial\mathbf{B}/\partial t$ at optical frequencies.

At long wavelengths ($\mathbf{k} \approx 0$) during the optical mode of vibration in an ionic crystal, the positive and negative ions suffer displacements in opposite directions giving rise to a net polarization \mathbf{P} . The macroscopic electric field \mathbf{E} and the displacement vector \mathbf{D} associated with it are given by the well-known relationship (10.15):

$$\mathbf{D} = \epsilon_0 \mathbf{E} + \mathbf{P}$$

Since there are no charges to have been introduced by an external source (or simply no free charges), we have

$$\text{div } \mathbf{D} = 0 \quad (10.109)$$

Further, the microscopic field $\mathbf{E}^{\text{micro}}(\mathbf{r})$ rapidly varying over a range of atomic distances is connected with the corresponding potential $\phi^{\text{micro}}(\mathbf{r})$ by

$$\mathbf{E}^{\text{micro}}(\mathbf{r}) = -\text{grad}_{\mathbf{r}} \phi(\mathbf{r})$$

Because the macroscopic field \mathbf{E} represents the average of $\mathbf{E}^{\text{micro}}$, the above relation applies in that case too. As stated in the beginning, we ignore the effect of the $-\partial\mathbf{B}/\partial t$ term in the Maxwell equation and write

$$\operatorname{curl} \mathbf{E} = \operatorname{curl} (-\operatorname{grad}_r \phi) = 0 \quad (10.110)$$

In ionic crystals owing to the cubic symmetry, ϵ is not a tensor and therefore \mathbf{D} , \mathbf{E} and \mathbf{P} are parallel (10.15). We take the spatial variation of these vectors as

$$\begin{aligned}\mathbf{D} &\sim R_e \mathbf{D}_0 \exp(i\mathbf{k} \cdot \mathbf{r}) \\ \mathbf{E} &\sim R_e \mathbf{E}_0 \exp(i\mathbf{k} \cdot \mathbf{r}) \\ \mathbf{P} &\sim R_e \mathbf{P}_0 \exp(i\mathbf{k} \cdot \mathbf{r})\end{aligned}\quad (10.111)$$

On imposing the condition (10.109), we get

$$\mathbf{k} \cdot \mathbf{D}_0 = 0, \text{ requiring that}$$

$$\text{either } \mathbf{D} = 0 \quad \text{or} \quad \mathbf{D}, \mathbf{E}, \mathbf{P} \text{ be perpendicular to } \mathbf{k}. \quad (10.112)$$

Similarly, when (10.111) is subjected to the condition (10.110), we get

$$\mathbf{k} \times \mathbf{E}_0 = 0, \text{ according to which}$$

$$\text{either } \mathbf{E} = 0 \quad \text{or} \quad \mathbf{D}, \mathbf{E} \text{ and } \mathbf{P} \text{ be parallel to } \mathbf{k}. \quad (10.113)$$

We see immediately below that one of the requirements under (10.112) combines with another, the compatible one under (10.113) to define a certain type of optical mode (longitudinal or transverse).

10.9.1 The Longitudinal Optical Mode

In a longitudinal mode the polarization \mathbf{P} is parallel to the direction of propagation of the wave, i.e. \mathbf{k} , as is one of the two allowed possibilities under (10.113). One of the two possibilities under (10.112) that must be considered to define this mode completely is $\mathbf{D} = 0$, since $\mathbf{P} \perp \mathbf{k}$ is already ruled out. Therefore, for a longitudinal optical mode,

$$\mathbf{E} = -\frac{\mathbf{P}}{\epsilon_0} \quad \text{and} \quad \epsilon = 0 \quad (\text{from 10.15}) \quad (10.114)$$

since,

$$\epsilon = \frac{\mathbf{D}}{\epsilon_0 \mathbf{E}} \quad \text{and} \quad \mathbf{D} = 0$$

10.9.2 The Transverse Optical Mode

In this case $\mathbf{P} \perp \mathbf{k}$, therefore, for a transverse optical mode,

$$\mathbf{E} = 0 \quad \text{and} \quad \epsilon = \infty \quad (10.115)$$

We must not forget here that (10.115) has been derived in the electrostatic approximation of the Maxwell's equation, $\operatorname{curl} \mathbf{E} = -\partial\mathbf{B}/\partial t$. Therefore, for an accurate description of the transverse optical modes, the condition $\epsilon = \infty$ must be replaced by a more general condition.

The transverse modes with angular frequency ω and wavevector \mathbf{k} propagate, provided

$$\epsilon(\omega) = \frac{k^2 c^2}{\omega^2} \quad [\text{from (10.106)}] \quad (10.116)$$

In view of this, the condition $\epsilon = \infty$ is acceptable only if the wavevectors of the optical modes are in accordance with $kc \gg \omega$. Since the magnitude of the optical phonon wavevector matches the order of the Debye wavevector, we have

$kc \gg k_D S$, where S is the speed of sound in the crystal

or

$$k \gg k_D \times \left(\frac{S}{c} \right) \quad (10.117)$$

Because the $S/c \approx 10^{-4}$ to 10^{-5} and k_D compares with the size of the Brillouin zone, it is concluded that the electrostatic approximation is applicable to those optical modes whose wavevectors are long enough and never be as small as a small fraction of a per cent of the Brillouin zone size when measured from $\mathbf{k} = 0$.

10.10 THE INTERACTION OF ELECTROMAGNETIC WAVES WITH OPTICAL MODES

We refer back to Section 10.5.2 dealing with the ionic polarizability of a diatomic ionic crystal in the presence of an electric field $E_{\text{loc}} [\sim E_0 \exp(-i\omega t)]$. This field can as well come from the one associated with an electromagnetic wave. Therefore, the theory of Section 10.5.2 forms the basis for the discussion in this section. At the outset it must be clear that the longitudinal optical modes cannot have any coupling with the transverse electromagnetic waves in the bulk of a crystal. We are concerned here with the coupling between the transverse optical phonons and the photons.

Let us first study the structure of the transverse modes all the way down to $k = 0$. This is done by making use of the relation (10.58) for the dielectric constant derived in Section 10.5.2:

$$\epsilon(\omega) = \epsilon_{\infty} + \frac{(\epsilon_s - \epsilon_{\infty}) \omega_T^2}{\omega_T^2 - \omega^2}$$

We plot ϵ versus ω using the above relation in Fig. 10.12. The intersection with the ω -axis (on which $\epsilon = 0$) gives the value of ω_L and the pole of $\epsilon(\omega)$ determines ω_T . It is significant that ϵ is negative between ω_T and ω_L , making k imaginary (10.106). This means that no radiation can propagate in the crystal over this range of frequencies. The region corresponds with the spread of the reststrahlen band which appears owing to strong reflection of the radiation. As mentioned in Section 10.5.2, there occurs a resonance at frequency ω_T where the frequencies and the wavevectors of the optical phonon and the photon are equal. In this condition the phonon-photon coupling becomes so substantial that it completely changes the nature of propagation and a forbidden gap is created which in no way can be tied to the periodicity of the crystal. The consequence of this coupling is implicitly contained in the dielectric function (10.58). The quantum of the coupled phonon-photon transverse wave field is commonly known as a *polariton*.

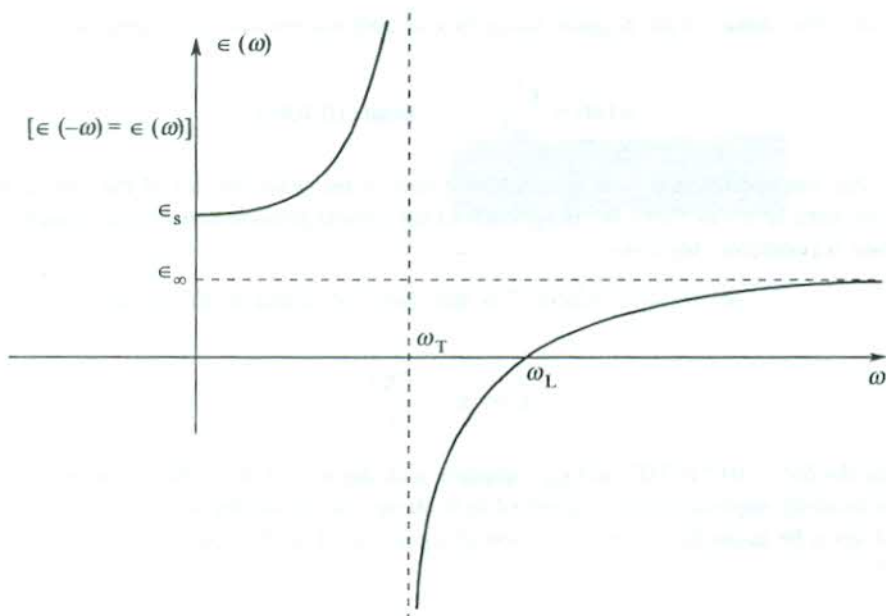


FIG. 10.12 Behaviour of the dielectric constant with change in frequency in a diatomic ionic crystal.

We give below a simple account of the transverse optical (TO) phonon-photon coupling and calculate the polariton frequency at $k = 0$.

The dispersion relation for the photons is [see (10.106)]

$$\epsilon(\omega)\omega^2 = \frac{k^2}{\mu_0 \epsilon_0}$$

or

$$\left(\frac{\epsilon_0 E + P}{\epsilon_0 E} \right) \omega^2 = \frac{k^2}{\mu_0 \epsilon_0}$$

or

$$P\omega^2 + \left(\epsilon_0 \omega^2 - \frac{k^2}{\mu_0} \right) E = 0 \quad (10.118)$$

If we do not consider the electronic polarization and neglect the damping term in (10.52), the polarization within the crystal can be written as

$$P = \frac{N_i e^2}{\mu(\bar{\omega}^2 - \omega^2)} E$$

or

$$\mu(\bar{\omega}^2 - \omega^2) P - N_i e^2 E = 0 \quad (10.119)$$

For the relations (10.118) and (10.119) to have a solution, the determinant of the coefficients of \mathbf{P} and \mathbf{E} in these relations must vanish. Therefore,

$$\begin{vmatrix} \omega^2 & \left(\epsilon_0 \omega^2 - \frac{k^2}{\mu_0} \right) \\ \mu(\bar{\omega}^2 - \omega^2) & -N_i e^2 \end{vmatrix} = 0 \quad (10.120)$$

For $k = 0$, it gives two roots:

$$\omega = 0 \text{ for the photon}$$

and

$$\omega^2 = \bar{\omega}^2 + \frac{N_i e^2}{\epsilon_0 \mu} \quad (10.121)$$

To remind, N_i is the density of ion pairs and μ is the reduced mass of an ion pair. The $\bar{\omega}$ is related to ω_T by (10.59) when the electronic polarization is also considered. Therefore, the polariton frequency at $k = 0$ may be given by

$$\omega^2 = \omega_T^2 \left(\frac{\epsilon_s + 2}{\epsilon_\infty + 2} \right) + \frac{N_i e^2}{\epsilon_0 \mu} \quad (10.122)$$

But we must appreciate that the resonance occurs for a finite value of k , where the coupling between the TO phonon and the photons is the strongest. It can be determined by the intersection of the photon dispersion curve (10.106) and the dispersion curve of TO phonons. This value of k turns out to be very small compared with the extent of the Brillouin zone. This region of resonance is often referred to as the *crossover region*.

Solutions to the dispersion relation for the transverse optical modes propagating in a diatomic ionic crystal are drawn in Fig. 10.13. There are two branches, one lying completely below ω_T and the other completely above ω_L . The appropriate dielectric constant to be used for frequencies below ω_T is ϵ_s , and ϵ_∞ for frequencies above ω_T (see Fig. 10.12). The corresponding dispersions (the dashed lines at $k = 0$) are represented accordingly. In the linear regions of each of the continuous curves, one mode is clearly phonon like. The curved regions are mixed in character and describe the dispersion of polaritons.

The theory discussed in this section also provides the relationship between ω_L and ω_T . When $\omega = \omega_L, \epsilon = 0$. Imposing this condition on (10.58), we have

$$\omega_L^2 = \frac{\epsilon_s}{\epsilon_\infty} \omega_T^2 \quad (10.123)$$

Relation (10.123) is known as the Lyddane-Sachs-Teller relation (addressed popularly as the LST relation). This relation has been tested by comparing the values of ω_L and ω_T , obtained from the neutron scattering experiment, with the measured values of the dielectric constant and index of refraction ($\bar{n} = \sqrt{\epsilon_\infty}$). Woods et al.* have observed excellent agreement between ω_L/ω_T and

* A.D.B. Woods et al., *Phys. Rev.*, **131**, 1025 (1963).

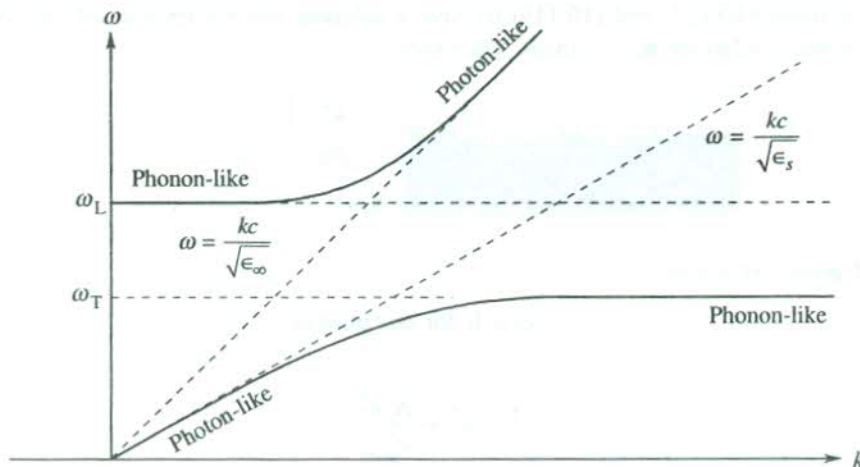


FIG. 10.13 Dispersion curves of coupled TO phonon and optical photon in a diatomic ionic crystal (in thick continuous lines). The curves for the uncoupled TO phonons and optical photons are shown by the dashed lines. There are two linear regions in each branch of the thick curves. In these regions one mode is clearly phonon-like and the other is clearly photon-like. The curved portions of the curve truly represent mixed modes, i.e. polaritons.

$(\epsilon_s/\epsilon_\infty)^{1/2}$ in NaI and KBr crystals. The mismatch is well within the limits of the experimental error. We will be back with the LST relation in Chapter 11, where it will be found useful in explaining the occurrence of ferroelectricity.

10.11 APPLICATION TO THE MOTION OF ELECTRONS IN POLAR CRYSTALS

Imagine an electron inside a polar (partially or completely ionic) crystal. The electrostatic field owing to the electron displaces each ion to a small extent. Thus a spatial distribution of lattice polarization is set up about the electron. The role of the neighbouring positive ions is more significant because they surround the electron with a positive screening cloud. As the electron moves, its polarization cloud must accompany it. Of course, the same ions cannot move along with the electron; the cloud is made up of just the neighbouring ions and these ions change as the electron moves. This way a deformation or a strain field propagates through the crystal with the moving electron. This quasielectron which is a system of the real electron plus the polarization cloud or the deformation field is called a *polaron*.

The coupling between an electron and its deformation field is more strong in ionic crystals than that in covalent crystals where the interaction of the electron with the neutral atoms is very weak. The polaron behaves as a heavier particle than the electron since the motion of a polaron may be interpreted as the motion of an electron that drags the heavy ion cores along with it.

The creation of a polaron is viewed as a consequence of the electron-lattice interaction which in analytical terms amounts to the electron-phonon interaction. The relatively low frequency longitudinal optical phonons are relevant to the theory of the polaron. The response of the lattice is limited dynamically by their frequency ω_L , that refers to the natural oscillations of dielectric polarization of the crystal. When the energy of the electron is more than $\hbar\omega_L$, an optical phonon is created with the electron getting decelerated and strongly scattered. Even for the slow moving electrons, we must

consider the virtual excitation and re-absorption of quanta in the optical modes, subscribing to the picture in which the electron is surrounded by a cloud of virtual phonons. The strength of the electron-phonon coupling is measured by a dimensionless interaction parameter,

$$\alpha = \frac{2(\text{the deformation energy})}{\hbar \omega_L} \quad (10.124)$$

where $\alpha/2$ can be visualized as the number of phonons that surround a slow moving electron in the crystal.

For small values of α , perturbation theory gives the following relation for the effective mass of the polaron:

$$m^* = m \left(1 + \frac{1}{6} \alpha \right) \quad (10.125)$$

Here m is the effective mass of the electron in the undeformed crystal. The value of m^* is determined from the cyclotron resonance studies. The values of α and m^*/m in a number of crystals have been given by Kittel.[†] In KCl the values are 3.97 and 2.5, respectively.

The electron associated with a polaron, with properties described above, moves in a band. Such a polaron is identified as a large polaron. In a small polaron, the associated electron remains mostly localized or trapped on a single ion. Both electrons and holes may be self-trapped by the asymmetric local deformations induced by them in the crystal lattice. This is feasible in a polar crystal when the band edge is degenerate. Since the valence band edge is more often degenerate than the conduction band edge, the holes are more likely to be self-trapped. They may, however, be released by thermal excitation. Such a small polaron is so sensitive to the graininess of the lattice that it moves only by hopping from cell to cell. The concept of a valence band in an ionic crystal thus becomes meaningless.

SUMMARY

1. The polarization \mathbf{P} in terms of the macroscopic electric field \mathbf{E} of the Maxwell's equation is given by

$$\mathbf{P} = (\epsilon - 1) \epsilon_0 \mathbf{E}$$

2. The macroscopic field \mathbf{E} is equal to the average of the electric field within the volume of the dielectric.
3. The electric field at an atomic site is

$$\mathbf{E}_{\text{loc}} = \mathbf{E}_0 + \mathbf{E}_{\text{dep}} + \mathbf{E}_L + \mathbf{E}_{\text{dip}}$$

where

\mathbf{E}_0 is the external field

\mathbf{E}_{dep} is the depolarization field

\mathbf{E}_L is the Lorentz field, the field at the centre of the fictitious cavity owing to the induced charges on the imaginary surface of the cavity.

\mathbf{E}_{dip} is the field at the centre of the cavity owing to dipoles within the cavity.

[†] C. Kittel, *Introduction to Solid State Physics*, 7th ed., p. 298 (John-Wiley, 1996).

4. The macroscopic field

$$\mathbf{E} = \mathbf{E}_0 + \mathbf{E}_{\text{dep}}$$

with $\mathbf{E}_{\text{dep}} = -\frac{1}{3\epsilon_0} \mathbf{P}$ for a sphere.

5. $\mathbf{E}_L = \frac{1}{3\epsilon_0} \mathbf{P}$, for spherical cavity

6. $\mathbf{p} = \alpha \mathbf{E}_{\text{loc}}$
where

\mathbf{p} is the atomic dipole moment
 α is the atomic polarizability

7. In electronic polarization the resonance frequency is shifted from the natural frequency of oscillation of the electronic shell (towards a lower value) because of the presence of a large density of polarizable electrons.

8. For a longitudinal optical mode

$$\mathbf{E} = -\frac{1}{\epsilon_0} \mathbf{P} \quad \text{and} \quad \epsilon = 0$$

For a transverse optical mode

$$\mathbf{E} = 0 \quad \text{and} \quad \epsilon = \infty$$

9. The dielectric constant of a cubic ionic crystal is

$$\epsilon(\omega) = \epsilon_{\infty} + \frac{(\epsilon_s - \epsilon_{\infty}) \omega_T^2}{\omega_T^2 - \omega^2}$$

10. Power dissipated per cubic metre of the dielectric is given by

$$W = \frac{1}{2} \omega \epsilon_0 E_0^2 \epsilon''(\omega)$$

$$= \frac{1}{2} \omega E_0 D_0 \sin \delta; \text{ with } \tan \delta = \frac{\epsilon''(\omega)}{\epsilon'(\omega)}$$

11. The complex index of refraction is given by

$$\bar{n}(\omega) = n + ik = \sqrt{\epsilon(\omega)}$$

n, k are the optical constants.

12. The real and imaginary parts of the dielectric constant are written as

$$\epsilon'(\omega) = n^2 - k^2; \quad \epsilon''(\omega) = 2nk$$

13. The reflectivity at normal incidence is given as

$$r = \frac{n + ik - 1}{n + ik + 1}$$

and the reflectance at normal incidence is of the form:

$$R = \frac{(n - 1)^2 + k^2}{(n + 1)^2 + k^2}$$

14. The uniform collective longitudinal oscillations of the electron gas against a background of fixed positive ions is given by

$$\Omega_p = \frac{\omega_p}{\sqrt{\epsilon_\infty}} \quad \text{with} \quad \omega_p = \left(\frac{N_0 e^2}{\epsilon_0 m} \right)^{1/2}, \text{ the plasma frequency}$$

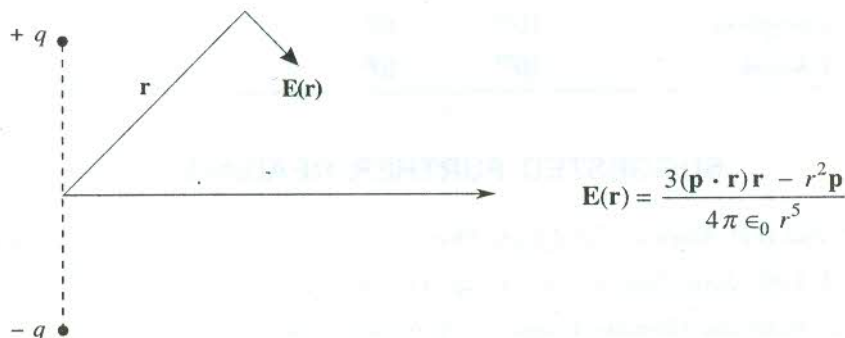
15. A quantum of coupled TO phonon-photon mode is called a *polariton*.

16. The relation $\frac{\omega_L^2}{\omega_T^2} = \frac{\epsilon_s}{\epsilon_\infty}$ is known as the LST relation.

17. The effective mass of the polaron (the combination of an electron and its strain field) is more than that of the electron in an undeformed crystal because of the additional mass associated with the deformation field being dragged by the moving electron in the form of a polarization cloud.

PROBLEMS

- 10.1 Find the components of the electric field resulting from charges $+q$ and $-q$ in the following figure. Add them vectorially to show that the resultant is given by



- 10.2** Assuming that an atom consists of a uniform sphere of negative charge with radius R surrounding a point positive charge, show that the polarizability is equal to $4\pi\epsilon_0 R^3$. Assume that the negative charge remains uniform even under the action of a field. If the diameter of argon atom be 3 Å, calculate the index of refraction of argon gas at NTP.
- 10.3** An infinite dielectric medium with dielectric constant ϵ has a spherical cavity of radius R cut within it. If a very small conducting sphere of radius r is placed at the centre of the cavity and a uniform electric field E_0 is produced within the main body of the dielectric, what will be the induced dipole moment of the sphere?
- 10.4** The resonance absorption exhibited by a medium shows a single absorption line at 6000 Å (in vacuum). When a beam of light of this wavelength travels through 2.5 cm in the medium, the intensity of light drops to $1/e$ of its initial value. Calculate the maximum value of the imaginary part of the index of refraction.
- 10.5** The complex index of refraction of a metal for infrared radiation ($\omega\tau \ll 1$) is expressed as

$$\sqrt{\epsilon(\omega)} = (n + ik) = 1 + 4\pi i\sigma_0/\omega \quad (\text{C.G.S})$$

where σ_0 is the electrical conductivity for static fields. Check that σ_0 has the unit s^{-1} in e.s.u. Assuming $\sigma_0 \gg \omega$ (leading to $n \approx k$), show that the reflectance of the metal approximately equals

$$[1 + (2\omega/\pi\sigma_0)^{1/2}]$$

- 10.6** Assume that the electrons and the nucleus of an atom form a spherical cloud of uniform density and radius r_0 . Taking r_0 as the Bohr radius, calculate the polarizability of hydrogen atom based on this model. How does it compare with the true polarizability?
- 10.7** Complete the following table, which lists the typical parameters for electrons in four different types of plasma.

	N_0 (m^{-3})	T (K)	ω_p (rad s^{-1})	λ_D (m)
Solar atmosphere	10^{18}	10^4		
Solar corona	10^{13}	10^6		
Ionosphere	10^{10}	10^3		
Tokamak	10^{19}	10^8		

SUGGESTED FURTHER READING

- Aschroft, N.W. and N.D. Mermin, *Solid State Physics*, Chap. 27 (Saunders College, 1988).
- Ibach, H. and H. Lüth, *Solid State Physics*, Chap. 11 (Springer, 1995).
- Ziman, J.M., *Electrons and Phonons*, Chaps. IV, V (Oxford Univ. Press, 1967).
- Ziman, J.M., *Principles of the Theory of Solids*, Chaps. 5, 8 (Cambridge Univ. Press, 1972).

Ferroelectric Crystals

The natural primitive cells of certain dielectric crystals can possess nonvanishing electric dipole moment, even in the absence of applied electric field. The crystal as a whole will thus have a polarization implying that it is spontaneously polarized. The spontaneously polarized dielectric crystals are called *pyroelectric crystals*. Though a proper interpretation for the spontaneous polarization is not straightforward, simple details of crystal structure surprisingly come handy in predicting if a crystal would be pyroelectric. When the centre of positive charge does not coincide with the centre of negative charge in a primitive cell, the primitive cell will possess an electric dipole moment even when there is no external electric field. This is, perhaps, the simplest way to look at the spontaneously polarized nature of pyroelectric crystals.

The shifting of the centre of positive charge from the centre of negative charge is exhibited in the lack of centre of inversion symmetry in the crystal. Out of 32 crystal point groups, 21 point groups do not have a centre of symmetry. Excepting one, which is very highly symmetric, the rest 20 point groups represent an extremely useful class of materials, commonly known as *piezoelectrics*. The piezoelectric crystals show electric polarization on being externally strained and conversely, show deformation when placed under the influence of an applied electric field. If it is confirmed that a crystal belongs to the class of 20 point groups under discussion, it can be predicted that the crystal would be piezoelectric. Among these 20, there are only 10 such groups in which the crystals are spontaneously polarized to be identified as pyroelectrics. At this point we have to examine the consequences of the following requirement on pyroelectric crystals. While maintaining the crystalline properties, the symmetry operations of a pyroelectric crystal must preserve the direction of polarization vector \mathbf{P} . This imposes severe restrictions on the point group symmetries as a result of which only 10 point groups are found to meet the conditions of pyroelectric crystals. The rotation is allowed about only one axis that is parallel to \mathbf{P} and there cannot exist mirror planes perpendicular to this axis. The structural scrutiny of crystal point groups (see Table 1.2) reveals that only the following point groups meet the restrictions of pyroelectric crystals:

$$\text{C}_n, \text{C}_{nv} \quad (n = 2, 3, 4, 6), \text{C}_1 \text{ and } \text{C}_{1h}$$

Thus the pyroelectric property too, like piezoelectricity, is solely determined by the symmetry properties of crystals.

The polarization in pyroelectric crystals is usually masked by surface charges that accumulate on the surface from the atmosphere and subsequently neutralize the layers of ions. But, when the temperature of the crystal is altered, the masking is no longer complete as the polarization changes because of the thermal expansion or contraction of the crystal. Owing to the thermal effect on polarization, these crystals are named pyroelectric (pyro means fire). The thermal effect accompanying deformations thus corroborates the piezoelectric property of these crystals. This only confirms that all pyroelectric crystals are piezoelectric, though the converse is not true. The description of pyroelectric

crystals remains grossly incomplete without the mention of ferroelectric crystals which are only part of the group of pyroelectrics. The ferroelectric crystals, however, have an additional property that the polarization in them can be changed and even reversed by an external electric field. On the other hand, the same is not possible in pyroelectrics even with the maximum electric field that may be applied without causing electrical breakdown. The additional feature of ferroelectrics that distinguishes them as a special class of pyroelectrics does not follow from the characteristics of crystal structure. It is established only on the basis of dielectric measurement.

Furthermore, the additional feature of ferroelectrics mentioned above converts the usual linear relationship between polarization and applied electric field into a hysteresis loop. The hysteresis effect finds a valid interpretation in the multiple domain theory according to which a bulk crystal is constituted of regions with varying direction of polarization. These regions are called *ferroelectric domains* (analogous to ferromagnetic domains).

The ferroelectric property is observed only below a certain characteristic temperature, called the *Curie point*. On heating the crystal above its Curie point, it shows paraelectric behaviour (normal dielectric behaviour). The Curie point is taken as a critical temperature or a transition temperature T_c that characterizes a phase transition. The theory of structural changes that bring about this transition forms the core of this chapter. At this stage it may suffice to treat the ferroelectric state simply as an ordered state of induced dipoles such that the total energy of the crystal in this state is lower than when the crystal shows no spontaneous polarization since the thermal energy at these temperatures is not strong enough to frustrate the ordering of dipoles.

The role of electric dipoles may further be appreciated by referring to an interesting class of solids which may apparently display permanent electric dipole moments. These substances are known as *electrets*. The materials, in fact, are polarized at high temperatures in an electric field, cooled in the field and then removed from the field. The process leaves the polarization 'frozen in'. As the moments thus produced may at the most survive a few years, the stable state of electrets would be unpolarized. Certain types of waxes, plastics and ceramics are some examples of electrets. Their applications are restricted because of the accumulation of surface charges that are attracted by the dipole field.

11.1 REPRESENTATIVE CRYSTAL TYPES OF FERROELECTRICS

The ferroelectric crystals may be classified into certain representative groups. Such a broad classification is given in Table 11.1. The table gives the Curie point T_c and the spontaneous polarization P_s for a number of common ferroelectric crystals. The electric susceptibility χ_E in the paraelectric phase is related to temperature by the Curie–Weiss law:[†]

$$\chi_E = \frac{C}{T - T_c} \quad (11.1)$$

where C is the Curie constant.

The ferroelectric crystals are also distinguished on the basis of the oscillatory nature of the atomic displacements that destroy the ferroelectric dipole order above the Curie temperature. In the ferroelectric phase of some crystals, the atomic displacements can be viewed as oscillations about a polar site. These oscillations take place about a non-polar site in the paraelectric phase. The phase

[†]The law gives a similar temperature dependence as that for the paramagnetic susceptibility χ_p . It will be derived in Chapter 13, giving due importance to magnetism which was discovered earlier than ferroelectricity.

Table 11.1 Data[†] on some representative ferroelectric crystals

Group	Crystal	T_c (K)	P_s $\text{Cm}^{-2}(10^{-2})$	At T (K)
Ilmenites and Perovskites	GeTe	670	—	—
	LiNbO_3	1480	71	296
	KNbO_3	710	30	600
	BaTiO_3	393	26	300
	SrTiO_3	32	3	4.2
KDP type	KH_2PO_4 (KDP)	123	4.7	100
	KD_2PO_4	213	5.5	100
	RbH_2PO_4	147	5.6	90
	KH_2AsO_4	97	5.0	78
TGS type	$(\text{NH}_2\text{CH}_2\text{COOH})_3 \cdot \text{H}_2\text{SO}_4$ (Triglycine sulphate)	322	2.8	275
Rochelle salt type	$\text{NaKC}_4\text{H}_4\text{O}_6 \cdot 4\text{H}_2\text{O}$ (Rochelle salt)	296 (upper) 255 (lower)	0.25	275

† Sources: F. Jona and G. Shirane, *Ferroelectric Crystals*, Pergamon (1962); E.C. Subbarao, *Ferroelectrics*, 5, 267 (1973).

transition that brings about this transformation in the nature of oscillations is called a *displacive phase transition*. These crystals are accordingly identified as *displacive type*. The well-known examples of this class are ionic crystals with ilmenite and perovskite structures. GeTe is the simplest ferroelectric crystal having the ilmenite structure (i.e. NaCl structure). We propose to take BaTiO_3 as the representative of perovskites for a discussion of its ferroelectric behaviour in Section 11.1.2.

There is another very interesting class of crystals in whose non-ferroelectric state the potential energy function around certain atomic sites is double-well or multiple-well shaped. On the transition to the ferroelectric state the atomic displacements about those sites are executed as oscillations in an ordered subset of the referred potential wells. It involves an order-disorder type of phase transition. Common examples of these crystals, classified as order-disorder type, are some hydrogen bonded solids, namely KDP type crystals. The motion of protons engaged is linked to the ferroelectric behaviour. Neutron diffraction experiments confirm that the phosphate groups are bound together by what is known as a hydrogen bond. The proton prefers one end of the bond in the ferroelectric state because the proton distribution is found to be asymmetrically contracted in this state. The replacement of hydrogen by deuterium in KDP type crystals raises the Curie point in an amazing proportion. Though the increase in the molecular weight is less than 2 per cent, the T_c rises from 123 K to 213 K in the deuterated KDP and from 96 K to 162 K in KD_2AsO_4 . This abnormal effect does not have explanation in the domain of classical physics. It is believed to be a consequence of the change in the de Broglie wavelength, affected by the variation in mass.

The above brief account certainly does no justice to the cause of ferroelectric crystals, a large number of which have found important applications. Unfortunately, a complete and befitting treatment demands the description of each crystal separately since there exists no comprehensive theory that may treat them in a collective fashion. For specific description we have selected Rochelle salt and BaTiO_3 as the two representative compounds whose ferroelectric properties are uniquely different.

11.1.1 Properties of Rochelle Salt

Rochelle salt ($\text{NaKC}_4\text{H}_4\text{O}_6 \cdot 4\text{H}_2\text{O}$) has the distinction of being the first compound that showed ferroelectric property. So, it is of historical importance as well. It was first prepared in 1672 by a pharmacist Seignette who lived in Rochelle. It represents the tartaric group of salts whose other well-known members are lithium ammonium tartrate and lithium tantalum tartrate. The most noteworthy characteristic of Rochelle salt is that it is ferroelectric between two temperatures (255 K and 296 K). On account of its two transition temperatures, Rochelle salt becomes a special and peculiar example of ferroelectrics.

The crystal structure of Rochelle salt is somewhat complex. Above 296 K and below 255 K the structure is orthorhombic. It has a monoclinic symmetry in the ferroelectric phase such that the angle β (between the c - and a -axes) differs from 90° and the spontaneous polarization is along the original orthorhombic a -axis. The original orthorhombic a -axis acts as the lone polar axis with two directions (\pm) along this axis.

Halblützel* has measured the dielectric constant of Rochelle salt along the three crystal axes over the whole useful range of temperatures. Figure 11.1 gives a logarithmic plot of these values. The Curie–Weiss law applies above 296 K and below 255 K. With the help of the experimental data it is easy to confirm that the two regions have different values of Curie constants. The dielectric constant

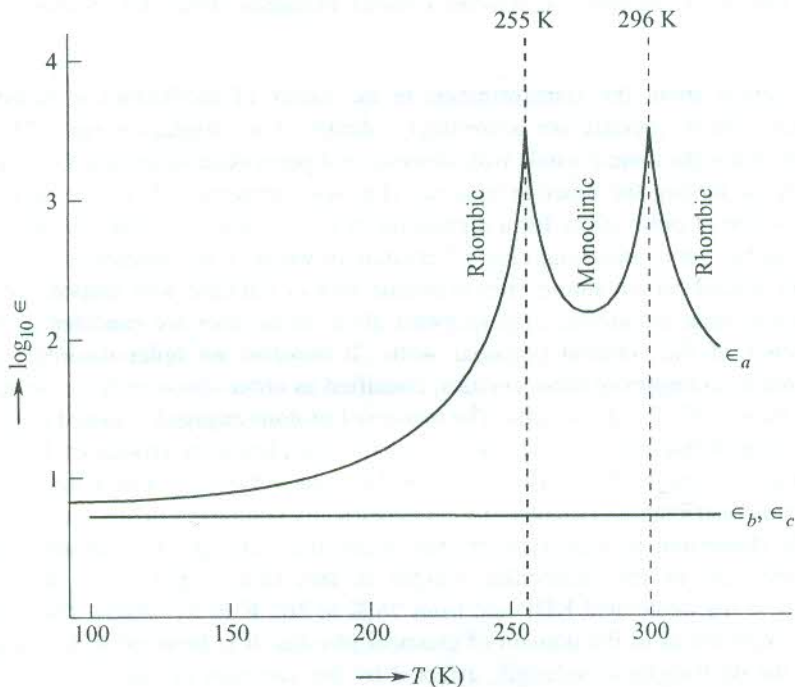


FIG. 11.1 Variation of the dielectric constants of Rochelle salt along a -, b - and c -axes with change in temperature*.

measured along the polar axis ϵ_a peaks at both the transition temperatures, assuming a value as high as 4000. The behaviour of spontaneous polarization* as a function of temperature is shown in Fig. 11.2. The lower curve represents Rochelle salt and the upper curve belongs to the deuterated salt.

* J. Halblützel, *Helv. Phys. Acta*, **12**, 489 (1939).

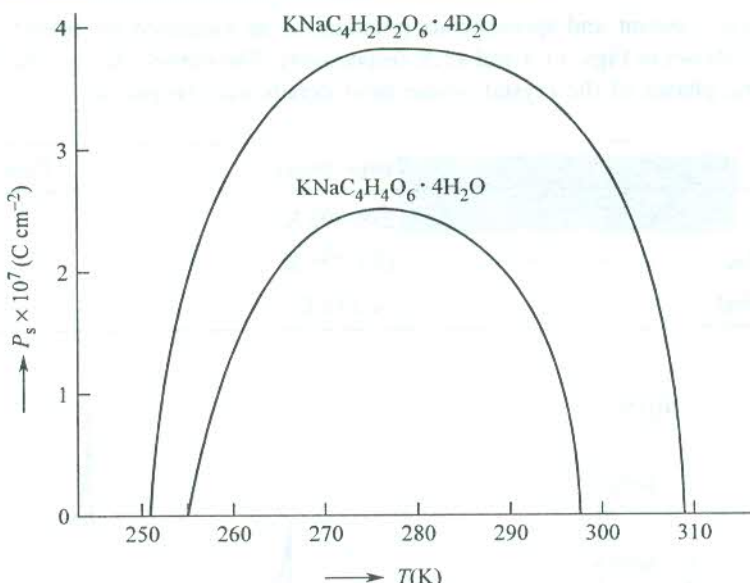


FIG. 11.2 Variation of the spontaneous polarization with change in temperature. The lower curve represents Rochelle salt and the upper curve the deuterated salt.

From the remarkable increase in polarization in the ferroelectric phase of the deuterated crystal, we might be tempted to infer that certain hydrogen bonds are involved in the mechanism of the transition. But the latest structural studies rule out this possibility. No definite theory has been developed so far to account for the ferroelectric properties of Rochelle salt and, therefore, the details of the transition mechanism remain obscure.

11.1.2 Properties of $BaTiO_3$

$BaTiO_3$ is the most important and most completely investigated representative of the perovskite type ferroelectrics. In the non-ferroelectric state (i.e. above 393 K) it has cubic symmetry as shown in Fig. 11.3(a). The Ba^{2+} ions are positioned at the corners, the O^{2-} ions at the centre of the faces and the Ti^{4+} ion is located at the centre of the cube. It has an arrangement of highly polarizable oxygen ions in the form of an octahedron with a small titanium ion at the centre [see Fig. 11.3(b)].

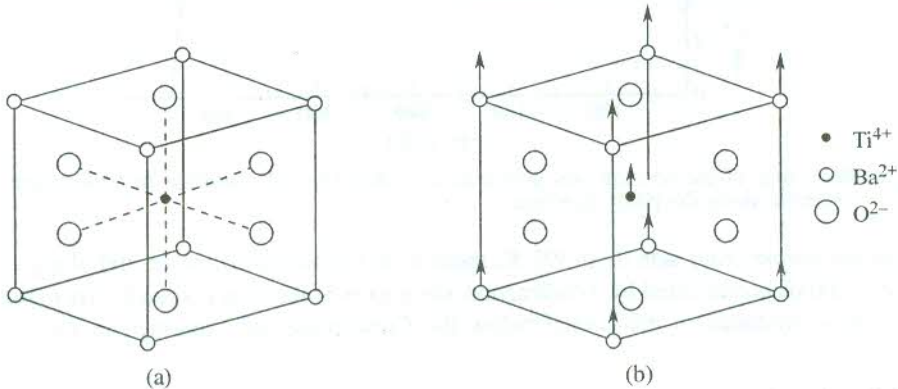


FIG. 11.3 (a) Unit cell of $BaTiO_3$ (perovskite structure). (b) Main distortion in $BaTiO_3$ unit cell that gives rise to ferroelectricity.

The dielectric constant and spontaneous polarization as measured by Merz* over a range of temperatures are shown in Figs. 11.4 and 11.5, respectively. The curves clearly indicate that there are three ferroelectric phases of the crystal whose brief details may be put as:

Crystalline symmetry	Temp. range	Direction of P_s
Tetragonal	278–393 K	[001]
Orthorhombic	193–278 K	[011]
Rhombohedral	< 193 K	[111]

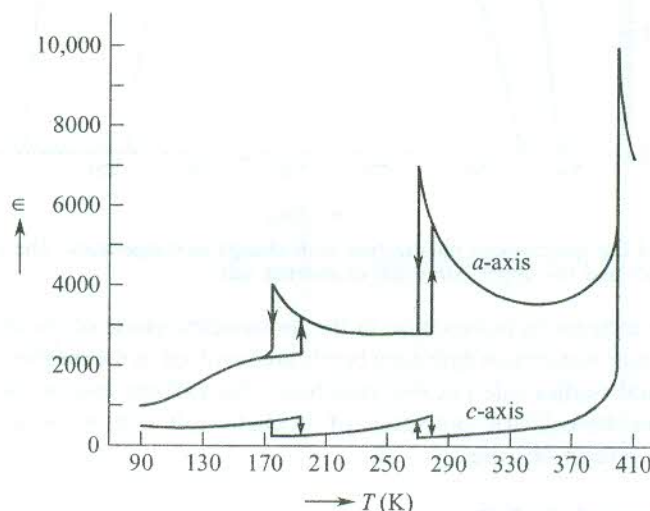


FIG. 11.4 Variation of the dielectric constant of BaTiO_3 with change in temperature.*

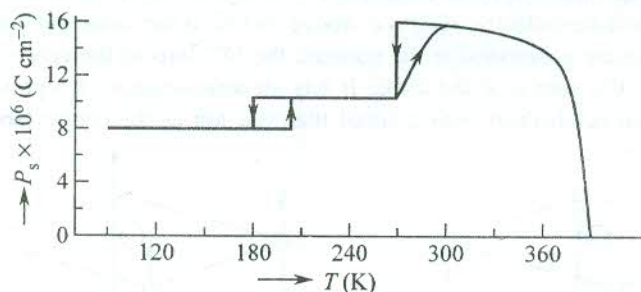


FIG. 11.5 Behaviour of the spontaneous polarization of BaTiO_3 with variation in temperature.* The P_s is measured along the [001] direction.

When the dipole order sets in at 393 K, there is an expansion of the crystal along one pseudo-cubic axis (c -axis) accompanied by a contraction along each of the axes perpendicular to this direction. The distortions produced in the crystal below the Curie point are explained in Fig. 11.3(b). The

* W.J. Merz, *Phys. Rev.*, **76**, 1221 (1949).

sublattice of all the Ba²⁺ and Ti⁴⁺ ions is shifted with respect to the sublattice of the O²⁻ ions, the displacement d being barely $\sim 0.1 \text{ \AA}$ at room temperature. This leads to the dipole moment per unit cell p , given by

$$p = 6e \cdot d = 0.96 \times 10^{-29} \text{ C m}$$

The dipole moment p can alternatively be estimated by multiplying P_s (as obtained from Fig. 11.5 at room temperature) by the unit cell volume. Treating the unit cell as a simple cube of edge 4 Å even in the ferroelectric state, we get $p = 0.15(4 \times 10^{-10})^3 = 0.96 \times 10^{-29} \text{ C m}$. Thus we find that this value is in perfect agreement with that obtained on the basis of the observed deformation of the unit cell. The order of magnitude gives a measure of the ferroelectric effect in BaTiO₃. The effect, however, is fairly large in some other perovskites (e.g. LiNbO₃).

The fact that Fig. 11.5 shows P_s along the [001] direction, warrants our further attention. This implies that we must multiply the values shown in the figure by $\sqrt{2}$ and $\sqrt{3}$ to obtain the actual values in the regions $193 \text{ K} < T < 278 \text{ K}$ and $T < 193 \text{ K}$, respectively, because the direction of P_s in these regions is along the [011] and [111] directions, respectively. It is then quite interesting to note that spontaneous polarization (same as the saturation polarization) remains almost constant below 300 K.

11.2 THEORY OF THE FERROELECTRIC DISPLACIVE TRANSITIONS

Although we plan to discuss formal thermodynamic theory later in this chapter, the theory that gives a good account of these transitions in perovskite type crystals merits a separate treatment on account of having stood the test of vast experimental data. These crystals generally undergo a displacive transition at the Curie point. We can follow two approaches in the pursuit of finding interpretation to a displacive transition. In one approach we talk of polarization catastrophe that refers to an unusual situation in which the polarization becomes infinitely large. In this condition the force exerted by the local electric field is greater than the elastic restoring force. This produces an asymmetric shift in the positions of the positive and negative ions. The shift is, however, limited to a finite displacement by the anharmonic restoring forces. We can alternatively follow the soft mode approach in which a transverse optical (TO) mode is frozen, i.e. its frequency vanishes at some point in the Brillouin zone below the Curie temperature. This TO mode is known as a soft mode. When $\omega_T = 0$, the crystal becomes unstable because of the absence of an effective restoring force.

11.2.1 Polarization Catastrophe

The Clausius–Mossotti relation (10.38) can be rearranged in the form

$$\epsilon = 1 + \frac{3(N_i\alpha_i + N_e\alpha_e)}{3\epsilon_0 - (N_i\alpha_i + N_e\alpha_e)} \quad (11.2)$$

where all of these symbols have their meaning as defined in Chapter 10. When

$$(N_i\alpha_i + N_e\alpha_e) = 3\epsilon_0 \quad (11.3)$$

the dielectric constant becomes infinite [from (11.2)], giving the state of polarization catastrophe.

Further,

$$\begin{aligned}\mathbf{P} &= (N_i \alpha_i + N_e \alpha_e) \mathbf{E}_{\text{loc}} \\ &= (N_i \alpha_i + N_e \alpha_e) \left(\mathbf{E} + \frac{\mathbf{P}}{3 \epsilon_0} \right)\end{aligned}\quad (11.4)$$

for a cubic crystal (using the Lorentz expression for \mathbf{E}_{loc}).

If $\mathbf{E} = 0$, then from (11.4) we have

$$\mathbf{P} \left(\frac{N_i \alpha_i + N_e \alpha_e}{3 \epsilon_0} - 1 \right) = 0 \quad (11.5)$$

But, when the polarization catastrophe occurs, the quantity within the brackets equals zero [from (11.3)]. This requires that

$$\mathbf{P} \neq 0 \quad (11.6)$$

for (11.5) to be true.

The result (11.6) is obtained with the condition that the macroscopic field \mathbf{E} ($= \mathbf{E}_0 + \mathbf{E}_1$) be zero which is possible only if the applied field \mathbf{E}_0 is zero, since then \mathbf{E}_1 (the depolarization field, caused by the induced charges) would also be zero.

In order to get an improved physical understanding of the above situation, we consider a highly polarizable ionic crystal of cubic symmetry. Let α denote the total polarizability and p the dipole moment of an ion pair. We assume that some transient stray field starts polarizing the ion pairs. The ion pairs will keep on polarizing until some resistance develops to stop the process. The resistance that finally stops the process of polarization exists in the form of anharmonic restoring forces. The dipole moment of a single ion pair with ion separation \mathbf{x} is

$$\mathbf{p} = q \cdot \mathbf{x} = \alpha \mathbf{E}_{\text{loc}} = \left(\frac{\alpha \mathbf{F}}{q} \right) \quad (11.7)$$

where \mathbf{F} is the restoring force that tends to bring the positive and negative ions together and q is the charge on each ion.

The work required to create N such dipoles in the unit volume of the crystal is

$$\epsilon_1 = N \int \mathbf{F} \cdot d\mathbf{x} = \frac{Nq^2}{\alpha} \int \mathbf{x} \cdot d\mathbf{x} = \frac{Np^2}{2\alpha} \quad [\text{using (11.7)}] \quad (11.8)$$

$$= \frac{P^2}{2N\alpha}$$

On the other hand, the energy density associated with the electrical displacement brought about by \mathbf{E}_{loc} is given by

$$\epsilon_2 = \int \mathbf{E}_{\text{loc}} \cdot d\mathbf{P}$$

$$\begin{aligned}
 &= \int \left(\mathbf{E} + \frac{\mathbf{P}}{3\epsilon_0} \right) \cdot d\mathbf{P} \\
 &= \frac{P^2}{6\epsilon_0} + \int \mathbf{E} \cdot d\mathbf{P}
 \end{aligned} \tag{11.9}$$

Since ϵ_1 is set against ϵ_2 , the net energy density of a polarized dielectric is

$$\epsilon_2 - \epsilon_1 = \frac{P^2}{2N\alpha} \left(\frac{N\alpha}{3\epsilon_0} - 1 \right) + \int \mathbf{E} \cdot d\mathbf{P} \tag{11.10}$$

This shows that even when $\mathbf{E} = 0$, $\epsilon_2 > \epsilon_1$, provided that

$$N\alpha \geq 3\epsilon_0 \tag{11.11}$$

The above condition in a general case is written in the form

$$\sum_j N_j \alpha_j \geq 3\epsilon_0 \tag{11.12}$$

where N_j stands for the density of the j th type of particles (ions/electrons) in the crystal and α_j denotes the polarizability of a single particle of this type.

The sign of equality in (11.12) describes the condition of polarization catastrophe (11.3) with

$$\sum_j N_j \alpha_j \equiv N_i \alpha_i + N_e \alpha_e \tag{11.13}$$

From relation (11.10) it follows that the energy of the crystal is smaller in the presence of induced dipoles than it is without them. The minimum value of $\sum_j N_j \alpha_j$ for which the ferroelectricity would occur is $3\epsilon_0$. Unfortunately, a simple situation that exactly corresponds to the polarization catastrophe has not been found in any real ferroelectric crystal. However, a small deviation in the value of $\sum_j N_j \alpha_j$ from $3\epsilon_0$ changes the value of ϵ (11.2) by a large amount. When we express $\sum_j N_j \alpha_j$ as

$$\sum_j N_j \alpha_j = 3\epsilon_0 - 3\beta \tag{11.14}$$

with $\beta \ll 1$ and using (11.2), we get

$$\epsilon \propto \frac{1}{\beta} \tag{11.15}$$

If we assume that β is a linear function of temperature near the Curie point and given by

$$\beta = \frac{T - T_c}{\eta} \tag{11.16}$$

η being a constant, then

$$\epsilon \propto \frac{1}{T - T_c} \quad (11.17)$$

The temperature dependence of ϵ as given by this relation is in excellent agreement with the observed behaviour in several perovskite crystals (Fig. 11.6).

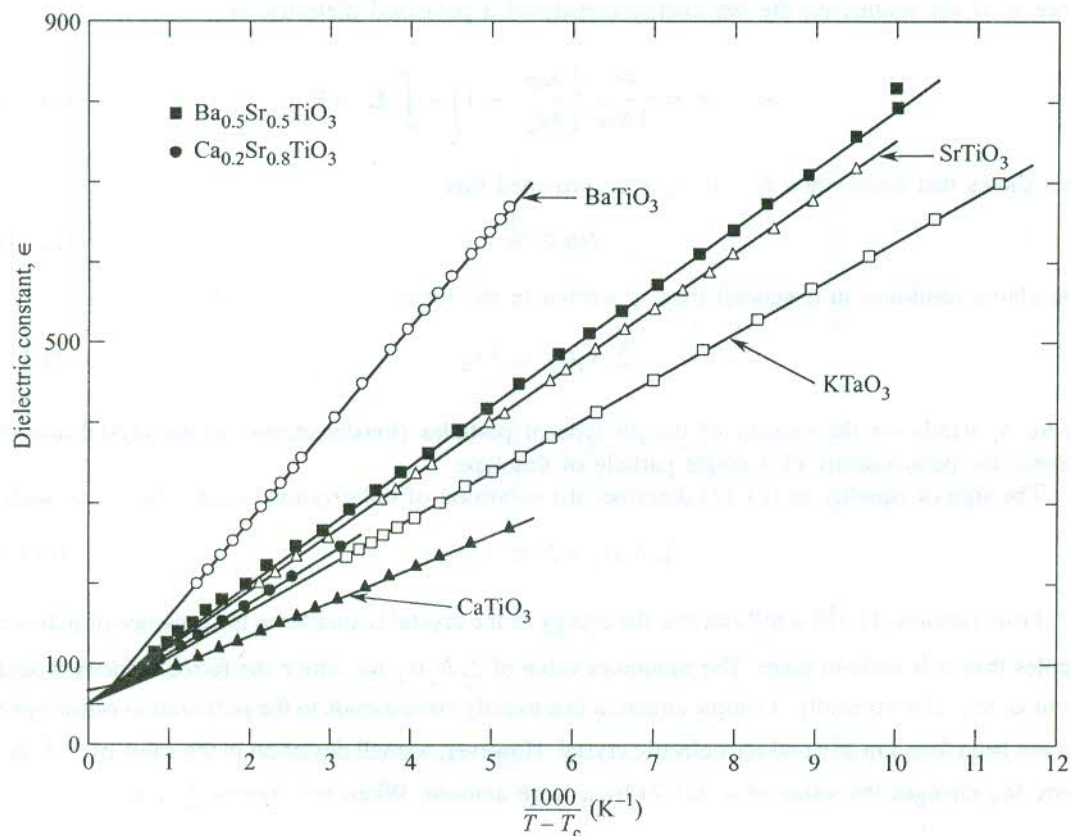


FIG. 11.6 Plot of the measured values of the dielectric constant versus $1/(T - T_c)$ in the non-ferroelectric phase ($T > T_c$) for certain perovskite crystals. [After G. Rupprecht and R.O. Bell, *Phys. Rev.*, **135**, A 748 (1964).]

The occurrence of ferroelectricity in perovskite crystals is understood conclusively to a large extent in view of the following two points, made in respect of barium titanate:

1. **The titanium ion motion.** The barium ions situated at the cube corners leave a big hole at the body centre position. Being smaller than the barium ion, the titanium ion is unable to fill the hole and is free to rattle around in the hole. Because the ionic polarizability is a measure of the ease of displacement, its value is greatly increased. In this case the potential well, in which the titanium ion moves, is somewhat flatter (Fig. 11.7) than the one under the condition of ordinary ionic bonding.

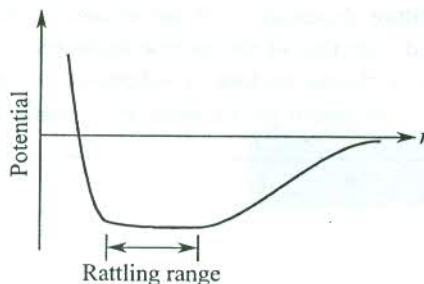


FIG. 11.7 Rattling of titanium ion in a potential well over a large volume, giving rise to a poorly defined equilibrium position of the titanium ion.

2. **The non-cubic symmetry around oxygen ions.** Unlike the barium and titanium ions, the oxygen ions are in the non-cubic environment. An oxygen ion has only two nearest neighbours in the form of titanium ions. Because of this reason, E_{loc} is not given by the Lorentz expression ($E + P/3\epsilon_0$) and instead found to be greater than this value.

A larger value of α envisaged under point 1 leads to a smaller value of the deformation energy ϵ_1 or the work required to create induced dipoles. Similarly, a larger value of E_{loc} as expected under point 2 implies that the dipolar attraction energy will be larger. Thus both the directions of change in α and E_{loc} are favourable to the onset of ferroelectricity.

11.2.2 ‘Frozen in’ Transverse Optical Phonons

As stated earlier, a ferroelectric state can be regarded as a ‘frozen in’ TO phonon. According to the LST relation (10.123)

$$\frac{\omega_{TO}^2}{\omega_{LO}^2} = \frac{\epsilon_\infty}{\epsilon_s}$$

showing that when the static dielectric constant ϵ_s increases, ω_{TO} decreases. Thus in the case of an infinitely large ϵ_s , which happens at the Curie point (T_c), ω_{TO} may even be zero. In practice, however, ϵ_s remains finite on approaching T_c . The TO modes in question are called *soft modes*. Such TO modes have surprisingly low frequencies. For example, BaTiO₃ has a soft mode of frequency 12 cm⁻¹ at 297 K which is low for a TO mode. We are not concerned here with LO phonons whose frequency is higher for the same value of the wavevector. At the transition point T_c when ω_{TO} approaches the zero value, the crystal becomes unstable and anharmonic elastic forces come into play. In the presence of anharmonic forces, ω_{TO} may show a temperature dependence of the form

$$\omega_{TO}^2 \propto (T - T_c) \quad (11.18)$$

On assuming that ω_{LO} are temperature independent, the LST relation in view of (11.18) gives

$$\frac{1}{\epsilon_s} \propto (T - T_c) \quad (11.19)$$

Experiments on several perovskite ferroelectrics strongly support the view that a large static dielectric constant (ϵ_s) is associated with a low frequency TO phonon (the soft mode). In view of

(11.18) and (11.19) the temperature dependence of the square of energy of a low frequency TO phonon can be directly compared with that of the inverse dielectric constant, as shown in Fig. 11.8 for a KTaO_3 crystal.* To have a clearer picture, a schematic representation of the temperature dependence of ϵ_s^{-1} , ω_{TO}^2 and the saturation polarization P_s is made in Fig. 11.9.

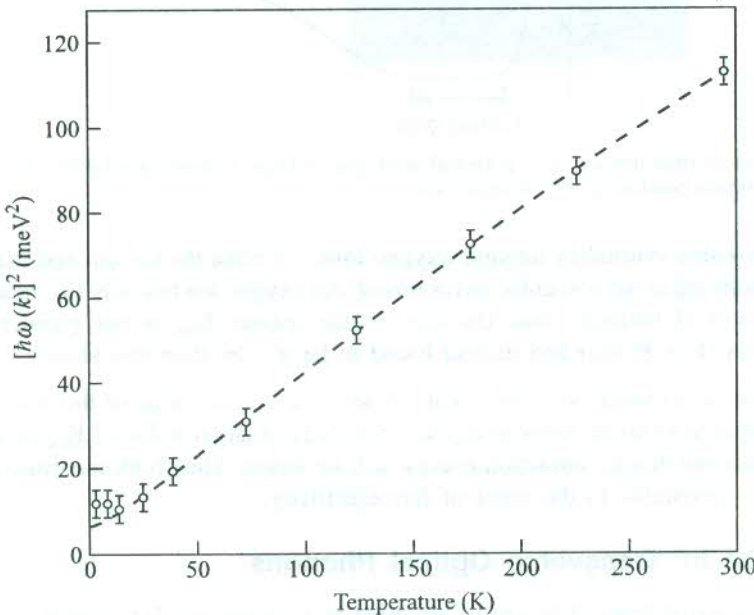


FIG. 11.8 Temperature dependence of a low frequency TO mode in KTaO_3 . The square of the phonon energy (points) is compared with the reciprocal of the dielectric constant (dashed line).

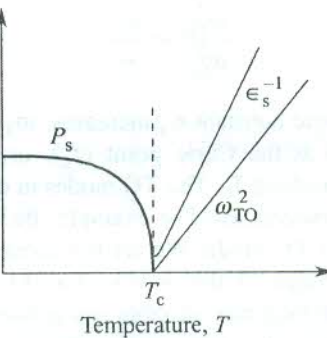


FIG. 11.9 Schematic view of the temperature dependence of the spontaneous polarization P_s , the reciprocal dielectric constant ϵ_s^{-1} and the square of the TO mode frequency ω_{TO}^2 for a ferroelectric crystal.

11.3 THERMODYNAMIC THEORY OF THE FERROELECTRIC TRANSITION

The features of a general thermodynamic theory as developed by Devonshire[†] are described in this

* G. Shirane et al., *Phys. Rev.*, **157**, 393 (1967).

† A.F. Devonshire, 'Theory of Ferroelectrics' in *Adv. Phys.*, **3**, 85 (1954).

section. Let x denote the relative displacement of the centres of the positive and negative charges in the crystal during a particular mode of vibration. If F_0 be the free energy of the unpolarized crystal, the free energy of the polarized crystal F is a function of the even powers of x . That is,

$$F - F_0 = \phi_2 x^2 + \phi_4 x^4 + \phi_6 x^6 + \dots \quad (11.20)$$

The constants ϕ are functions of all other displacements and given by their thermal average values. They are thus functions of temperature. Since the electric polarization P is proportional to the displacement x , we have

$$F - F_0 = \frac{1}{2} \lambda_2 P^2 + \frac{1}{4} \lambda_4 P^4 + \frac{1}{6} \lambda_6 P^6 + \dots \quad (11.21)$$

The constants λ are automatically the functions of temperature. The numerical factors are introduced to facilitate calculations.

Consider first the paraelectric phase of the crystal, i.e. for $T > T_c$. If a small electric field E is applied in the absence of any external pressure, the following thermodynamic relation holds good:

$$dF = -S dT + E dP \quad (11.22)$$

where S represents the entropy of the crystal.

Since for small E , P will also be small, and hence we retain only the first term in (11.21) neglecting all other terms in the first approximation. Then, using (11.22) we have

$$E = \left(\frac{\partial F}{\partial P} \right)_T = \lambda_2 P \quad (11.23)$$

We may define the electric susceptibility χ_P in the paraelectric phase by

$$\frac{1}{\chi_P} = \epsilon_0 \left(\frac{dE}{dP} \right) = \epsilon_0 \lambda_2 \quad [\text{from (11.23)}] \quad (11.24)$$

(see 10.12)

Using the Curie-Weiss law (11.1), we have

$$\epsilon_0 \lambda_2 = \frac{T - T_c}{C}$$

or

$$\lambda_2 = C_1(T - T_c) \quad (11.25)$$

where C_1 is another constant.

Relation (11.25) shows that λ_2 increases linearly with the rise in temperature. As a result of this temperature dependence, λ_2 varies from positive values to negative values as the temperature is lowered from above T_c to below T_c .

In the state of thermal equilibrium, the free energy is minimum which requires that

$$\left(\frac{\partial F}{\partial P} \right)_T = 0$$

Applying this condition to (11.21) in the absence of the applied electric fields, we have

$$\lambda_2 P + \lambda_4 P^3 + \lambda_6 P^5 + \dots = 0 \quad (11.26)$$

The spontaneous polarization is bound to satisfy (11.26) and

$$P_s(\lambda_2 + \lambda_4 P_s^2 + \lambda_6 P_s^4 + \dots) = 0 \quad (11.27)$$

We find that $P_s = 0$ is always a root of (11.27). For this solution the free energy has a minimum provided λ_2 is positive ($\frac{\partial^2 F}{\partial P^2} = \lambda_2$). However, if λ_2 , λ_4 and λ_6 are all positive and higher order terms are neglected, the condition (11.27) is satisfied only for $P_s = 0$. Thus $P_s = 0$ corresponds to the only minimum of the free energy and the paraelectric phase exists for the positive sign of λ_2 , λ_4 and λ_6 .

When the temperature is lowered through the transition point, λ_2 goes from positive to negative values while passing through $\lambda_2 = 0$ at the transition point. There are two interesting situations that are identified in terms of the signs of λ_2 , λ_4 and λ_6 . These characterize the two different types of transitions, namely the second-order and first-order types.

11.3.1 Second-order Transitions

When λ_2 varies from positive to negative as the temperature is lowered and λ_4 , λ_6 , \dots are all positive, the free energy changes as shown in Fig. 11.10(a). Assuming that the terms beyond the second term in (11.27) are negligible, we get

$$P_s^2 = -\frac{\lambda_2}{\lambda_4} = \frac{C_1(T_c - T)}{\lambda_4} \quad (11.28)$$

Hence P_s is a continuous function of temperature and falls continuously to zero at $T = T_c$ as shown in Fig. 11.10(b).

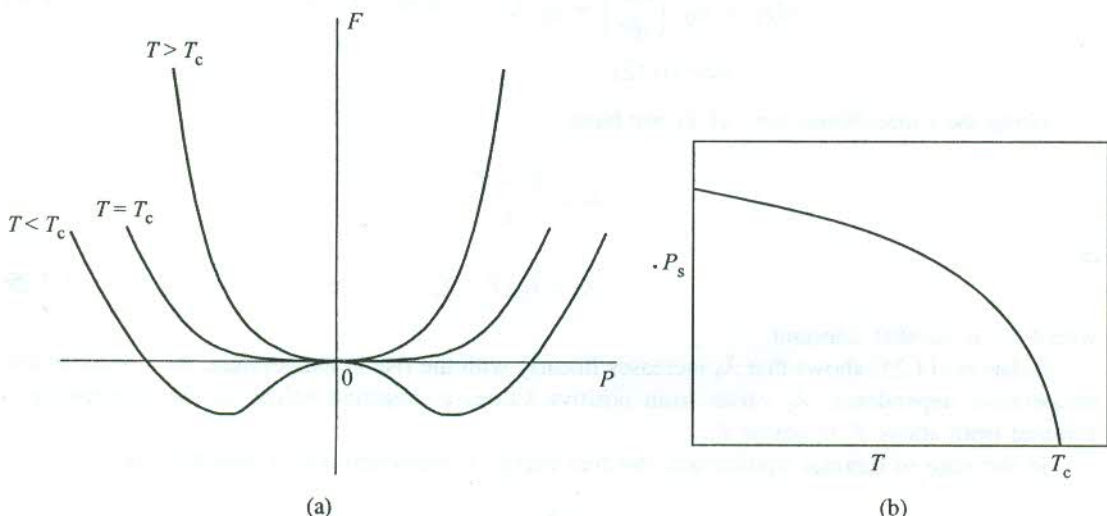


FIG. 11.10 (a) Free energy as a function of polarization as the temperature is varied near a second-order phase transition. (b) Temperature dependence of the spontaneous polarization (the order parameter) below the transition temperature T_c in a second-order phase transition.

It is useful to examine the spontaneously polarized state in terms of the frequency of normal modes. From the forms of the free energy (11.20) and (11.21), it follows that

$$\phi_2 \text{ or } \lambda_2 \propto \omega_i^2(k)$$

and hence in view of (11.25),

$$\omega_i^2(k) \propto (T - T_c) \quad (11.29)$$

where $\omega_i(k)$ is the frequency of the normal mode i (actually a TO mode). The transition takes place when $\omega_i(k) \rightarrow 0$. This decrease in the mode frequency is called *softening*. It means that the harmonic restoring forces are becoming very weak, permitting a large displacement which is limited solely by the anharmonic forces. A small positive value of $\omega_i^2(k)$ or λ_2 means that the crystal lattice is soft and close to instability. Below T_c , λ_2 is negative and so is $\omega_i^2(k)$ which implies that the unpolarized lattice is unstable and the crystal is in the spontaneously polarized ferroelectric state.

The understanding of the above type of transition remains incomplete without a discussion on the free energy in the state of thermal equilibrium. We saw a little earlier that the free energy minimum in the ferroelectric phase occurs for a non-zero value of P_s , given by (11.28) and not by $P_s = 0$. At $P_s = 0$, there is a local maximum (since $\lambda_2 < 0$) and not the minimum as in the paraelectric phase. This means that the minimum of the free energy in the ferroelectric state is shifted to a point where $P_s \neq 0$. In other words, the minimum occurs for a non-zero value of the relative displacement (say \bar{x}). This implies that the distortion sets in below the Curie temperature and increases proportionally to $(T_c - T)^{1/2}$. Note that both F and P_s are continuous at $T = T_c$, but the slope $\frac{\partial P_s}{\partial T}$ is discontinuous.

The free energy minimum refers to the value at the thermal equilibrium F_e which we obtain by putting the value of P_s^2 from (11.28) in (11.21). This gives

$$F_e = F_0 - \frac{C_1^2 (T_c - T)^2}{2 \lambda_4} \quad (11.30)$$

The heat capacity is given by

$$\begin{aligned} C_V &= \frac{\partial}{\partial T} T^2 \frac{\partial}{\partial T} \left(\frac{F_e}{T} \right) \\ &= \frac{C_1^2 T}{\lambda_4} \end{aligned} \quad (11.31)$$

It falls discontinuously to zero at $T = T_c$ (see Fig. 11.11). But there is no latent heat at the transition. Since the discontinuities are in the second derivatives of the free energy, such a transition is called a *second-order transition*. In the terminology of the Landau theory of phase transitions the spontaneous polarization P_s serves here as an order parameter. The continuous fall of the order parameter to zero at the transition point [Fig. 11.10(b)] is another significant feature of the second-order transitions.

The transitions in Rochelle salt, KH_3PO_4 and LiTaO_3 are some examples of the second-order transition. The transition to the superconducting state is the most popular example of this type of transition.

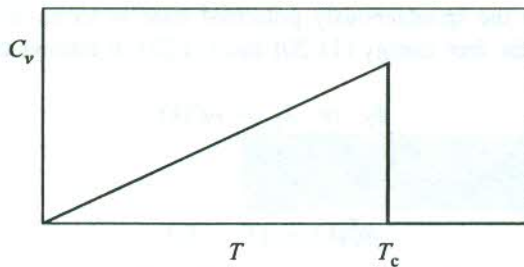


FIG. 11.11 Temperature dependence of specific heat showing anomaly at a second-order phase transition.

11.3.2 First-order Transitions

We saw above that when λ_2 is negative and λ_4 positive, the transition is of the second-order type. We now examine a situation where λ_4 is negative. Positive values of λ_6 are considered to restrain the free energy from going to minus infinity. In accordance with (11.25), λ_2 varies from positive to negative as the crystal is cooled through the Curie point. The corresponding free energy curves are depicted in Fig. 11.12(a). The thermal equilibrium condition, $\partial F/\partial P = 0$, in the absence of the applied electric field gives

$$\lambda_2 P_s + \lambda_4 P_s^3 + \lambda_6 P_s^5 = 0 \quad (11.32)$$

which implies that either $P_s = 0$, or

$$\lambda_2 + \lambda_4 P_s^2 + \lambda_6 P_s^4 = 0 \quad (11.33)$$

At $T = T_c$, the free energy in the paraelectric state is equal to that in the ferroelectric state, i.e.

$$F_0(T_c) = F(T_c) \quad (11.34)$$

Using (11.34) in (11.21), we have

$$0 = \frac{1}{2} \lambda_2 P_s^2(T_c) + \frac{1}{4} \lambda_4 P_s^4(T_c) + \frac{1}{6} \lambda_6 P_s^6(T_c) + \dots \quad (11.35)$$

Then, using (11.33), we get

$$\lambda_2 + \lambda_4 P_s^2(T_c) + \lambda_6 P_s^4(T_c) = 0 \quad (11.36)$$

Substituting the value of λ_2 from (11.36) in (11.35) and solving for $P_s^2(T_c)$, we get

$$P_s^2(T_c) = - \frac{3}{4} \left(\frac{\lambda_4}{\lambda_6} \right) = \frac{3}{4} \frac{|\lambda_4|}{\lambda_6} \quad (11.37)$$

and with

$$\lambda_2 = \frac{3}{16} \left(\frac{\lambda_4^2}{\lambda_6} \right) \quad (11.38)$$

$$P_s^4(T_c) = \frac{3\lambda_2}{\lambda_6} \quad (11.39)$$

Note that in Fig. 11.12(a) at the transition point there are two minima of free energy with equal value; one at $P_s(T_c) = 0$ in the paraelectric phase and the other for the value of $P_s(T_c)$ given by (11.37) in the ferroelectric phase. Thus there is a jump [see Fig. 11.12(b)] in the value of P_s at T_c , meaning thereby that the spontaneous polarization (the order parameter) drops discontinuously to zero at $T = T_c$ when a ferroelectric crystal is heated slowly. Such transitions are called the *first-order transitions*. The other important property of these transitions is that there is a latent heat at the transition. A well-known example of this type of transition is the upper transition in a BaTiO_3 crystal.

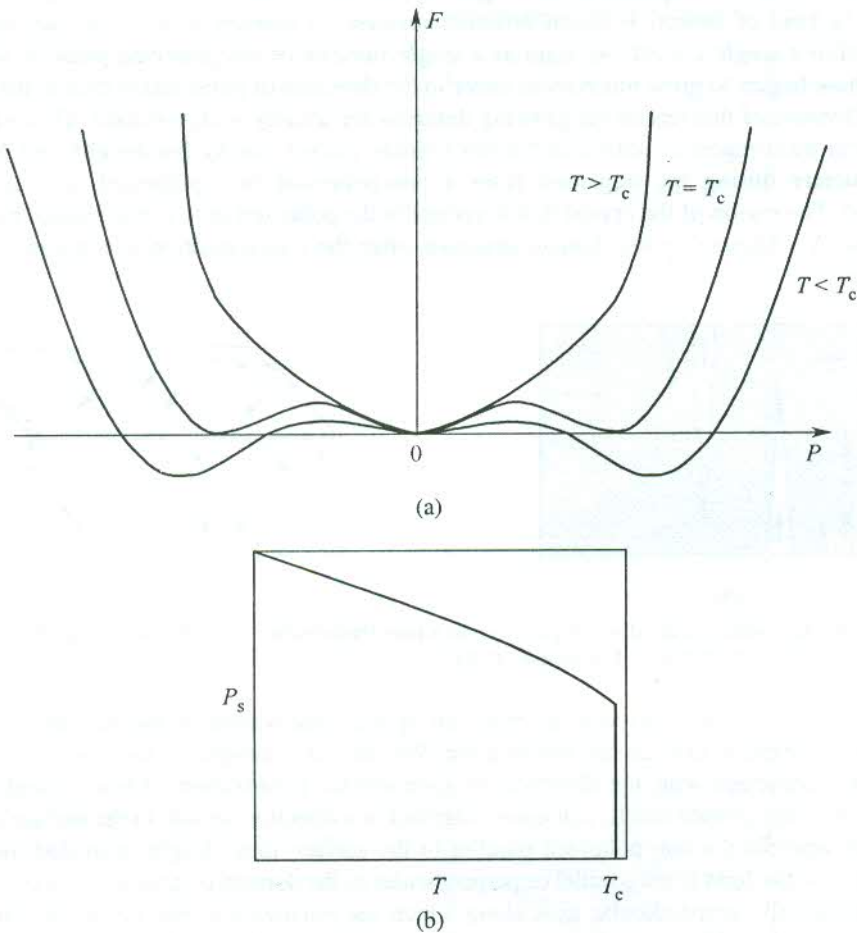


FIG. 11.12 (a) Free energy as a function of polarization as the temperature is varied near a first-order phase transition. (b) Fall of the spontaneous polarization (the order parameter) below the transition point T_c in a first-order phase transition.

11.4 FERROELECTRIC DOMAINS

A ferroelectric crystal need not necessarily show an observable evidence of spontaneous polarization. When the crystal is cooled from the paraelectric phase through the Curie temperature, the polarized phase may be nucleated at several points in the crystal. These nuclei normally differ in the direction of polarization since there may be several equivalent crystallographic directions in which the

spontaneous polarization can occur. For example, in BaTiO_3 the spontaneous polarization may occur along one of the three edges, giving six possible directions for the spontaneous polarization. Thus, as the nuclei grow through the crystal in the ferroelectric phase, they form several regions or domains differing in their direction of polarization. The vector sum of these polarizations may not be always big enough to show up macroscopically.

Polarization is accompanied by some distortion of the unit cell and the domain walls are consequently in a state of strain. The dimensional changes, however, are relatively small. Though the domain walls act as interruptions in the regularity of the crystal, they are not regarded as grain boundaries (a kind of defect) between different crystals. A domain wall is, instead, treated as a subgrain within a single crystal. As soon as a single nucleus of the polarized phase is formed, the polarized phase begins to grow much more faster in the direction of polarization than in the transverse directions. Because of this reason the growing domains are usually wedge-shaped. This was revealed by the optical birefringence studies on barium titanate carried out by Forsbergh* and Merz.[†] The domain structure during the transition from a non-polarized to a polarized state is shown in Fig. 11.13(a). The region of the crystal that is yet not in the polarized state is represented by the cross-hatched area. A schematic of the domain structure, after the transformation is complete, is given in Fig. 11.13(b).

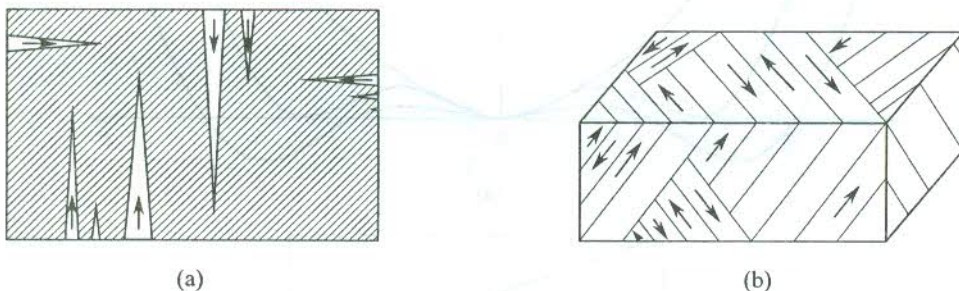


FIG. 11.13 (a) Schematic of the domain growth into a non-ferroelectric (paraelectric) phase. (b) Schematic of the domain structure in a single crystal.

As referred above, it is possible to make an optical observation of the ferroelectric domains because the ferroelectric crystals are birefringent. We take the example of barium titanate in which the optic axis coincides with the direction of spontaneous polarization. When viewed through a microscope between crossed nicols, a domain polarized in a direction normal to the surface of a crystal appears dark whereas the one polarized parallel to the surface looks bright, provided the direction of polarization of the light is not parallel or perpendicular to the domain polarization. As a consequence of the three mutually perpendicular axes along which the polarization may occur, the directions of polarization in the neighbouring domains are either at 90° or at 180° . These directions have given origin to the concept of 90° and 180° walls. A wall separating regions of antiparallel polarization is called a 180° wall. A 90° wall may be defined similarly.

The ferroelectric domains are regarded as the electrical analogues of the ferromagnetic domains despite the fact that there are some interesting differences in their origin and growth. On application of an electric field to a ferroelectric crystal, the number and size of domains that are polarized in the

* P.W. Forsbergh, Jr., *Phys. Rev.*, **76**, 1187 (1949).

† W.J. Merz, *Phys. Rev.*, **88**, 421 (1952).

field direction increase. As a result of this effect, upon the reversal of the field direction a hysteresis in the P versus E curve is observed. The size of ferroelectric domains increases because of the growth in the forward direction (the direction of polarization) and not sideways. Practically, there is little sideways motion of the domain walls. But in ferromagnetic domains it is just the reverse. A change in the direction of magnetization is achieved because of the growth of favourably-oriented domains such that the growth is facilitated mainly by a sideways motion of the domain walls. Another significant difference between the two sets of domains, lies in the thickness of a domain wall. It is estimated by calculating the energy per unit area of the wall and then minimizing it with respect to the thickness of the wall. The thickness of a ferromagnetic domain wall is found to be about 300 lattice constants in contrast to a considerably small value of the order of a few lattice spacings for a ferroelectric domain wall. Accordingly, the energy associated with a wall in the former case is relatively much small.

11.5 ANTIFERROELECTRICITY

Like ferroelectrics there is another group of solids which has induced, ordered electric dipoles below a characteristic temperature but shows no spontaneous bulk polarization. In these crystals the neighbouring lines of atoms are associated with antiparallel polarizations because of which the bulk polarization of the crystal vanishes. Crystals exhibiting this property are called *antiferroelectric* crystals and the property is known as *antiferroelectricity*. The structural requirements for the ferroelectric and antiferroelectric phases being common, a number of well-known antiferroelectric crystals are found to be isomorphous with some ferroelectrics. For example, ammonium dihydrogen phosphate (ADP) which is antiferroelectric is isomorphous with potassium dihydrogen phosphate (KDP).

Perovskite type crystals are known to be susceptible to several types of deformation with almost equal energy difference between them. In many of them the coupling through the oxygen octahedra causes adjacent lines of basic cells to be polarized in opposite directions. Below a certain temperature the resultant deformation is such that the total energy in the antiparallel arrangement of adjacent lines of dipoles is lower, when compared separately to that in the state of fully parallel arrangement of dipoles and to that in the state with no induced dipoles. Lead zirconate (PbZrO_3) is a notable example of these perovskites. It shows two antiferroelectric phases, one each ferroelectric and paraelectric phase over different ranges of temperature.

11.6 PIEZOELECTRICITY

Requirements for a crystal to show piezoelectric behaviour were discussed in the beginning of the chapter. The piezoelectric crystals get electrically polarized when stressed and conversely get strained when polarized (placed in the electric field). This phenomenon is called *piezoelectricity* and it is of great technological importance. We showed earlier that all ferroelectrics are piezoelectrics and that its converse is not true. For example, quartz is piezoelectric but it does not possess the ferroelectric property.

The foremost condition for a crystal to be piezoelectric is the absence of the centre of symmetry. Figure 11.14(a) shows the array of a simple two-dimensional ionic crystal with no centre of symmetry. It is evident that a compressive force F [Fig. 11.14(b)] decreases the electric dipole moment (hence the polarization) and a tensile force F [Fig. 11.14(c)] increases the same. This is essentially the piezoelectric effect. We must appreciate that the displayed crystal [Fig. 11.14(a)] could well be a ferroelectric crystal.

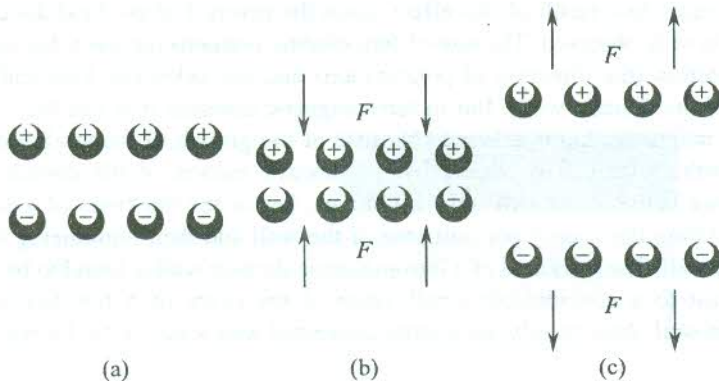


FIG. 11.14 (a) A two-dimensional ionic crystal with no centre of symmetry. (b) Compression under the action of force F decreases the polarization. (c) Extension of structure under the action of force F increases the polarization.

Next we take up another example to show how the symmetry of a non-centrosymmetric crystal controls firstly the magnitude and direction of polarization when the crystal is stressed and secondly the crystal dimensions when the crystal is polarized. Consider a molecule of a hypothetical ionic solid which at equilibrium has three electric dipoles of equal magnitude distributed over 360° at an interval of 120° as shown in Fig. 11.15(a). The molecule belongs to the point group 3 m and its net dipole moment is zero. But if the molecule together with the crystal is stressed or compressed along a direction parallel or antiparallel to one of the three directions of the dipole moment, a net dipole moment would appear [see Fig. 11.15(b) and (c)]. Similarly, a molecule may be distorted by an electric field applied along one of the three arrows shown in the Fig. 11.15(a). The electric field produces an elongation or contraction of the crystal along the field direction and a length change of opposite sign in the lateral direction. An applied field that is perpendicular to one of the three dipole directions in Fig. 11.15(a) finds itself perpendicular to a mirror plane of symmetry and, therefore, is rendered ineffective in changing the crystal dimensions.

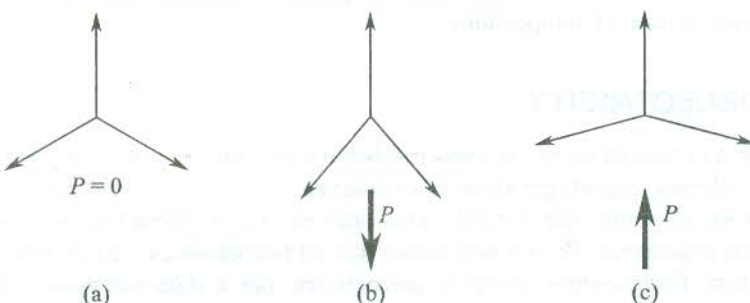


FIG. 11.15 Response of a piezoelectric molecule to strain: (a) Directions of polarization (in accordance with symmetry) in a molecule within an undistorted crystal in the state of equilibrium. The net polarization of the molecules is zero. (b) A vertical tension or a horizontal compression causing a net polarization. (c) A vertical compression or a horizontal tension causing a net polarization.

Because of lack of centre of inversion and complex structure of piezoelectrics, their electrical behaviour under strain or strain behaviour under an electric field is not isotropic in nature. Nevertheless,

a simple picture of the phenomena can be presented in a schematic one-dimensional notation by the following equations:

$$P = \sigma d + \epsilon_0 E \chi; \quad e = \sigma s + E d \quad (11.40)$$

where P is the polarization, σ the stress, d the piezoelectric strain constant, ϵ_0 the permittivity of free space, E the electric field, χ the dielectric susceptibility, e the strain and s the elastic compliance constant.

In real crystals, however, the tensile, compressional or shear strains produced by an electric field may develop in different directions and depend on the crystal orientation and the field direction. In view of this fact the piezoelectric strain constants, that form a third rank tensor, are defined as

$$d_{ik} = \left(\frac{\partial e_k}{\partial E_i} \right)_{\sigma}$$

where $i \equiv x, y, z$ and $k \equiv xx, yy, zz, xy, yz, zx$.

Depending on the application and the desired behaviour, a crystal is cut so as to have the parallel faces of the crystal in a specific orientation. An X -cut is defined as a section cut from the crystal such that the x -axis of the crystal is perpendicular to the parallel crystal faces. The axes in some common piezoelectric crystals are shown in Fig. 11.16. In order to obtain certain desirable properties the crystals are sometimes given oblique cut, i.e. cut at angles different from 90° with the principal axes.

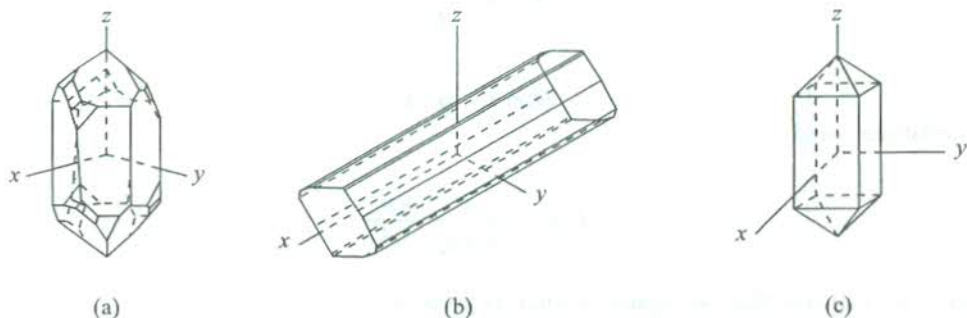


FIG. 11.16 Orientations of axes that are used to describe some common piezoelectric crystals: (a) Quartz, (b) Rochelle salt, and (c) ADP.

11.7 ELECTROSTRICTION

It may not be out of place to discuss a more universal phenomenon of deformation in crystals that is caused by an applied electric field. It refers to the deformations in ionic crystals and the effect is commonly known as *electrostriction*. In the first approximation, the deformation of a piezoelectric crystal is proportional to the applied electric field and the stress induced polarization varies linearly with the strain produced (11.40). But in ionic crystals, which do not have to be necessarily piezoelectric, the strain is much smaller and proportional to the square of the electric field. We can understand the origin of electrostriction by appreciating that the dipoles created by the applied electric field would interact with each other (Fig. 11.17). The in-line dipoles attract each other with a repulsive force acting perpendicular to the direction of polarization.

Let p denote the moment of a dipole, and r the separation between two neighbouring in-line dipoles. The value of the electric field caused by a dipole at its in-line neighbour may be written as



FIG. 11.17 Production of electrostriction by attraction among the in-line dipoles. This attraction exceeds the repulsion from the side-by-side dipoles.

$$E = \frac{1}{4\pi \epsilon_0} \frac{2p}{r^3} \quad (11.41)$$

The energy of a dipole in this field $U(r)$ and the corresponding attractive force F are related as

$$F = - \frac{dU(r)}{dr}$$

and

$$U(r) = -\mathbf{p} \cdot \mathbf{E}$$

These relations yield

$$F = - \frac{1}{4\pi \epsilon_0} \frac{6p^2}{r^4} \quad (11.42)$$

Similarly, we can find that the repulsive force is given by

$$F = \frac{1}{4\pi \epsilon_0} \frac{3p^2}{r^4} \quad (11.43)$$

Since $p = \alpha E$, the attractive force can be expressed as

$$F = - \frac{1}{4\pi \epsilon_0} \left(\frac{6\alpha^2}{r^4} \right) E^2 \quad (11.44)$$

To a first approximation the strain or deformation u may be assumed to follow the Hooke's law and then

$$u = - \frac{F}{f}$$

where f is the usual force constant in the direction of the in-line dipoles.

With the use of (11.44) in the above relation, we get

$$u = \frac{1}{4\pi\epsilon_0} \left(\frac{6\alpha^2}{fr^4} \right) E^2 \quad (11.45)$$

Thus there will occur a compression in the field direction and an extension perpendicular to the field direction. The above treatment holds good for permanent dipoles as well on account of the effective dipole moment being proportional to the electric field.

11.8 APPLICATIONS OF PIEZOELECTRIC CRYSTALS

It may be recalled that all ferroelectrics are piezoelectrics, though the converse is not true. As a result, ferroelectric materials have been frequently used in many applications that are based on the principle of piezoelectricity. But, because of the importance of properties such as mechanical and thermal strength the use of certain piezoelectric crystals (e.g. quartz which is non-ferroelectric) becomes inevitable. There are a very large number of piezoelectric applications whose complete listing at this place is a formidable task. We describe below only a few of them which span all the significant areas of applications:

1. Crystals shaped to have a prescribed mechanical resonance frequency are used as narrow band electrical filters. Only those electrical signals whose frequency coincides with the mechanical vibrational frequency pass through the crystal and all others are rejected.
2. When an a.c. voltage at one of the resonant frequencies of the crystal is impressed perpendicular to a certain pair of parallel faces, the amplitude of oscillation at this frequency grows. The constancy of the elastic constants of the crystal controls the stability of the oscillator. Specially-cut quartz discs are used for this purpose. Due to a very low value of the coefficient of thermal expansion for quartz, a fairly high level of stability is achieved.
3. Piezoelectric oscillators are used to convert mechanical pulses into electrical ones and vice versa. The crystal in these devices works as a transducer. The acoustic pulses are used in underwater search (sonars) and other applications. The acoustic pulses are generated by the piezoelectric transducers, excited by electric fields in almost all such cases. The generation of ultrasonic waves is invariably accomplished by exploiting the above principle.
4. The highest possible efficiency is a desirable attribute of every device. Rochelle salt, being a sensitive and inexpensive transducer, has been used in phonographs. A shaped ceramic block of barium strontium titanate or lead zirconium titanate (PZT) should, however, be preferred since these materials are very sensitive and resistive to heat and moisture.
5. The piezoelectric effect in synthetic polyvinylidenefluoride (PVF_2) is about five times stronger than that in quartz. Being flexible and easy to handle like ultrasonic transducers, the PVF_2 films are frequently used in applications such as monitoring blood pressure and respiration.
6. The piezoelectric materials are used as delay lines. When an electrical signal is converted into an acoustic one at one end of a quartz rod, the signal passes along the rod as an acoustic wave, travelling at the velocity of sound. At the other end, the acoustic wave may be converted into an electrical signal. The initial signal is thus delayed. Such an arrangement is often used in communication devices.

SUMMARY

1. Pyroelectric, ferroelectric and piezoelectric crystals lack centre of inversion symmetry.
2. A pyroelectric crystal belongs to one of the following point groups:
 C_n, C_{nv} ($n = 2, 3, 4, 6$), C_1 and C_{1h}
3. All ferroelectric crystals are piezoelectric, but the converse is not true.
4. Polarization catastrophe occurs when

$$\sum_j N_j \alpha_j = 3\epsilon_0$$

5. The soft modes are low frequency TO modes (e.g. 12 cm^{-1} in BaTiO_3 at 293 K). The soft mode frequency tends to zero as the transition temperature is approached.
6. The free energy of a ferroelectric crystal is given by

$$F - F_0 = \frac{1}{2} \lambda_2 P^2 + \frac{1}{4} \lambda_4 P^4 + \frac{1}{6} \lambda_6 P^6 + \dots$$

where

F_0 is the free energy of the unpolarized crystal

F is the free energy of the polarized crystal

P is the electric polarization

$\lambda_2, \lambda_4, \lambda_6, \dots$ are constants that depend on temperature.

7. A transition is of the second-order type if λ_2 is negative and $\lambda_4, \lambda_6, \dots$ are positive. The order parameter (P_s , in ferroelectrics) falls continuously to zero at the transition point. The specific heat drops discontinuously to zero at the transition point.
8. A transition is of the first-order type if λ_4 is negative and λ_2, λ_6 are positive. The order parameter falls discontinuously to zero at the transition point. There is a latent heat at the transition.

PROBLEMS

- 11.1 Explain why ZnS could be piezoelectric but not diamond, although the atomic arrangement is the same in both the crystals.
- 11.2 Two dipoles, each having a polarizability α , are at a fixed distance a . If they form a ferroelectric state, set up the relationship between a and α .
- 11.3 Consider an ionic crystal with cubic symmetry at every lattice point. Calculate its ferroelectric Curie point taking the total polarizability of the crystal as given by

$$\alpha = \left(0.5 + \frac{100}{T} \right) \times 10^{-30} \text{ m}^3$$

- 11.4** Atoms of polarizability α are arranged in a line with a as the interatomic separation. Prove that the array can polarize spontaneously if

$$\alpha \geq \frac{a^3}{4 \sum n^{-3}}$$

where the sum is carried out over all positive integers.

- 11.5** The SrTiO_3 crystal has the perovskite structure, but is not ferroelectric. Determine a likely reason on the basis of a comparison between the barium and strontium ions.

- 11.6** The resonant frequency of a quartz crystal is given by

$$v_0 = \frac{1}{2l} \sqrt{\frac{Y}{\rho}}$$

where l is the dimension that determines the mode of oscillation of the crystal, Y is the Young's modulus and ρ is the density of quartz. Determine the useful sizes of the crystal for oscillators in kHz and MHz ranges (for quartz, $Y = 10^{10} \text{ N m}^{-2}$, $\rho = 2500 \text{ kg m}^{-3}$).

SUGGESTED FURTHER READING

- Bruce, A.D. and R.A. Cowley, *Structural Phase Transitions* (Taylor and Francis, 1981).
 Fröhlich, H., *Theory of Dielectrics* (Oxford, 1986).
 Lines, M.E. and A.M. Glass, *Ferroelectrics and Related Materials* (Oxford, 1977).
 Toledano, J.-C. and P. Toledano, "Landau Theory of Phase Transitions: Application to structural, incommensurate, magnetic and liquid crystal systems" (*World Scientific*), 1987.
 Zheludev, I.S., *Physics of Crystalline Dielectrics* (Plenum, 1971).

Imperfections in Crystals

It is a well-established fact that there exist no perfect crystals. Every crystalline structure shows some deviation or the other from the regular atomic arrangement, as prescribed by the symmetry and structure of the respective unit cell. These deviations from the ideal crystal structure are called *imperfections*. Imperfections could be of several types, as we will see below. The presence of imperfections or defects is not accounted by the translational symmetry of the perfect crystal though it forms the basis of most of the interpretations in perfect crystals. We may obviously be curious to know how the translational symmetry in a crystal is consistent with laws of thermodynamics since these laws are applied to describe the growth of crystals all of which have some imperfections. We know that the Helmholtz free energy

$$F = U - TS \quad (12.1)$$

must be minimum in the state of equilibrium at a certain temperature. In (12.1) U stands for the internal energy and S for the entropy. We take the advantage of the following statistical statement of entropy,

$$S = k_B \ln W \quad (12.2)$$

where W is the number of possible ways in which the elements of a system may be distributed.

Now, we take the case of a defect that can be localized at a lattice point. In a perfect crystal there can be only one way (i.e. $W = 1$) to arrange atoms at different sites and, therefore, the entropy in this case would be zero [see (12.2)]. On the other hand, a defect at a site within a unit cell makes the unit cell look different from others. In this case there can be as many ways of arranging the defect as the number of sites within the unit cell. The entropy is given by

$$S = k_B \ln N \quad (12.3)$$

where N is the number of sites in the unit cell.

Relation (12.3) expresses the contribution of the defect to the entropy of the crystal. Thus any increase in the defect concentration raises the entropy which in turn lowers the free energy at a finite temperature. In the equilibrium state there is a finite concentration of imperfections in the crystal. In the above example we considered only one type of defect. But, as a necessary consequence of the inherent disorder associated with finite temperature, all kinds of imperfections (one can imagine) could be present, though some of them might be very small in number. The concentration of a particular type of imperfection depends on the type of the crystal lattice, the binding energy of the lattice and the structure of the imperfection itself. The imperfections are crucial to the interpretation of several properties of crystals that are not accounted by the translational symmetry. To name a few: colour of crystals, enhancement of conductivity of pure semiconductors, plasticity, strength of crystals, luminescence and diffusion of atoms in solids are some such significant examples.

Imperfections play a pivotal role even in the very existence of the solid state. It will be clear through discussions on the strength of crystals and the process of crystal growth, taken up towards the end of the chapter.

For a systematic description of imperfections, we classify them broadly as follows:

1. Point imperfections
2. Line imperfections
3. Planar imperfections

12.1 POINT IMPERFECTIONS OR POINT DEFECTS

The well-established forms in which point defects are found in crystals are the following:

(a) **Vacancy.** A normal lattice site from where the atom or ion is missing, is known as *Schottky defect* (Fig. 12.1).

(b) **Interstitial atom.** An atom located at a position that is not a normal lattice site (Fig. 12.1), known as *Frenkel defect*.

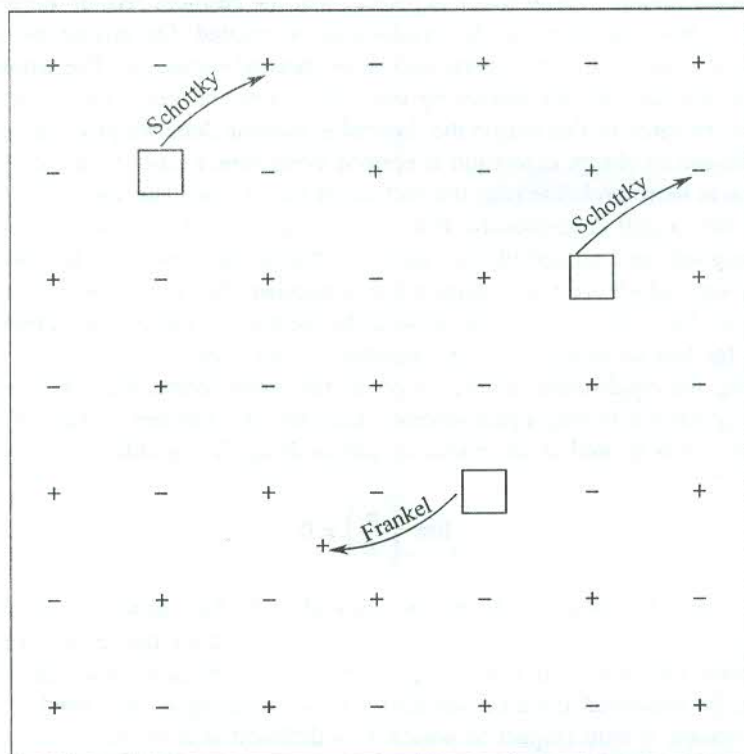


FIG. 12.1 Formation of Schottky and Frenkel defects in a diatomic ionic crystal—arrows indicate the direction of displacement of ions. The creation of a Schottky defect results in the production of a pair of positive ion and negative ion vacancies to meet the charge neutrality requirement. The formation of a Frenkel defect implies the creation of a pair of a lattice vacancy and an interstitial position. The symbol \square denotes a vacancy.

(c) **Colour centre.** A bound system results from a charge compensation mechanism. This bound system, known as *colour centre*, has a quantized scheme of energy levels and absorbs visible light in some crystals. These crystals thus show colour which are otherwise colourless.

(d) **Excitons.** Quantized electron–hole pair excitations.

(e) **Polarons.** Quantized polarization waves (introduced in Section 10.10)

A detailed account of these point defects is given below.

Schottky defects

A Schottky defect as described above is a vacancy at a normal lattice site which is otherwise occupied by an atom or ion in a perfect crystal. We base our discussion in this subsection on ionic crystals with NaCl structure which are easy to handle theoretically on account of their simple structure. In this case there can be two kinds of Schottky defects—one type representing the cation vacancies and the other corresponding to the anion vacancies. The two types of vacancies must be equal in number to maintain the charge neutrality of the crystals. Therefore, if a Schottky defect in a unit cell is a cation vacancy, there must be another unit cell within the crystal which has an anion vacancy representing the Schottky defect of the other type.

Suppose we have found a crystal which is perfect near the absolute zero of temperature. We may be curious to know how vacancies in this crystal can be created. On raising the temperature the thermal agitations are excited and the crystal undergoes thermal expansion. The whole of the thermal energy supplied is not used up for increasing the lattice constant, but a part of it is consumed in vacancy formation. Because of this reason the thermal expansion does not proceed continuously with rise in temperature and an abrupt expansion is noticed every time a pair of vacancies is formed. The vacancy formation is more probable near the surface of the crystal. The vacancies from the surface flit in and out of the crystal continuously. But as the temperature rises, more vacancies diffuse in, than those diffusing out until an equilibrium state is achieved. It is easier to follow the diffusion of vacancies than of ions which are many times more in number. The present situation is analogous to that of a nearly filled band where it is easier to describe the transport of charge in terms of the motion of holes that are far less in number than the number of electrons.

For calculating the equilibrium concentration at any finite temperature, it is assumed that the number of vacancy pairs n is very much smaller than the total number of sites N available in the crystal. The number n is treated as an extensive thermodynamic variable satisfying the condition

$$\lim_{N \rightarrow \infty} \left(\frac{n}{N} \right) \neq 0$$

implying that the limit does not vanish, but is required to be less than unity since $n \ll N$. This condition is always met for point defects in crystals. As the vacancy pair concentration approaches its equilibrium value, the Helmholtz free energy F touches a minimum value. Thus the equilibrium concentration can be evaluated thermodynamically by minimizing F . We need to express F as a function of the variable n with respect to which F is differentiated in the process of applying the condition for F to be minimum. If E_v be the energy of a vacancy pair, the increase in internal energy owing to production of n pairs is

$$U = nE_v \quad (12.4)$$

For calculating entropy S we have to determine the number of ways of picking n molecules from N sites. For the first molecule there are N ways, for the second $(N - 1)$, for the third $(N - 2)$ and for the n th $(N - n + 1)$. This gives the number of ways as

$$N(N - 1)(N - 2) \dots (N - n + 1)$$

Since the order of taking molecules does not matter, we divide the above expression by $n!$ making the number of ways to be equal to

$$\frac{N(N - 1)(N - 2) \dots (N - n + 1)}{n!} = \frac{N!}{(N - n)! n!} \quad (12.5)$$

It should be marked that we have not accounted for the number of ways of picking the components of the pair. These are N for the first pair, $(N - 1)$ for the second and so on. Therefore, each factor in the estimate (12.5) must be squared to get the total number of ways W , which is then expressed as

$$W = \left[\frac{N!}{(N - n)! n!} \right]^2 \quad (12.6)$$

and, therefore, from (12.2), we get

$$S = 2k_B \ln \left(\frac{N!}{(N - n)! n!} \right) \quad (12.7)$$

Relation (12.7) gives the configurational entropy which is different from thermal entropy. The former is determined by the number of ways the atoms can be distributed over the lattice sites whereas the latter is determined by the number of ways the thermal energy of the crystal can be distributed among the modes of vibration. Vacancies may also have thermal entropy because of the changes in the frequency spectrum or change in volume of the crystal. This contribution being relatively very small is ignored here.

On substituting U and S from (12.4) and (12.7), respectively, into (12.1), we obtain

$$F = nE_v - 2k_B T \ln \left(\frac{N!}{(N - n)! n!} \right) \quad (12.8)$$

Using Stirling formula[†]: $\ln X! \equiv X[\ln X - 1]$ in (12.8), we have

$$F = nE_v - 2k_B T [N \ln N - n \ln n - (N - n) \ln (N - n)]$$

and

$$\frac{\partial F}{\partial n} = E_v + 2 k_B T \ln \left(\frac{n}{N - n} \right) \quad (12.9)$$

For F to be minimum, $\frac{\partial F}{\partial n} = 0$. This gives

[†] Valid for large values of X .

$$E_v = 2k_B T \ln \left(\frac{N-n}{n} \right)$$

or

$$\left(\frac{n}{N-n} \right) = \exp \left(-\frac{E_v}{2k_B T} \right) \quad (12.10)$$

Since $N \gg n$, the above relation reduces to

$$\frac{n}{N} = \exp \left(-\frac{E_v}{2k_B T} \right) \quad (12.11)$$

An estimate of these concentrations near the melting point can be made in alkali halides by using $T = 10^3$ K and $E_v = 1$ eV. This gives the value of n/N as 10^{-5} , i.e. about $10^{24}/\text{m}^3$. It is implied in these calculations that the number of cation vacancies is equal to the number of anion vacancies. In no way it is meant that the vacancy pairs are tied together. On account of having an effective charge associated with them, they tend to pair up or move together. But it is not necessary that they exist adjacent to each other. In pure alkali halides the most common vacancies are the Schottky defects.

Frenkel defects

The process of an interstitial occupation is accompanied by the creation of a vacancy. If N_i be the number of interstitial positions in the crystal, the different ways W in which n Frenkel defects can be produced is given by the relation

$$W = \frac{N!}{(N-n)! n!} \cdot \frac{N_i!}{(N_i-n)! n!} \quad (12.12)$$

The Helmholtz free energy in this case is then expressed as

$$F = nE_i - k_B T \ln \left[\frac{N!}{(N-n)! n!} \cdot \frac{N_i!}{(N_i-n)! n!} \right] \quad (12.13)$$

where E_i denotes the energy required for removing an atom from a lattice site to an interstitial position.

Proceeding on lines parallel to those for Schottky defects and taking $n \ll N$ and $n \ll N_i$, we obtain the following relation

$$n = (NN_i)^{1/2} \exp \left(-\frac{E_i}{2k_B T} \right) \quad (12.14)$$

In pure silver halides, the most common vacancies are the Frankel defects.

It can be shown that vacancies bear the same relation to ionic conduction as holes do to electronic conduction. Lattice vacancies are created in alkali halide crystals with the addition of divalent elements while the growth of the crystal is in progress. For example, when a triatomic molecule like CaCl_2 is added to a KCl crystal, a cation vacancy is produced. The Ca^{2+} occupies a

normal K^+ site and the two Cl^- enter the Cl^- sites. On requirement of charge neutrality, one K^+ site near the Ca^{2+} site must be left vacant during the crystal growth (Fig. 12.2).

K^+	Cl^-	K^+	Cl^-	K^+	Cl^-
Cl^-	Ca^{2+}	Cl^-	K^+	Cl^-	K^+
K^+	Cl^-	<input type="checkbox"/>	Cl^-	K^+	Cl^-
Cl^-	K^+	Cl^-	K^+	Cl^-	K^+
K^+	Cl^-	K^+	Cl^-	K^+	Cl^-
Cl^-	K^+	Cl^-	K^+	Cl^-	K^+

FIG. 12.2 Creation of a positive ion vacancy caused by the addition of traces of $CaCl_2$ in KCl during crystal growth.

We might expect the density of the crystal to increase on account of Ca^{2+} being heavier than K^+ . But this can happen only if no vacancies are present. The density in fact is lowered because of the presence of vacancies that effectively increase the volume of the unoccupied space within the crystal. Lattice defects are generally investigated by measuring the ionic conductivity. The data at not too high temperature show that the ionic conductivity of alkali halide and silver halide crystals increases linearly with increase in the amount of divalent element added. While the current flows the monovalent metal deposits at the cathode, establishing that the role of divalent addition is limited to the production of vacancies. The vacancies enhance the diffusion of monovalent atoms forming the basis for current flow. The diffusion of a lattice vacancy is equivalent to the diffusion of the metal ion in the opposite direction. Basic mechanisms of diffusion are shown in Fig. 12.3.

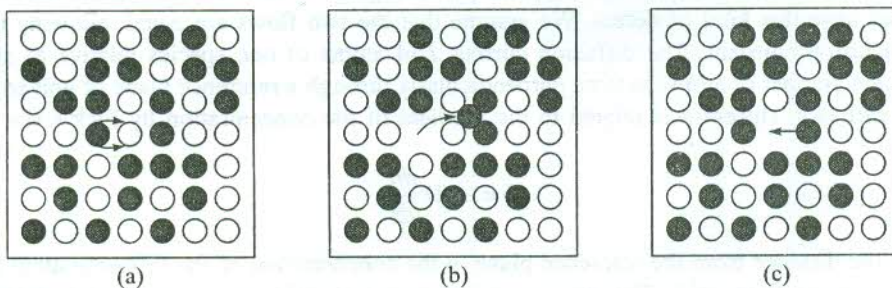


FIG. 12.3 Basic mechanisms of diffusion: (a) Atoms interchange positions by rotation about a midpoint. (b) Atoms move through interstitial sites. (c) Atoms exchange positions with vacant lattice sites.

As vacancies require energy for their formation, they should contribute to the heat capacity. Their formation can be regarded as an extra degree of freedom, in addition to the $3N$ vibrational modes. The corresponding additional contribution to the heat capacity is noticeable near the melting point, in particular. Figure 12.4 shows this contribution in silver bromide as a sudden rise over the value $3Nk_B$ (normal value at high temperatures), as the melting point is approached.

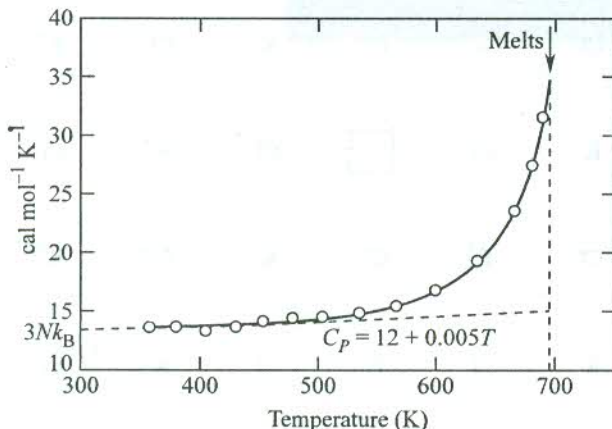


FIG. 12.4 Variation of heat capacity of silver bromide near the melting point. Excess heat capacity (over $3Nk_B$) is attributed to vacancy formation.

Diffusion

In the absence of electric field, lattice defects move in a random fashion. But, on applying a field the defects move with a velocity that depends upon the magnitude of the field. This introduces the concept of mobility μ , defined as the drift velocity per unit electric field. The mobility is related to a quantity known as the *diffusion constant*, D , by the Einstein relation

$$\mu k_B T = qD \quad (12.15)$$

where q is the charge on a defect or an atom whose diffusion may be under study.

The so-called diffusion laws connect the rate of flow of an atom with the concentration or the thermodynamic potential that causes the flow. In general, the diffusion has at least two components, each diffusing in opposite directions. This means that in an interstitial diffusion the empty interstitial spaces form the second component. It would be analogous to the flow of vacant lattice sites in crystals that have this kind of defect. We assume that the two flows are equal, allowing us to use a single diffusion constant. The diffusion current J of atoms of one species relative to another is defined as the number of atoms passing perpendicularly through a reference plane of unit area in unit time. The diffusion current J is related to the gradient of the concentration by Fick's law

$$J = - D \frac{dn}{dx} \quad (12.16)$$

where x is the distance from the reference plane, n the concentration of the diffusing atom and t the time. Thus units of D are m^2/s . The minus sign indicates that diffusion occurs away from regions of higher concentration. It is further assumed that D is independent of concentration in a given medium at a given temperature. This assumption may, however, be true only as a first approximation.

Let us consider the diffusion of impurity atoms between interstitial sites. The treatment of the diffusion of lattice vacancies proceeds on identical lines. For diffusion, an atom is required to migrate over the potential barrier provided by its nearest neighbours. The probability of each try that the atom jumps over the potential hill is $\exp\left(-\frac{E_a}{k_B T}\right)$, E_a being the height of the barrier (or the activation energy). If the characteristic atomic vibrational frequency is v_0 , the atom will make v_0 tries in one second to cross over the potential barrier. Therefore, the probability per second or the number of times the atom actually crosses the barrier in one second is

$$v = v_0 \exp(-E_a/k_B T) \quad (12.17)$$

where v is also known as the *jump frequency*. The other process that may contribute to diffusion is quantum mechanical tunnelling. But it is significant only in the diffusion of the light nuclei.

Consider two adjacent parallel planes having impurity atoms in interstitial sites. When the two planes are separated by one unit of lattice constant a and the total concentration of impurity atoms

is denoted by n , the number of these atoms per unit area on one plane will be $na\left(=\frac{na^3}{a^2}\right)$. The corresponding number on the other plane can be written as $\left[na + a\frac{d(na)}{dx}\right]$. Therefore, the number of atoms that move between the two planes in unit time through their unit area is

$$(va^2) \frac{dn}{dx}$$

Thus we get another statement of the Fick's law, written as

$$J = (v_0 a^2) \exp\left(-\frac{E_a}{k_B T}\right) \frac{dn}{dx} \quad (12.18)$$

On comparing (12.18) with (12.16), we find that

$$\begin{aligned} D &= (v_0 a^2) \exp(-E_a/k_B T) \\ &= D_0 \exp(-E_a/k_B T) \end{aligned} \quad (12.19)$$

This relation gives the temperature dependence of the diffusion constant. Its value shows a great variation for various impurities at a given temperature. For common metals and Ge and Si, its value lies in the range 10^{-50} to 10^{-20} m²/s. The constant D_0 is experimentally found not to vary much with temperature. Its value for carbon impurity in alpha iron is about 2×10^{-6} m²/s. The representative values of D_0 and E_a for a number of impurities in various host crystals have been given by Kittel.*

From the ionic conductivity data obtained at different temperatures it is possible to estimate the values of energy of formation of a vacancy pair and the jump activating energy. The conductivity is expressed as

$$\begin{aligned} \sigma &= nq\mu \\ &= \left(\frac{nq^2 v_0 a^2}{k_B T}\right) \exp\left(-\frac{E_a}{k_B T}\right) \quad [\text{using (12.15) and (12.19)}] \end{aligned} \quad (12.20)$$

* C. Kittel, *Introduction to Solid State Physics*, 7th ed., Chap. 18, p. 545 (John Wiley, 1996).

In the temperature range over which the number of vacancies is controlled by the number of divalent metal ions, the vacancy concentration is independent of temperature. The slope of $\ln \sigma$ versus $(1/k_B T)$ plot then gives the jump activation energy of positive ion vacancies E_a^+ . There is another range of temperature in which thermal activation energy determines the defect concentration and the proportion of vacancies is given by $\exp\left(-\frac{E_v}{2k_B T}\right)$, E_v being the energy of formation of a vacancy pair. The slope of $\ln \sigma$ versus $1/k_B T$ plot in this case provides the value of $\left(E_a^+ + \frac{1}{2} E_v\right)$. Thus the conductivity data over a wide range of temperatures enable us to determine the jump activation energy and the energy of formation of a vacancy pair.

Colour centres

The band gap of ionic crystals is about 6 eV which is equivalent to the energy of a photon of wavelength 2000 Å (i.e. in the ultraviolet region). The ionic polarizability is found to resonate at 50 microns, falling in the far infrared region. Therefore, these crystals are expected to be transparent in the visible region, as is actually the case with alkali halides. But with certain treatment, these crystals can be coloured or made to show colour.

On the requirement of charge neutrality, vacancies of one constituent of a diatomic ionic crystal are balanced either by an equal number of interstitials of the same constituent (Frenkel) or by an equal number of vacancies of the other constituent (Schottky). The missing charge of a negative ion vacancy may also be compensated by an electron localized or trapped[†] in the vicinity of the point defect whose charge the electron is replacing. The negative ion vacancy together with the trapped electron can be regarded as a bound system that is characterized by a quantized set of energy levels. Similar to the case of single isolated atoms, these levels give rise to a series of absorption lines in the optically forbidden band between $\hbar\omega_{TO}$ and $\hbar\omega_{LO}$, as discussed in Chapter 10. The band covers the visible region. The bound system as described above and other such defect-electron structures, that absorb in the visible region imparting colour to an otherwise transparent perfect crystal, are called *colour centres*.

Colour centres have been extensively studied in alkali halides. They are usually coloured in the following ways:

- (i) Adding chemical impurities
- (ii) Heating the crystal in the vapour of the alkali metal and then cooling it quickly
- (iii) Irradiating the crystal with x-rays, γ -rays, neutron or electron beams
- (iv) Conducting electrolysis

By heating the crystal in the vapour of the alkali metal, an excess number of alkali atoms are incorporated into the crystal and as such we could expect the mass density to increase. But the density practically decreases in proportion to the concentration of excess alkali atoms. When an alkali atom from the vapour diffuses into the crystal, it occupies a pre-existing cation vacancy. Since the equilibrium concentration must be maintained, a new cation vacancy is formed. But to maintain charge neutrality an anion vacancy must also be created simultaneously. Therefore, the net result of putting one alkali atom into the crystal is to increase the size of the crystal by one alkali atom and by one anion vacancy. This increases the vacancy concentration causing a decrease in density.

[†] A negative ion vacancy acts as a centre of a positive charge and, therefore, it can trap an electron.

F-centres

We saw above that the excess alkali atoms enter the crystal at the pre-existing cation vacancies. While diffusing from the surface the atom is ionized and then occupies a cation vacancy. The liberated valence electron is trapped at an anion vacancy and forms a hydrogen atom-like bound system (see Fig. 12.5). This bound system is known as an *F*-centre (*F* stands for Farbe, a German word that means colour). The above model of *F*-centre was originally conceived by de Boer and confirmed by the electron spin resonance studies. Pohl* was the first to study the experimental properties of *F*-centres in detail. Figure 12.6 shows the central absorption band caused by *F*-centre in several alkali halide crystals.

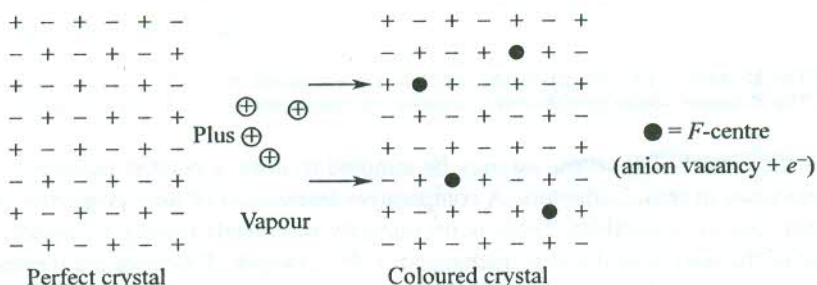


FIG. 12.5 An excess of alkali ions being produced in a crystal by heating it in the vapour of the alkali metal. Highly localized excess electrons occupy the corresponding negative ion vacancies.

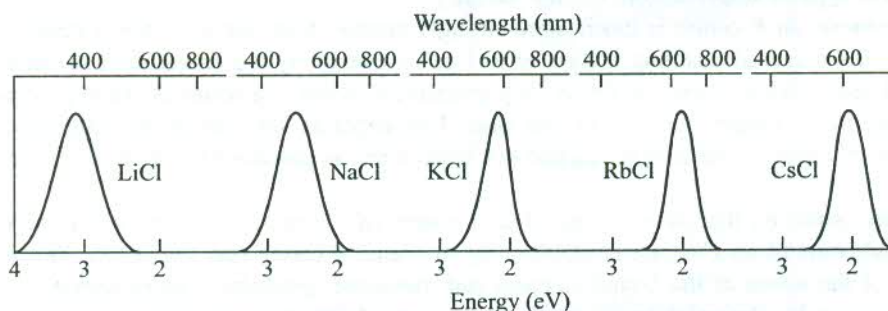


FIG. 12.6 *F*-centre absorption bands in certain alkali halide crystals. [After R.W. Pohl, *Proc. Phys. Soc.*, **49**, 3 (1937).]

The qualitative features of the spectra produced by *F*-centres are strikingly similar to those of ordinary atomic spectra in many respects. However, the basic difference lies in the symmetry around the *F*-centre which is cubic and not spherical as is the case with isolated atoms. The cubic crystal field splits the orbitally degenerate energy levels making the spectra of *F*-centres relatively complicated. A complete analysis using the crystal field theory demonstrates that *F*-centre is not the only way the electrons and vacancies can combine to colour the crystal. There are two other possibilities:

* R.W. Pohl, *Proc. Phys. Soc.*, **49**, 3 (1937).

- (a) The *M*-centre [Fig. 12.7(a)], in which two electrons are bound to two neighbouring anion vacancies in (100) plane.
- (b) The *R*-centre [Fig. 12.7(b)], in which three electrons are bound to three neighbouring anion vacancies in (111) plane.

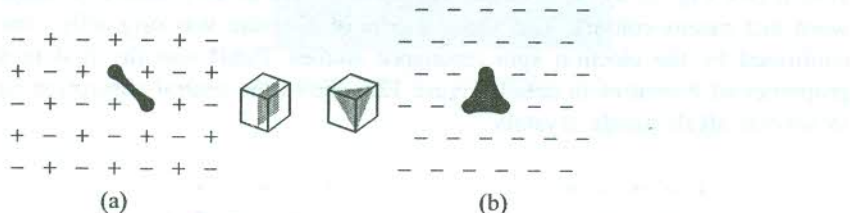


FIG. 12.7 (a) The *M*-centre—two neighbouring negative ion vacancies in a (100) plane binding two electrons.
 (b) The *R*-centre—three neighbouring negative ion vacancies in a (111) plane binding three electrons.

In view of the model of *F*-centre we may be tempted to draw a parallel between *F*-centres and bound donor electrons in semiconductors. A comparative assessment of their properties demonstrated that they are not exactly equivalent. There is no impurity in crystals having *F*-centres. The *F*-band is characteristic of the host crystal and is unchanged if, for example, *F*-centres are formed by heating the crystal in the vapour of a different alkali metal. This implies that the electron is no longer associated with the atom which released it in the process of ionization. This contrasts the behaviour of a donor electron that is bound to its parent impurity atom. The electron in an *F*-centre is bound to a different type of imperfection, i.e. the vacancy.

Furthermore, an *F*-centre is much more strongly bound. Also, the *F*-centre is strongly coupled to the rest of the crystal enabling it thereby to lose its energy by the emission of phonons. On the other hand, the isolated atoms can decay only radiatively which is a relatively slow process, i.e. the excited state has a longer lifetime[†] in this case. This explains why the optical absorption spectra produced by *F*-centres consist of bands and not sharp lines, as produced by the excitation of isolated atoms.

Another centre *F*_A that may be treated as a cousin of *F*-centre is formed when one of the six nearest neighbours of an *F*-centre is replaced by an impurity cation (see Fig. 12.8). This lowers the symmetry of the levels of the bound electron and, therefore, produces a more complex absorption spectrum caused by the splitting of levels in a crystal field of lower symmetry. It is, however, interesting to note that the formation of an *F*_A-centre is often energetically favourable.

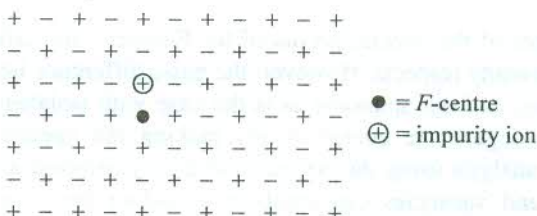


FIG. 12.8 The *F*_A-centre—an impurity ion replacing one of the six nearest-neighbour positive ions that surround an *F*-centre.

[†] The linewidth is inversely proportional to the lifetime of the excited state of concern.

The *M*- and *R*-centres described earlier, are examples of more complex centres. They may be regarded as members of the *F*-centre family since they represent the grouping of two and three *F*-centres, respectively.

Trapped-hole centres

By heating an alkali halide crystal in a halogen gas, it should, in principle, be possible to introduce alkali metal vacancies. A hole then could be bound to such a vacancy, producing an antimorph to the *F*-centre. But no such antimorphs are observed in alkali halides. Though holes can be trapped by point imperfections, there exists no evidence for these imperfections to be cation vacancies. A V_k -centre is the best known trapped-hole centre in which a hole binds two neighbouring anions (see Fig. 12.9). The optical absorption spectrum of the V_k -centre is interpretable as that of a negative halogen molecular ion in a crystal (say, Cl_2^- in KCl). Another example is the *H*-centre which is thought to result from the binding by a hole of an interstitial chlorine ion to a symmetrically positioned lattice ion (Fig. 12.10).

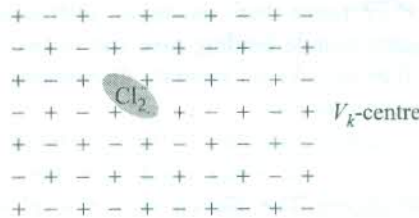


FIG. 12.9 The V_k -centre—two neighbouring negative ions bound by a hole.



FIG. 12.10 The *H*-centre—an interstitial chlorine ion bound by a hole to a symmetrically situated lattice chlorine ion. The resulting singly-ionized chlorine molecule occupies a single chlorine ion site.

The structure and properties of colour centres are investigated by electron paramagnetic resonance and optical absorption studies. A typical absorption spectrum of colour centres in a KCl crystal is shown in Fig. 12.11. The peaks attributed to different centres are marked accordingly.

Excitons

We described above some of the most common point defects. There is a subtle possibility when an atom in a perfect crystal can be regarded as a point defect. This refers to the situation when only one of the atoms in a perfect crystal is in an excited state and the rest are in the ground state. In this picture the single excited atom is treated as a defect and known as a *Frenkel exciton*. The excitation may be transferred from atom to atom because of the coupling between atoms. On being excited, a valence electron is transferred to the conduction band leaving behind a hole in the

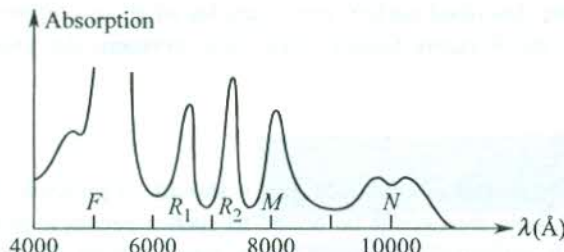


FIG. 12.11 Absorption spectrum of KCl showing peaks caused by various colour centres.

valence band. The electron and the hole may be bound by the Coulomb attractive force acting between them. The bound electron-hole pair is called an *exciton*. The exciton being neutral does not transport charge, though it does carry energy as it moves through the crystal. This means that by the movement of excitons the energy is transported through the crystal without the atoms themselves having to move out from their equilibrium positions. This results in fast movement of excitons. Excitons, in fact, move much more faster than vacancies, interstitial or substitutional impurities.

Two limiting cases of the electron-hole binding give rise to two types of excitons—the Frenkel and Mott-Wannier excitons. Before we take up separate discussions on these excitons, we describe below the general features of exciton levels.

In reflection and absorption spectra of insulators, there is enough evidence to suggest that there exist energy levels immediately below the lower conduction band edge, though the crystals are expected to be transparent in this region. The discrete energy level structure belongs to the exciton that represents a bound electron-hole pair. When a photon of energy greater than the forbidden gap is incident on an insulating crystal, a free electron and a free hole are likely to be produced as already described. The threshold photon energy in a direct absorption process equals the band gap. But in an indirect phonon assisted absorption process the threshold is lower by the phonon energy, as discussed in section 9.2.3.

When the group velocities of the electron and the hole created are equal, i.e. $d\varepsilon_c/d\mathbf{k} = d\varepsilon_v/d\mathbf{k}$ (ε_c and ε_v refer to the electron and hole energies in the conduction and valence band, respectively), the two particles may be bound by the Coulomb attractive force between them and thus an exciton formed. In the process a part of the incident photon energy goes as the binding energy, bringing thereby the exciton energy to a level that is lower than the lower conduction band edge even when the threshold is equal to the band gap E_g . A schematic of the exciton levels is shown in Fig. 12.12 which also illustrates the concept of the exciton binding energy E_x . The usual range of variation of the exciton binding energy is from 1 meV to 1 eV. Its value in a number of semiconductor and ionic crystals has been given by Kittel.* Excitons are unstable and prone to a recombination process in which the electron drops into the hole in the valence band with the emission of a photon or phonons.

Frenkel excitons

Excitons are examined in two limiting cases: one in which the exciton is small and tightly bound and the other in which it is weakly bound and its size can be equal to many lattice distances. The former is called a *Frenkel exciton* while the latter is known as *Mott-Wannier exciton*. In a Frenkel exciton the excitation is strongly localized on or near a single atom. Both the electron and the hole are on the same atom with no restriction on the whereabouts of the pair within the crystal. Frenkel

* C. Kittel, *Introduction to Solid State Physics*, 7th ed., p. 314 (John Wiley, 1996).

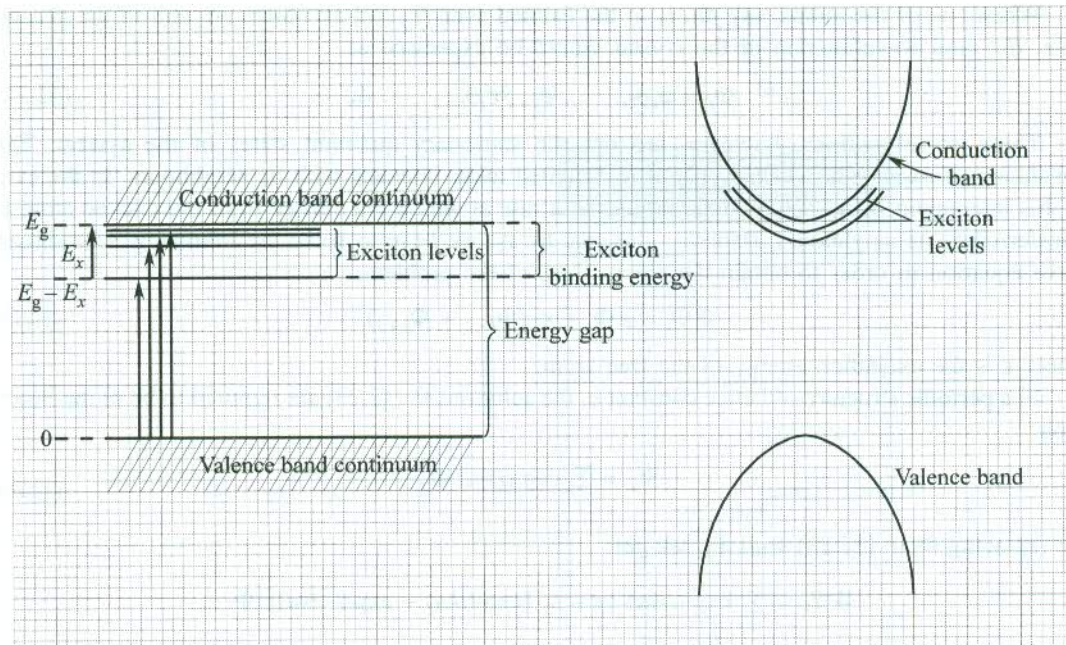


FIG. 12.12 Exciton levels of a solid of simple band structure with both conduction and valence band edges at $\mathbf{k} = 0$. The exciton binding energy is equal to the depth of the exciton ground state below the conduction band minimum.

envisaged an excited electron describing an orbit of atomic dimension around an atom with a vacant valence state. Since the coupling between the neighbouring atoms facilitates the transfer of excitation from atom to atom, the empty valence state, though instantaneously on one atom, behaves as a mobile hole (see Fig. 12.13).

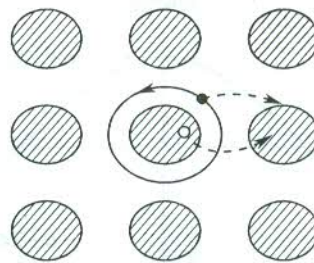


FIG. 12.13 Motion of a Frenkel exciton.

Thus a Frenkel exciton is like an electron bound in a relatively deep impurity state except that it is mobile. The Frenkel picture is applicable to the solidified rare gases and some ionic crystals.

Let us consider the translation of Frenkel excitons in a crystalline ring of N identical atoms. If ϕ_j be the ground state wavefunction of the j th atom in the ring, the ground state of the crystal may be represented by the wavefunction

$$\Phi_0 = \phi_1 \phi_2, \dots, \phi_{N-1} \phi_N \quad (12.21)$$

provided that the interaction between the atoms is ignored.

When one of the atoms, say j th, is in the excited state Ψ_j and all others are still in the ground state, the total wavefunction of the crystal would be expressed as

$$\Phi_j = \phi_1 \phi_2 \dots \phi_{j-1} \Psi_j \phi_{j+1} \dots \phi_N \quad (12.22)$$

These wavefunctions, however, are not the stationary quantum states of the system. The translation of exciton is possible only if the excited atom interacts with its neighbours. In the case of this interaction being active, there would be a rate at which the energy from the excited atom is transferred to its neighbours. Denoting this rate by ε_T , we have to solve the following Schrödinger wave equation in order to obtain the eigenvalues of the problem,

$$\mathcal{H} \Phi_j = \varepsilon \Phi_j + \varepsilon_T (\Phi_{j-1} + \Phi_{j+1}) \quad (12.23)$$

where ε is the excitation energy of the free atom.

In a periodic structure of lattice constant a , the solutions to (12.23) are required to be of the Bloch type

$$\Psi_k = \sum_j \exp(ika) \Phi_j \quad (12.24)$$

On replacing Φ_j in (12.23) with Ψ_k , we get

$$\begin{aligned} \mathcal{H} \Psi_k &= \sum_j \exp(ika) \{ \varepsilon + \varepsilon_T [\exp(ika) + \exp(-ika)] \} \Phi_j \\ &= [\varepsilon + 2\varepsilon_T \cos ka] \Psi_k \end{aligned} \quad (12.25)$$

Thus we have the eigenvalues

$$\varepsilon_k = \varepsilon + 2\varepsilon_T \cos ka \quad (12.26)$$

The allowed set of k values is the same (4.9) as obtained in Section 4.2.1 by applying periodic boundary conditions. Relation (12.26) shows that the energy of Frenkel excitons is minimum at the zone boundary ($k = \pm \pi/a$) and maximum at the zone centre ($k = 0$) (see Fig. 12.14).

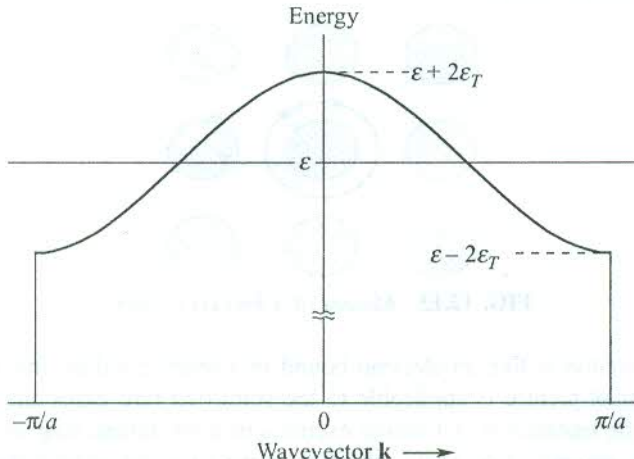


FIG. 12.14 Dispersion curve for a Frenkel exciton, obtained with the positive nearest-neighbour transfer interaction ε_T .

Examples of Frenkel excitons. (1) Solidified inert gases—two lowest transitions in crystalline xenon occur at 8.4 eV and 9.55 eV. These are clearly Frenkel excitons (see Fig. 12.15). (2) Alkali

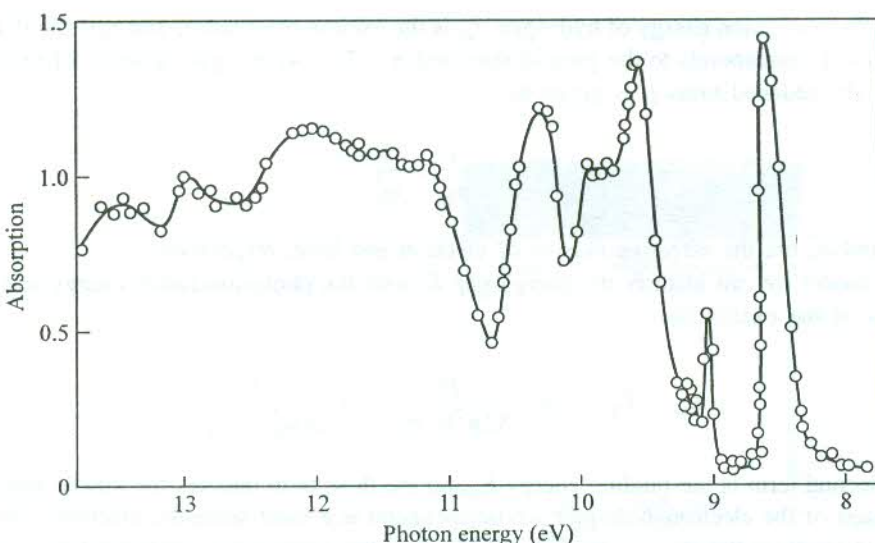


FIG. 12.15 Absorption spectrum of solid xenon between 8.0 and 14.0 eV. [After G. Baldini, *Phys. Rev.*, **128** 1562 (1962)].

halide crystals show Frenkel excitons in the vacuum ultraviolet region. A doublet structure observed in NaBr is a significant example of Frenkel excitons. The splitting is attributed to the effect of spin-orbit coupling. (3) In molecular crystals the covalent bonding within a molecule is much more stronger than the van der Waals coupling that holds molecules together in the crystal. There is no noticeable shift in the energy of excitations of individual molecules when the respective excitations are measured in crystalline samples. These are ideal examples of Frenkel excitons.

Mott-Wannier excitons

These are weakly bound excitons with a separation of many lattice distances between the electron and hole. This model works exceedingly well to account for the excitonic absorption in covalently bonded crystals, such as Group IV semiconductors. It is also applicable to many partially ionic, partially covalent crystals (e.g. Group III-IV semiconductors). We saw in Chapter 9 that the shallow donor or acceptor impurity levels in semiconductors could be described by analogy with hydrogen atoms. The Mott-Wannier picture of exciton is a similar one and its simplest mathematical description is given by the so-called hydrogenic model. The exciton binding energy E_x can be deduced by following the arguments of section 9.4.1 and replacing the effective mass by the reduced mass μ of the electron-hole pair. By analogy with (9.27) and (9.25), we write

$$r_{\text{ex}} = n^2 \left(\frac{m \epsilon_s}{\mu} \right) r_0 \quad (12.27)$$

and

$$\begin{aligned} E_x &= - \frac{1}{n^2} \left(\frac{\mu}{m \epsilon_s^2} \right) E_H \\ &= - \frac{1}{n^2} \frac{\mu e^4}{32 \pi^2 \epsilon_0^2 \epsilon_s^2 \hbar^2} \end{aligned} \quad (12.28)$$

where E_H is the ionization energy of hydrogen, r_{ex} is the exciton orbit radius and r_0 is the Bohr radius. The state $n = 1$ corresponds to the ground state and $n = 2, 3, 4$, etc. give a series of excited states of exciton. The reduced mass μ is given by

$$\frac{1}{\mu} = \frac{1}{m_e^*} + \frac{1}{m_h^*}$$

where m_e^* and m_h^* are the effective masses of electron and hole, respectively.

In this model we can identify the energy gap E_g with the photo-ionization energy and write the total energy of the exciton as

$$\varepsilon_{nk} = E_g - \frac{1}{n^2} \frac{\mu e^4}{32\pi^2 \hbar^2 \epsilon_0^2 \epsilon_s^2} + \frac{\hbar^2 k^2}{2(m_e^* + m_h^*)} \quad (12.29)$$

where the second term is the binding energy E_b and the third term denotes the kinetic energy of the centre of mass of the electron-hole pair whose inclusion is a must since the electron-hole pair can move almost freely in the crystal (see Fig. 12.16). \mathbf{k} is the wavevector corresponding to the centre of mass motion of the two particles.

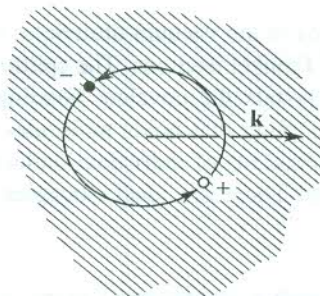


FIG. 12.16 Motion of the Mott-Wannier exciton.

Various relations given above imply that the Coulomb force between the electron and hole is reduced to $1/\epsilon_s$ of the value in vacuum (ϵ_s being the static dielectric constant of the crystal). For semiconductors, ϵ_s is of the order of 10 and therefore the exciton spectrum for $\mathbf{k} = 0$ is a strongly compressed hydrogen spectrum and the binding energies lie below 0.1 eV. On the same account the spatial extent of the Mott-Wannier exciton is much larger than that of the hydrogen atom (~ 10 Bohr radii). This in a way justifies the application of the simple hydrogenic model with the use of a macroscopic dielectric constant.

When excitons are generated by photon absorption and no other particles are involved, the energy conservation demands that the wavevector of the exciton be equal to that of the photon. Since the photon wave vector is small, the third term in (12.29) can be dropped in such a case. This explains why in an optical absorption experiment, exciton states with $\mathbf{k} = 0$ are not seen. As the energy separation of the exciton state from the lower conduction band edge is rather small, the excitonic character of the optical absorption can be investigated only by experiments conducted at low temperatures. The excitonic absorption in GaAs observed at 21 K is shown in Fig. 12.17.

In Fig. 12.15 the two smaller peaks at 9.1 eV and 9.2 eV are identified in the Mott-Wannier model

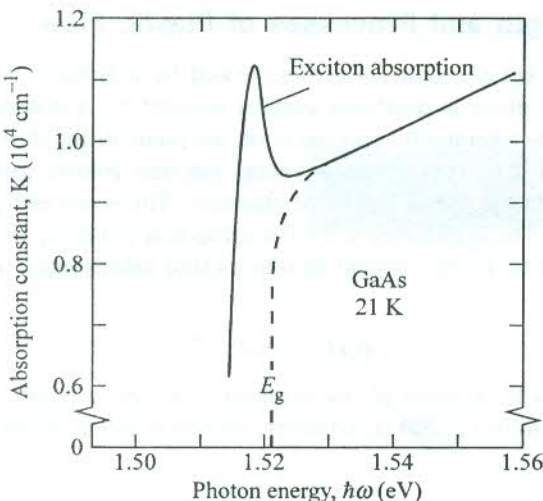


FIG. 12.17 Absorption in a GaAs crystal near the band gap energy E_g at 21 K. The dashed curve shows absorption in the absence of exciton excitation. [After M.D. Sturge, *Phys. Rev.*, **127**, 768 (1962).]

as the $n = 2$ and $n = 3$ lines of a series in which the 8.4 eV line is the lowest. We may recall the 8.4 eV line to have been attributed to a Frenkel exciton. But it must not surprise us to have both types of excitons in one crystal because the condition on orbit size for the Mott-Wannier model in the present case is met for $n \geq 2$ and not for $n = 1$.

Polarons

An electron on being excited to the conduction band of a perfect ionic crystal may often be favoured to move in a spatially localized level with a local deformation in the ionic arrangement being carried along. The deformation is produced by the electron field that effectively polarizes the lattice, as a result of which the electron field is screened and the electrostatic energy lowered. Since perfect crystals are considered to be free of deformations, the quasi-particle composed of an electron and its strain field, known as a *polaron*, is viewed as another point defect which is observed to be fairly mobile. A brief theoretical account of polarons was given in Section 10.10 where they were not treated as defects but as a complication in the theory of electron mobility in ionic crystals.

12.2 LINE IMPERFECTIONS: DISLOCATIONS

Single crystals show far less strength than they would have according to the theory of elasticity. This anomalous behaviour is attributed to the movement of certain line imperfections in crystals under the action of a deforming force. These imperfections are commonly known as *dislocations*. All crystals, except those grown under very special conditions, usually have a high concentration of dislocations. In contrast to a point defect that directly affects one lattice point or a few immediately adjacent lattice points, a dislocation is a line source of imperfection. A general dislocation may follow any curved route through a crystal.

How crucial is the role of dislocations in limiting the strength of a crystal can be appreciated by comparing the measured values with the corresponding theoretical estimates. An approximate estimate of the theoretical elastic limit can be had by calculating the critical stress at which the crystal becomes unstable and the shear occurs.

12.2.1 Shear Strength and Processes of Plastic Flow

Consider a crystal with a set of parallel planes separated by a distance d (Fig. 12.18). Suppose in a shear deformation each plane is displaced parallel to itself by a distance x , with respect to the nearest plane below it. The interatomic separation on the plane in the direction of the displacement in an undeformed crystal is a . The additional energy per unit volume associated with the shear of the crystal is obtained with the use of theory of elasticity. This extra energy, say $\phi(x)$, is quadratic in x for small values of x . The displacement $x = 0$ corresponds to the equilibrium state of the crystal. For the shear deformation of a cubic crystal in which (100) planes move along the [010] direction, $\phi(x)$ is related to x by

$$\phi(x) = 2(x/d)^2 C_{44} \quad (12.30)$$

where C_{44} is the appropriate stiffness elastic constant. The above relation fails for large x .

The more general form of (12.30) is, however, written in terms of the shear modulus G

$$\phi(x) = \frac{1}{2} \left(\frac{x}{d} \right)^2 G \quad (12.31)$$

The $\phi(x)$ versus x plot is shown in Fig. 12.19(a). As the displacement increases from the zero value, the extra energy per unit volume increases. It becomes maximum at $x = a/2$ where the shear could

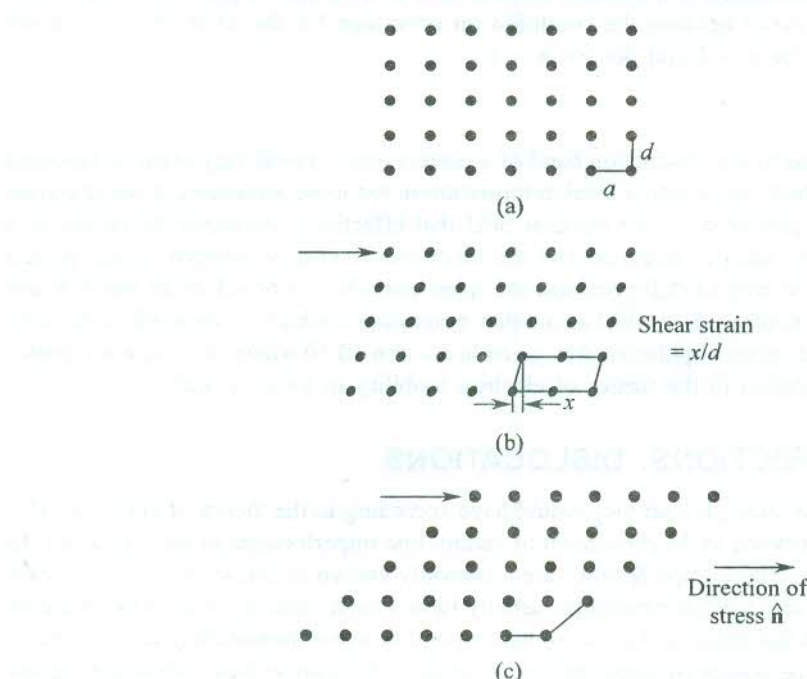


FIG. 12.18 Progressive deformation under increasing shear stress: (a) Perfect crystal. (b) Deformed crystal. (c) Crystal deformed to the limit such that the new interior configuration and the original undeformed crystal appear identical.

go either way and refers to the zero value of stress. At an extreme displacement $x = a$, the interior displacement configuration [see Fig. 12.18(c)] can in no way be distinguished from the undeformed crystal if we overlook small surface effects. $\phi(x)$ then obviously drops to zero. It indicates to the fact that $\phi(x)$ is a periodic function of x with period a , i.e. $\phi(x + a) = \phi(x)$. This has no inconsistency with relation (12.31) if $x \ll a$.

If the crystal has N planes of area S , its volume is $V = NSd$ and, therefore, the additional energy acquired by it in maintaining a relative displacement of x between two successive parallel planes as shown in Fig. 12.18(b) may be written as

$$\Phi(x) = V\phi(x) \quad (12.32)$$

The shear stress σ is defined as the force per unit area on a single plane that maintains the displacement x . We can express it as

$$\begin{aligned} \sigma &= \frac{1}{NS} \frac{d}{dx} (\Phi) \\ &= d \left(\frac{d\phi}{dx} \right) \quad [\text{using (12.32)}] \end{aligned} \quad (12.33)$$

Relation (12.33) implies that the behaviour of σ must be identical with that of the first derivative of ϕ . The σ versus x curve [Fig. 12.19(b)] in conjunction with the ϕ versus x plot [Fig. 12.19(a)] clearly vindicates this contention. The shear stress becomes maximum (σ_c) at a

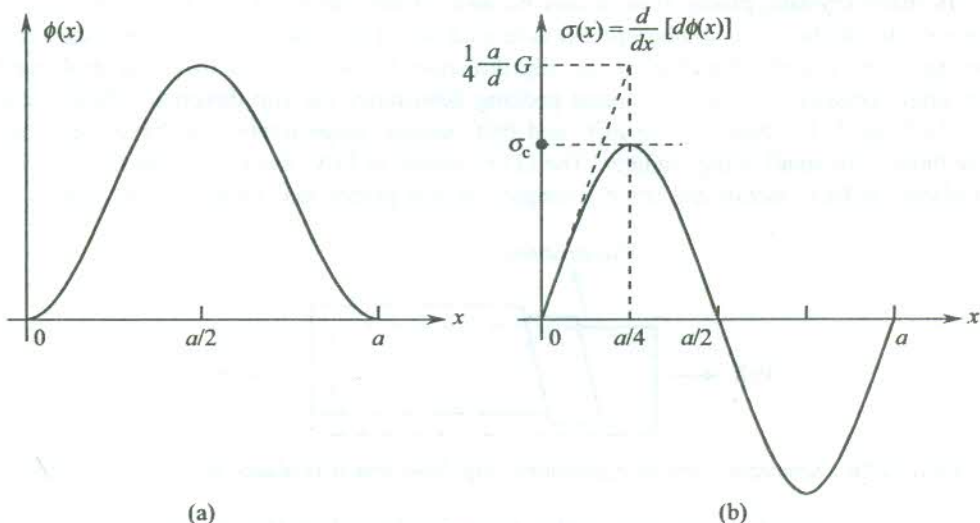


FIG. 12.19 (a) Variation of the additional energy per unit volume, $\phi(x)$, with relative displacement x . (b) Plot of shear stress σ versus the relative displacement x . Note that σ is proportional to the first derivative of $\phi(x)$. The curves are in consistency with this fact.

displacement between 0 and $a/2$. Since our treatment is valid strictly for small values of x and these fall on the linear portion of the curve in Fig. 12.19(b), it is obligatory to extrapolate the linear region out to the point of the maximum of the actual curve ($x = a/4$) and evaluate $d\phi/dx$ at this point for a reasonable, though still approximate, estimate of σ_c . This yields

$$\begin{aligned}\sigma_c &\approx d \left[\frac{d}{dx} \left(\frac{1}{2} \frac{x^2}{d^2} G \right) \right]_{x=a/4} \\ &= \frac{1}{4} \left(\frac{a}{d} \right) G\end{aligned}\quad (12.34)$$

At shear stress greater than σ_c , one plane slides over another, or in other words the crystal undergoes *slip*. Since G is typically of the order 10^{10} to 10^{11} N m $^{-2}$, σ_c must be of a similar order of magnitude. On the other hand, the measured values of σ_c even in some best grown pure single crystals are lower by a factor as large as 10^4 . In view of this flagrant disparity, attempts were made to improve the theoretical estimate by identifying the true form of intermolecular forces and the available configurations of mechanical stability to the lattice. On these considerations, Mackenzie* was able to show that the ideal shear strength comes down to $G/30$ corresponding to a critical shear angle of about 2 degrees. Since this small improvement does not make any headway towards the resolution of the problem, a suspicion develops over the genuineness of the process of slip on which the estimate of (12.34) is based. Extensive experimental studies have, however, now established that slip occurs by the motion of dislocation lines.

Even though we have not taken to a proper discussion on dislocations so far, a few introductory remarks on *slip* and *twinning* are desirable here because they are the well-known modes of plastic deformation.

Slip. In many crystals, plastic flow occurs because of the sliding of one part of the crystal as a unit relative to another. The sliding process is termed *slip*. The plane on which slip occurs is known as the slip plane and the direction as the slip direction. Figure 12.20 shows a general translation slip in single crystals. The line of closest packing determines the slip direction. These correspond to the [110] and [111] directions in FCC and BCC metals, respectively. The likely slip planes are usually those with small Miller indices. The (111) planes in FCC metals and the (110), (112), and (123) planes in BCC metals are some examples of slip planes that underline this point.

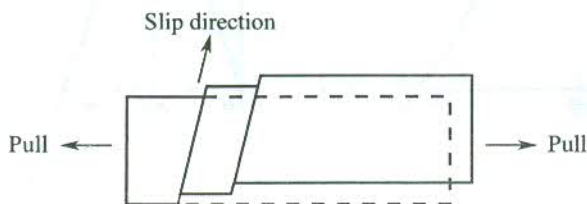


FIG. 12.20 Schematic view of translational slip. Note that it produces an increase in length.

If the displacement or the slip vector measures less than the shortest lattice translation vector, the crystalline order cannot be maintained. This gives rise to *stacking fault* such as the regular sequence of ABC ABC ABC ... of the closest-packed planes in FCC crystals appearing as ABC AB ABC The slip plane has a large number of dislocations produced by the multiplication of a dislocation segment pinned at each end (called a Frank-Read source) under the influence of an applied shear stress.

* J.K. Mackenzie, *Thesis*, Bristol (1949).

Twinning. It is another mode of plastic deformation observed usually either in HCP or BCC structures. Twinning represents a shearing motion of atomic planes over one another in which the magnitude of translation of each plane is proportional to its distance from a particular plane known as the *twinning plane*. A twinning plane acts as a mirror plane of symmetry at which when one portion of the twinned crystal is reflected the other portion is produced (or constructed).

12.2.2 Dislocation Types

Experiments have confirmed that there are few pure crystals that are not plastic. Germanium and silicon crystals are not plastic at room temperature and fail or yield only by fracture. As mentioned in the preceding section, the weakness and plastic deformation of crystals are attributed to the presence of dislocations and their movement. We describe below two simplest straight-line dislocations—the *edge* and *screw* types. Though there are several of other types, they can generally be interpreted as modifications or combinations of these two.

Edge dislocations

An edge dislocation is formed when either a row of atoms is removed from a crystal lattice or a row of atoms is displaced at unit lattice distance. Figure 12.21(a) illustrates a pure edge dislocation in which one of the planes of atoms terminates at certain level within the crystal and thus resembles a knife blade embedded in a block of cheese with one edge of the knife on level with the top surface of the block. The direction of the line of atoms in the incomplete plane determines the line (or direction) of dislocation. The vector representing the lattice displacement is called the *Burgers vector* \mathbf{b} . We see that in an edge dislocation the Burgers vector is perpendicular to the dislocation line.

The motion of an edge dislocation is equivalent to slip. In the presence of a shearing stress there is a considerable lattice strain at an edge dislocation, compressive on one side and extensive on the other, facilitating the motion. Figure 12.21(b) explains how the motion of an extra plane across the crystal takes place at the cost of little energy. The motion is equivalent to a slip of one lattice vector. It is analogous to the movement of a wriggle across a rug which is easier than the motion of the rug as a whole. The calculated value of the stress required to move an edge dislocation comes to less than 10^4 N m^{-2} . It shows how easily crystals can be plastically deformed in the presence of dislocations.

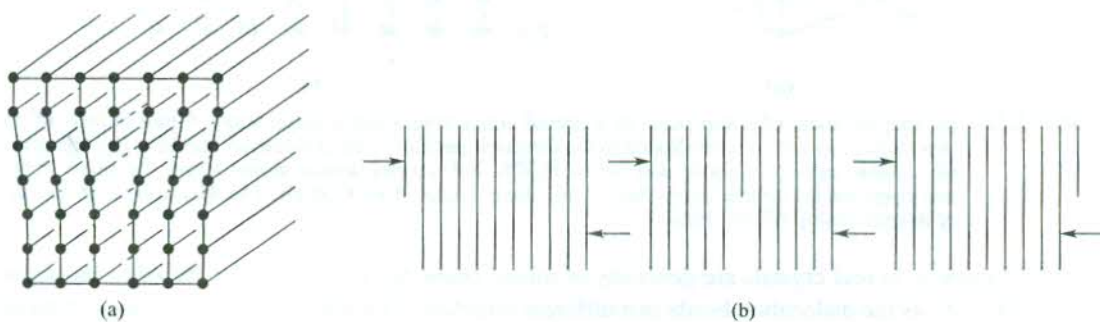


FIG. 12.21 (a) An idealized form of an edge dislocation. (b) Motion of an edge dislocation under applied stress, producing slip.

Screw dislocation

A screw dislocation, as sketched in Fig. 12.22, may be thought to have been accomplished by the following procedure. First, cut a perfect crystal partway through, then force the material on one side of the cut to move up with respect to the material on the other side by one unit of atomic spacing, and finally glue the material on the two sides in this condition. The dislocation marks the boundary between the displaced and undisplaced parts of the crystal. The Burgers vector is again used to describe the displacement. It is parallel to the dislocation line for a pure screw dislocation.

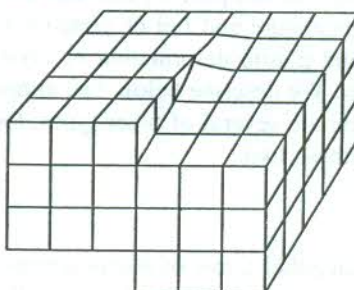


FIG. 12.22 An idealized form of a screw dislocation.

Figure 12.23 shows the relative displacement of atoms in the displaced part of the crystal. A screw dislocation may be pictured as a spiral arrangement of lattice planes in which on going once completely around the dislocation axis we move from one plane to the immediate next.

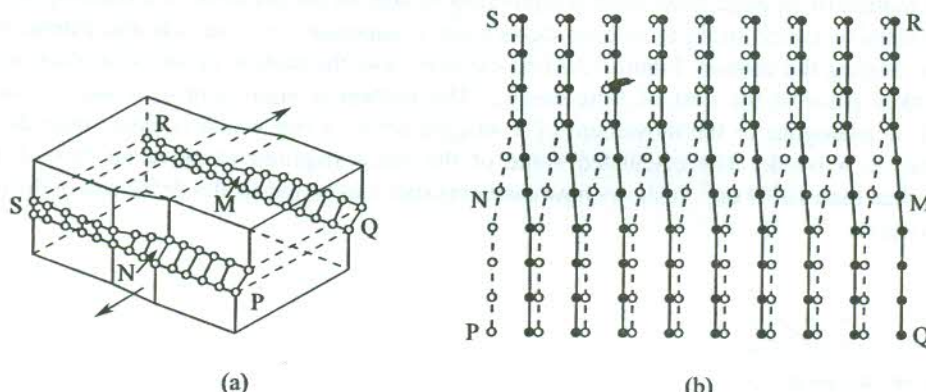


FIG. 12.23 (a) Displacement of a slip plane in a crystal containing a screw dislocation. A part PQMN of the slip plane is shown to have slipped in the direction parallel to the dislocation line MN. (b) The atoms (in a cubic structure) above and below PQRS. Full circles denote atoms above the plane PQRS and open circles denote atoms below the plane. [After A.H. Cottrell, *The Mechanical Properties of Matter* (John Wiley, 1964).]

Dislocations in real crystals are generally of mixed character. Proportions of the edge and screw characters vary as the dislocation bends in a different direction. The Burgers vector, however, remains unchanged throughout the length of the dislocation. The dislocation is either a closed or an open loop, terminating only on an outer surface or a grain boundary (to be defined in Section 12.4). The chemical etching is often helpful in locating the termination point of an open dislocation loop since

the etch prefers to attack the strained part revealing thereby an *etch pit*. These studies on tellurium single crystals made by Blakemore et al.[†] serve as an excellent proof to this effect.

With the application of mechanical stress, dislocations easily sweep through a crystal. A moving dislocation generates point defects until its movement is *pinned* either by impurities or by the path of some other dislocation (work hardening).

Dislocations have energies which do not favour their existence in the state of thermal equilibrium. They are introduced in a non-equilibrium state during the solidification of the crystal, and continue to exist at lower temperatures. A quantity, dislocation density (the number of dislocations crossing per unit area) is used as an indicator of the degree of imperfection of a crystal. The value ranges from 10^{15} or 10^{16} m^{-2} in heavily deformed metals to well below 10^5 m^{-2} in the best crystals of germanium and silicon. Common techniques employed for estimating dislocation densities are: electron microscopy, x-ray transmission and reflection, decoration and etch pits.

12.3 STRESS FIELDS OF DISLOCATIONS

With the knowledge of the magnitudes and directions of stresses introduced into an ideal crystal by the presence of a dislocation, the forces on a dislocation caused by the presence of another one can be calculated. This enables us to give a semi-quantitative description of the behaviour of dislocation networks. Since the calculations for screw dislocations are simpler, we derive the expressions for this case and only quote results for the edge dislocations.

Screw dislocation

Consider a cylindrical crystal that has been sheared in the axial direction. The shearing, as shown in Fig. 12.24, amounts to producing a screw dislocation along the crystal axis with Burgers vector \mathbf{b} . Since the original length (peripheral) that has undergone displacement is $2\pi r$, the shear strain would be

$$\gamma = \frac{b}{2\pi r} \quad (12.35)$$

Then, the corresponding shear stress is

$$\sigma = G\gamma = \frac{Gb}{2\pi r} \quad (12.36)$$

where G is the shear modulus.

We can express the elastic energy dE_S of the shell of volume dV caused by the presence of the dislocation as

$$dE_S = \frac{1}{2} G\gamma^2 dV$$

[†] J.S. Blakemore, et al., *J. Appl. Phys.*, **31**, 2226 (1960).

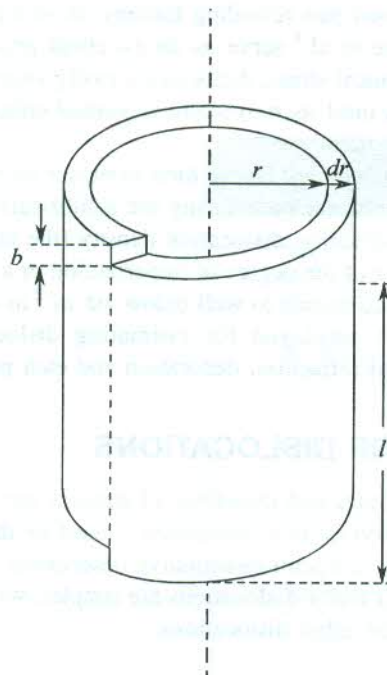


FIG. 12.24 Shell of a deformed cylindrical crystal surrounding a screw dislocation marked by the dotted line.

$$\begin{aligned}
 &= \frac{1}{2} G \left(\frac{b}{2\pi r} \right)^2 \cdot (2\pi r l dr) \\
 &= \left(\frac{Gb^2}{4\pi} \right) \frac{dr}{r} l
 \end{aligned} \tag{12.37}$$

This gives the elastic energy E_S per unit length of the screw dislocation as

$$\begin{aligned}
 E_S &= \int_{r_1}^{r_2} \left(\frac{Gb^2}{4\pi} \right) \frac{dr}{r} \\
 &= \left(\frac{Gb^2}{4\pi} \right) \ln \left(\frac{r_2}{r_1} \right)
 \end{aligned} \tag{12.38}$$

where r_1 and r_2 are the lower and upper limits for the radius of the cylinder, strained because of the presence of the dislocation. The choice of r_1 and r_2 is not obvious. Investigations suggest that little error would be introduced if we let $\ln \left(\frac{r_2}{r_1} \right) = 4\pi$ in relation (12.38). It gives

$$E_S \approx Gb^2 \tag{12.39}$$

Edge dislocation

In this the strain energy E_e per unit length is found as

$$E_e = \frac{Gb^2}{4\pi(1-\nu)} \ln \left(\frac{r_2}{r_1} \right) \quad (12.40)$$

where ν denotes the Poisson ratio which measures approximately ~ 0.3 for metals.

Using $\ln \left(\frac{r_2}{r_1} \right) = 4\pi$, in (12.40), we have

$$E_e \approx \frac{Gb^2}{1-\nu} \quad (12.41)$$

which is slightly higher than E_s .

The above mathematical exercise reveals two interesting features of dislocations:

- (i) The fact that the energy is proportional to b^2 , implies that dislocations with minimum possible b will be most stable, i.e. the most stable dislocations occur in directions of close packing.
- (ii) The energy increases with the length of the dislocation, meaning thereby that there is a ‘line tension’ along the dislocation. Since the elastic energy per unit length is equivalent to the force, the tension may be given by

$$T \approx Gb^2 \quad (12.42)$$

12.4 PLANAR IMPERFECTIONS: GRAIN BOUNDARIES

A junction of two single crystals of different orientations along a common planar surface is called a *grain boundary*. The grain boundary is characteristic of crystalline solids and is not found in amorphous materials. These planar imperfections are very common in polycrystalline materials which consist of a large number of crystals bound to one another along interfaces behaving as grain boundaries. When the difference in orientation of single crystals intervened by a grain boundary is small, we have a low-angle grain boundary. On annealing (cooling slowly), a random array of edge dislocations in a crystal often coalesce to develop low-angle grain boundaries. The movement involved in the process lowers the total energy of the crystal, showing thereby that the crystal prefers to be free of dislocations over the largest possible volume. The two common examples are the *tilt* and *twist* grain boundaries. The former is formed from a linear sequence of edge dislocations (Fig. 12.25) whereas the latter results from a sequence of screw dislocations. Generally, the low-angle grain boundaries are a mixture of these two.

Burgers gave a model for a symmetrical low-angle grain boundary as shown in Fig. 12.25. Denoting the average distance between the dislocations by D , the tilt angle θ is expressed as $\theta = b/D$, where b is the magnitude of the Burgers vector. This model is strongly supported by experiments. Vogel et al.* carried out x-ray and optical investigations of germanium single crystals

* F. L. Vogel, W.G. Pfann, H.E. Corey, and E.E. Thomas, *Phys. Rev.*, **90**, 489 (1953).

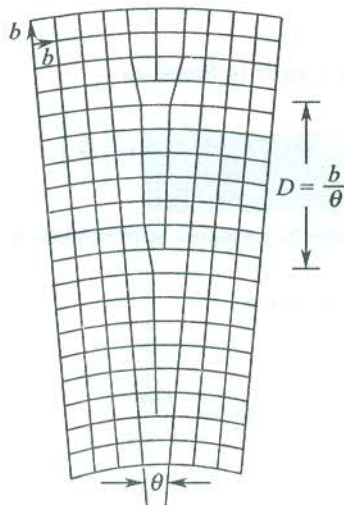
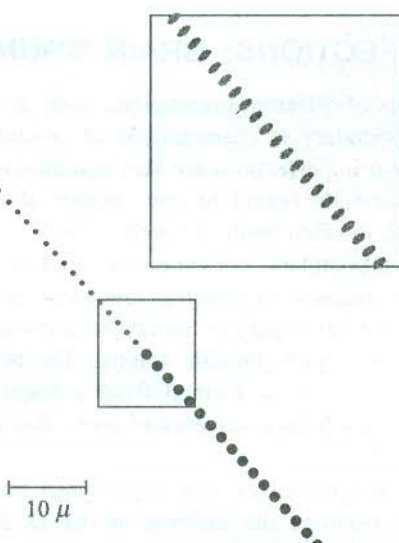


FIG. 12.25 View of a typical low-angle grain boundary.

and concluded that the results verified the model. A germanium crystal grown along the [100] direction from a seeded melt was etched with an acid to reveal the grain boundaries. The grain boundaries were found to consist of regularly spaced conical pits as evidenced in the optical micrograph (Fig. 12.26), recorded under high magnification. Each pit is believed to represent a single dislocation penetrating through the surface. The distance between the pits is obtained by counting and the angle θ determined from the x-ray diffraction measurements. Vogel and co-workers found the calculated and measured values of D and θ to be in a remarkably good agreement.

FIG. 12.26 Optical micrograph of lineage boundary in a germanium single crystal when viewed in the face, transverse to the growth direction. [After F.L. Vogel, W.G. Pfann, H.E. Corey, and E.E. Thomas, *Phys Rev.*, **90**, 489 (1953)].

Washburn and Parker[†] studied the motion of low-angle grain boundaries in zinc single crystals under the action of a suitable stress. They observed that the boundaries move normal to themselves and concluded that the low-angle grain boundaries can be interpreted as arrays of dislocations, supporting the view gathered from other investigations.

12.5 ROLE OF DISLOCATIONS IN CRYSTAL GROWTH

Consider the process of growing a large crystal by exposing a small piece of crystal to a vapour of the same atoms. The deposition of atoms at those lattice sites will be preferred whose surrounding sites are occupied in the original small crystal. This is so because of a relatively strong attractive force of neighbouring atoms in comparison with the weak attractive force to the surface of a perfect crystal. It means that the growth of a seed crystal is faster in the presence of an imperfection in the seed. Theoretical estimates of the growth rate for ideal crystals, especially in the condition of low supersaturation, are lower than the observed growth rates by many orders of magnitude. It is, perhaps, the largest ever recorded disagreement between theory and experiment. The fast observed growth rates are attributed to the presence of dislocations.

Frank* has compiled an excellent review of the phenomena under discussion here. The large disagreement recorded above is attributed, primarily to the difficulty of nucleating a new monolayer on a completed plane of a perfect crystal. But if the crystal contains a screw dislocation, the local helical mould in the growing crystal can wind endlessly about the screw dislocation like a spiral, without necessitating the nucleation of a new plane. A picture of such a growth pattern of a single screw dislocation in SiC crystal is shown in Fig. 12.27.

The development of a spiral step in the growth of a crystal having a screw dislocation is shown in Fig. 12.28. If the growth is taken as independent of the direction of the edge in the plane of the surface, the growth pattern would resemble an Archimedes spiral

$$r = a\theta \quad (12.43)$$

where a is a constant.

The level of supersaturation determines the limiting minimum value of curvature near the dislocation. A too small radius of curvature approaches the equilibrium curvature with the evaporation of an appropriate number of atoms on the curved edge. Each part of a step that is away from the origin acquires new atoms at a constant rate dr/dt . The growth of the crystal proceeds by virtue of rotation of the spiral at an angular speed $d\theta/dt$, which is required to be a constant for a uniform growth.

Whiskers

The kind of crystal growth we discussed above can lead to thin and long crystals wound around a single dislocation. We call them *whiskers*. The presence of a single axial screw dislocation in a whisker is unable to cause yielding, because in bending the crystal the direction of the shear stress on the dislocation is not parallel to its Burgers vectors. Hence, slip cannot occur for this direction of stress, endowing whiskers with elastic properties that are close to theoretical predictions for perfect crystals. Herring and Galt** measured a shear stress of the order of $G/100$ in whiskers of tin

[†] J. Washburn and E.R. Parker, *J. Metals*, **4**, 1076 (1952).

^{*} F.C. Frank, *Advances in Physics*, **1**, 91 (1952).

^{**} C. Herring and J.K. Galt, *Phys. Rev.*, **85**, 1060 (1952).



FIG. 12.27 Phase contrast micrograph of spiral growth pattern in SiC crystal of 126 R unit cell modification (rhombohedral). Step height, $h = 109 \pm 5 \text{ \AA}$ (Mag. $\times 90$). (Courtesy A.R. Verma)

of radius $\sim 1 \mu\text{m}$. This value is about 1000 times more than that in bulk tin, giving credence to the theoretical estimates for perfect crystals [$\sim G/30$, as mentioned in Section 12.2.1].

12.6 STRENGTH OF ALLOYS

There are other important properties of solids that can be manipulated to advantage by exploiting the characteristics of dislocations. Strength of engineering materials is one such example. On account of their wide ranging applications, alloys attract special attention in this regard. Realizing that the motion of dislocations under the action of a deforming force is the main cause of weakness of crystals, the following methods are used to raise the yield strength of alloys:

1. The dislocations are mechanically blocked by introducing tiny particles of a second phase into the crystal lattice. For example, in the hardening of steel, particles of iron carbide are precipitated into iron. Similarly, particles of Al_2Cu are precipitated into aluminium for hardening of aluminium.
2. The dislocations are pinned in solid solutions by solute atoms. Since a foreign atom prefers

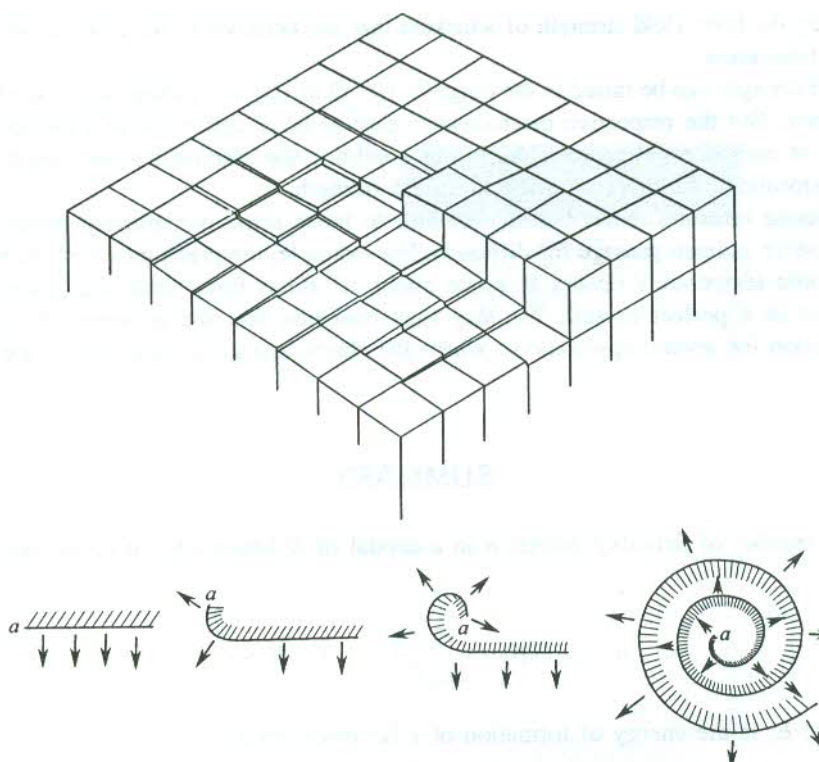


FIG. 12.28 The intersection of a screw dislocation with a free surface to produce a spiral step. [After F.C. Frank, *Discussions Faraday Soc.*, **5**, 48 (1949).]

to dissolve itself near a dislocation than elsewhere, the pinning is easily accomplished by this method.

3. Slip can be impeded by short range or local order, found in most of the concentrated solid solutions. When the number of like neighbour bonds in an alloy is different from that expected statistically, the alloy can have only short range order. A disordered phase is first produced by quenching (cooling quickly) from a high temperature and then some ordering is introduced by heat treatment at a lower predetermined temperature. This produces a sizable increase in strength, something impossible in the presence of long range order. In a long range order, atoms of one kind occupy preferred lattice sites and a super lattice is produced where correlation occurs over many lattice sites that is conducive to slip. The order-hardening in 18 carat gold is accomplished by the precipitation of an ordered AuCu phase.
4. Crystalline materials gain in strength even when they are highly enriched with dislocations. Large dislocation densities make it more difficult for a dislocation to move across a slip plane which at these densities is threaded by many dislocations. The method, known as *work-hardening* or *strain-hardening* is, however, useful at temperatures low enough so as not to allow annealing.

In addition, the yield strength may also be increased by preparing dislocation-free crystals. Such a perfection in crystal growth is attainable to some extent only in crystals of small size. This is

exemplified by the high yield strength of whiskers that are believed to have grown around a single axial-screw dislocation.

The yield strength can be raised to the range of 10^{-3} G to 10^{-2} G by using any of the four methods described above. But the respective mechanisms cease to be effective above a certain temperature where diffusion rates become appreciable. In this condition the precipitated particles that hinder the motion of dislocations dissolve, lowering the yield strength.

Fast diffusion rates are, nevertheless, welcome to boost some precipitation reactions in solids. Dislocations serve as open passage for diffusion. For example, the precipitation of tin from lead-tin solution at room temperature occurs at a rate about 10^8 times faster than what may be expected from diffusion in a perfect crystal. We may thus conclude that the presence of dislocations in crystals is a boon for several applications, where the characteristics of dislocations are exploited to advantage.

SUMMARY

1. The number of Schottky defects n in a crystal of N lattice sites at temperature T is given by

$$n = N \exp\left(-\frac{E_v}{2k_B T}\right) \quad \text{for } N \gg n$$

where E_v is the energy of formation of a Schottky defect.

2. The number of Frenkel defects in a crystal of N lattice sites and N_i interstitial sites at temperature T is given by

$$n = (NN_i)^{1/2} \exp\left(-\frac{E_i}{2k_B T}\right) \quad \text{for } n \ll N, N_i$$

where E_i is the energy required for removing an atom from a lattice site to an interstitial position.

3. Diffusion constant at a temperature T is given by

$$D = (v_0 a^2) \exp\left(-\frac{E_a}{k_B T}\right)$$

where v_0 is the characteristic atomic vibration frequency, a is the lattice constant and E_a the activation energy.

4. The energy of a Frenkel exciton is

$$\epsilon_k = \epsilon + 2\epsilon_T \cos ka$$

where ϵ is the excitation energy of the free atom and ϵ_T denotes the rate at which the energy from an excited atom is transferred to its neighbours.

5. The binding energy of a Mott-Wannier exciton is

$$E_x = - \frac{1}{n^2} \frac{\mu e^4}{32 \pi^2 \epsilon_0^2 \epsilon_s^2 \hbar^2}$$

with $\frac{1}{\mu} = \frac{1}{m_e^*} + \frac{1}{m_h^*}$

6. The theoretical critical shear stress for perfect crystals is given by

$$\sigma_c \cong \frac{1}{4} \left(\frac{a}{d} \right) G$$

where

a is the atomic separation in a plane

d is the interplanar spacing

G is the shear modulus

The more reasonable estimate of the ideal sheer stress is $G/30$, with $G = 10^{10}$ to 10^{11} N m $^{-2}$.

7. The strain energy per unit length of a screw dislocation, $E_s \cong Gb^2$ where b is the magnitude of the Burgers vector.

The strain energy per unit length of an edge dislocation is

$$E_e \cong \frac{Gb^2}{1-\nu}, \text{ where } \nu \text{ is the Poisson ratio.}$$

PROBLEMS

- 12.1 Calculate the atomic percentage of interstitials and vacancies at the melting point in copper. Take the formation energies, respectively, as 4.5 and 1.5 eV.
- 12.2 A perfect crystal of KCl is doped with 10^{24} CaCl₂ molecules per m³. Estimate the fractional change of density assuming that (a) no vacancies are introduced owing to doping, (b) one positive ion vacancy is created for each CaCl₂ molecule.
- 12.3 Given that the energy required to remove a sodium atom from the inside of a sodium crystal to the boundary is 1 eV, calculate the number of Schottky vacancies at room temperature. Assuming that a neighbouring sodium atom has to cross over a potential barrier of 0.5 eV and the atomic vibration frequency be 10^{12} , calculate the diffusion coefficient for radioactive sodium in normal sodium at room temperature.
- 12.4 If the energy required to create a vacancy in a solid be 2 eV, show that the relative density of vacancies to atoms will always be less than 10^{-8} per cent unless the melting point is higher than 1000 K.
- 12.5 Show that in a crystal having N lattice points and N' possible interstitial positions, the number n of Frenkel defects in equilibrium condition is given by

$$E_i = k_B T \ln \left[\frac{(N - n)(N_i - n)}{n^2} \right]$$

Show further that for $n \ll N, N_i$

$$n \approx (NN_i)^{1/2} \exp \left(-\frac{E_i}{2k_B T} \right)$$

where E_i denotes the energy required for removing an atom from a lattice site to an interstitial position.

- 12.6 Apply simple Bohr model to predict the energy of the F -centre absorption in KCl, taking $1s \rightarrow 2p$ as the absorption transition. The refractive index of KCl is 1.49.
- 12.7 What is the smallest Burgers vector parallel to a [111] direction that a dislocation in an FCC crystal may have?
- 12.8 A crystalline cube of side L contains an edge dislocation with Burgers vector \mathbf{b} . It is subjected to a shear stress σ on the upper and lower faces in the direction of slip. On energy balance consideration show that the magnitude of force \mathbf{F} on the dislocation per unit length is given by $F = b\sigma$.
- 12.9 A single crystal of copper has a low angle tilt boundary on (010) plane with the tilt axis parallel to the [001] direction. If the spacing of dislocations in the boundary is 1.5×10^{-6} m, determine the tilt angle.
- 12.10 The elastic displacement round an isolated dislocation of Burgers vector \mathbf{b} is $\mathbf{b}\theta/2\pi$, where θ is the angular coordinate around the dislocation line. Show that two parallel dislocations with Burgers vectors \mathbf{b}_1 and \mathbf{b}_2 and a distance r apart in a crystal of shear modulus G repel each other with a force whose magnitude per unit length is approximately given by $Gb_1b_2/2\pi r$.

SUGGESTED FURTHER READING

- Farge, Y. and M. Fontana, *Electronic and Vibrational Properties of Point Defects in Ionic Crystals* (North-Holland, 1979).
- Flynn, C.P., *Point Defects and Diffusion* (Oxford, 1972).
- Friedel, J., *Dislocations* (Pergamon Press, 1964).
- Hull, D. and D.J. Bacon, *Introduction to Dislocations*, 3rd ed. (Pergamon Press, 1984).
- Markham, J.J., *F-Centres in Alkali Halides* (Academic Press, 1966).
- Nabarro, F.R.N., *Theory of Crystal Dislocations* (Dover, 1987).
- Schulman, J.H. and W.D. Compton, *Color Centres in Solids* (Pergamon Press, 1962).
- Whelan, M.J., *Worked Examples in Dislocations* (Institute of Metals, 1990).

Diamagnetism and Paramagnetism

Unlike the dielectric response, the magnetic response of most of the solids is dominated by permanent dipoles. The existence of magnetic dipoles, whether permanent or induced, can be explained only on the basis of quantum theoretical considerations. If we regard matter as made up of charged particles, there can be no magnetic moment in the state of thermal equilibrium of a strictly classical system even in the presence of an applied magnetic field. Thus magnetism is essentially a quantum effect. The two fundamental forms of magnetism, *diamagnetism* and *paramagnetism*, have their origin in induced and permanent magnetic moments, respectively. The impossibility of magnetism in the domain of classical physics may be argued in the following way. As the magnetic field is switched on, the electronic circulating currents having an associated magnetic moment are induced in the system. But these currents are destroyed by collisions in tending to bring the system finally to the state of thermal equilibrium.

None of the derivations of relations in classical physics including those for magnetic susceptibility is self-consistent. The permanent atomic magnetism (paramagnetism) cannot be accounted for without restricting the circulating electrons to the discrete stationary orbits as required in the Bohr's quantum theoretical model of the hydrogen atom. In the classical picture, there can be no magnetic moment associated with the current of circulating electrons because electrons in accelerated motion would radiate and finally fall on the nucleus, causing the atomic structure to collapse. Diamagnetism, where the applied magnetic field is pushed out of the system, can be appreciated similarly by realizing that the discrete quantum states occupied by electrons are stable to a certain extent only against external perturbations, like the magnetic field in the present case.

We define below the fundamental physical quantities that concern the magnetic properties of materials. In vacuum, the intensity of the applied magnetic field \mathbf{H} and the magnetic induction \mathbf{B} are related by the equation

$$\mathbf{B} = \mu_0 \mathbf{H} \quad (13.1)$$

where μ_0 is the permeability of free space ($\mu_0 = 4\pi \times 10^{-7} \text{ V s/A m}$).

The magnetic state of a system is specified by its magnetization \mathbf{M} , defined as the magnetic moment per unit volume. \mathbf{M} is related to \mathbf{B} and \mathbf{H} by

$$\mathbf{B} = \mu_0(\mathbf{H} + \mathbf{M}) \quad (13.2)$$

For convenience in discussions it is a practice to introduce an external induction such that

$$\mathbf{B}_0 = \mu_0 \mathbf{H} \quad (13.3)$$

Mostly, there is a linear relationship between \mathbf{B}_0 and \mathbf{M} given by

$$\mu_0 \mathbf{M} = \chi \mathbf{B}_0 \quad (13.4)$$

Since \mathbf{r} is perpendicular to linear velocity (say, \mathbf{v}), (13.6) may be rewritten as

$$\begin{aligned}\mu_l &= -\left(\frac{e}{2m}\right)(\mathbf{r} \times \mathbf{p}) \\ &= -\left(\frac{e}{2m}\right) (\text{orbital angular momentum})\end{aligned}\quad (13.7)$$

where e is the electronic charge, m the electron mass, and \mathbf{p} its linear momentum.

Using simple methods of Newtonian mechanics, we can study the motion of an electron within an atom or ion in the presence of a steady magnetic field. The characteristic feature of the motion in this condition is that the plane of the electron orbit precesses about the direction of the magnetic field [see Fig. 13.1(a)]. This amounts to precession of the orbital angular momentum vector \mathbf{l} associated with the electron motion around the central nucleus [see Fig. 13.1(b)]. The precession is superposed on the electron's orbital motion in the central field of the nucleus which to a first order in the magnetic field remains almost the same as in the absence of the magnetic field. The frequency of precession is, however, much smaller than the frequency of the orbital motion of the electron. The precession is called the 'Larmor precession'.

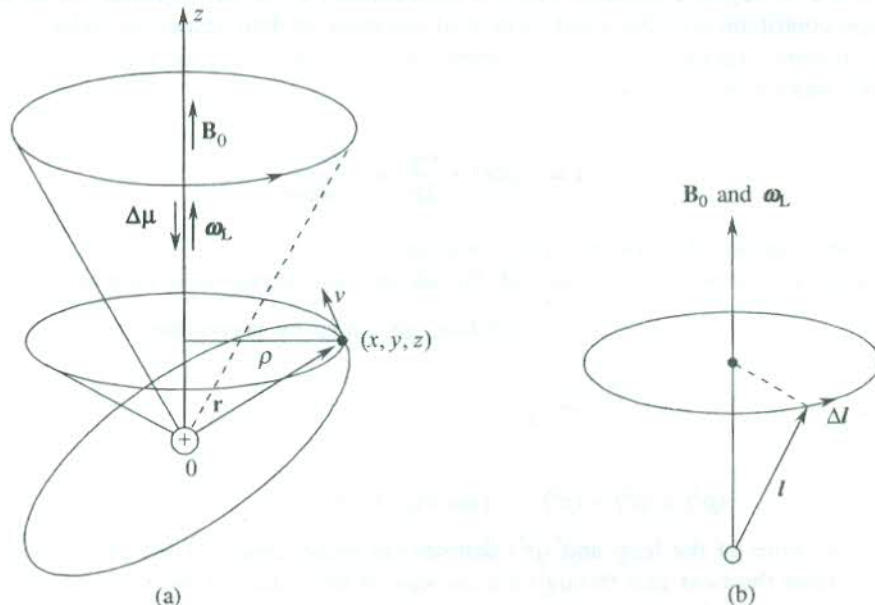


FIG. 13.1 Effect of the magnetic field on orbital motion of an electron. The field \mathbf{B}_0 is perpendicular to the orbit plane: (a) The precession of the electron orbit. ω_L denotes the angular frequency of precession and $\Delta\mu$ denotes the induced magnetic moment. (b) The precession of the angular momentum \mathbf{l} in the field.

The magnetic moment associated with the orbital angular momentum \mathbf{l} according to (13.7) is

$$\mu_l = -\left(\frac{e}{2m}\right) \mathbf{l} \quad (13.8)$$

This dipole, when acted upon by a magnetic field \mathbf{B}_0 (actually the magnetic induction), experiences a torque given by

$$\frac{d\mathbf{l}}{dt} = \mu_l \times \mathbf{B}_0 = \left(\frac{e}{2m} \right) \mathbf{B}_0 \times \mathbf{l} \quad (13.9)$$

The above equation that serves as the equation of motion of \mathbf{l} is a well-known equation in mechanics, describing precession of the characteristic angular frequency

$$\omega_L = \frac{eB_0}{2m} \quad (13.10)$$

where ω_L is commonly known as the 'Larmor frequency'.

Alternatively, the vector relationships as depicted in Fig. 13.1(b) give

$$\Delta\mathbf{l} = \omega_L \times \mathbf{l} \cdot dt \quad (13.11)$$

On comparing (13.11) with (13.9), we reproduce the value of ω_L as given by (13.10).

The precession of the electron orbit produces its own loop current and, therefore, magnetic moment. It is this magnetic moment which is responsible for the diamagnetism of an atom or ion. The average contribution of the usual motion of electrons in their respective orbits is zero in this model, as already explained. The loop current in the atomic or ionic system produced by the precessional motion is

$$I = -(Ze) \times \frac{\omega_L}{2\pi} = -\frac{Ze^2 B_0}{4\pi m} \quad (13.12)$$

where Z is the number of electrons in the atom or ion.

The magnetic moment associated with the above loop current is written as

$$\mu = I \times \text{area of the loop generated by precession}$$

$$= -\frac{Ze^2 B_0}{4m} \langle \rho^2 \rangle \quad (13.13a)$$

with

$$\langle \rho^2 \rangle = \langle x^2 \rangle + \langle y^2 \rangle \quad [\text{see Fig. 13.1(a)}] \quad (13.13b)$$

Here ρ is the radius of the loop and $\langle \rho^2 \rangle$ denotes the mean square of the perpendicular distance of electrons from the field axis through the nucleus. If the radius of the orbit around the nucleus be r , the mean square distance of electrons from the nucleus is given by

$$\langle r^2 \rangle = \langle x^2 \rangle + \langle y^2 \rangle + \langle z^2 \rangle \quad (13.14)$$

When the charge distribution is spherically symmetric,

$$\langle x^2 \rangle = \langle y^2 \rangle = \langle z^2 \rangle \quad (13.15)$$

Then, using (13.14) and (13.15) in (13.13b), we get

$$\langle \rho^2 \rangle = \frac{2}{3} \langle r^2 \rangle \quad (13.16)$$

Substituting this value of $\langle \rho^2 \rangle$ in (13.13a), we get the following expression for the magnetization

$$\mathbf{M} = - \frac{NZe^2\mathbf{B}_0}{6m} \langle r^2 \rangle \quad (13.17)$$

where N is the number of atoms per unit volume of the system and Z is the atomic number.

Then, the diamagnetic susceptibility is expressed as

$$\chi = \frac{\mu_0 \mathbf{M}}{\mathbf{B}_0} = - \frac{\mu_0 NZe^2}{6m} \langle r^2 \rangle \quad (13.18)$$

The relation (13.18) is known as the Langevin's relation for the diamagnetic susceptibility. The diamagnetic susceptibility of isolated atoms or ions can be calculated with the knowledge of $\langle r^2 \rangle$ whose appropriate determination is feasible only in a quantum mechanical approach. van Vleck* has discussed some other models of intricate nature, including the diamagnetism of molecules with electron-pair bonds.

For typical densities and orbital sizes of electrons in solids, relation (13.18) gives a susceptibility of approximately -10^{-5} . This is fairly comparable with the measured values which for a few materials are given below:

Materials	Bi	Hg	Ga	Cu	Si
χ	-1.6×10^{-4}	-2.9×10^{-5}	-2.3×10^{-5}	-9.5×10^{-6}	-4.2×10^{-6}

Diamagnetism is an essential property of all substances. On account of being weak, it is masked in paramagnetic materials under the background of their positive susceptibility.

13.2 LANGEVIN'S THEORY OF PARAMAGNETISM

The classical treatment of paramagnetism is also due to Langevin. Consider a solid containing N magnetic atoms per unit volume, each bearing a magnetic moment μ . An assembly of randomly oriented magnetic moments (dipoles) defines the ground state of this solid in the absence of a magnetic field. The energy of a dipole in the magnetic field \mathbf{B}_0 is

$$U = -\mu \cdot \mathbf{B}_0 \quad (13.19)$$

Any increase in the magnetic field should produce preferential orientation of the dipoles with the field. This orientation at the same time is resisted by the thermal disorder in the solid. The orientation produces the magnetization \mathbf{M} whose magnitude in the state of thermal equilibrium may be expressed as

$$\mathbf{M} = N\mu \overline{\cos \theta} \quad (13.20)$$

where $\overline{\cos \theta}$ is the average over a distribution in thermal equilibrium, θ being the angle between μ and \mathbf{B}_0 .

Using the Boltzmann statistical law of distribution, the relative probability of finding a dipole in an element of solid angle $d\Omega$ is expressed as $\exp\left(-\frac{U}{k_B T}\right)$ and

* J.H. van Vleck, *The Theory of Electric and Magnetic Susceptibilities* (Oxford, 1952).

$$\overline{\cos \theta} = \frac{\int \exp\left(-\frac{U}{k_B T}\right) \cos \theta d\Omega}{\int \exp\left(-\frac{U}{k_B T}\right) d\Omega} \quad (13.21)$$

Since the limits of integration must include all solid angles,

$$\overline{\cos \theta} = \frac{\int_0^\pi 2\pi \sin \theta \cos \theta \exp\left(\frac{\mu B_0 \cos \theta}{k_B T}\right) d\theta}{\int_0^\pi 2\pi \sin \theta \exp\left(\frac{\mu B_0 \cos \theta}{k_B T}\right) d\theta}$$

Letting $\cos \theta = x$, and $\frac{\mu B_0}{k_B T} = a$

$$\begin{aligned} \overline{\cos \theta} &= \frac{\int_{-1}^1 x \exp(ax) dx}{\int_{-1}^1 \exp(ax) dx} = \frac{d}{da} \ln \int_{-1}^1 \exp(ax) dx \\ &= \coth a - \left(\frac{1}{a}\right) \\ &\equiv L(a) \end{aligned} \quad (13.22)$$

where $L(a)$ is called the 'Langevin function'.

Then, from (13.20)

$$M = N \mu L(a) \quad (13.23)$$

A schematic plot of the Langevin function $L(a)$ is given in Fig. 13.2, showing that it saturates when a or $\frac{\mu B_0}{k_B T} \gg 1$. It suggests that the saturation can be easily achieved at low temperatures.

The initial slope is linear as indicated by the dashed line. In this region, $\frac{\mu B_0}{k_B T} \ll 1$ or $\mu B_0 \ll k_B T$

that conforms to the use of low magnetic fields at which the experiments are done. For $B = 1$ T and μ of the order of a Bohr magneton (10^{-23} J/T), $\mu B_0 = 10^{-23}$ J which is about one hundredth of $k_B T$ at room temperature ($\sim 10^{-21}$ J). Thus the initial linear part of the curve, ideally refers to the experimental conditions at room temperature. The value of $L(a)$ in this limit ($a \ll 1$) comes to $a/3$.

Therefore, using $L(a) \approx \frac{a}{3} = \frac{\mu B_0}{3k_B T}$ in (13.23), we get

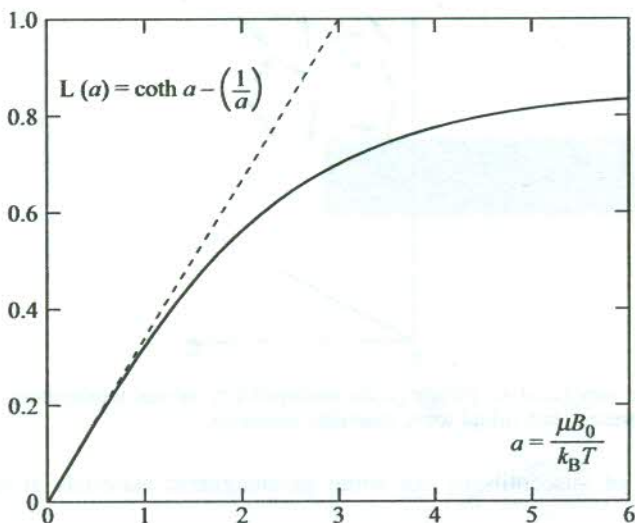


FIG. 13.2 Variation of Langevin function $L(a)$ as a function of $a = \frac{\mu B_0}{k_B T}$. The dashed line indicates the initial slope.

$$M = \frac{N\mu^2 B_0}{3k_B T} \quad (13.24)$$

and

$$\chi = \frac{\mu_0 M}{B_0} = \frac{\mu_0 \mu^2 N}{3k_B T} \quad (13.25)$$

or

$$\chi = \frac{C}{T} \quad (13.26)$$

with

$$C = \frac{\mu_0 \mu^2 N}{3 k_B} \quad (13.27)$$

Relation (13.26) is called the ‘Curie law’ and C is known as the ‘Curie constant’. According to the Curie law, the plot of $1/\chi$ versus T is a straight line as shown in Fig. 13.3. While the law is obeyed in a large number of paramagnetic solids, deviations at low temperatures are observed in some others. The deviations can be justified on the ground that the dipolar orientation is complicated by the rules of quantum mechanics in respect of the space quantization of angular momentum.

With $N = 5 \times 10^{28} \text{ m}^{-3}$ and $\mu = 1 \text{ Bohr magneton}$, we have

$$\chi = \frac{0.13}{T} \quad (13.28)$$

The numbers obtained from (13.28) are of the order of the typical measured values. The

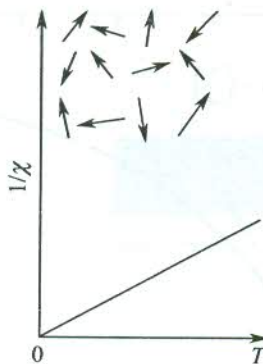


FIG. 13.3 Plot of the reciprocal of paramagnetic susceptibility versus temperature. The randomly oriented arrows represent individual ionic magnetic moments.

experimental values of susceptibility for some paramagnetic materials at room temperature are given below:

Material	Cr	Al	Ca	Na	O ₂ (at NTP)
χ	$+2.7 \times 10^{-4}$	$+2.2 \times 10^{-5}$	$+1.9 \times 10^{-5}$	$+9.1 \times 10^{-6}$	$+1.9 \times 10^{-6}$

13.3 THEORY OF ATOMIC MAGNETIC MOMENT

In this section we apply the principles of quantum theory to calculate the atomic magnetic moment. We begin by subjecting the electrons of an atom or ion to the Bohr's quantization condition, according to which their orbital angular momentum is constrained to be a multiple of \hbar . This requires (13.8) to be written as

$$\begin{aligned} \mu &= -\left(\frac{e\hbar}{2m}\right)l; \quad \text{with } (\mathbf{r} \times \mathbf{p}) = \hbar l \\ &= -\mu_B l \end{aligned} \quad (13.29)$$

where l denotes the orbital angular momentum of an electron, and

$$\begin{aligned} \mu_B &= \frac{e\hbar}{2m} = 5.7884 \times 10^{-5} \text{ eV/T} \\ &= 9.2742 \times 10^{-24} \text{ J/T} \end{aligned} \quad (13.30)$$

Here μ_B is called the 'Bohr magneton'. According to (13.29) the magnetic moment associated with the orbital motion is a multiple of the Bohr magneton.

The magnetic moment caused by electron spin can be calculated similarly. It may not be out of place to remind readers that the electron spin is purely a quantum mechanical concept. It is simply impossible to provide an interpretation to it that may conform to any form of motion we come across in our day-to-day life. The spin quantum number $s = \pm 1/2$ characterizes the angular momentum associated with the electron spin. It is a standard practice to express spin magnetic moment as

$$\mu_s = -g_0\mu_B s \quad (13.31)$$

where the quantity g_0 is called the electronic *g*-factor. The above relation is often used to define the Bohr magneton. Because $g_0 = 2.0023$ for a free electron, one Bohr magneton is taken as almost an exact measure of the magnetic moment of a spinning electron.

For the calculation of the magnetic moment of an atom or ion which generally has more than one electron, we require to determine the total angular momentum. This is accomplished by combining vectorially the individual orbital and spin angular momenta by following either the L-S coupling or the J-J coupling scheme, whichever may be valid for the element of the atom under consideration. The two schemes have been tested for all the elements of the periodic table and the response in this respect may be found in standard books on atomic physics. Suppose, we have a case for the L-S coupling (also known as the Russel-Saunders coupling) to be used. In this scheme, the orbital quantum numbers of individual electrons are added vectorially to get the net orbital angular momentum as $\hbar\mathbf{L}$ ($= \hbar \sum_i \mathbf{l}_i$). Similarly, the vectorial combination of individual spin quantum numbers gives the gross spin angular momentum expressible as $\hbar\mathbf{S}$ ($= \hbar \sum_i \mathbf{s}_i$). Then, the total angular momentum is written as

$$\hbar\mathbf{J} = \hbar\mathbf{L} + \hbar\mathbf{S} \quad (13.32)$$

where J denotes the total angular momentum quantum number. The associated atomic or ionic magnetic moment μ precesses around the direction of \mathbf{J} . The μ is customarily related to \mathbf{J} as*

$$\begin{aligned} \mu &= -\mu_B(\mathbf{L} + g_0\mathbf{S}) \\ &= -g\mu_B \mathbf{J} \end{aligned} \quad (13.33a)$$

with

$$\mathbf{L} + g_0\mathbf{S} = g\mathbf{J} \quad (13.33b)$$

where g is called the Landé splitting factor.

For the Russel-Saunders type of coupling[†] (or L-S coupling), the Landé splitting factor is given by

$$g = 1 + \frac{J(J+1) + S(S+1) - L(L+1)}{2J(J+1)} \quad (13.34)$$

If we take the value of g_0 as 2.0000 instead of 2.0023, to a good approximation the magnetic moment may be expressed as

$$\mu = -\mu_B(\mathbf{L} + 2\mathbf{S}) \quad (13.35)$$

The above discussion suggests that the presence of a permanent magnetic moment is crucial to the magnetic behaviour of a system. This concerns atoms or ions with partially filled shells. The magnetic moment of a system can be estimated by calculating L and S (hence J) of individual atoms or ions of the system. It is accomplished with the help of the Pauli exclusion principle and the

* Relation (13.33b) is valid only within the $(2J+1)$ dimensional set of states that form the degenerate atomic ground state in the absence of a magnetic field. For details, see N.W. Ashcroft and N.D. Mermin, *Solid State Physics*, Ch. 31, p. 654 (Saunders College, 1988).

[†] We must appreciate that J is always a good quantum number of an atom. But, if L-S coupling (the spin-orbit coupling) is insignificant, L and S can also be good quantum numbers. In this limit, the Hamiltonian of the atom can be taken to commute with \mathbf{L} and \mathbf{S} as well as with \mathbf{J} . Hence the states of the atom can be described by quantum numbers L, L_z, S, S_z, J and J_z , indicating that they are eigenstates of the operators $\mathbf{L}^2, \mathbf{L}_z, \mathbf{S}^2, \mathbf{S}_z, \mathbf{J}^2$ and \mathbf{J}_z with eigenvalues $L(L+1), L_z, S(S+1), S_z, J(J+1)$, and J_z , respectively.

Hund's rules that describe the manner in which the electrons are assigned to various quantum states within a partially-filled shell of an atom or ion in its ground state.

13.3.1 Hund's Rules

Quantum numbers for the spin, orbital, and total angular momentum in the ground state of an atom or ion with a partially-filled shell are derived by applying the following rules:

The first rule. The electron spins are added so as to get the maximum possible S , as permitted by the Pauli principle.

The second rule. The orbital momenta are combined to get the maximum value for L that is consistent with S determined by the first rule.

The third rule. For a partially-filled shell,

$$J = L - S \text{ for a shell less than half-filled}$$

$$= L + S \text{ for a shell more than half-filled}$$

A few examples are discussed below to illustrate the application of the Hund's rules.

Example 1. Consider the Cr^{3+} ion which is a transition metal ion of the iron group. Its $3d$ shell is partially filled and contains 3 electrons, i.e. short of 7 electrons to be completely occupied. In this case $l = 2$; so the allowed m_l values [$(2l + 1)$ in number] are: 2, 1, 0, -1, -2, characterizing five different degenerate orbitals. For the maximum values of S and L , as required under the first and second rules, the filling of electrons in the orbitals is as follows:

m_l	2	1	0	-1	-2
	↑	↑	↑		

where (\uparrow) denotes an electron with $m_s = +1/2$

The above filling arrangement gives

$$L = \sum m_l = 3 \text{ (the sum is taken over the occupied orbitals)}$$

$$S = \sum m_s = 3/2$$

Since the shell is less than half-filled, in accordance with the third rule, we have

$$J = L - S = 3/2$$

The energy states are conventionally designated as

$$M_{X_A}$$

where $M = (2S + 1)$, the multiplicity

$A = J$, the total angular momentum quantum number

$$X = S \quad P \quad D \quad F \quad G \quad H \dots$$

for $L = 0 \quad 1 \quad 2 \quad 3 \quad 4 \quad 5 \dots$

Because our calculations are for the ground state, the ground state of Cr^{3+} ion is ${}^4F_{3/2}$.

Example 2. Let us take the next example of a rare earth ion, Ho^{3+} in which $4f^{10}$ represents the electronic configuration of the incomplete shell ($4f$). For this shell, $l = 3$, therefore, the filling of electrons in various allowed orbitals can be shown as

m_l	3	2	1	0	-1	-2	-3
	$\downarrow\uparrow$	$\downarrow\uparrow$	$\downarrow\uparrow$	\uparrow	\uparrow	\uparrow	\uparrow

This gives $L = 6$ and $S = 2$. Since the shell is more than half-filled, $J = 6 + 2 = 8$. Thus the ground state is 5I_8 .

Example 3. We take an interesting case where an ion is short of one electron to make it half-filled. Consider Mn^{3+} or Cr^{2+} whose 3d shell has four electrons with the filling as shown below:

m_l	2	1	0	-1	-2
	\uparrow	\uparrow	\uparrow	\uparrow	

Therefore, $L = 2$ and $S = 2$. According to Hund's third rule, $J = L - S = 0$, giving the ground state as 3D_0 .

Examples 1 and 2 deal with ions having a non-vanishing total angular momentum. These ions, as expected, show paramagnetic behaviour. On the other hand, Example 3 gives a case where an ion with a partially filled shell has no net angular momentum, a situation similar to that with ions having only completely-filled shells. In this case both L and S are independently nonzero unlike in the latter case where both of these are independently zero. As we will see later in Section 13.5, the atoms or ions in Example 3 show a second-order paramagnetism. It is regarded as a correction to the diamagnetic term, though of opposite sign. The susceptibility associated with this correction at low temperatures is found to be temperature independent. It is famous in literature as van Vleck paramagnetism.

13.4 QUANTUM THEORY OF MAGNETIC SUSCEPTIBILITY: A QUANTUM MECHANICAL FORMULATION

Magnetization (also known as the intensity of magnetization) of a quantum mechanical system having N magnetic ions per unit volume at $T = 0$ is defined as

$$M(B_0) = -N \frac{\partial E_0(B_0)}{\partial B_0} \quad (13.36)$$

where $E_0(B_0)$ is the ionic ground state energy in the presence of the field B_0 .

In the state of thermal equilibrium at temperature T , the thermal average of the magnetization of each excited state of energy $E_n(B_0)$ gives the measure of magnetization, i.e.

$$M(B_0, T) = \frac{\sum_n M_n(B_0) \exp\left(-\frac{E_n}{k_B T}\right)}{\sum_n \exp\left(-\frac{E_n}{k_B T}\right)} \quad (13.37)$$

where

$$M_n(B_0) = -N \frac{\partial E_n(B_0)}{\partial B_0} \quad (13.38)$$

The thermodynamical definition of magnetization is given as

$$M = -N \frac{\partial F}{\partial B_0} \quad (13.39)$$

where F is the magnetic Helmholtz free energy. The free energy F is defined by the well-known rule of statistical mechanics written as

$$\exp\left(-\frac{F}{k_B T}\right) = \sum_n \exp\left[\frac{-E_n(B_0)}{k_B T}\right] \quad (13.40)$$

The general definition of susceptibility gives

$$\chi = \mu_0 \frac{\partial M}{\partial B_0} = -\mu_0 N \frac{\partial^2 F}{\partial B_0^2} \quad (13.41)$$

But, in most of the cases, M is found to be very accurately linear in B_0 for attainable field strengths. In such a case, the definition of χ reduces to

$$\chi = \frac{\mu_0 M}{B_0} \quad [\text{see (13.5)}]$$

The theory discussed so far makes it abundantly clear that the determination of energy shifts of various ionic states induced by a magnetic field is a prerequisite to the calculation of susceptibility. The exercise is carried out below in a quantum mechanical approach.

The part of the Hamiltonian operator of the energy of an atomic dipole in a magnetic field \mathbf{B}_0 owing to its orbital magnetic moment $\boldsymbol{\mu}_L$ is

$$\Delta H_L = -\boldsymbol{\mu}_L \cdot \mathbf{B}_0 = \mu_B L \cdot \mathbf{B}_0 \quad (13.42)$$

Similarly, the interaction energy owing to electron spin gives another term in the Hamiltonian operator as

$$\Delta H_S = -\boldsymbol{\mu}_S \cdot \mathbf{B}_0 = g_0 \mu_B \mathbf{S} \cdot \mathbf{B}_0 = g_0 \mu_B S_z B_0 \quad (13.43)$$

where

$$\mathbf{S}_z = \sum_i \mathbf{s}_z^i \quad \text{with } \mathbf{s}_z^i = \frac{1}{2} \boldsymbol{\sigma}_i \quad (\boldsymbol{\sigma}_i \text{ is a Pauli spin matrix})$$

It is assumed here that the magnetic field is applied along the z -direction. In the presence of a magnetic field, the linear momentum of an electron is given by

$$\mathbf{p}_{\text{field}} = \mathbf{p} + e\mathbf{A}(\mathbf{r}) \quad (13.44)$$

where \mathbf{p} is the linear momentum of the electron in the absence of the field and \mathbf{A} denotes the vector potential of the field to which it is related as

$$\mathbf{B}_0 = \text{curl } \mathbf{A} \quad \text{with } \text{div } \mathbf{A} = 0 \quad (13.45)$$

For a homogeneous field, a possible choice of the vector potential is

$$\mathbf{A} = -\frac{1}{2} \mathbf{r} \times \mathbf{B}_0 \quad (13.46)$$

As a result, we can write the kinetic energy part of the Hamiltonian as

$$\begin{aligned} H_{\text{kin}} &= \frac{1}{2m} \sum_i \left(\mathbf{p}_i - \frac{e}{2} \mathbf{r}_i \times \mathbf{B}_0 \right)^2 \\ &= T_0 + \mu_B \mathbf{L} \cdot \mathbf{B}_0 + \frac{e^2}{8m} B_0^2 \sum_i (x_i^2 + y_i^2) \end{aligned} \quad (13.47)$$

where T_0 is the kinetic energy in the absence of the field and $\hbar \mathbf{L} = \sum_i \mathbf{r}_i \times \mathbf{p}_i$.

Combining the spin term (13.43) with (13.47), we get the total interaction Hamiltonian (the field dependent) in the form

$$\Delta H = \mu_B (\mathbf{L} + g_0 \mathbf{S}) \cdot \mathbf{B}_0 + \frac{e^2}{8m} B_0^2 \sum_i (x_i^2 + y_i^2) \quad (13.48)$$

Changes in energy affected by (13.48) even with the strongest magnetic fields that can be produced in a laboratory are very small on the scale of atomic excitation energies. Hence it may be justified to follow the ordinary perturbation approach for calculating the changes in electron energies induced by a magnetic field.

The dependence of susceptibility on the second derivative of energy (13.41) indicates that it would suffice to confine the perturbation calculations to second-order terms. If energy E_n changes by ΔE_n on applying the field, this change according to the standard result of the second-order perturbation theory is expressed as

$$\Delta E_n = \langle \phi_n | \Delta H | \phi_n \rangle + \sum_{n' \neq n} \frac{|\langle \phi_n | \Delta H | \phi_{n'} \rangle|^2}{E_n - E_{n'}} \quad (13.49)$$

where ϕ_n denotes the eigenfunction of the n th energy state.

On substituting ΔH from (13.48) and retaining terms up to those in quadratic in B_0 , we obtain

$$\begin{aligned} \Delta E_n &= \mu_B \mathbf{B}_0 \cdot \langle \phi_n | \mathbf{L} + g_0 \mathbf{S} | \phi_n \rangle + \sum_{n' \neq n} \frac{|\langle \phi_n | \mu_B \mathbf{B}_0 \cdot (\mathbf{L} + g_0 \mathbf{S}) | \phi_{n'} \rangle|^2}{E_n - E_{n'}} \\ &\quad + \frac{e^2}{8m} B_0^2 \langle \phi_n | \sum_i (x_i^2 + y_i^2) | \phi_n \rangle \end{aligned} \quad (13.50)$$

This relation serves as the basis for the description of magnetic susceptibility of individual atoms, ions or molecules. It can also be applied to ionic and molecular solids by computing the susceptibility ion by ion, provided the concerned solid may be regarded as a collection of only slightly deformed ions. We show below how it accounts for diamagnetism or paramagnetism at atomic level.

13.4.1 Diamagnetism

Consider the case of a solid composed of ions whose all electronic shells are filled. An ion has zero spin and orbital angular momentum in its ground state represented by the wavefunction ϕ_0 , i.e.

$$\mathbf{J} |\phi_0\rangle = \mathbf{L} |\phi_0\rangle = \mathbf{S} |\phi_0\rangle = 0 \quad (13.51)$$

In relation (13.50), only the last term contributes to the field-induced shift in the ground state energy:

$$\begin{aligned}\Delta E_0 &= \frac{e^2}{8m} B_0^2 \langle \phi_0 | \sum_i (x_i^2 + y_i^2) | \phi_0 \rangle \\ &= \frac{e^2}{12m} B_0^2 \langle \phi_0 | \sum_i r_i^2 | \phi_0 \rangle \quad [\text{under (13.15)}]\end{aligned} \quad (13.52)$$

In the state of thermal equilibrium ions are generally in their ground state, excepting the situation at high temperatures. Therefore, the susceptibility of a solid with N atoms or ions per unit volume at room temperature is given as

$$\begin{aligned}&= -\mu_0 N \frac{\partial^2 \Delta E_0}{\partial B_0^2} \\ &= -\frac{\mu_0 Ne^2}{6m} \langle \phi_0 | \sum_i r_i^2 | \phi_0 \rangle\end{aligned} \quad (13.53)$$

If there are Z electrons in an ion, the mean square radius of the ion may be defined by

$$\langle r^2 \rangle = \frac{\langle \phi_0 | \sum_i r_i^2 | \phi_0 \rangle}{Z} \quad (13.54)$$

This leads to

$$\chi = -\frac{\mu_0 NZ e^2}{6m} \langle r^2 \rangle \quad (13.55)$$

which is surprisingly the same as (13.18), obtained on the basis of purely classical considerations.

13.4.2 Paramagnetism

The paramagnetism is attributed generally to ions with a partially-filled shell. There arise two cases of partially-filled shells. In one case, $J \neq 0$ and paramagnetism follows from the first term in relation (13.50). Being the leading term, it determines the major paramagnetic effect. Its magnitude is so large that the other two terms can simply be ignored at the first instance. In the other case, $J = 0$ which refers to ions whose partially-filled shell is one electron short of being half-filled. The paramagnetism in this case appears only as a second-order effect. We discuss here the first case and treat the second in the following section.

The ionic ground state in the present case in the absence of a magnetic field is $(2J + 1)$ -fold degenerate. This produces difficulty in calculating the Landé splitting factor (g -factor). Furthermore, the relation

$$\mathbf{L} + g_0 \mathbf{S} = g \mathbf{J}$$

holds good only within the ground state multiplet of $(2J + 1)$ states in zero field. Only when the separation between the ground state multiplet in zero field and the first excited state multiplet is much greater than $k_B T$, is there a sizeable contribution from the states of the ground state multiplet to the free energy. This is usually the case in practice. Only in this event, the above relation allows us to treat the first term in (13.50) to be equal to the interaction energy $(-\mu \cdot \mathbf{B}_0)$, with μ being given by

$$\mu = -\mu_B g J$$

The calculation of susceptibility, nevertheless, is not straightforward on account of the degenerate character of the ground state. When the field becomes zero, the splitting of the $(2J + 1)$ lowest lying states would be smaller than $k_B T$, rendering it unjustifiable to substitute the free energy with the ground state energy as is possible in the case of a non-degenerate ground state. Therefore, for the calculation of susceptibility we have to take recourse to a method based on principles of statistical mechanics as detailed below.

Consider a system containing identical ions with angular momentum J . Assuming that only the lowest $(2J + 1)$ states are thermally excited with appreciable probability, we can define the magnetic Helmholtz free energy F by the fundamental statistical mechanical rule (13.40):

$$\begin{aligned} \exp\left(-\frac{F}{k_B T}\right) &= \sum_{J_z=-J}^J \exp\left(-\frac{E_J^z}{k_B T}\right) \\ &= \sum_{J_z=-J}^J \exp\left(-\frac{g\mu_B J_z B_0}{k_B T}\right) \end{aligned} \quad (13.56)$$

with the applied magnetic field in the z -direction.

The sum is in a geometrical progression and it can be easily evaluated, leading to

$$\exp(-\beta F) = \frac{\exp\left[\beta\gamma B_0 \left(J + \frac{1}{2}\right)\right] - \exp\left[-\beta\gamma B_0 \left(J + \frac{1}{2}\right)\right]}{\exp\left(\frac{\beta\gamma B_0}{2}\right) - \exp\left(-\frac{\beta\gamma B_0}{2}\right)} \quad (13.57)$$

with $\beta = \frac{1}{k_B T}$ and $\gamma = g\mu_B$.

If there are N such ions per unit volume, the magnetization can be written as

$$\begin{aligned} M &= -N \frac{\partial F}{\partial B_0} \\ &= N\gamma J B_J(x) \end{aligned} \quad (13.58)$$

where $B_J(x)$ is called the 'Brillouin function', defined by

$$B_J(x) = \left(\frac{2J+1}{2J} \right) \coth \left(\frac{2J+1}{2J} x \right) - \frac{1}{2J} \coth \left(\frac{1}{2J} x \right) \quad (13.59)$$

with

$$x = \beta\gamma JB_0 \quad (13.60)$$

$$= \frac{g\mu_B}{k_B T} \frac{JB_0}{T} = \frac{\mu B_0}{k_B T}$$

The experimental plot of the magnetic moment versus B_0/T for certain materials is shown in Fig. 13.4. It shows that as $T \rightarrow 0$, the magnetic moment approaches saturation, i.e. each ion approaches complete alignment with the field. This implies that $[J_z]$ acquires its maximum value J which may be possible only if $k_B T \ll \gamma B_0$. This condition refers to that of the lowest temperatures and highest fields. Such a condition is, however, usually not realized in practice. On the contrary, over a wide

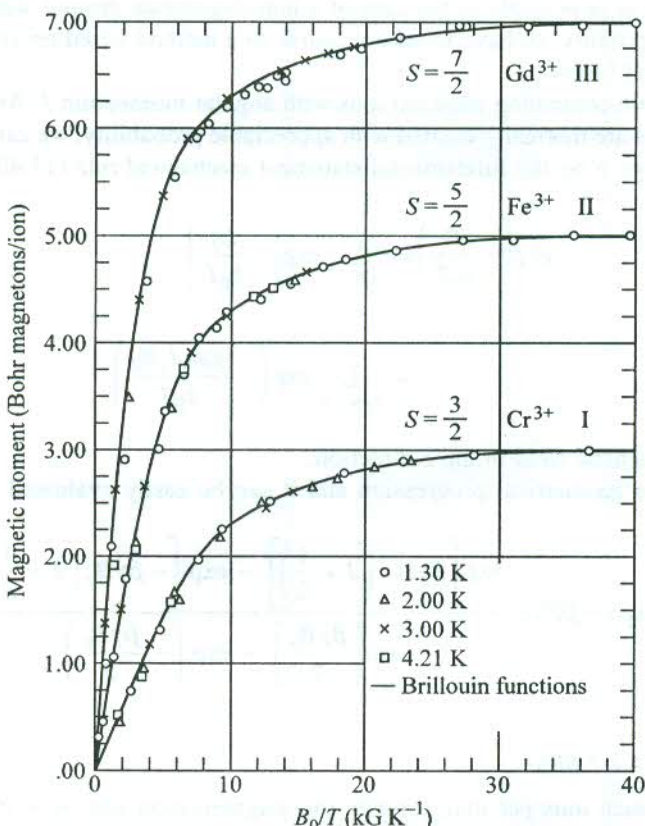


FIG. 13.4 Magnetic moment versus B_0/T plot showing saturation at higher fields for spherical samples: I—potassium chromium alum, II—ferric ammonium alum and III—gadolinium sulphate octahydrate. [After W.E. Henry, *Phy. Rev.*, **88**, 559 (1952).]

range of temperature and fields the condition $k_B T \gg \gamma B_0$ is nicely applicable. In this limit x is small and

$$\begin{aligned}\coth x &= \frac{1}{x} + \frac{1}{3}x - \frac{1}{45}x^3 + \dots \\ &\approx \frac{1}{x} + \frac{1}{3}x\end{aligned}\quad (13.61)$$

and

$$B_J(x) \approx \left(\frac{J+1}{3J} \right) x \quad (13.62)$$

Using (13.62) with (13.58), we get

$$\begin{aligned}\chi &= \frac{\mu_0 N J(J+1) g^2 \mu_B^2}{3 k_B T} \\ &= \frac{\mu_0 N p^2 \mu_B^2}{3 k_B T}\end{aligned}\quad (13.63)$$

where p is the 'effective Bohr magneton number', given by

$$p = g[J(J+1)]^{1/2} \quad (13.64)$$

Relation (13.63) can be put in the form of the Curie law $\chi = C/T$, where C is Curie constant, defined by

$$C = \frac{\mu_0 N p^2 \mu_B^2}{3 k_B} \quad (13.65)$$

The paramagnetic susceptibility (13.63) is greater than the diamagnetic susceptibility (13.55) by a factor of about 500 at room temperature. This confirms that in a solid containing ions that have a partially-filled shell with $J \neq 0$, the contribution from the partially-filled shell to the total susceptibility dominates the diamagnetic contribution from filled shells.

13.4.3 Application to Magnetic Ions in Solids: Effect of the Crystal Field

In this section we examine how well the theory of paramagnetism of free ions is applicable to paramagnetic solids. The Curie law (13.63) is obeyed very well in insulating solids containing rare earth ions. The p -values (the effective Bohr magneton numbers) are derived from the coefficient of $1/T$ in (13.63) using the measured values of χ . These are in exceedingly good agreement with those calculated with (13.64) for all rare earth ions* excepting samarium and europium. For both of these ions the J -multiplet lying just above the ground state is very close in energy as a consequence of which a couple of assumptions made in the derivation of the Curie law remain no more valid:

* N.W. Ashcroft and N.D. Mermin, *Solid State Physics*, Table 31.3 (Saunders College, 1988).

- (i) The second term in (13.50) that is ignored in the derivation of the Curie law becomes important because the denominators ($E_n - E_{n'}$) are now very small.
- (ii) There is an appreciable probability of thermally exciting some ions from the state(s) of lowest J to higher states, contrary to what is assumed for deriving the Curie law.

These observations explain the discrepancy noticed in respect of samarium and europium ions. In addition, our analysis is not applicable to the latter since J is equal to zero in that case. The excellent agreement in respect of all other ions, however, leads to the conclusion that the rare earth ions can be treated as free ions even in solids.

Let us now take up the case of 3d transition metal ions (the iron group). Other transition metal ions (4d and 5d) will not be discussed here in view of their complex behaviour. In the case of 3d transition metal ions, although the Curie law is obeyed, the experimental p -values* are not accounted for by (13.64). The agreement is close only if J is replaced by S in the relation, assuming that L is zero though S will be still given by the Hund's rules. This phenomenon is known as *quenching of the orbital angular momentum* and attributed to the crystal field effect. The crystal field effect is stronger in transition metal ions since their partially filled d-shell (3d in the iron group) happens to be the outermost shell. The electrons in the d-shell are thus directly exposed to the electric field created by ions surrounding the magnetic ion of concern. The coupling between L and S is largely broken so that the states are no longer specified by their J values. Further, the $(2L + 1)$ sublevels belonging to a certain L and degenerate in the free ion may be split by the crystal field. The splitting decreases the contribution of the orbital motion to the magnetic moment.

On the other hand, the crystal field effect for rare earth ions is almost negligible since their partially-filled shell (4f) lies deep inside the ion, sheltered by 5s and 5p shells. This explains why these ions behave as almost free ions even when they are embedded in crystals.

The symmetry of a crystal field is determined by the arrangement of ions around the magnetic ion. Since the symmetry is never spherical in a crystal, the basis for the application of the Hund's rules prevails no more. Under the action of an asymmetrical (noncentral) crystal field, the plane of the electron orbit moves about and the precession of the orbital angular momentum sets in. As a result, all the three components of the orbital angular momentum (L_x, L_y, L_z) may average out to zero, though L^2 may still be a constant of motion with the mean value $L(L + 1)$. This contrasts with the behaviour in a central field where in accordance with the quantum theory one component of L , usually L_z , and L^2 are constant. For a magnetic field along the z -direction, the contribution of orbital motion to magnetic moment is proportional to the quantum expectation value of L_z . Therefore, when L_z averages out to zero, the orbital angular momentum, and hence the orbital magnetic moment, is said to be quenched.

13.5 van VLECK PARAMAGNETISM

In this section we discuss the case of a partially-filled shell with $J = 0$, giving a non-degenerate ground state for which calculations are simpler. To repeat, it is the case of ions whose partially-filled shell is one electron short of being half filled (see Example 3 in Section 13.3.1). In a filled shell too, $J = 0$. But the present case is different in the sense that the second term in (13.50) does not vanish here, though it does so for ions having only completely occupied shell, simply because L and S

*N.W. Ashcroft and N.D. Mermin, *Solid State Physics*, Table 31.4 (Saunders College, 1988).

are both independently zero for a completely filled shell. Hence the shift in the ground state energy induced by the magnetic field in the present case is written as

$$\Delta E_0 = \frac{e^2}{8m} B_0^2 \langle \phi_0 | \sum_i (x_i^2 + y_i^2) | \phi_0 \rangle - \sum_n \frac{|\langle \phi_0 | \mu_B \mathbf{B}_0 \cdot (\mathbf{L} + g_0 \mathbf{S}) | \phi_n \rangle|^2}{E_n - E_0} \quad (13.66)$$

If the system has N such ions per unit volume,

$$\begin{aligned} \chi &= -\mu_0 N \frac{\partial^2 \Delta E_0}{\partial B_0^2} \\ &= -\mu_0 N \left[\frac{e^2}{4m} \langle \phi_0 | \sum_i (x_i^2 + y_i^2) | \phi_0 \rangle - 2\mu_B^2 \sum_n \frac{|\langle \phi_0 | (\mathbf{L}_z + g_0 \mathbf{S}_z) | \phi_n \rangle|^2}{E_n - E_0} \right] \end{aligned} \quad (13.67)$$

The first term with a negative sign (depending on the diagonal matrix element) in (13.67) represents the usual Langevin's diamagnetic susceptibility (13.55). The second term is positive because the energy of excited state E_n is always greater than the ground state energy E_0 . It indicates the preference of the magnetic moment for aligning with the field direction (z -direction) which is a definite evidence of paramagnetism. This term may be regarded as a correction to the diamagnetic contribution. It must be stressed that the paramagnetism being discussed is fairly weak since it appears through a non-diagonal matrix element as a second-order term. In view of this fact, the overall magnetic behaviour of ions is determined by the balance between two weak terms of opposite sign.

The paramagnetic term is required to be examined in two extreme limits:

1. $(E_n - E_0) \ll k_B T$

In this limit the excess population in the ground state over the excited state of energy E_n is approximately equal to $\frac{N(E_n - E_0)}{2k_B T}$. This would give a magnetization

$$M = \frac{NB_0 \mu_B^2}{k_B T} \sum_n |\langle \phi_0 | (\mathbf{L}_z + g_0 \mathbf{S}_z) | \phi_n \rangle|^2 \quad (13.68)$$

and

$$\chi = \frac{\mu_0 N \mu_B^2}{k_B T} \sum_n |\langle \phi_0 | (\mathbf{L}_z + g_0 \mathbf{S}_z) | \phi_n \rangle|^2 \quad (13.69)$$

The above contribution is of the usual Curie form with the difference that the magnetization occurs here by polarization of the states of the system and not by the usual redistribution of ions among the spin states. We also observe that χ does not depend on the separation of excited states from the ground state.

2. $(E_n - E_0) \gg k_B T$

In this condition, almost all the ions stay in the ground state with little probability of being excited to higher states in the state of thermal equilibrium. Also, in this limit the free energy is just the ground state energy. Treating all the ions to be in the ground state,

$$M = 2NB_0\mu_B^2 \sum_n \frac{|\langle \phi_0 | (\mathbf{L}_z + g_0 \mathbf{S}_z) | \phi_n \rangle|^2}{E_n - E_0} \quad (13.70)$$

and therefore,

$$\chi = 2\mu_0 N\mu_B^2 \sum_n \frac{|\langle \phi_0 | (\mathbf{L}_z + g_0 \mathbf{S}_z) | \phi_n \rangle|^2}{E_n - E_0} \quad (13.71)$$

This expression denotes a temperature independent paramagnetism which is commonly known as the van Vleck paramagnetism.

13.6 PAULI PARAMAGNETISM

The contribution of conduction electrons to the magnetic moment of a metal is discussed in this section. It is interesting to find that the conduction electrons, apart from producing diamagnetism on account of their angular momentum, also exhibit a temperature independent paramagnetism, known as 'Pauli paramagnetism'. These electrons can be safely treated in the independent electron approximation as they are neither localized in space like those in filled shells nor favoured by the Pauli principle to be localized on different ions. However, the complex response of the orbital motion to the magnetic field poses serious difficulties for an accurate calculation of the magnetic properties. In view of this fact, we settle for an oversimplified model in which the electron is considered to have a spin magnetic moment but no charge and the response of the orbital motion is completely ignored. As a result the calculations become far more easier and even the free energy does not figure in calculations.

The degeneracy between the electrons of opposite spin that share the same orbital is resolved by a magnetic field. In a metal this causes a redistribution of electrons between the two spin orientations and, therefore, gives rise to a magnetic moment. Each electron with its spin parallel to the field lines contributes a magnetic moment $-g_0\mu_B/2$ and the one with spin antiparallel to the field contributes $g_0\mu_B/2$ to the magnetic moment of the system of conduction electrons. If n_{\pm} denotes the number of electrons per unit volume with spin parallel (+) or antiparallel (-) to the external induction B_0 , the magnetization will be given by

$$\begin{aligned} M &= -\frac{1}{2} g_0 \mu_B n_+ + \frac{1}{2} g_0 \mu_B n_- \\ &= -\frac{1}{2} g_0 \mu_B (n_+ - n_-) \end{aligned} \quad (13.72)$$

The electrons with spin parallel and magnetic moment antiparallel to \mathbf{B}_0 are in states whose energy has been increased by $\frac{1}{2} g_0 \mu_B B_0$ with respect to the zero field condition. Similarly, for the electrons with spin antiparallel and magnetic moment parallel to the field, the energy is lowered by $\frac{1}{2} g_0 \mu_B B_0$. The energy parabola splits into two parabolae (Fig. 13.5) that are separated by $g_0 \mu_B B_0$ on the energy axis. The figure shows the separation as $2\mu_B B_0$ under the assumption, $g_0 = 2$, since the conduction electrons can be treated very nearly like free electrons. Henceforth, this assumption shall apply to all our discussions.

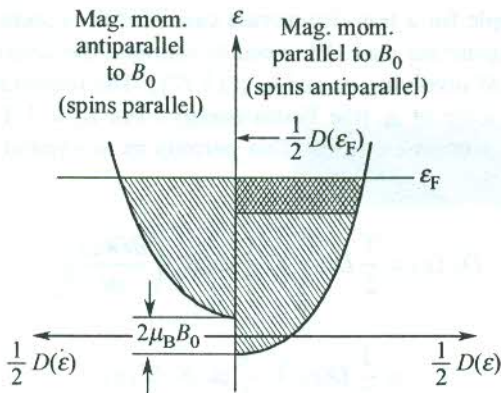


FIG. 13.5 Relative shift energy parabolae referred to parallel and antiparallel spin states of conduction electrons in a magnetic field B_0 . The cross-hatched area represents excess (uncompensated) electron spins parallel to B_0 , that account for the net magnetic moment.

Suppose $D_{\pm}(\epsilon)$ represents the density of energy levels at energy ϵ belonging to the two sets of electrons with densities n_+ and n_- in the presence of the field. Then,

$$D_{\pm}(\epsilon) = \frac{1}{2} D(\epsilon) \quad (13.73)$$

where $D(\epsilon)$ is ordinary density of levels in the absence of the field.

The energy of each electronic level with spin parallel to the field lines is raised by $\mu_B B_0$. This implies that the number of levels with energy ϵ for this spin species in the presence of the field is the same as with $(\epsilon - \mu_B B_0)$ in the absence of the field. That is,

$$D_+(\epsilon) = \frac{1}{2} D(\epsilon - \mu_B B_0) \quad (13.74a)$$

Similarly,

$$D_-(\epsilon) = \frac{1}{2} D(\epsilon + \mu_B B_0) \quad (13.74b)$$

The number of electrons per unit volume for the two sets of spin orientations is

$$n_{\pm} = \int D_{\pm}(\epsilon) f(\epsilon) d\epsilon \quad (13.75)$$

where $f(\epsilon)$ is the Fermi-Dirac distribution function

$$\frac{1}{\exp\left(\frac{\epsilon - \mu}{k_B T}\right) + 1}$$

As usual the chemical potential μ is estimated by requiring the total electron density n to be consistent with

$$n = n_+ + n_- \quad (13.76)$$

The calculations are simple for a non-degenerate case. But the conduction electrons or for that matter metals belong to a degenerate case. We need to estimate the density of levels $D_{\pm}(\varepsilon)$ for the calculation of magnetization M involving n_+ and n_- [(13.72)]. The important variation of the density of levels $D(\varepsilon)$ occurs on the scale of ε_F (the Fermi energy). For $B_0 = 1$ T, $\mu_B B_0 \sim 10^{-4} \varepsilon_F$ which is very small compared to the electron energies. This permits us to expand $D_{\pm}(\varepsilon)$ [given by (13.74)] as

$$\begin{aligned} D_{\pm}(\varepsilon) &= \frac{1}{2} D(\varepsilon) \mp \frac{1}{2} \mu_B B_0 \left(\frac{\partial D(\varepsilon)}{\partial \varepsilon} \right)_0 \\ &= \frac{1}{2} D(\varepsilon) \mp \frac{1}{2} \mu_B B_0 D'(\varepsilon) \end{aligned} \quad (13.77)$$

Using (13.77) with (13.75), we get

$$n_{\pm} = \frac{1}{2} \int D(\varepsilon) f(\varepsilon) d\varepsilon \mp \frac{1}{2} \mu_B B_0 \int D'(\varepsilon) f(\varepsilon) d\varepsilon \quad (13.78)$$

Putting these values in (13.76), we find that the overall electron density, as expected for moderate fields, does not change on the application of a magnetic field:

$$n = \int D(\varepsilon) f(\varepsilon) d\varepsilon \quad (13.79)$$

Using (13.76) with (13.72) gives the magnetization

$$\begin{aligned} M &= \mu_B^2 B_0 \int D'(\varepsilon) f(\varepsilon) d\varepsilon \\ &= \mu_B^2 B_0 \int D(\varepsilon) \left(-\frac{\partial f}{\partial \varepsilon} \right) d\varepsilon \quad (\text{on integrating by parts}) \end{aligned} \quad (13.80)$$

At $T = 0$, $-\frac{\partial f}{\partial \varepsilon} = \delta(\varepsilon - \varepsilon_F)$, therefore, at absolute zero, $D(\varepsilon)$ should be rightfully replaced by $D(\varepsilon_F)$.

But in practice we are always concerned with non-zero temperatures. As may be seen in Fig. 6.10, the variation of f at temperatures not too high[†] ($\sim 10^4$ K) is maximum around ε_F . Since the experiments are performed at temperatures far below 10^4 K, $D(\varepsilon_F)$ determines the all important density of levels and it can replace $D(\varepsilon)$ in (13.80) without involving a meaningful error. Then, (13.80) becomes

$$\begin{aligned} M &= \mu_B^2 B_0 D(\varepsilon_F) \int \left(-\frac{\partial f}{\partial \varepsilon} \right) d\varepsilon \\ &= \mu_B^2 B_0 D(\varepsilon_F) \end{aligned} \quad (13.81)$$

[†] At $T \neq 0$, corrections to $(-\partial f / \partial \varepsilon)$ are of the order of $(k_B T / \varepsilon_F)^2$. See N.W. Ashcroft and N.D. Mermin, *Solid State Physics*, Ch. 2 (Saunders College, 1988).

and

$$\chi = \frac{\mu_0 M}{B_0} = \mu_0 \mu_B^2 D(\varepsilon_F) = \frac{3\mu_0 \mu_B^2 N}{2k_B T_F} \quad (13.82)$$

with

$$D(\varepsilon_F) = \frac{3N}{2\varepsilon_F} = \frac{3N}{2k_B T_F} \quad [\text{see (6.37)}]$$

where N is the total number of electrons in the system and T_F is the Fermi temperature ($\sim 10^4$ K).

The result (13.82) determines the Pauli paramagnetic susceptibility; a contribution from the conduction electrons that is essentially temperature independent and not accounted by calculations based on classical statistics. As remarked in Section 6.1.1, it is identified as one of the most prominent gains of using quantum statistics. The use of Fermi-Dirac statistics in the above treatment is in conformity with the antisymmetric character of the spinning electrons. The expression is ideally valid at $T = 0$, though applicable in the limit $T \ll T_F (= \varepsilon_F/k_B)$. The Pauli susceptibility is measured by making use of the nuclear magnetic resonance (NMR) technique, to be discussed in Section 13.9.2. The measured values are in fairly good agreement with those calculated for the electrons with (13.82). These are of the order of 10^{-6} , i.e. of the size of typical diamagnetic susceptibilities. Thus the Pauli susceptibilities are about hundreds of times smaller than the paramagnetic susceptibilities of magnetic ions.

In addition to the Pauli paramagnetism, there is a diamagnetic contribution too from the conduction electrons. A magnetic field induces an orbital motion creating a magnetization that is antiparallel to the field lines. The magnetism thus produced is known as 'Landau diamagnetism'. For free electrons,

$$\chi_{\text{Landau}} = -\frac{1}{3} \chi_{\text{Pauli}} \quad (13.83)$$

A comparative view of various forms of paramagnetism and diamagnetism is provided by Fig. 13.6 with the help of a χ versus T plot.

13.7 NUCLEAR PARAMAGNETISM

In addition to the orbital motion and the spin of electrons, the nuclear spin also contributes to the magnetic moment of atoms. The nuclear magnetic moment is expressed in units of the nuclear magneton in analogy with the Bohr magneton defined by

$$\mu_n = \frac{e\hbar}{2M_P} = 5.051 \times 10^{-27} \text{ J/T} \quad (13.84)$$

where M_P is the proton mass.

Comparing (13.84) with (13.30) we see that the nuclear magneton is smaller than the Bohr magneton in the ratio of the proton mass to the electron mass ($\sim 10^3$). Therefore, the static nuclear paramagnetism is masked by the electron paramagnetism in paramagnetic substances. Solid hydrogen

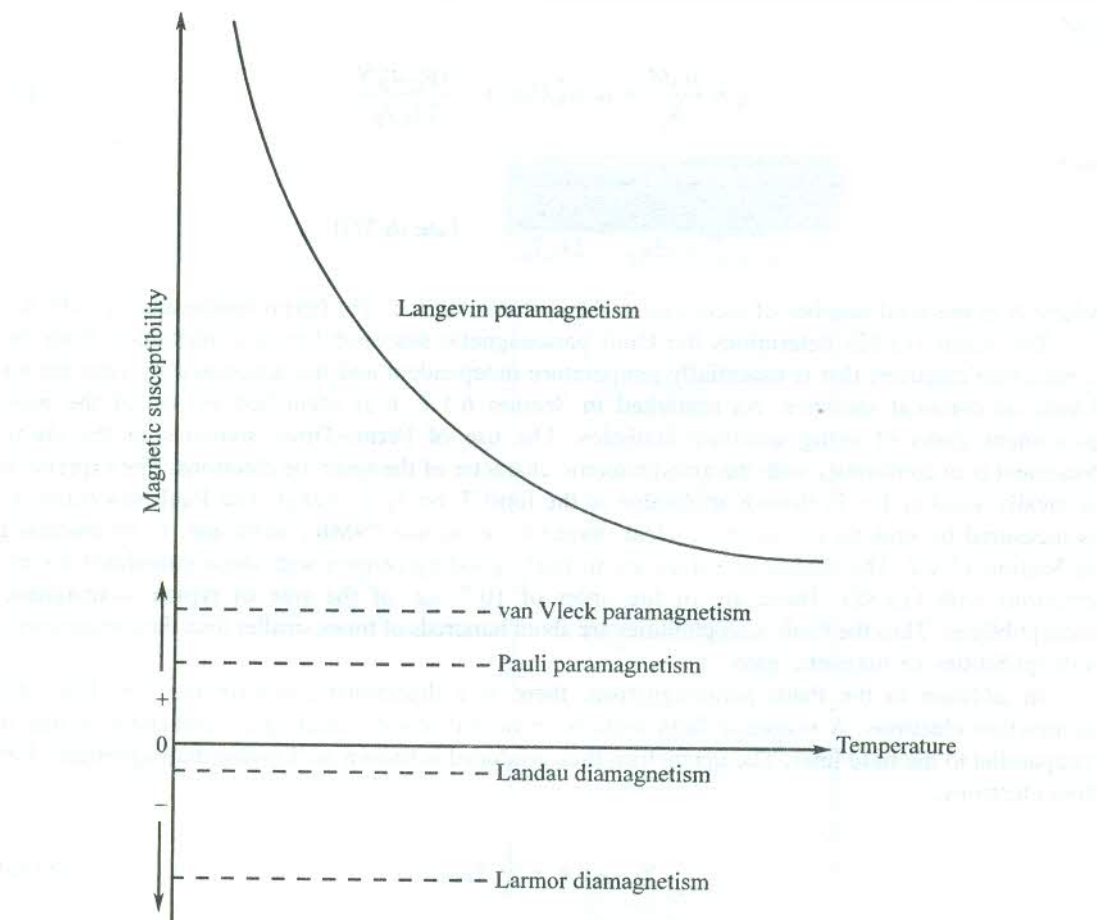


FIG. 13.6 A comparative view of various forms of paramagnetism and diamagnetism, giving χ versus T plot.

shows nuclear paramagnetism, though its electron configuration suggests diamagnetism only. The value of proton magnetic moment (2.793 nuclear magnetons) is verified by these measurements. Heavy nuclei are found to possess even smaller magnetic moments. The method of nuclear magnetic resonance (NMR) is used to determine the nuclear magnetic moments. The nuclear magnetic moments, being very small compared to the electronic components, are almost ignored while discussing static magnetization.

13.8 COOLING BY ADIABATIC DEMAGNETIZATION

The cooling of a system, in principle, can be produced by an isothermal reduction of its entropy by some operation, followed by an adiabatic (isentropic) reversal of the operation. All that is required is to find a system whose entropy can be lowered. For cooling below 1 K, for which the adiabatic demagnetization has been used, the selection of an appropriate system is not easy because at these low temperatures there is hardly any entropy left in any system. There may be

only some solids as there are no gases or liquids suitable for the purpose. The lattice entropy[†] of solids is, however, not encouraging. At 1 K for a solid with $\theta_D = 100$ K it is merely $\sim 10^{-4} Nk_B$. The choice falls on paramagnetic solids which possess appreciable spin entropy because of the random orientations of atomic magnetic moments.

A magnetic field is applied to reduce the entropy of a paramagnetic salt immersed in liquid helium. The creation of a more ordered state of spins leads to the reduction of entropy. The liquid helium absorbs any heat liberated in the process. The salt is then removed from the liquid helium bath and the magnetic field is switched on under adiabatic conditions implying that the entropy remains unchanged. The field is switched off slowly to ensure that the system passes through states always in thermal equilibrium. As we will explain below, the temperature will have to fall if the entropy is to remain unchanged even after the magnetic field is completely withdrawn. In order to preserve the cooling thus produced, no heat should flow into the spin system. The most likely source of heat is the lattice entropy. Therefore, it is most important that the lattice entropy of the salt be smaller than its spin entropy to disallow heating. Salts containing rare earth elements because of their larger magnetic moments adequately satisfy the above condition and, therefore, used for adiabatic demagnetization.

We learn from the above discussion that the method of adiabatic demagnetization can be applied in a limited range of temperatures over which the spin entropy dominates its lattice counterpart. In practice, the method is useful for cooling from a few K down, at the best, to 10^{-3} K.

Consider an entirely disordered spin system at high temperatures where the thermal disorder overpowers magnetic interactions that could produce any preferential spin orientations. A spin system of N ions, each of spin J , has $(2J + 1)$ states in total over which the spins are distributed. If W represents the number of possible ways of distribution in a quantized spin system, the entropy S of the system is defined by

$$S = k_B \ln W \quad (13.85)$$

where

$$W = (2J + 1)^N \quad (13.86)$$

Therefore,

$$S = Nk_B \ln (2J + 1) \quad (13.87)$$

showing that the entropy is temperature independent in the absence of a magnetic field.

For $J = 1/2$, the entropy is equal to $Nk_B \ln 2$. It shows that even for a two-level system the spin entropy is far greater than the lattice entropy around 1 K ($\sim 10^{-4} Nk_B$). On the application of a magnetic field B_0 , the $(2J + 1)$ states are separated in energy and the entropy is lowered when the lower levels gain in population. When the magnetic field is withdrawn adiabatically, the temperature falls so that the entropy may remain unchanged as required in an adiabatic change. We attempt below to find a theoretical basis for this phenomenon.

[†] The lattice entropy is defined as

$$S = \int_0^T C_V \cdot \frac{dT}{T} = \int_0^T \frac{12\pi^4 Nk_B}{5} \left(\frac{T}{\theta_D} \right)^3 \cdot \frac{dT}{T} = 78 Nk_B \left(\frac{T}{\theta_D} \right)^3$$

with

$$C_V = \frac{12\pi^4 Nk_B}{5} \left(\frac{T}{\theta_D} \right)^3 \quad [\text{see (5.39)}]$$

The entropy is defined in terms of the Helmholtz free energy F and the internal energy U as

$$\begin{aligned} S &= \frac{U - F}{T} \\ &= k_B \beta(U - F) \quad \text{with } \beta = \frac{1}{k_B T} \end{aligned} \quad (13.88)$$

Further, we learn from relation (13.40) that for a system of non-interacting paramagnetic ions, βF depends on B_0 only through the product βB_0 . This requires F to be of the form

$$F = \frac{1}{\beta} f(\beta B_0) \quad (13.89)$$

where $f(\beta B_0)$ denotes a function of the product (βB_0) .

Since U can be expressed as

$$U = \frac{\partial}{\partial \beta} (\beta F) \quad (13.90)$$

we can write the entropy using (13.88) as

$$S = k_B \beta^2 \frac{\partial F}{\partial \beta} \quad (13.91)$$

or

$$S = k_B [-f(\beta B_0) + \beta B_0 f'(\beta B_0)] \quad [\text{using (13.89)}] \quad (13.92)$$

Relation (13.92) indicates that S , too, depends on the product βB_0 . Thus, when S is constant, we would require that βB_0 remains constant, i.e. $B_0/T = \text{constant}$, which we can write as

$$\frac{(B_0)_{\text{initial}}}{T_{\text{initial}}} = \frac{(B_0)_{\text{final}}}{T_{\text{final}}}$$

or

$$T_{\text{final}} = \frac{(B_0)_{\text{final}}}{(B_0)_{\text{initial}}} \times T_{\text{initial}} \quad (13.93)$$

Instead of withdrawing the field completely, if we decrease it adiabatically to a certain value, according to (13.93), then, $T_{\text{final}} < T_{\text{initial}}$.

The lower limit of temperature that can be approached is determined by the validity of (13.92). In principle, we could even reach the absolute zero, if the relation were absolutely valid. Had it really been true, the zero-field entropy would not have been found to be temperature dependent as shown in Fig. 13.7. The observed temperature dependence leads to the conclusion that the entropy will really drop to zero as the absolute zero is approached, a result that is consistent with the third law of thermodynamics. Therefore, the condition (13.93) must fail at small fields to account for the temperature dependence of the zero-field entropy. In fact, even after the magnetic field is completely withdrawn there remains a magnetic field, though weak, mainly contributed by magnetic interactions between paramagnetic ions. This field in some cases may be as large as 100 gauss around 1 K. When

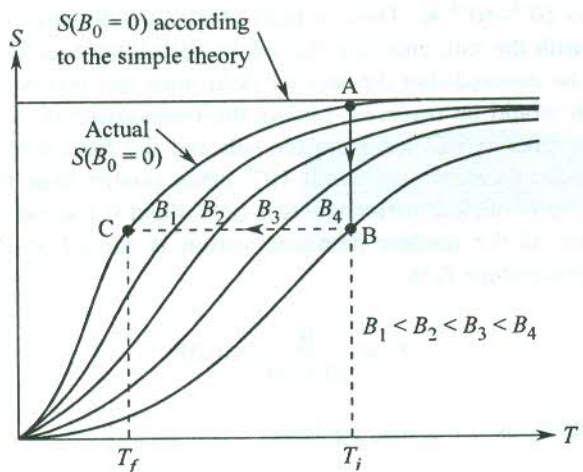


FIG. 13.7 Plot of entropy versus temperature cooling curves for interacting spins at various values of external induction B_0 in an adiabatic demagnetization process. The top horizontal line refers to the constant zero-field entropy $Nk_B \ln(2J+1)$ of non-interacting spins. The actually observed zero-field entropy shows temperature dependence, represented by the curve passing through the point C.

this aspect and other effects, such as strong crystal field splittings at low temperatures, are taken into consideration, the temperature dependence in question is properly explained using the resultant modified expression for entropy.

The process of cooling by adiabatic demagnetization is explained in Fig. 13.7 with the help of S versus T curves for different magnetic fields. Initially, the paramagnetic salt rests immersed in liquid helium. The vertical line AB represents the first step of operation where the entropy is isothermally reduced from its initial value at A to a lower value at B by applying a magnetic field B_4 . Notice that the point A lies on the zero-field S versus T curve and the point B on a curve obtained in the presence of the field B_4 . There are other curves for fields lower than B_4 — $B_3 > B_2 > B_1$. The S versus T behaviour in the absence of a magnetic field as predicted by simple theory and as observed is shown by two separate curves.

In the next step, the salt is removed from the liquid helium bath and the field reduced under adiabatic conditions (but slowly) through $B_3, B_2, B_1 \dots$ to zero value. The operation is represented by the horizontal line BC. The intersections of BC with various S versus T curves gives the temperature $T_3 > T_2 > T_1$ corresponding to the fields B_3, B_2 and B_1 at three different stages during the process of adiabatic demagnetization. The lowest temperature approached is shown as T_f symbolized by the point C on the observed zero-field curve. As mentioned earlier, the lowest temperatures produced by adiabatic demagnetization are in the range of 10^{-3} K.

For approaching temperature below 10^{-3} K, a cascade process involving nuclear demagnetization is employed. The process consists of two steps. In the first step the cooling is produced by the demagnetization of an electron-spin system. It is followed in the next step by a further lowering of temperature resulting from demagnetization of a nuclear spin system in which the electron spin paramagnet acts as the reservoir.

Kurti et al.* carried out the first experiment on nuclear magnetization using copper as the nuclear spin system. An adiabatic demagnetization is performed in the usual way bringing the salt

* N. Kurti, F.N.H. Robinson, F.E. Simon and D.A. Sophr, *Nature*, 178, 450 (1956).

and the copper down to 10^{-2} – 10^{-3} K. Then, a field of 20–30 kilogauss is applied locally to the copper kept in contact with the salt, enabling the salt to absorb the heat released when the copper is magnetized. It must be ensured that the second field must not involve the salt, otherwise the path of demagnetization would be reversed, raising the temperature (C to B in Fig. 13.7). After being magnetized, the copper is isolated from the salt and the field turned off.

Since nuclear magnetic moments are about 10^{-3} times smaller than the electronic moments, the residual magnetic field in nuclear paramagnets is only about 0.1 gauss in contrast to 100 gauss in electron-spin systems. If the nuclear demagnetization is started at $B_0 = 50$ kilogauss and $T_i = 0.01$ K, the final temperature T_f is

$$T_f = \frac{B'_0}{50 \times 10^3} \times 0.01$$

Taking the residual field B'_0 as 0.1 gauss, we have

$$T_f \approx 10^{-7} \text{ K}$$

In their historic experiment, Kurti et al. started the magnetization at 0.02 K and could approach 1.2×10^{-6} K. According to the latest available reports, the lowest temperature approached so far is 280×10^{-12} K, achieved with the use of rhodium nuclei.[†]

13.9 MAGNETIC RESONANCE

It was shown in Section 13.3 that every magnetic moment μ has an angular momentum \mathbf{J} associated with it. When a constant magnetic field \mathbf{B}_0 is applied, the field exerts a torque on μ . The torque makes \mathbf{J} to precess around the direction of the field as discussed in Section 13.1. The motion represents effectively the precession of the system, just as the precession of a spinning top, with the Larmor frequency ω_L [given by (13.10) for an electron orbit]. As a result, a magnetic dipole in the presence of a constant magnetic field is characterized with a natural frequency ω_L . This reveals that permanent magnetic dipoles are prone to show resonant behaviour in contrast to the normally observed behaviour of permanent electric dipoles. The induced electric dipoles, nevertheless, do show resonance because they have a natural frequency.

The magnetic resonance is observed by applying a second magnetic field which is alternating and perpendicular to the dc field. The source of this additional field is a radio-frequency radiation. The resonance occurs when the frequency of precession becomes equal to the frequency of rf radiation under conditions, favourable for resonance absorption. In experiment, the rf radiation is fed at a fixed frequency and the matching precession frequency is set by searching (varying) the dc magnetic field. The rf magnetic field produces a torque on the magnetization that is parallel to the dc field. The rf field bends the magnetic moment away from the dc field, causing the amplitude of precession to increase. The precession with an increasing amplitude in the present case produces the favourable condition for resonance. As in any resonant system, the damping comes into play through relaxation processes that limit the amplitude of precession. The above is a classical interpretation of the magnetic resonance. A description based on quantum physics will be taken up after making a few introductory remarks in the following paragraph.

[†] P.J. Hakonen et al., *Phys. Rev. Lett.*, **70**, 2818 (1993).

In view of the form of magnetism discussed in this chapter, two types of magnetic resonances are of basic importance. They are: electron paramagnetic resonance (EPR) and nuclear magnetic resonance (NMR). The EPR in solids is mostly concerned with spin angular momentum since the crystal field generally quenches the orbital angular momentum. It was shown in Section 13.4.3 that the quenching is nearly complete in crystals containing 3d-transition metal ions. When the quenching is not complete the orbital contribution is reflected in small splittings of states, caused by the crystal field. If the quenching can be treated as complete, the paramagnetic atom or ion appears to have a free spin. Therefore, to be precise, the resonance in such a case should better be referred to as electron spin resonance (ESR). In this section, we discuss ESR and NMR phenomena that are linked with the magnetic moments of spinning electrons and spinning nuclei, respectively.

13.9.1 Electron Spin Resonance (ESR)

We saw in Section 13.3 that the contribution of electron spin to the magnetic moment of an atom or ion is

$$\begin{aligned}\mu &= -g_0\mu_B S \\ &= -g_0(e/2m)\hbar S \\ &= \gamma_e \hbar S\end{aligned}\quad (13.94)$$

where γ_e is a constant known as the *magnetogyric ratio* and the subscript e stands for electron. It is defined as the ratio of the magnetic moment to the angular momentum:

$$\gamma_e = \mu/\hbar S = -g_0(e/2m) \quad (13.95)$$

with $g_0 = 2.0023$. If we can consider[†] the electrons to be spinning freely and take $g_0 = 2$, then $\gamma_e = -(e/m)$.

According to quantum mechanics, the eigenvalue of the spin operator S is $\sqrt{S(S+1)}$ and, therefore, the magnitude of magnetic moment may be expressed as

$$\mu = \gamma_e \hbar \sqrt{S(S+1)} \quad (13.96)$$

For simplicity, we now consider the case of an unpaired spinning electron in a homogeneous environment. Its spin angular momentum ($\hbar\sqrt{S(S+1)}$) is calculated using $S = |m_s|$ with $m_s = \pm 1/2$. The value thus obtained is $\sqrt{3}\hbar/2$. Under the influence of a magnetic field \mathbf{B}_0 , the angular momentum is space quantized and has two allowed orientations in the present case^{††} [(since $S = 1/2$), as shown in Fig. 13.8(a)]. The respective components along the field direction are $\hbar/2$ and $-\hbar/2$ with the angular momentum being inclined at an angle $\cos^{-1}(1/\sqrt{3})$ with the field direction.

Further, the magnetic moment interacts with the magnetic field, affecting a change in the electron energy. The electron energy in the presence of the magnetic field can be written as

$$U = U_0 + \Delta U \quad (13.97)$$

[†] In the case where the total spin quantum number $S = 0$ and the orbital motion contributes to the magnetic moment ($L \neq 0$), then $\gamma_e = -e/2m$.

^{††} For magnetic field along the z-direction, the angular momentum $\hbar S$ has $(2S+1)$ orientations corresponding to S_z values: $-S, -(S-1), \dots, 0, \dots, (S-1), S$.

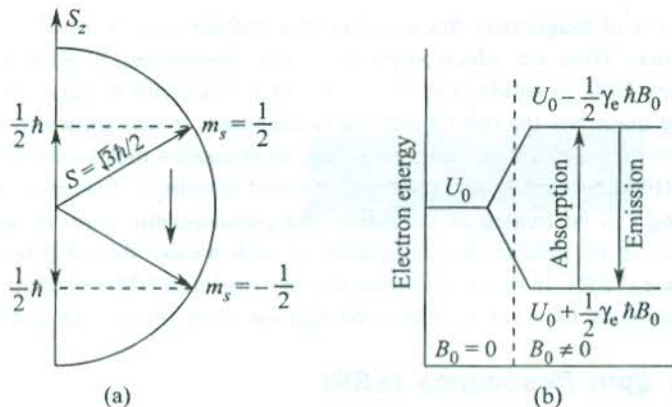


FIG. 13.8 (a) Two possible orientations of the spin angular momentum of an electron relative to the direction of a magnetic field. (b) Splitting of a one-electron energy level in a magnetic field. The two levels differ in energy by $\gamma_e \hbar B_0$. For a photon of this energy, resonance absorption occurs.

where U_0 is the electron energy in the absence of the field and

$$\Delta U = -\mu \cdot B_0 = -\mu_z B_0 \quad (\text{if the field is along the } z\text{-direction}). \quad (13.98)$$

Therefore,

$$U = U_0 \pm \frac{1}{2} \gamma_e \hbar B_0 \quad (13.99)$$

$$\left(\text{since } \mu_z = \pm \frac{1}{2} \gamma_e \hbar, \text{ for } S_z = \pm \frac{1}{2} \right)$$

Thus an electron level with energy U_0 splits in the presence of a magnetic field B_0 into two levels [see Fig. 13.8(b)] with energies $\left(U_0 - \frac{1}{2} \gamma_e \hbar B_0\right)$ and $\left(U_0 + \frac{1}{2} \gamma_e \hbar B_0\right)$. This is essentially the manifestation of the Zeeman effect, removing the degeneracy of states with $m_s = \pm 1/2$. The two levels are separated in energy by the amount $\gamma_e \hbar B_0$. The frequency of transition between these levels, $\gamma_e B_0$, has reference to the Larmor frequency in classical picture. So, if rf photons of frequency, $\gamma_e B_0$, were fed into the system, a resonant absorption of the radiation would take place. As already stated, in actual experiment, the frequency of the rf radiation is kept fixed at certain value ω_0 and the magnetic field searched for a value B_0 , satisfying the condition

$$\hbar \omega_0 = \gamma_e \hbar B_0 \quad (13.100)$$

or

$$\omega_0 = \gamma_e B_0$$

The experimental assembly for a magnetic resonance measurement is given in Fig. 13.9.

For ESR, where the electron spin is involved,

$$\begin{aligned} \gamma_e &= \frac{2\mu_B}{\hbar}, \quad \text{taking } g_0 = 2 \\ &= 17.587 \times 10^{10} \text{ s}^{-1} \text{ T}^{-1} \end{aligned}$$

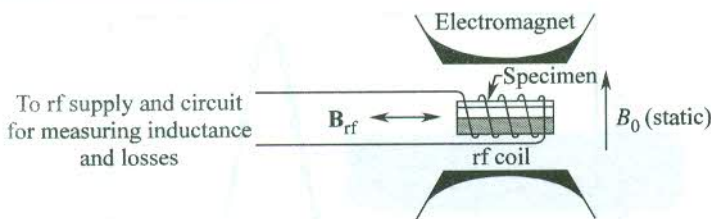


FIG. 13.9 Experimental set-up for a magnetic resonance measurement.

Using this value of γ_e , the frequency of rf radiation that would produce resonance can be expressed as

$$v_0(\text{GHz}) = 28.0 B_0(\text{T}) \quad (13.101)$$

For an induction field of 10 T, $v_0 = 28 \text{ GHz}$ (wavelength $\sim 1 \text{ cm}$). These frequencies are covered by the microwave region of the e.m. radiation. In experiment, a klystron is used as the source of microwaves. These days frequencies up to 50 GHz and fields up to 1.5 T (15 kilogauss) are very common. The use of a high frequency-high field combination not only provides a higher resolution but also improves the absorption probability.

Let N_1 and N_2 denote the spin population in the lower and upper levels, respectively, in the present system with $m_s = \pm 1/2$. Their ratio at the thermal equilibrium is written as

$$\left(\frac{N_2}{N_1} \right)_0 = \exp \left[- \frac{\gamma_e \hbar B_0}{k_B T} \right] \quad (13.102)$$

Generally, for temperatures at which the experiments are performed, $\gamma_e \hbar B_0 / k_B \ll T$ (for $B_0 = 1.0 \text{ T}$, it is $\sim 1 \text{ K}$). In this limit it is easy to show that the population difference $(N_1 - N_2)$ at thermal equilibrium is given by

$$(\Delta N)_0 \approx N \left(\frac{\gamma_e \hbar B_0}{2 k_B T} \right) = N \left(\frac{h v_0}{2 k_B T} \right) \quad (13.103)$$

where N is the total spin density ($N_1 + N_2$). The $(\Delta N)_0$ is usually very small compared to N . Though relation (13.103) shows that $(\Delta N)_0$ is proportional to v_0 , the experimental setting is often manipulated to make the ESR sensitivity closely proportional to v_0^2 . Also, for a large absorption probability $(\Delta N)_0$ should be reasonably large. These considerations indicate the desirability of performing the experiment at high fields and low temperature. Accordingly, the use of a high frequency high field combination is very much welcome.

The ESR was observed for the first time in MnSO_4 by Zavoisky* using a radio frequency in the MHz range and a field less than 0.01 T. The resonance is attributed to the unpaired spins of Mn^{++} ($S = 5/2$, $L = 0$). The resonance could barely be detected because of poor resolution. Zavoisky was later able to get a well resolved resonance (see Fig. 13.10) by increasing v_0 and B_0 .

Substances containing paramagnetic ions show EPR. The EPR is also observed in a few compounds with an even number of electrons including molecular oxygen and organic biradicals.

* E. Zavoisky, *J. Phys. (USSR)*, 9, 211, 245 (1945).

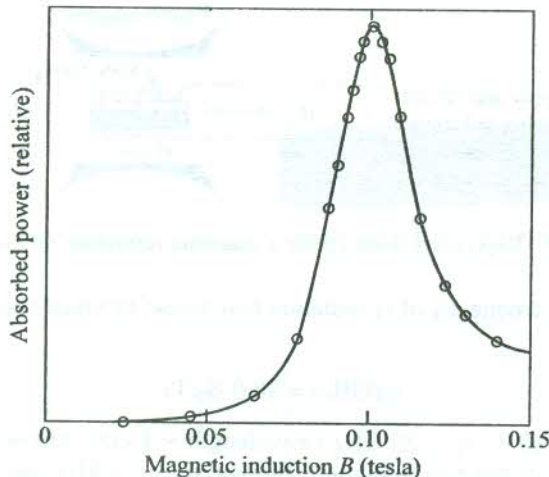


FIG. 13.10 The ESR of Mn^{2+} ions in MnSO_4 at room temperature (for $v_0 = 2.75 \text{ GHz}$). The Mn^{2+} ion has five unpaired electrons in the 3d shell ($L = 0, S = 5/2$). (After E. Zavoisky, *J. Phys. (USSR)*, **10**, 197 (1946)).

The fine structure of the resonance line is especially useful in studying the electronic structure of point defects such as *F*-centre in alkali halides and the donor impurity in semiconductors.

13.9.2 Nuclear Magnetic Resonance (NMR)

The principle of NMR is the same as that of the ESR with modification in expressions affected on account of replacing the electron spin S by the nuclear spin I . The nuclear energy under the influence of a magnetic field B_0 acting along the z -direction changes by an amount expressible as

$$\begin{aligned} U &= -\gamma_n \hbar \mathbf{I} \cdot \mathbf{B}_0 \\ &= -\gamma_n \hbar B_0 I_z \end{aligned} \quad (13.104)$$

with $I_z = -I, -(I-1), \dots, 0, \dots, (I-1), I$.

For the simplest case involving a proton,

$$\begin{aligned} \gamma_n &= \frac{2\mu_p}{\hbar} = 2.675 \times 10^8 \text{ s}^{-1} \text{ T}^{-1} \\ (\text{Using } \mu_p &= 1.4106 \times 10^{-26} \text{ J T}^{-1}) \end{aligned}$$

This value of γ gives the resonance frequencies in the range of MHz:

$$v_0(\text{MHz}) = 42.58 B_0(T) \quad (13.105)$$

So far as solids are concerned there are three most important aspects of studies for which the NMR technique has been widely exploited: (i) Structure, (ii) Molecular rotation, and (iii) Pauli susceptibility (appearing as the Knight shift in NMR).

Analysis in respect of the first two cases is carried out on the basis of general features of NMR such as the structure, width and shape of the resonance line. Details of the actual analysis may be dispensed with in a book like this that emphasizes the basic principles. Nevertheless, a suitable

account of relaxation processes that affect the features of magnetic resonance in a significant way is given at a later stage in this chapter.

Estimation of the Pauli susceptibility of metals by NMR, on the other hand, is especially significant because there is hardly any other experimental method that meets this purpose. In practice, a measurement of the bulk magnetic moment induced by a magnetic field in metals gives the sum of the Pauli paramagnetic susceptibility, the Landau diamagnetic susceptibility (see Section 13.6) and the Larmor diamagnetic susceptibility. Generally, it is not easy to isolate any of these contributions experimentally. The NMR study, nevertheless, provides an indirect method of estimating the Pauli susceptibility. The basis of measurement lies in the fact that the magnetic moments of the ionic nuclei couple more strongly to the spin magnetic moments of the conduction electrons than to fields produced by the translational motion of electrons.

The magnetic field acting directly on the nucleus determines the frequency of resonance. The field in non-paramagnetic materials differs by a small diamagnetic correction from the actually applied field. At a fixed frequency, the resonance thus occurs for a value of the magnetic field that is shifted from what would be expected in the absence of the diamagnetic correction. This shift is known as the *chemical shift*. There is, however, a stronger correction to the field in metals caused by the magnetic field of the spin magnetic moment of the conduction electrons. The same external magnetic field, in which the nuclei precess, also creates imbalance in the electronic spin populations in the parallel and antiparallel alignments with the field (see Fig. 13.5). We saw in Section 13.6 that the imbalance is responsible for the net magnetic moment and, therefore, for the Pauli paramagnetism of the conduction electron gas. The net electronic magnetic moment has its own field leading to a modified field at the nucleus. At a fixed frequency, the resonance of a spin is observed at a slightly different magnetic field in a metal than in a non-paramagnetic solid containing the metallic element. The observed shift, known as the *Knight shift*, is proportional to the Pauli susceptibility. But this estimate is not precise because the Knight shift is also proportional to the square of the magnitude of the conduction electron wavefunction at the nucleus. The actual Pauli susceptibility is obtained by incorporating this correction which is calculated with the knowledge of wavefunctions that are generally derived from the atomic s-shells.

13.9.3 Spin Relaxation

Consider again the simplest spin systems of an unpaired electron and proton to study the effect of spin relaxation on magnetic resonance. We are concerned with a two-level system in the presence of a dc magnetic field. Both upward and downward transitions are induced by the microwave photons at rates proportional to N_1 and N_2 , the population of the lower and upper levels respectively. For the absorption of the microwave power, the population difference $\Delta N (=N_1 - N_2)$ must maintain a positive value during the measurement. It is essential that ΔN remains at the equilibrium value (13.103) while the magnetic field is swept near resonance. This is ensured by restricting the microwave power input to a reasonably low level, usually determined by the mechanicsm of spin relaxation because of which the spin system falls back to the lower energy level.

Spin-lattice relaxation

The crystal lattice, usually represented by lattice vibrations, participates in this kind of spin relaxation. It occurs through mainly three types of processes:

- (i) **Direct process.** The spin-phonon coupling induces the relaxation with the emission of a low frequency ($\omega_0 = \gamma B_0$) acoustic phonon. The relaxation time τ_1 that represents the process varies with temperature T as $1/T$.
- (ii) **Raman process.** In certain solids this process competes with the direct process effectively at higher temperatures. A phonon of frequency ω , already present in the system at these temperatures, is inelastically scattered to cause relaxation with the emission of a phonon of frequency $(\omega + \omega_0)$. In this case, $\tau_1 \propto T^{-7}$ or T^{-9} .
- (iii) **Orbach process.** It is different from the Raman process in the sense that it is a two-stage phonon process in which the system at higher energy first goes to a further higher state by the absorption of a phonon of energy Δ present in the system, and then relaxes to the lower energy state with the emission of a phonon of energy $(\Delta + \hbar\omega_0)$. The temperature

dependence of the relaxation time is expressed as $\tau_1 \propto \exp\left(\frac{\Delta}{k_B T}\right)$.

In the absence of any spin relaxation, the equation of motion describing the precession of angular momentum $\hbar\mathbf{J}$ (see Section 13.1) is

$$\hbar \frac{d\mathbf{J}}{dt} = \boldsymbol{\mu} \times \mathbf{B}_0 \quad (13.106)$$

with

$$\begin{aligned} \mathbf{J} &= \mathbf{S} \text{ for a pure ESR} \\ &= \mathbf{I} \text{ for NMR} \end{aligned}$$

Relation (13.106) can be rewritten as

$$\frac{d\boldsymbol{\mu}}{dt} = \gamma \boldsymbol{\mu} \times \mathbf{B}_0 \quad (\text{since } \boldsymbol{\mu} = \gamma \hbar \mathbf{J}) \quad (13.107)$$

and

$$\frac{d\mathbf{M}}{dt} = \gamma \mathbf{M} \times \mathbf{B}_0 \quad (13.108)$$

where \mathbf{M} is the magnetization given by $(N_1 - N_2)\boldsymbol{\mu}$ or $(\Delta N)\boldsymbol{\mu}$, with N_1, N_2 defined as the spin population per unit volume of the lower and upper energy levels, respectively, in the two-level spin system.

When the field is applied along the z-direction, the magnetization at thermal equilibrium will be along the z-direction, i.e.

$$M_z = (\Delta N)_0 \boldsymbol{\mu} \quad \text{with} \quad M_x = 0 \quad \text{and} \quad M_y = 0$$

In the presence of the spin-lattice relaxation the magnetization M_z at any instant tends to approach the equilibrium value M_0 at the rate given by

$$\frac{dM_z}{dt} = \frac{M_0 - M_z}{\tau_1} \quad (13.109)$$

Integrating (13.109), we get

$$M_z(t) = M_0 \left(1 - \exp\left(-\frac{t}{\tau_1}\right) \right) \quad (13.110)$$

Accordingly, the spin-lattice relaxation modifies the equation of motion (13.108) to the form

$$\frac{dM_z}{dt} = \gamma(\mathbf{M} \times \mathbf{B}_0)_z + \frac{M_0 - M_z}{\tau_1} \quad (13.111)$$

The above equation states that besides precessing around the magnetic field, M_z tends to relax to the equilibrium value M_0 .

Spin-spin relaxation

In a static magnetic field \mathbf{B}_0 along the z -direction, if the transverse components of magnetization M_x and M_y are not zero to start with, they decay to zero since their values at thermal equilibrium are zero. The decay takes place through another type of relaxation known as the *spin-spin relaxation*. This occurs owing to the influence (as a result of the local field contribution) of one magnetic atom on others. The decay rate of the transverse magnetization is set by the spin-spin relaxation time τ_2 . The factor $1/\tau_2$ gives the rate constant for the loss of phase coherence of a set of spins with e.m. field applied in the x - or y -direction. In this sense, τ_2 is also identified as the dephasing time. The loss of phase coherence of a set of spins causes an increased fluctuation in the magnetic field exerted by spins on each other. As a consequence to this, the spins show resonance over a small range of the magnetic field values, providing thus a finite width to the resonance line.

Equations of motion for the transverse components of magnetization are written as

$$\frac{d\mathbf{M}_x}{dt} = \gamma(\mathbf{M} \times \mathbf{B}_0)_x - \frac{\mathbf{M}_x}{\tau_2} \quad (13.112)$$

$$\frac{d\mathbf{M}_y}{dt} = \gamma(\mathbf{M} \times \mathbf{B}_0)_y - \frac{\mathbf{M}_y}{\tau_2} \quad (13.113)$$

The relations (13.111) to (13.113) are called *Bloch equations*. They are solved to derive several important properties of a magnetic system from its magnetic resonance measurement.

The net effect of relaxation is demonstrated by the combined relaxation time τ given by

$$\frac{1}{\tau} = \frac{1}{\tau_1} + \frac{1}{\tau_2} \quad (13.114)$$

τ is effectively determined by the shorter of τ_1 and τ_2 . It is usually deduced from the width of the resonance line.

13.9.4 Line Width and Line Shape

For the sake of completeness, let us first have a cursory look at the causes of the line width. The main sources are identified as follows:

- (i) **Spontaneous emission.** It is responsible for the natural line width which is negligibly small compared to the width due to other sources.

- (ii) **Spin-lattice relaxation.** It is represented by the relaxation time τ_1 , as defined in Section 13.9.3.
- (iii) **Spin-spin relaxation (Magnetic dipole-dipole interaction).** It is represented by the relaxation time τ_2 , as described in Section 13.9.3. It is absent in liquids and gases because of rapid rotation of molecules which effectively averages out the magnetic fields.
- (iv) **Inhomogeneous magnetic field (an experimental limitation).** The static magnetic field may vary over the volume of the sample. There is a contribution to the overall line broadening because of the superposition of lines from the spins in the different parts of the sample.
- (v) **Electric quadrupole coupling.** It occurs in the NMR of nuclei with $I > 1/2$, where the electric quadrupole moments interact with the electric field gradients. The contribution in this case is relatively much small.

At first sight, the gain from a magnetic resonance measurement is appreciated in the form of knowledge about the effective g -factor that is crucial to the study of magnetic properties of a system. In fact, much more information is derived from this measurement. For example, the width and shape of the resonance line furnish information about the environment of spins. At this stage it must be impressed on the reader's mind that precise information about the symmetry around a paramagnetic centre, especially in crystalline solids, is determined from the fine structure and hyperfine structure of the resonance line. Being topics of advanced level, they are not discussed here.

In a magnetic resonance measurement, the absorbed rf power P can be plotted as a function of the magnetic field B . But a greater sensitivity is achieved with a phase-sensitive detection method, which gives dP/dB versus B plot. Bloch* considered the upward and downward stimulated transitions for a spin system where B/v_0 is swept at a linear rate through the resonance condition in an NMR measurement. But the theory applies equally well to EPR. Bloch has shown that when the deviation of the value of ΔN from $(\Delta N)_0$ (the value at thermal equilibrium) is negligibly small throughout the sweep of B/v_0 , the resonance line has a Lorentzian shape expressed as

$$P = \frac{P_{\max}}{1 + \frac{(B - B_0)^2}{\xi^2}} \quad (13.115)$$

where B_0 is the value at resonance and the parameter ξ is determined from the measure of the separation $\Delta B_{1/2}$ between the half-power points. Using simple calculus, we can show that

$$\Delta B_{1/2} = 2\xi \quad (13.116)$$

and

$$\Delta B_{pp} = \frac{2\xi}{\sqrt{3}} = \frac{\Delta B_{1/2}}{\sqrt{3}} \quad (13.117)$$

where ΔB_{pp} denotes the separation between the positive and negative peaks in the dP/dB plot.

The P and dP/dB plots for the EPR of DPPH (solid 1,1-diphenyl-2-picryl-hydrazyl) are shown in Fig. 13.11. The DPPH line is often taken as standard for the calibration of a spectrometer.

* F. Bloch, *Phys. Rev.*, **70**, 460 (1946).

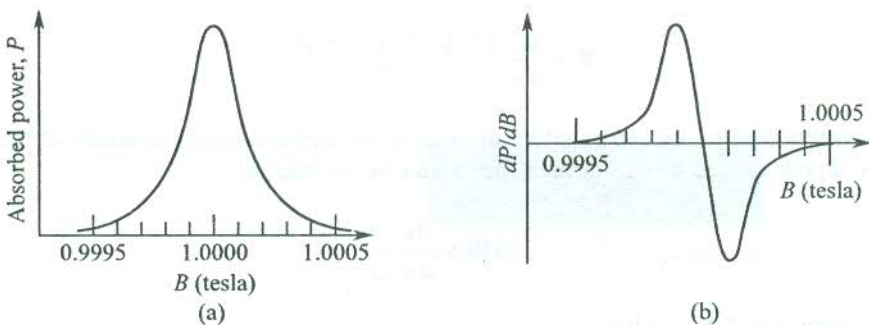


FIG. 13.11 (a) EPR absorption line for DPPH at room temperature ($v_0 = 28$ GHz). (b) The corresponding plot of the first derivative of the line.

The line width in units of frequency is given by the reciprocal of the net relaxation time τ which is estimated from

$$\tau \equiv \frac{1.1 \times 10^{-11}}{g \xi} \text{ s} \quad (13.118)$$

when ξ is expressed in units of tesla.

In case the value of ΔN happens to be much different from $(\Delta N)_0$, the resonance line assumes a Gaussian shape

$$P = P_{\max} \exp \left[-\frac{(B - B_0)^2}{\xi^2 \ln 2} \right] \quad (13.119)$$

giving again $\Delta B_{1/2} = 2\xi$ but a larger ΔB_{pp} and a relationship between ξ and τ that differs from (13.118).

The NMR line behaves differently by the way of its width being practically independent of τ_1 , even though τ_1 continues to determine the rate of spin transitions induced without creating saturation. In a nuclear spin system, τ_1 can become appreciably large at low temperatures. Pound (1951) reported the value of τ_1 as 300 s at room temperature for ^{7}Li in LiF crystal. Harping on the consequences of this slow response, he along with Purcell* founded the concept of 'population inversion' in a nuclear spin system where the spin population density is greater in a higher energy state than that in the ground state. The spin populations being given by the Boltzmann distribution at thermal equilibrium, the inversion of population must be viewed as accompanied by the cooling of the spin system. Thus, for a spin system at low temperatures, it is very much likely that a negative value of temperature would have to be assigned to the system when in an excited state at thermal equilibrium under the condition of population inversion. The concept of population inversion and negative temperature was exploited later in the same decade in the discovery of masers and lasers.

The magnetic dipolar interaction is usually the main contributor (through a small τ_2) to the large width of an NMR line in a solid. The magnetic field caused by a magnetic dipole† of strength μ at a distance r in a rigid lattice is

* E.M. Purcell and R.V. Pound, *Phys. Rev.*, **81**, 279 (1951).

† Relation (13.120) is comparable with the corresponding relation (10.2) for an electric dipole.

$$\mathbf{B} = \frac{\mu_0}{4\pi} \frac{[3(\mu \cdot \mathbf{r})\mathbf{r} - r^2\mu]}{r^5} \quad (13.120)$$

If two nearest dipoles are separated by distance a , the approximate magnitude of the magnetic field at one dipole caused by the nearest other can be written as

$$|\Delta \mathbf{B}| \approx \frac{\mu_0}{4\pi} \frac{\mu}{a^3} \quad (13.121)$$

For protons with $a = 2 \text{ \AA}$, we have

$$|\Delta \mathbf{B}| \approx 10^{-7} \times \frac{1.4106 \times 10^{-26}}{8 \times 10^{-30}} \text{ T}$$

$$\approx 2 \times 10^{-4} \text{ T}$$

The observed resonance line reflects the effect of the vector sum of fields mainly caused by all the nearest magnetic dipoles. Relation (13.121) essentially gives the line broadening contributed by the magnetic dipole-dipole interaction.

SUMMARY

1. The (Larmor) diamagnetic susceptibility of N atoms of atomic number Z is given by

$$\chi = -\frac{\mu_0 N Z e^2}{6m} \langle r^2 \rangle, \text{ where } \langle r^2 \rangle \text{ is the mean square atomic radius. This relation is known}$$

as the Langevin's relation for the diamagnetic susceptibility.

2. According to the classical theory, the relation for paramagnetic susceptibility of atoms with a permanent magnetic moment μ is given by

$$\chi = \frac{\mu_0 \mu^2 N}{3 k_B T} \quad \text{for} \quad \mu B_0 \ll k_B T \quad (\text{Curie-Langevin expression})$$

where N denotes the number of atoms per unit volume.

3. The magnetic moment of an atom is

$$\mu = -\mu_B (\mathbf{L} + g_0 \mathbf{S}) = -g\mu_B \mathbf{J}$$

4. When an atom or ion is in its ground state, its electrons in the same shell acquire the maximum value of S in accordance with the Pauli principle and maximum L as may be consistent with the maximum S . The value of J is $(L + S)$ for a shell more than half-filled and $(L - S)$ for a shell less than half-filled.

5. $J = 0$ for completely-filled shells and shells that are one electron short of being half-filled.

6. The magnetic Helmholtz energy F is defined as

$$\exp(-F/k_B T) = \sum_n \exp[-E_n(B_0)/k_B T]$$

where E_n is the electronic energy in the n th state in the presence of field B_0 .

7. The magnetic susceptibility of a system is defined in terms of the Helmholtz free energy F as

$$\chi = -\mu_0 N \frac{\partial^2 F}{\partial B_0^2}$$

where N is the number of atoms/ions per unit volume.

8. According to quantum mechanics, the change in the energy of an ion in its n th state when placed in a magnetic field B_0 is

$$\begin{aligned} \Delta E_n &= \mu_B \mathbf{B}_0 \cdot \langle \phi_n | \mathbf{L} + g_0 \mathbf{S} | \phi_n \rangle + \sum_{n' \neq n} \frac{|\langle \phi_n | \mu_B \mathbf{B}_0 \cdot (\mathbf{L} + g_0 \mathbf{S}) | \phi_{n'} \rangle|^2}{E_n - E_{n'}} \\ &\quad + \frac{e^2}{8m} B_0^2 \langle \phi_n | \sum_i (x_i^2 + y_i^2) | \phi_n \rangle \end{aligned}$$

where the first term gives rise to paramagnetism because of the permanent magnetic moment; the second term leads to weak paramagnetism including van Vleck paramagnetism which is temperature independent (for a partially-filled shell with $J = 0$) and the last term refers to Larmor diamagnetism.

9. According to the quantum theory, the paramagnetic susceptibility of ions with $J \neq 0$ (with permanent ionic magnetic moment μ) is given by

$$\chi = \frac{\mu_0 N p^2 \mu_B^2}{3 k_B T} \text{ in the limit } \mu B_0 \ll k_B T, \text{ where } p \text{ is the 'effective Bohr magneton number'}$$

defined as

$$p = g[J(J+1)]^{1/2}.$$

and N is the number of ions per unit volume.

10. The paramagnetic susceptibility of conduction electrons (metals) is independent of temperature for $k_B T \ll \epsilon_F$ and expressed as

$$\chi = \frac{3N\mu_0\mu_B^2}{2\epsilon_F} = \frac{3N\mu_0\mu_B^2}{2k_B T_F}$$

where N is the total number of electrons.

11. The frequency of magnetic resonance is

$$\omega_0 = \gamma B_0, \text{ where } \gamma = \frac{\mu}{\hbar J} \text{ (the magnetogyric ratio)}$$

12. The Bloch equations are

$$\frac{d\mathbf{M}_x}{dt} = \gamma(\mathbf{M} \times \mathbf{B})_x - \frac{\mathbf{M}_x}{\tau_2}$$

$$\frac{d\mathbf{M}_y}{dt} = \gamma(\mathbf{M} \times \mathbf{B})_y - \frac{\mathbf{M}_y}{\tau_2}$$

$$\frac{d\mathbf{M}_z}{dt} = \gamma(\mathbf{M} \times \mathbf{B})_z + \frac{\mathbf{M}_0 - \mathbf{M}_z}{\tau_1}$$

13. The shapes of the magnetic resonance line:

$$\text{Lorentzian: } P = \frac{P_{\max}}{1 + \frac{(B - B_0)^2}{\xi^2}}$$

$$\text{Gaussian: } P = P_{\max} \exp \left[-\frac{(B - B_0)^2}{\xi^2 \ln 2} \right]$$

$$\text{with } \Delta B_{1/2} = 2\xi.$$

14. Line width due to magnetic dipole-dipole interaction in a rigid lattice is given by

$$|\Delta\mathbf{B}| \approx \frac{\mu_0}{4\pi} \frac{\mu}{a^3}$$

where a is the separation between the two nearest dipoles.

PROBLEMS

13.1 The wavefunction of the hydrogen atom in its ground state is

$$\psi = \frac{1}{(\pi a_0^2)^{1/2}} \exp \left(-\frac{r}{a_0} \right)$$

Assuming the charge density to be given by

$$\rho(x, y, z) = e|\psi|^2$$

show that

$$\langle r^2 \rangle = 3a_0^2$$

and calculate the molar diamagnetic susceptibility of atomic hydrogen.

- 13.2 Ampere defined classically the magnetic moment of electron owing to its orbital motion as the average over the orbit of $-e/2(\mathbf{r} \times \mathbf{v})$.

Prove that our definition, $\mu = \partial E / \partial B_0$, reduces to this form by showing from (13.47) that

$$\mu = -\frac{e}{2m} \sum_i \mathbf{r}_i \times \left(\mathbf{p}_i - \frac{e}{2} \mathbf{r}_i \times \mathbf{B}_0 \right)$$

and

$$\mathbf{v}_i = \frac{\partial \mathbf{H}}{\partial \mathbf{p}_i} = \frac{1}{m} \left(\mathbf{p}_i - \frac{e}{2} \mathbf{r}_i \times \mathbf{B}_0 \right)$$

- 13.3 (a) Show that the following formulae summarize the Hund's rules for a shell of angular momentum l containing n electrons:

$$S = 1/2 [(2l + 1) - |2l + 1 - n|]$$

$$L = S [2l + 1 - n]$$

$$J = |2l - n| S$$

- (b) For a given LS -multiplet, verify that

$$(2L + 1)(2S + 1) = \sum_{|L-S|}^{|L+S|} (2J + 1)$$

- (c) Find the ground state of

- (i) Eu²⁺ in the configuration 4f⁷5s²p⁶
- (ii) Dy³⁺ in the configuration 4f⁹5s²p⁶
- (iii) Tm³⁺ in the configuration 4f¹²5s²p⁶

- 13.4 A magnetic field B_0 , when applied on an atom with a spherically symmetric charge distribution $\rho(r)$, induces a diamagnetic current. Show that the magnetic field produced by the diamagnetic current at the nucleus is

$$\Delta B_0 = -\left(\frac{eB_0}{3m}\right)V_0$$

where V_0 is the electrostatic potential at the nucleus, given by

$$V_0 = \int_0^\infty \frac{\rho(r)}{r} 4\pi r^2 dr$$

- 13.5 When a system of electron spins is placed in a magnetic field of 2 Wb/m² at a certain temperature, the number of the spins parallel to field lines is twice the number of the spins antiparallel to the field. Determine the temperature.

- 13.6 The most important contribution to the paramagnetism of copper sulphate comes from the copper ions which have spin 1/2 and may be treated as non-interacting. Show that the magnetization in field B_0 is given by

$$M = N\mu_B = \tanh\left(\frac{\mu_B B_0}{k_B T}\right)$$

where N is the number of ions per unit volume.

- 13.7 In benzene, the carbon atoms form a regular hexagon of side 1 Å. One outer electron from each carbon atom has a wavefunction that extends round the whole ring of atoms (the other three are in sp^2 atomic orbitals). Make a rough estimate of the contribution of these electrons to the diamagnetic susceptibility of liquid benzene (density 0.88 g cm⁻³; molecular wt. = 76).
- 13.8 An ion has a partially-filled shell of angular momentum J with Z electrons in the completely filled shells. Show that the ratio of the Curie law paramagnetic susceptibility to the Larmor diamagnetic susceptibility is

$$\frac{\chi_{\text{para}}}{\chi_{\text{dia}}} = - \frac{2J(J+1)}{Zk_B T} \frac{\hbar^2}{m\langle r^2 \rangle}$$

- 13.9 A magnetic field is applied to a salt containing Cu²⁺ ions. Cu²⁺ has 9 electrons in the 3d shell. What magnetic field must be applied to the salt when at 1 K, so that 99 per cent of the ions are in the lowest energy state?
- 13.10 For quantized states we cannot use the Langevin function $L(x)$ given by (13.22) to compute susceptibilities, but instead, the Brillouin function $B_J(x)$ as given by (13.59) must be used. Show that $B_J(x) \rightarrow L(x)$ as $J \rightarrow \infty$, with $x = \mu B_0 / k_B T$.
- 13.11 For temperatures very small compared to the Fermi temperature, show that the temperature dependent correction to the Pauli susceptibility is

$$\chi(T) = \chi(0) \left(1 - \frac{\pi^2}{6} (k_B T)^2 \left[\left(\frac{D'}{D} \right)^2 - \frac{D'}{D} \right] \right)$$

where D , D' and D'' are the density of levels and its derivatives at the Fermi energy. Show that for electrons it reduces to

$$\chi(T) = \chi(0) \left(1 - \frac{\pi^2}{12} \left(\frac{k_B T}{\epsilon_F} \right)^2 \right)$$

- 13.12 (a) Show that for a crystal containing N paramagnetic ions with $S = 1/2$ and $g_0 = 2$, the spin entropy can be expressed by

$$S = \frac{N\Delta}{2T} \tanh\left(\frac{\Delta}{2k_B T}\right) + Nk_B \ln(2) \cosh\left(\frac{\Delta}{2k_B T}\right)$$

with $\Delta = 2\mu_B B_0$

- (b) For cooling by adiabatic demagnetization, why is it not possible to start with the nuclear demagnetization, without going through the process of electron-spin demagnetization?

SUGGESTED FURTHER READING

- Abragam, A., *Nuclear Magnetism* (Oxford, 1961).
- Ashcroft, N.W. and N.D. Mermin, *Solid State Physics* (Saunders College, 1988).
- Blakemore, J.S., *Solid State Physics* (W.B. Saunders, 1974).
- Chakravarty, A.S., *Introduction to Magnetic Properties of Solids* (John Wiley, 1980).
- Hudson, R.D., *Principles and Applications of Magnetic Cooling* (Elsevier, 1972).
- Kittel, C., *Introduction to Solid State Physics*, 7th ed. (John Wiley, 1996).
- Slichter, C.P., *Principles of Magnetic Resonance*, 3rd ed. (Springer, 1990).
- van Vleck, J.H., *The Theory of Electric and Magnetic Susceptibilities* (Oxford, 1932).
- White, R.M., *Quantum Theory of Magnetism* (Springer, 1982).

Ferromagnetism, Antiferromagnetism and Ferrimagnetism

A system of non-interacting magnetic ions is expected to be thermally disordered at any temperature in the absence of an applied magnetic field. The vector magnetic moment of each ion would then average to zero as confirmed by (13.20). Nevertheless, there are plenty of solids in which individual magnetic ions have nonvanishing average vector moments below a critical temperature T_c . This points towards a possible correlation or interaction among magnetic ions, leading to the ordering of magnetic moments as revealed by experiments. These solids are regarded as magnetically ordered.

The magnetic ordering may or may not lead to a net magnetization for the solid as a whole. There arise three distinct cases of ordering:

1. The individual localized magnetic moments may combine, even in the absence of an applied magnetic field, to produce a macroscopic bulk magnetization reflecting the existence of microscopic ordering. Such a magnetization is known as *spontaneous magnetization* and the solids exhibiting this property are called *ferromagnets*. An array of local magnetic moments with the same magnitude and average direction describes the simplest model of ferromagnets. It is represented by the first of the three arrays in Fig. 14.1(a) for a linear ferromagnet.
2. The individual local moments may add up to zero, resulting in no bulk magnetization. The solids with this type of ordering have been identified as *antiferromagnets*. Two possible arrays of local moments for a linear antiferromagnet are drawn in Fig. 14.1(b).
3. The primitive cell of some solids showing spontaneous magnetization contains several magnetic ions which may necessarily not be identical. Such a possibility makes it desirable to adopt a rather restrictive definition of ferromagnets, according to which all the local moments are required to have a positive component along the direction of spontaneous magnetization. The solids that show spontaneous magnetization but do not satisfy this requirement are described as *ferrimagnets*. We will show later that the spontaneous magnetization that is acquired by ferrimagnets is relatively much small. The possible orderings for a linear ferrimagnet are shown in Fig. 14.1(c).

14.1 WEISS THEORY OF FERROMAGNETISM

Ferromagnetic materials have been known for many years. Of these only five (Fe, Co, Ni, Gd and Dy)

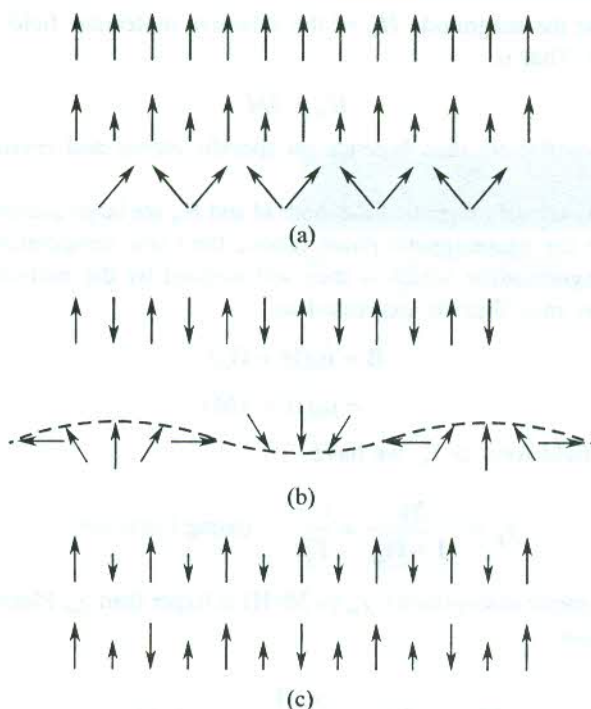


FIG. 14.1 Possible orderings of atomic moments in a linear (a) ferromagnet, (b) antiferromagnet, and (c) ferrimagnet.

are elements (all metals) and the rest are alloys and insulating compounds (see Table 14.1). In similarity with ferroelectrics, ferromagnetic materials exhibit hysteresis in the relationship between magnetic induction B and intensity of the applied magnetic field H . Ferromagnetism is clearly revealed by a macroscopic magnetic field which in one of the simplest approaches is recognized as the mean molecular field. It is apparent from what we said in the beginning that ferromagnetism arises because of the cooperative alignment of permanent atomic dipoles which may be supposed to be caused by the mean molecular field. The concept of mean field was introduced by Pierre Weiss* through his theory that provides a satisfactory explanation to ferromagnetism. The Weiss mean field theory is based on the following two hypotheses.

1. In ferromagnetic solids of macroscopic dimensions, there are a number of small regions, called *domains*, that are spontaneously magnetized.
2. There exists a molecular magnetic field within each domain and the field tends to produce a parallel alignment of the individual localized atomic moments.

While describing the properties of magnetic domains later in this chapter we will find that the explanation to the hysteresis revealed by the B - H curve follows from these hypotheses. It must, however, be remarked here that spontaneous magnetization refers to a single domain whereas the remanent magnetization (for $H = 0$) refers to the specimen as a whole.

* P. Weiss, *J. Phys. Radium*, **4**, 661 (1907).

Weiss observed that the magnitude H_m of the effective molecular field should be proportional to the magnetization M . That is,

$$H_m = \lambda M \quad (14.1)$$

where λ is the Weiss coefficient that depends on specific atoms and crystal structure but not on temperature.

In the absence of an external magnetic field, both M and H_m are large quantities in the ferromagnetic phase of a solid. But in the paramagnetic phase (above the Curie temperature T_c), an external field is needed to initiate magnetization which is then self-assisted by the molecular field it builds. The total magnetic induction may thus be expressed as

$$\begin{aligned} \mathbf{B} &= \mu_0(\mathbf{H} + \mathbf{H}_m) \\ &= \mu_0(\mathbf{H} + \lambda\mathbf{M}) \end{aligned} \quad (14.2)$$

and in a weak applied field for $T > T_c$, we have

$$\chi_p = \frac{\mathbf{M}}{\mathbf{H} + \mathbf{H}_m} = \frac{C}{T} \quad (\text{using Curie law}) \quad (14.3)$$

The observable magnetic susceptibility $\chi_m (= \mathbf{M}/\mathbf{H})$ is larger than χ_p . Placing the value of \mathbf{H}_m from (14.1) in (14.3), we obtain

$$\mathbf{M} = \chi_m \mathbf{H} = \frac{\chi_p \mathbf{H}}{(1 - \lambda \chi_p)} \quad \text{for } T > T_c \quad (14.4)$$

or

$$\chi_m = \frac{\mathbf{M}}{\mathbf{H}} = \frac{\chi_p}{1 - \lambda \chi_p} = \frac{C}{T - \lambda C} = \frac{C}{T - T_c} \quad (14.5)$$

with

$$T_c = \lambda C \quad (14.6)$$

In view of (14.5), χ_m has a singularity at $T = T_c = \lambda C$. The spontaneous magnetization shows up for $T \leq T_c$, since there can be a finite M for $H = 0$ even when χ_m is infinite. Relation (14.5) states the Curie-Weiss law that is known to explain the observed variation of susceptibility above the Curie temperature T_c (Fig. 14.2) in most of the ferromagnetic solids. Using the value of C from (13.27) in (14.6), the Weiss coefficient can be written as

$$\lambda = \frac{T_c}{C} = \frac{3k_B T_c}{\mu_0 N g^2 S(S+1) \mu_B^2} \quad (14.7)$$

The use of S in place of J in the above relation implies that the contribution of the orbital motion can be treated as negligible, letting the effective Bohr magneton number to be determined entirely by the spin of the unpaired electrons.

Relation (14.7) gives the value of λ for iron as $\sim 10^3$. Using the value of spontaneous magnetization M_s as $1.74 \times 10^6 \text{ A m}^{-1}$ (Table 14.1), we obtain $H_m \sim 10^9 \text{ A m}^{-1}$ or the value of magnetic induction $\mu_0 H_m \approx 10^3 \text{ T}$. On the other hand, the order of magnitude of the field produced by a magnetic ion regarded as a dipole at a nearest ion at distance a equals $\sim \mu_0 \mu_B / 4\pi a^3 \approx 0.1 \text{ T}$. These small dipolar

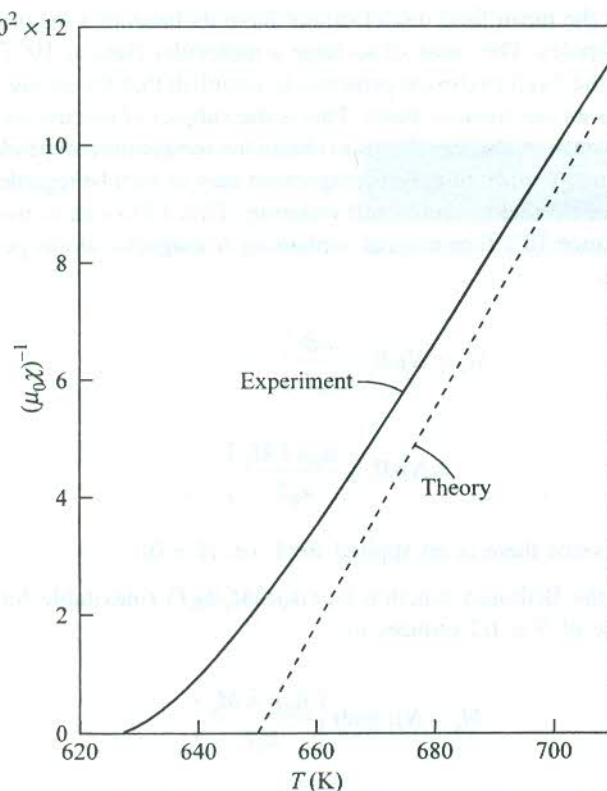


FIG. 14.2 Reciprocal of the susceptibility for nickel as a function of temperature above the Curie temperature on the mean field theory. The experimental curve shows the typical results on nickel. [After P. Weiss and R. Forrer, *Ann. Phys.*, **15**, 153 (1926).]

Table 14.1 Selected ferromagnetic solids[†] with Curie temperatures T_c and saturation magnetization M_s at $T = 0$ K

Substance	T_c (K)	M_s (gauss)
Fe	1043	1752
Co	1388	1446
Ni	627	510
Gd	293	1980
Dy	85	3000
MnAs	318	870
MnBi	670	675
Au_2MnAl	200	323
Cu_2MnIn	500	613
EuO	77	1910
GdCl_3	2.2	550

[†] Sources: F. Keffer, *Handbuch der Physik*, vol. 18, pt. 2 (Springer, New York, 1966); P. Heller, *Rep. Progr. Phys.*, **30** (pt. II), 731 (1967).

fields clearly indicate that the mean field model cannot have its basis in a magnetostatic coupling of the permanent magnetic dipoles. The cause of so large a molecular field as 10^3 T was discovered by Heisenberg* who applied the Pauli exclusion principle to establish that the strong interaction between adjacent magnetic ions has an electrostatic basis. This is the subject of discussion of the next section.

The mean field approximation also enables us to obtain the temperature-dependence of spontaneous magnetization below the Curie temperature. Ferromagnetism may as well be regarded as paramagnetism with a massive molecular field that produces self-ordering. This allows us to use (13.58) to express the spontaneous magnetization of a ferromagnet containing N magnetic atoms per unit volume, each of magnetic moment μ , as

$$\begin{aligned} M_s &= N\mu B_J \left(\frac{\mu B}{k_B T} \right) \\ &= N\mu B_J \left(\frac{\mu_0 \mu \lambda M_s}{k_B T} \right) \end{aligned} \quad (14.8)$$

with $B = \mu_0 H_m = \mu_0 \lambda M_s$ (since there is no applied field, i.e. $H = 0$) (14.9)

Replacing J by S in the Brillouin function $B_J (\mu_0 \mu \lambda M_s / k_B T)$ (inevitable for transition metals), relation (14.8) for the case of $S = 1/2$ reduces to

$$M_s = N\mu \tanh \left(\frac{\mu_0 \mu \lambda M_s}{k_B T} \right) \quad (14.10)$$

The solution to this transcendental equation for nonzero M_s is determined graphically as in Fig. 14.3 to give a curve for $M_s(T)$ which falls from a saturated value at $T = 0$ to zero at $T = T_c$ (see Fig. 14.4).

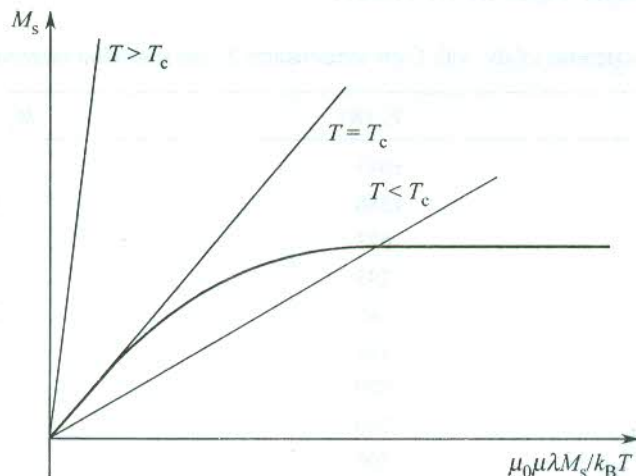


FIG. 14.3 Graphical solution of equation (14.10). For $T > T_c$, there is only one solution at $M_s = 0$. For temperatures below T_c , the curves have a second intersection that gives the other solution.

* W. Heisenberg, *Z. Physik*, **49**, 619 (1928).

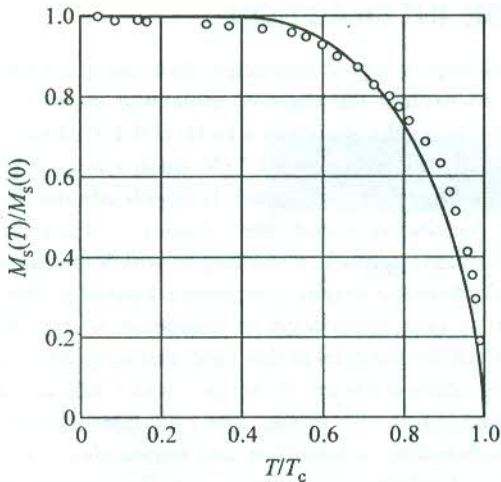


FIG. 14.4 Saturation magnetization of nickel as a function of temperature for $S = 1/2$ on the molecular field model. Open circles denote the experimental points. [After P. Weiss and R. Forrer, *Ann. Phys.*, **15**, 153(1926).]

The energy per unit volume U is written as

$$U = -M_s H_m = -\lambda M_s^2 \quad (14.11)$$

which gives the heat capacity C_V as

$$C_V = -2 \lambda M_s \left(\frac{\partial M_s}{\partial T} \right) \quad (14.12)$$

According to (14.12), C_V rises to a maximum at T_c and then falls abruptly to zero as shown in Fig. 14.5. The mean field theory thus predicts an anomaly in the heat capacity at T_c which is confirmed by experiments. The transition from the paramagnetic to the ferromagnetic phase is typically a second-order type as is demonstrated by the continuous fall of spontaneous magnetization, being treated as an order parameter (see Fig. 14.4).

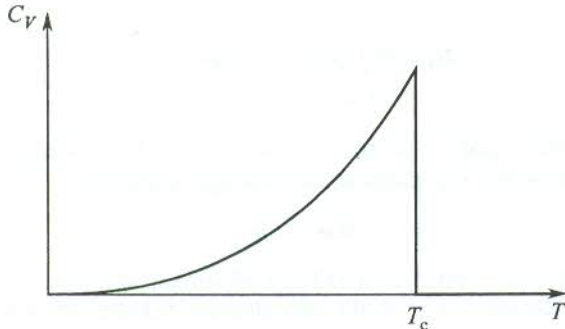


FIG. 14.5 Heat capacity anomaly as predicted on mean field theory.

14.2 THE EXCHANGE INTERACTION

The inadequacy of the magnetic dipole-dipole interaction to account for ferromagnetism is proved by the failure of the interaction to explain the massive molecular mean fields and fairly high Curie temperatures. In iron, an atomic magnetic dipole in a field of 0.1 T caused by the nearest dipole (see Section 14.2) has a magnetic interaction energy $\sim 10^{-4}$ eV. Such a weak magnetic coupling is expected to break down above $(1.6 \times 10^{-23}/k_B) K \approx 1$ K, which is hopelessly much smaller than the observed Curie temperature (1043 K). As already stated, the solution to this puzzle has been provided by Heisenberg in a quantum mechanical approach, according to which the cause of the magnetic ordering lies in an interaction of the electrostatic origin, commonly known as the *exchange interaction*.

The exchange interaction is best understood in insulators where the magnetic ions are well separated, though the theory is not simple even in this case. For simplicity, we consider the interaction within a hydrogen molecule regarding it a solid of two atoms and thus avoiding complications arising in a real solid containing approximately 10^{23} atoms. The principles involved are then generalized for application to real solids. It is, however, a laborious and intricate exercise to carry over these ideas to metals because of the required subtle modifications. Let \mathbf{R}_A and \mathbf{R}_B denote the position vectors of the two protons A and B, respectively, and \mathbf{r}_1 and \mathbf{r}_2 define locations of the two electrons labelled as 1 and 2, respectively. The extent to which the antiparallel ($S = 0$) spin arrangement is more favourable than the parallel is determined by the singlet-triplet energy splitting. We now proceed below to obtain an expression for this splitting. It is quite pleasant to find that the expression obtained justifies the need of viewing the source of magnetic interaction as an exchange interaction.

The two-electron Hamiltonian of a hydrogen molecule can be expressed as the sum of three parts:

$$\mathcal{H} = H_1 + H_2 + H_I \quad (14.13)$$

with

$$H_i = -\frac{\hbar^2}{2m} \nabla_i^2 - \frac{e^2}{4\pi\epsilon_0} \left[\frac{1}{|\mathbf{r}_i - \mathbf{R}_A|} + \frac{1}{|\mathbf{r}_i - \mathbf{R}_B|} \right], \quad i = 1, 2 \quad (14.14)$$

and

$$H_I = \frac{e^2}{4\pi\epsilon_0} \frac{1}{|\mathbf{r}_1 - \mathbf{r}_2|} \quad (14.15)$$

When the electron-electron interaction H_I is ignored, the two-electron Schrödinger equation is written as

$$(H_1 + H_2) \psi(1, 2) = \xi \psi(1, 2) \quad (14.16)$$

$(1 \equiv \mathbf{r}_1; 2 \equiv \mathbf{r}_2)$

The Hamiltonian in this equation comprises one-electron Hamiltonians and solutions to this equation can be derived from the one-electron Schrödinger equation

$$H\psi = \varepsilon\psi \quad (14.17)$$

Let ψ' and ψ'' denote the solutions to (14.17) of lowest energies ε' and ε'' ($\varepsilon' < \varepsilon''$). The symmetric solution of the lowest energy to the two-electron Schrödinger equation (14.16) is

$$\psi_s(1, 2) = \psi'(1) \psi''(2) \quad (14.18)$$

with

$$\xi_s = 2\epsilon'$$

This is clearly a singlet state meeting the requirement of the Pauli principle. The lowest antisymmetric solution is a triplet:

$$\psi_t(1, 2) = \psi'(1) \psi''(2) - \psi'(2) \psi''(1) \quad (14.19)$$

with

$$\xi_t = \epsilon' + \epsilon''$$

We are thus led to the result $\xi_s < \xi_t$ which is in fact a general theorem for the two-electron systems. The ground state energy ($2\epsilon'$) is determined by the symmetric solution (14.18) which is not expected to be a proper solution to the exact two-electron Schrödinger equation that includes the electron-electron Coulomb interaction as well. Actually, it turns out to be a thoroughly bad solution when the protons are far separated because the solution fails to deal effectively with the electron-electron interaction in this situation mainly because of the structures of ψ' and ψ'' . The specialized case of a solid in which $N = 2$ and the protons are well-separated, is most elegantly handled in the tight-binding approximation, generally used for the band structure calculations (see Section 7.8). In this approach, the one-electron stationary-state wavefunctions ψ' and ψ'' are taken as linear combinations of atomic stationary-state wavefunctions ϕ_A and ϕ_B centred at lattice points R_A and R_B , respectively:

$$\begin{aligned} \psi' &= \phi_A + \phi_B \\ \psi'' &= \phi_A - \phi_B \end{aligned} \quad (14.20)$$

Accordingly, the two-electron wavefunctions (14.18) and (14.19) change to

$$\psi_s(1, 2) = \phi_A(1)\phi_B(2) + \phi_B(1)\phi_A(2) + \phi_A(1)\phi_A(2) + \phi_B(1)\phi_B(2) \quad (14.21)$$

and

$$\psi_t(1, 2) = 2[\phi_B(1)\phi_A(2) - \phi_A(1)\phi_B(2)] \quad (14.22)$$

where $\phi_\alpha(i)$ stands for an orbital of the hydrogen atom α at which the electron i is localized.

The structure of (14.21) reveals that states in which both electrons are located on the same atom ('ionic states') are equally represented in this form of $\psi_s(1, 2)$. The corresponding terms (the last two) describe a hydrogen molecule as a H^- ion and a bare proton which may be acceptable (though far from being accurate), provided we ignore the repulsive Coulomb term (the electron-electron interaction) or at least absorb it into the effective potential of the ions. Therefore, in order to include the effect of the electron-electron interaction, especially when the protons are well-separated, the ionic states be better omitted. This is essentially the Heitler-London approximation according to which (14.21) reduces to

$$\psi_s(1, 2) = \phi_A(1)\phi_B(2) + \phi_B(1)\phi_A(2) \quad (14.23)$$

The singlet-triplet splitting is then estimated from

$$\xi_s - \xi_t = \frac{\langle \psi_s | \mathcal{H} | \psi_s \rangle}{\langle \psi_s | \psi_s \rangle} - \frac{\langle \psi_t | \mathcal{H} | \psi_t \rangle}{\langle \psi_t | \psi_t \rangle} \quad (14.24)$$

where \mathcal{H} is the complete Hamiltonian inclusive of the electron-electron interaction.

With a little bookkeeping, it can be shown that this splitting in the limit of large spatial separation is given by

$$\frac{1}{2}(\xi_s - \xi_t) = \frac{e^2}{4\pi\varepsilon_0} \int \left(\frac{1}{|\mathbf{R}_A - \mathbf{R}_B|} + \frac{1}{|\mathbf{r}_1 - \mathbf{r}_2|} - \frac{1}{|\mathbf{r}_1 - \mathbf{R}_A|} - \frac{1}{|\mathbf{r}_2 - \mathbf{R}_B|} \right) \times \phi_A^*(1) \phi_A(2) \phi_B^*(2) \phi_B(1) d\mathbf{r}_1 d\mathbf{r}_2 \quad (14.25)$$

Since the matrix element represented by the integral is between two states that differ only through the exchange of the coordinates of the two electrons, the singlet-triplet splitting is justifiably referred to as the *exchange splitting*. In the same spirit, the source of splitting, when viewed as the source of magnetic interaction, is called the *exchange interaction* and the integral as the *exchange integral*, customarily denoted by J_{ex} . This implies that

$$(\xi_s - \xi_t) = 2J_{\text{ex}} \quad (14.26)$$

14.3 THE HEISENBERG MODEL

The spin-dependence of energy of a spin configuration is implicitly carried through the total wavefunction which is a product of the spatial and spin functions. In this section, we discuss the Heisenberg model for a two-electron system in a hydrogen molecule. We will define a spin-dependent Hamiltonian whose eigenvalues are the same as those of the original Hamiltonian in certain limit as discussed below. This Hamiltonian is called the *spin Hamiltonian*.

When the protons in a hydrogen molecule are well separated, the ground state wavefunction describes two independent hydrogen atoms. Since each electron can have two spin orientations, the ground state is fourfold degenerate. But when the protons are not far apart, ξ_s is no more equal to ξ_t and a splitting of the fourfold degeneracy occurs. The splitting, however, is quite small compared to other excitation energies of the system. If $k_B T$ is small, $\sim (\xi_s - \xi_t)$, then only the lowest four-state manifold can be thermally populated. The analysis of many properties especially at thermal equilibrium becomes far more easier if other excited states are simply overlooked. We can then use a linear combination of these four lowest states to represent the ground state wavefunction of the system. The eigenvalues of the corresponding Hamiltonian (the spin Hamiltonian) operator will then have the same eigenvalues as those of the original Hamiltonian within the energy range of the lowest four states whose spin is contained in the eigenfunctions.

Each individual electron spin operator satisfies $S_i^2 = \frac{1}{2}\left(\frac{1}{2} + 1\right) = \frac{3}{4}$, requiring the total spin operator \mathbf{S} to satisfy

$$\mathbf{S}^2 = (\mathbf{S}_1 + \mathbf{S}_2)^2 = \frac{3}{2} + 2\mathbf{S}_1 \cdot \mathbf{S}_2 \quad (14.27)$$

Using the result that the eigenvalue of \mathbf{S}^2 is $S(S+1)$ in states of spin S , we obtain the eigenvalue of the operator $\mathbf{S}_1 \cdot \mathbf{S}_2$ from (14.27) as

$$-\frac{3}{4} \text{ in the singlet } (S=0) \text{ state}$$

and

$$+\frac{1}{4} \text{ in the triplet } (S=1) \text{ state}$$

$$(14.28)$$

In view of (14.28), the spin Hamiltonian can be manipulated to have the form:

$$\mathcal{H}^{\text{spin}} = \frac{1}{4} (\xi_s + 3\xi_l) - (\xi_s - \xi_l) \mathbf{S}_1 \cdot \mathbf{S}_2 \quad (14.29)$$

Making use of (14.28) together with (14.27), we can easily verify that

$$\mathcal{H}^{\text{spin}} \psi_s = \xi_s \psi_s$$

and

$$\mathcal{H}^{\text{spin}} \psi_l = \xi_l \psi_l$$

shifting the origin to $\frac{1}{4}(\xi_s + 3\xi_l)$,

$$\mathcal{H}^{\text{spin}} = -2J_{\text{ex}} \mathbf{S}_1 \cdot \mathbf{S}_2 \quad [\text{using (14.26)}] \quad (14.30)$$

It is essentially this term in the Hamiltonian that gives rise to the so called Weiss molecular field. The value of J_{ex} is usually obtained from a spin wave resonance measurement.

Relation (14.30) works fairly well for real solids where \mathbf{S}_1 and \mathbf{S}_2 may be regarded as spins on two neighbouring atoms. It would, however, be wrong to infer that \mathbf{S}_1 is directly coupled with \mathbf{S}_2 . In the quantum mechanical picture, it can be shown that the exchange integral J_{ex} is a negative quantity for a small separation $|\mathbf{R}_A - \mathbf{R}_B|$ between the neighbouring magnetic atoms. As a consequence of this, the parallel alignment of spins becomes unfavourable because of the resulting positive sign of the spin Hamiltonian that is associated with a positive value of the exchange energy. This is consistent with what we found in the Heitler-London model. For ferromagnetism, the spacing $|\mathbf{R}_A - \mathbf{R}_B|$ must be larger than a certain critical distance, ensuring a positive value to J_{ex} and, therefore, the parallel alignment of spins. This places a requirement of the minimum spacing of magnetic atoms in a ferromagnet. The ferromagnetic behaviour of Fe, Co and Ni is consistent with this requirement, whereas the consequence of this condition is not observed in other transition metals with smaller atomic numbers. It is equally important to emphasize that ferromagnetism also requires the magnetic neighbours not to be far apart because the exchange integral J_{ex} gradually falls to zero for large values of $|\mathbf{R}_A - \mathbf{R}_B|$, as is evident in Fig. 14.6. The negative values of J_{ex} relate to the antiferromagnetic behaviour where the spins are ordered antiparallel so as to be in the lower energy configuration.

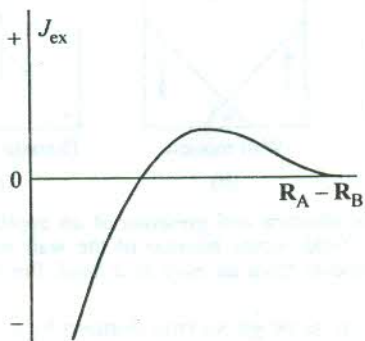


FIG. 14.6 A schematic of the variation of the exchange integral with distance between the two nearest magnetic ions.

While dealing with atoms with electrons of unpaired spins, we must be aware that states are to be filled in accordance with the Pauli principle so as to acquire a minimum electrostatic energy. It is sheer an accident in such a state of energy that a parallel spin alignment (or the spontaneous magnetization) emerges for an appropriate spacing $| \mathbf{R}_A - \mathbf{R}_B |$, producing ferromagnetism. Despite having the maximum possible unpaired spins for iron group elements, manganese in its elemental form (with a half-filled 3d shell) does not show ferromagnetism because of the small Mn-Mn distance, whereas in some of its compounds (e.g. MnSb, MnAs) the Mn-Mn spacing is large enough to make the exchange integral positive, thus letting them behave as ferromagnets. The importance of the Heisenberg theory of exchange interaction is emphasized through its success in accounting for the cause of magnetic ordering or massive molecular fields (and hence the high Curie temperatures). The gains of the theory in no way imply that the Weiss mean field theory be discarded. In fact, the physical theory of ferromagnetism is still often discussed in the framework of mean field theory on the ground of simplicity.

14.4 FERROMAGNETIC DOMAINS

Though pieces of ferromagnetic materials are normally found in the non-magnetized state, they can be magnetized (below T_c) with the application of a magnetic field. In order to explain this property of ferromagnetic solids Weiss, as indicated in Section 14.1, proposed the existence of an array of small magnetic domains that are randomly magnetized in the absence of an applied field. Each domain is magnetized to a saturated value M_s because of the parallel alignment of the atomic magnetic moments over its volume. The individual randomly oriented \mathbf{M}_s vectors may add to zero [Fig. 14.7(a)] in the absence of a field, giving no macroscopic magnetization (or spontaneous magnetization). An applied magnetic field may at the best create an ideal parallel alignment of the magnetic moments over the whole volume of the specimen with the same uniform distribution of parallel moments as within a domain along the direction of whose magnetization the magnetic field is applied. In view of this fact, the saturated value of the magnetic moment per unit volume (recognized as the saturation magnetization) of the specimen as a whole will at the most be equal to M_s and can never exceed this value.

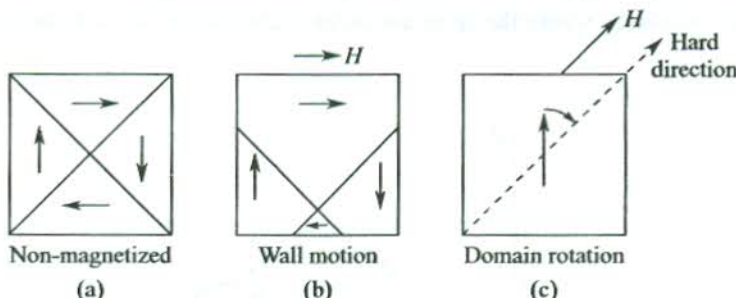


FIG. 14.7 Domain structure in the absence and presence of an applied field: (a) A non-magnetized state. (b) Magnetization by a field occurs because of the wall motion. (c) Magnetization caused by a rotation of domain moments from an *easy* to a *hard* direction.

Each domain is separated from its neighbouring domain by a domain wall called the *Bloch wall*. On applying a magnetic field, the magnetization of a specimen may occur either by the growth of a favourably-oriented (i.e. $\mathbf{M}_s \parallel \mathbf{H}$) domain at the expense of the neighbouring domains, i.e. by the motion of domain walls [Fig. 14.7(b)] or by the rotation of domains [Fig. 14.7(c)].

The first direct evidence for the existence of domains was found by Bitter* in powder patterns. In this technique a drop of colloidal suspension of finely divided ferromagnetic powder is placed on a carefully prepared surface of the ferromagnetic material under study. Because of the presence of strong local magnetic fields near the domain boundaries the particles collect along these directions and the domains can be observed under a microscope (Fig. 14.8). Typically, the dimensions of a single domain are of the order of 0.1 to 1.0 mm. A sample so small that it contained only one domain would exhibit permanent magnetization M_s , regardless of the presence of an applied magnetic field.

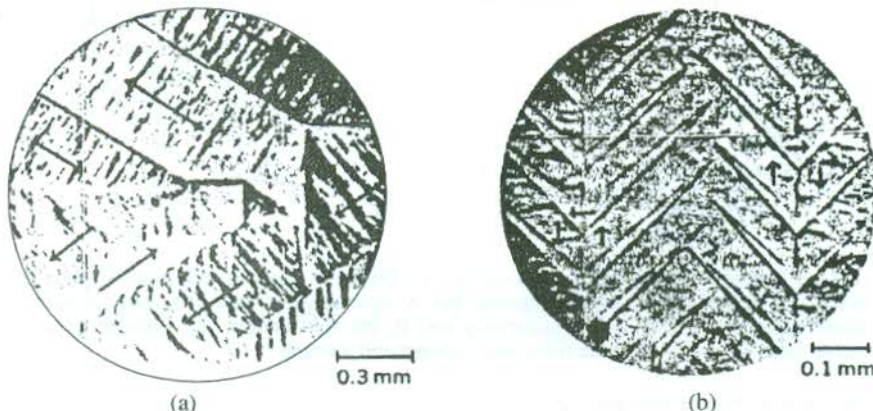


FIG. 14.8 Domain structures under a microscope: (a) For permalloy (78% Ni, 22% Fe) in which stable magnetization occurs along [111] directions and the resulting domains are separated by 180°, 90°, and 71° walls. (b) For iron containing 4% silicon; the cube edges [100] are the easy directions of magnetization and domains form 180° and 90° walls as viewed from a surface that is almost a cube face. The direction of magnetization within a domain is determined by observing the growth or contraction of the domain in a magnetic field. [After S. Chikazumi, *Physics of Magnetism* (Wiley, 1964).]

14.4.1 Technical Magnetization Curve

A representative magnetization curve is given in Fig. 14.9(a), showing dominant magnetization processes in different regions of the curve. The magnetic induction B of a multidomain ferromagnetic solid is plotted as a function of the applied magnetic field H in Fig. 14.9(b). The magnetic field is varied to carry out magnetization along the path indicated by the arrow. The technical magnetization curve traces a hysteresis loop. The hysteresis loop is interpreted easily in terms of the two magnetization processes described in Section 14.4 and the information available on Fig. 14.9(a). We define below two technical terms associated with the hysteresis curve.

Remanence, B_r

When the magnetic field is withdrawn ($H = 0$) after attaining the saturation point, the magnetic induction does not vanish but has a finite magnitude ($\mu_0 M_s$), referred to as the *remanence*.

Coercivity, H_c

Coercivity is defined as the reverse magnetic field that reduces the magnetic induction to zero, starting from saturation. The coercivity is often referred to as the coercive force.

* F. Bitter, *Phys. Rev.*, 38, 1903 (1931).

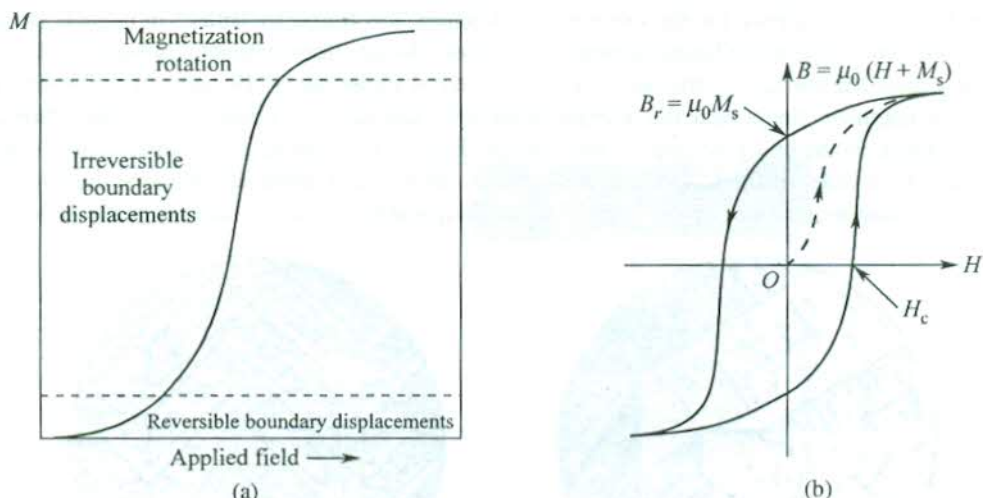


FIG. 14.9 (a) A schematic of the magnetization curve. Different regions are marked with the respective dominant processes of magnetization. (b) A hysteresis loop for a multidomain sample of a ferromagnetic solid; H_c is the coercivity and B_r the remanence. The dashed curve represents the initial path of magnetization for a non-magnetized sample.

The occurrence of hysteresis, regarded as a consequence of the domain structure, is accompanied by a loss of energy during the magnetization cycle. This implies the involvement of the domain structure in determining the efficiency of ferromagnetic devices. For example, a material to be used as a transformer core should have low coercivity in order that it incurs a low energy loss when taken round a cycle. A low coercivity relates to the high permeability which is ensured by using a pure, homogeneous and well-oriented material. The easy movement of domain walls in such a specimen may conform to a value of relative permeability as high as 4×10^6 . A permanent magnet is another important application for which a material of high coercivity is required. A high value of coercivity may be achieved by impeding the domain wall movements. This, in principle, can be accomplished in small crystallites whose size must be below a certain characteristic critical size (~ 0.1 mm to 1 mm) so as to exhibit single domain attributes, ruling out the presence of any domain walls. In practice, specimens are made heterogeneous on a fine scale by precipitating in them a second metallurgical phase.

14.4.2 Anisotropy Energy

In the derivation of the spin Hamiltonian (14.30), the spin-orbit coupling was ignored and the exchange coupling between neighbouring spins was taken as perfectly isotropic, depending only on the angle between them. But the spins in a real ferromagnetic solid are coupled to the charge density via spin-orbit coupling (Fig. 14.10). Therefore, the energy of spins will depend to some extent on their absolute orientation with respect to the crystal axes, as well as on their relative orientation with respect to one another. The part of spin energy that depends on the absolute orientation of spins with respect to the crystal axes is known as the *magnetocrystalline* or *anisotropy* energy.

The anisotropy energy directs the magnetization along certain crystallographic axes called directions of easy magnetization. The directions of easy magnetization in iron, which is cubic, are its cube edges, as evidenced in Fig. 14.11. The body diagonals ([111] directions) that appear as hard directions of magnetization in iron are the easy directions in nickel, also a cubic crystal. In cobalt, the hexagonal axis is the only preferred direction of magnetization.

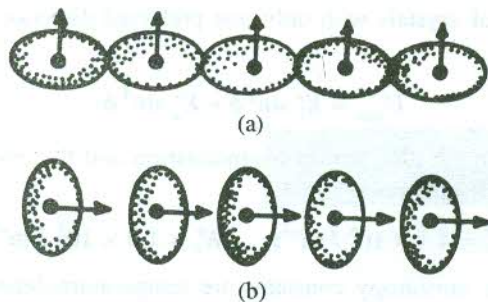


FIG. 14.10 An asymmetric electron charge distribution with different anisotropy energies for two different spin directions relative to the crystal axes. Changes in the exchange energy and electrostatic interaction energy take place with the rotation of the spin direction to which the asymmetry is tied. Due to the spin-orbit interaction, the charge distribution appears as spheroidal which is otherwise taken as spherical.

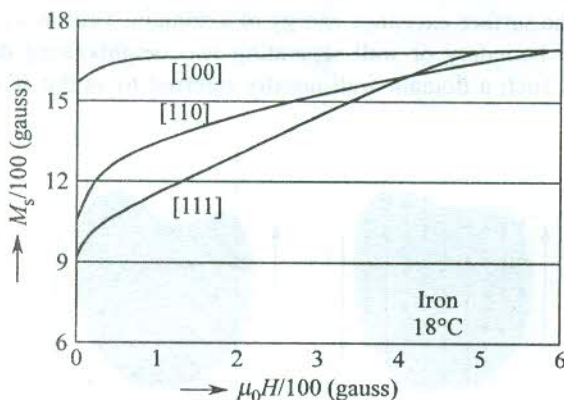


FIG. 14.11 Magnetization curves for a single crystal of iron at 291 K for different directions of the field relative to the crystal axes. [After R.G. Piety, *Phys. Rev.*, **50**, 1173 (1936).]

In order to obtain an expression for the anisotropy energy in terms of the direction of magnetization, the crystalline symmetry must be brought into consideration. For a cubic crystal magnetized in an arbitrary direction, the direction cosines α_1 , α_2 , α_3 are defined with reference to the cube edges. On account of the cubic symmetry, the expression for the anisotropy energy must be an even power of each α and be invariant under interchanges of α s among themselves. So $(\alpha_1^2 + \alpha_2^2 + \alpha_3^2)$ is the lowest order combination that satisfies the symmetry requirements. Being identically equal to unity, this combination cannot be associated with anisotropy effects. The leading term that accounts for the anisotropy energy is the next order combination $(\alpha_1^2\alpha_3^2 + \alpha_2^2\alpha_3^2 + \alpha_3^2\alpha_1^2)$. Despite the fact that this term by itself explains the experimental results on iron and nickel quite well, one more term of further allowed higher degree, namely $\alpha_1^2\alpha_2^2\alpha_3^2$ is retained and the rest neglected. The anisotropy energy density of a cubic crystal may thus be expressed as

$$U_{\text{anis}} = K_1(\alpha_1^2\alpha_2^2 + \alpha_2^2\alpha_3^2 + \alpha_3^2\alpha_1^2) + K_2\alpha_1^2\alpha_2^2\alpha_3^2 \quad (14.31)$$

The constants K_1 and K_2 are determined from experiment; for iron at room temperature:

$$K_1 = 4.2 \times 10^4 \text{ J m}^{-3}; \quad K_2 = 1.5 \times 10^4 \text{ J m}^{-3} \quad (14.32)$$

The expression in the case of crystals with only one preferred direction of magnetization, such as cobalt, is simpler:

$$U_{\text{anis}} = K'_1 \sin^2 \phi + K'_2 \sin^4 \phi \quad (14.33)$$

where ϕ is the angle between the direction of magnetization and the easy axis (hexagonal axis, for cobalt). For cobalt, at room temperature

$$K'_1 = 4.1 \times 10^5 \text{ J m}^{-3}; \quad K'_2 = 1.0 \times 10^5 \text{ J m}^{-3} \quad (14.34)$$

It may be observed that the anisotropy constants are temperature-dependent.

14.4.3 The Bloch Wall

The change in direction of the magnetization on moving from one domain to its adjacent domain does not take place in a single step, as erroneously indicated by Fig. 14.12(a), since it is unnecessarily costly in exchange energy. The reversal of spin direction, in fact, is spread out over many spins [Fig. 14.12(b)], lowering the surface exchange energy of a domain. Thus in a real ferromagnetic solid there cannot exist a sharp boundary or wall separating two neighbouring domains magnetized in different directions and as such a domain wall usually referred to as the *Bloch wall* would have a finite thickness.

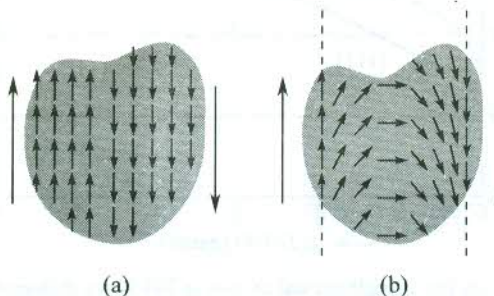


FIG. 14.12 Change of the magnetization direction (or the spin orientation) across a domain wall (the Bloch wall): (a) An abrupt boundary. (b) A boundary with a finite width over which a gradual change in spin direction takes place. Since the former is more costly in exchange energy, the latter corresponds to the picture of a real crystal.

If the spin reversal is uniformly distributed over n spins, then each spin within the wall will differ in orientation from its immediate neighbour by an angle π/n . In a crude classical interpretation of the spin Hamiltonian (14.30), we can express the exchange energy of successive spin pairs as

$$\varepsilon_{\text{ex}} = -2J_{\text{ex}} S^2 \cos\left(\frac{\pi}{n}\right) \approx -2J_{\text{ex}} S^2 \left[1 - \frac{1}{2}\left(\frac{\pi}{n}\right)^2\right] \quad (14.35)$$

which is more than the minimum value ($-2J_{\text{ex}}S^2$) for a single pair.

The cost of creating a 180° spin rotation down a line of $(n+1)$ spins will be

$$n[\varepsilon_{\text{ex}} - (-2J_{\text{ex}} S^2)] = \frac{\pi^2}{2n} (2J_{\text{ex}} S^2) \quad (14.36)$$

This amount is lower than the cost of one-step or abrupt reversal by the factor $\pi^2/2n$.

In the absence of any other consideration, the width of the transition layer, the so-called Bloch wall, would broaden out to a thickness limited only by dipolar interactions. But we must appreciate that there is an anisotropy energy associated with the wall on account of spins in the transition layer being largely directed away from easy directions of magnetization. Since the anisotropy energy acts to reduce the width of the transition layer, the thickness of a Bloch wall, in practice, is determined by a balance between exchange and anisotropy energies.

Let us consider the example of a simple cubic lattice for calculating the energy density of a Bloch wall. Imagine a wall parallel to the cube face separating two oppositely magnetized domains. The energy has contributions from exchange and anisotropy energies and so, the energy per unit area σ of the wall may be expressed as

$$\sigma = \sigma_{\text{ex}} + \sigma_{\text{anis}} \quad (14.37)$$

Relation (14.36) gives an approximate value of the exchange energy for each line of spins normal to the wall. The number of lines per unit area of the wall is $1/a^2$ where a is the lattice constant. This gives

$$\sigma_{\text{ex}} = \frac{\pi^2 J_{\text{ex}} S^2}{na^2} \quad (14.38)$$

The anisotropy energy per unit area of the wall is

$$\begin{aligned} \sigma_{\text{anis}} &= \text{anisotropy constant} \times \text{wall thickness} \\ &= K \cdot (na) \end{aligned} \quad (14.39)$$

Therefore,

$$\sigma = \frac{\pi^2 J_{\text{ex}} S^2}{na^2} + Kna \quad (14.40)$$

The number n is determined by requiring σ to be minimum (i.e. $\partial\sigma/\partial n = 0$) for this number. Applying this condition, we get

$$n = \left(\frac{\pi^2 J_{\text{ex}} S^2}{Ka^3} \right)^{1/2} \quad (14.41)$$

Placing this value of n in (14.40), we have

$$\sigma = 2\pi \left(\frac{KJ_{\text{ex}} S^2}{a} \right)^{1/2} \quad (14.42)$$

The estimated orders of magnitude for iron are

$$n \approx 300 \quad \text{and} \quad \sigma \approx 10^{-3} \text{ J m}^{-2}$$

14.4.4 Origin of Domains

The domain structure has its origin in the possibility of lowering the energy of the system. The total energy has contributions from exchange, anisotropy and magnetic energies.

The origin of domains can be understood with the help of structures drawn in Fig. 14.13, each representing a cross-section through a ferromagnetic single crystal. Figure 14.13(a) refers to a specimen with a single domain, i.e. the specimen is in the state of saturation magnetization (the maximum possible value). In such a specimen, the magnetic energy (arising on account of dipolar interaction) has a very high value $(1/2\mu_0) \int B^2 dV$. The magnetic energy is substantially reduced in the configuration shown in Fig. 14.13(b), since the spatial extension of the field has become very small. In fact such a subdivision is paid for in exchange energy, since the spins near the boundary of a domain experience unfavourable exchange interactions with misaligned spins in the domain wall. Because of the short range nature of exchange interaction, it is only the spins near the domain boundary whose exchange energy will be raised. In contrast, on the formation of domains the magnetic energy of every spin reduces on account of the long range of dipolar interactions. As we saw in Section 14.4.3, there is an energy associated with a domain wall, meaning thereby that some energy is always spent in creating a domain. Therefore, the subdivision into domains continues until the reduction in magnetic energy is less than the increase in energy to form another domain and its boundary, the Bloch wall.

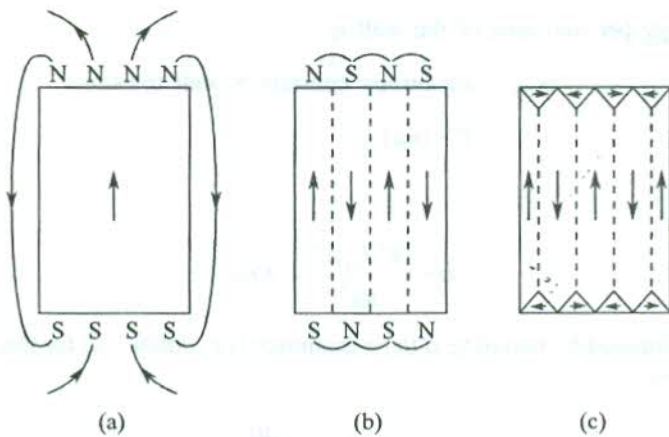


FIG. 14.13 The origin of domains. [After C. Kittel, *Rev. Mod. Phys.*, 17, 541 (1949).]

Figure 14.13(c) shows a domain structure whose magnetic energy is zero. The presence of prism domains at the top and bottom of the crystal are responsible for the zero magnetic energy. Such domains are called *closure domains*. The wall separating a closure domain and a vertical domain is inclined at an angle of 45° with the magnetization directions in both types of domains. In view of this, the normal component of the magnetization is continuous across the boundary and there is no field (hence no energy) associated with the magnetization because there are no free poles. The energy required to produce a closure domain is essentially determined by the anisotropy energy of the crystal.

Solids showing antiferromagnetic, ferroelectric, antiferroelectric, ferroelastic and superconducting properties also have domain structures. Domain structures are often quite complicated and may not be as simple as described above.

14.5 NÉEL MODEL OF ANTIFERROMAGNETISM

When the exchange interaction between magnetic ions in a solid is such as to favour antiferromagnetic spin alignment within each domain, there is a tendency for an ordering at low temperatures in which up and down spins alternate in the structure. As stated in the beginning of the chapter, these solids with no gross magnetization are identified as antiferromagnetic materials. Néel* used the Weiss mean field theory to demonstrate that this property is observed below a certain critical temperature known as the Néel temperature T_N above which the paramagnetic behaviour is observed. A list of antiferromagnetic materials with their Néel temperatures is given in Table 14.2.

Table 14.2 Selected antiferromagnetic solids[†] with Néel temperatures T_N

Substance	T_N (K)	Substance	T_N (K)
MnO	122	KFeF ₃	115
MnF ₂	67.34	CoO	291
MnCl ₂	2	CoF ₂	37.7
RbMnF ₃	54.5	KCoF ₃	125
KMnF ₃	88.3	NiO	600
FeO	198	Cr	311
FeF ₂	78.4	VS	1040

[†] Source: F. Keffler, *Handbuch der Physik*, vol. 18, pt. 2 (Springer, New York 1966).

In the Heisenberg model for an antiparallel spin alignment of two adjacent magnetic ions to correspond to the lowest energy configuration, the exchange integral J_{ex} is required to be a negative quantity. But it is by no means a sufficient condition for a real crystal to possess the antiferromagnetic property. In fact, a three-dimensional array of magnetic ions must be favourably disposed to the creation of magnetic sublattices that may oppose the magnetization of each other. The simplest picture arises when the spins up and down fall on two separate interpenetrating sublattices[†] of an identical structure. Two examples of antiferromagnetic ordering are displayed in Fig. 14.14. Figure 14.14(a) shows the ordering on a BCC lattice that can be interpreted as two interpenetrating SC lattices, one

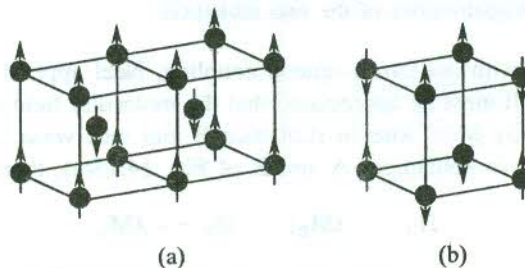


FIG. 14.14 Simple antiferromagnetic spin orders: (a) On a BCC lattice composed of two interpenetrating SC lattices, one with spins up and the other with spins of the same kind down. (b) On an SC lattice in which the spins of the same kind form two interpenetrating FCC lattices.

* L. Néel, *Ann. Phys.*, 18, 5 (1932); 5, 232 (1936).

† Four or even more sublattices are required for the distribution of magnetic ions to interpret the antiferromagnetic order of some crystals.

having the spins up and others the spins down. Similarly, the ordering on an SC lattice shown in Fig. 14.14(b) can be imagined as a combination of two FCC lattices with opposite spins. It can be verified for both the examples that the spin magnetic moments in a unit cell sum to zero moment (realizing that the moment at a corner contributes only 1/8th of its value).

The first experimental evidence* of antiferromagnetism was found in MnO which is also a case with two sublattices. The ordering of Mn^{2+} ions in $RbMnF_3$ [Fig. 14.15(a)] is one of the simplest with Mn^{2+} ions on an SC lattice. Let Mn^{2+} ions with spin up be on sublattice A and those with spin down on sublattice B. Figure 14.15(b) shows the temperature variation of magnetization M_A and M_B belonging to the two sublattices. They sum to zero at temperatures below T_N and drop independently to zero at T_N .

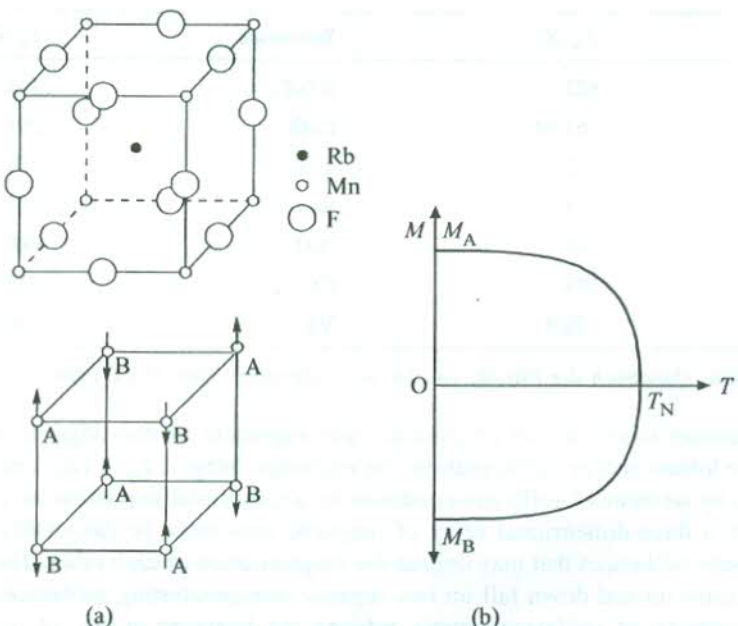


FIG. 14.15 (a) Unit cell structure of $RbMnF_3$ (antiferromagnetic, $T_N = 54.5$ K). The directions of spin moments of the magnetic ion Mn^{2+} are shown by arrows. (b) Temperature dependence of the equal and opposite magnetizations of the two sublattices.

In a model treatment with antiferromagnetic coupling, Néel applied the mean field theory to each sublattice separately. It must be appreciated that the molecular field experienced by Mn^{2+} ions in sublattice A is created by Mn^{2+} ions in sublattice B and vice versa. If H_A and H_B denote the respective molecular fields in sublattices A and B of Fig. 14.15(a), then

$$H_A = -\lambda M_B; \quad H_B = -\lambda M_A \quad (14.43)$$

where λ is positive and the minus sign corresponds to an antiparallel interaction; the interaction of parallel spins in a sublattice with its own molecular field is neglected. Then, by analogy with (14.3) for a ferromagnet, we have

* H. Bizette, C.F. Squire and B. Tsai, *Compt. Rend.*, **207**, 449 (1938).

$$\mathbf{M}_A = \frac{C}{2T} (\mathbf{H} - \lambda \mathbf{M}_B) \quad (14.44a)$$

$$\mathbf{M}_B = \frac{C}{2T} (\mathbf{H} - \lambda \mathbf{M}_A) \quad (14.44b)$$

where \mathbf{H} is the intensity of the applied magnetic field and $C/2$ is the appropriate Curie constant for one-half of the magnetic ions on each sublattice.

The saturation magnetizations of sublattices A and B are equal and opposite below the Néel temperature T_N . Equations (14.44) have a nonzero solution for M_A and M_B in the absence of an applied field if

$$\begin{vmatrix} 2T & \lambda C \\ \lambda C & 2T \end{vmatrix} = 0 \quad (14.45)$$

This determines the Néel temperature given by

$$T_N = \frac{\lambda C}{2} \quad (14.46)$$

which is a constant for a material.

Equations (14.44) are solved for M_A and M_B to obtain the susceptibility at $T > T_N$ in the form

$$\chi_m = \frac{\mathbf{M}_A + \mathbf{M}_B}{\mathbf{H}} = \frac{C}{T + \frac{\lambda C}{2}} = \frac{C}{T + T_N} \quad (14.47)$$

But experimental observations are not entirely in agreement with the predictions of (14.47). They are, instead, explained by

$$\chi_m = \frac{C}{T + \theta} \quad T > T_N \quad (14.48)$$

where the ratio θ/T_N is usually greater than one. The discord between theory and experiment can be accounted for with the use of more complicated models that consider the influence of distant magnetic ions.

The observed temperature variation of the susceptibility of antiferromagnetic solids is shown in Fig. 14.16, together with those for paramagnetic and ferromagnetic solids for the purpose of a comparative study. The susceptibility of antiferromagnetic solids is not infinite at $T = T_N$, but has a weak cusp. It shows considerable anisotropy for a single crystal sample at temperatures below T_N . The susceptibility has different values for the magnetic field applied parallel and perpendicular to the direction of the sublattice magnetization. The behaviour of susceptibility in this temperature range is well accounted by experiments and can be appreciated even qualitatively. For a magnetic field acting perpendicular to the direction of magnetization the spins are tilted easily even at absolute zero, leading to a constant susceptibility as shown in Fig. 14.16(c). But when the field is parallel to the direction of magnetization, it is hard to cause spin flips. The magnetization is opposed by the full molecular

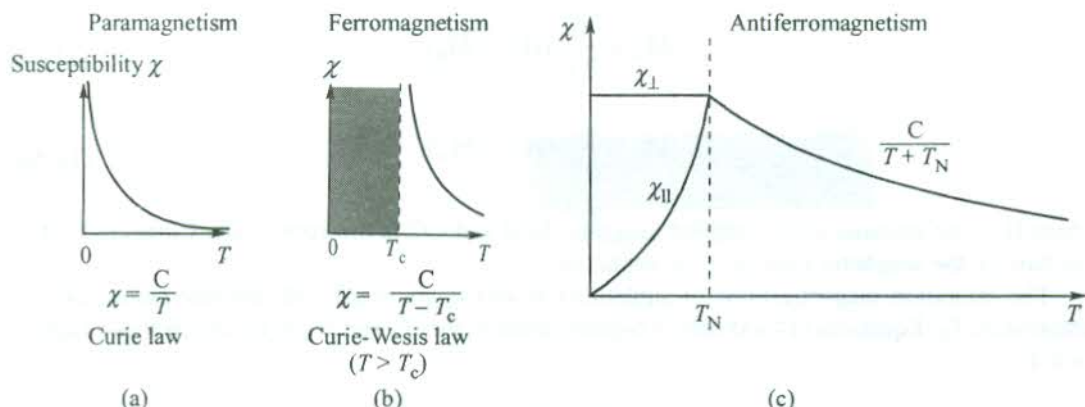


FIG. 14.16 Schematics of the susceptibility as a function of temperature in paramagnetic, ferromagnetic and antiferromagnetic solids.

field in this case and the susceptibility drops to zero as $T \rightarrow 0$ K with the two sublattice magnetizations of equal magnitude. On rise of temperature to T_N , the molecular field weakens and the susceptibilities for the two orientations of the magnetic field become comparable.

At temperatures $T \geq T_N$, the spin magnetic moments become entirely free because of the collapse of exchange coupling, and the susceptibility is back to the usual paramagnetic behaviour described by the Curie law.

The transition from an ordered magnetic phase to the disordered paramagnetic phase in all types of magnetic crystals is accompanied by a maximum in the heat capacity at the critical temperature that is much sharper than the break predicted by molecular field theory (see Fig. 14.5). Data from most carefully performed experiments suggest the following variation for the heat capacity:

$$C_V \propto \log |T - T_c| \quad (14.49)$$

which shows singularity at $T = T_c$. But the nature of singularity is such that $\int C_V dT$ remains finite, ruling out the involvement of latent heat, i.e. showing the transition as second-order type. The observed anomaly in an antiferromagnetic crystal ($\text{NiCl}_2 \cdot 6\text{H}_2\text{O}$) is depicted in Fig. 14.17.

14.6 NÉEL MODEL OF FERRIMAGNETISM

In view of the Néel sublattice model we need to elaborate on the definition of ferrimagnetism, given earlier in this chapter. Néel explored the consequences of the possibility that the magnetic moments of the two sublattices be unequal and anti-parallel. The corresponding configuration of spins is identified as a ferrimagnetic state that is usually characterized by a relatively weak spontaneous magnetization. A list of the selected ferrimagnetic materials is given in Table 14.3. This happens generally because of the presence of unidentical magnetic ions in the crystal. Néel* applied this concept of ferrimagnetism to explain the magnetic properties of an important group of magnetic oxides, known as *ferrites*. Ferrites are represented by the general formula, $\text{MO} \cdot \text{Fe}_2\text{O}_3$ where M can be any one of the divalent atoms: Fe, Co, Ni, Cu, Zn, Mg and Cd. These include lodestone ($\text{Fe}_3\text{O}_4 = \text{FeO} \cdot \text{Fe}_2\text{O}_3$) whose spontaneously magnetized pieces were used by ancient navigators as their primitive compasses. Lodestone is commonly known by the name *magnetite*.

* L. Néel, *Ann. Phys.*, 3, 137 (1948).

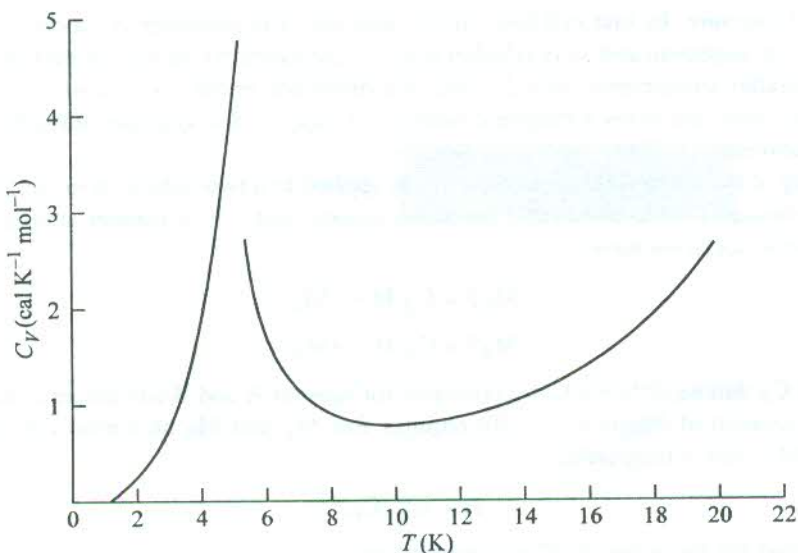


FIG. 14.17 Heat capacity anomaly in an antiferromagnetic crystal ($\text{NiCl}_2 \cdot 6\text{H}_2\text{O}$). [After W.K. Robinson and S.A. Friedberg, *Phys. Rev.*, **117**, 402 (1960).]

Table 14.3 Selected ferrimagnetic solids[†] with critical temperatures T_f and saturation magnetization M_s at $T = 0$ K

Substance	T_f (K)	M_s (gauss)
Fe_3O_4 (magnetite)	858	510
CoFe_2O_4	793	475
NiFe_2O_4	858	300
CuFe_2O_4	728	160
MnFe_2O_4	573	560
$\text{Y}_3\text{Fe}_5\text{O}_{12}$ (YIG)	560	195

† Source: F. Keffer, *Handbuch der Physik*, vol. 18, pt. 2 (Springer, New York, 1966).

In a Fe_3O_4 formula unit, there is one Fe^{2+} ion (with $3d^6$ configuration; $S = 2$) and two Fe^{3+} ions (with $3d^5$ configuration; $S = 5/2$). If the spins of all these ions were in a parallel alignment, the magnetic moment per formula unit would be about $14\mu_B$ ($= 4\mu_B + 2 \times 5\mu_B$). But the observed value is only $4.07\mu_B$, suggesting thereby that Fe_3O_4 must not be having an entirely parallel arrangement of spins, as is really confirmed by the neutron diffraction measurements. The magnetic ions are found to be distributed over two different symmetry sites: the tetrahedral and octahedral. These two sets of sites may be regarded to fall on two different sublattices. The spins of all ions at one type of site are in parallel alignment. But if the spins at tetrahedral sites point up, the spins at octahedral sites point down. Further, while Fe^{3+} ions are equally distributed over two sets of sites, the Fe^{2+} ions occupy only octahedral sites. Because of this distribution, only Fe^{2+} ions contribute to the net magnetic moment, equalling about $4\mu_B$ per formula unit. Thus we see that the model gives a value that is in exceedingly good agreement with the experimental value. Magnetite is a cubic ferrite having the

spinel* crystal structure. Its unit cell has 8 tetrahedral sites (on sublattice A) occupied by Fe^{3+} ions in parallel spin arrangement and 16 octahedral sites (on sublattice B), equally shared by Fe^{3+} and Fe^{2+} ions also in parallel arrangement such that the spin directions in the two sublattices are opposite to each other. This structure gives a magnetic moment of $32\mu_B$ ($= 8 \times 4\mu_B$) per unit cell, in agreement with the experimental value.

Continuing in the mean field approximation as applied to a two-sublattice model, we proceed to set up an expression for the observable magnetic susceptibility. In a manner similar to that of an antiferromagnetic solid, we have

$$\mathbf{M}_A T = C_A (\mathbf{H} - \lambda \mathbf{M}_B) \quad (14.50a)$$

$$\mathbf{M}_B T = C_B (\mathbf{H} - \lambda \mathbf{M}_A) \quad (14.50b)$$

where C_A and C_B denote different Curie constants for ions on A and B sublattices in that order. The simultaneous solution of equations (14.50) requires that \mathbf{M}_A and \mathbf{M}_B be nonzero in the absence of an applied field below a temperature,

$$T_f = \lambda (C_A C_B)^{1/2} \quad (14.51)$$

where T_f is called the ferrimagnetic Curie temperature.

Solving (14.50) for M_A and M_B at $T > T_f$, we have

$$\chi_m = \frac{M_A + M_B}{H} = \frac{T(C_A + C_B) - 2\lambda C_A C_B}{T^2 - T_f^2} \quad (14.52)$$

The more complicated form of (14.52) points towards a possible less straightforward behaviour for the susceptibility than what follows from the Curie–Weiss law. The $(1/\chi)$ versus T plot derived from the experimental values for magnetite and shown in Fig. 14.18 furnishes a sufficient proof to this effect. The curvature of the plot is a characteristic feature of ferrimagnetic materials. But the saturation magnetization is found to fall from a maximum at very low temperatures to zero at the ferrimagnetic Curie temperature T_f in a manner generally similar to that of a ferromagnetic solid.

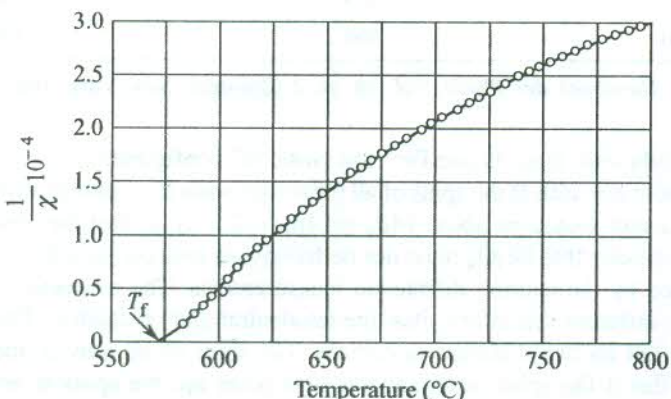


FIG. 14.18 Inverse susceptibility as a function of temperature for magnetite, Fe_3O_4 .

* See C. Kittel, *Introduction to Solid State Physics*, 7th ed., p. 460 (John Wiley, 1996).

Ferrites are known to be poor conductors of electricity. Several members of this family, crystallizing in spinel structure have been used as rf transformer cores and toroidal cores serving as primary information storage in most of the computers developed about three decades ago.

There is another group of ferrimagnets that have found important applications. These are iron garnets with general formula, $M_3Fe_5O_{12}$ where M is a trivalent metallic atom such as yttrium or one of the rare-earth elements and Fe is the trivalent ferric ion ($S = 5/2, L = 0$). An example of iron garnets is $Y_3Fe_5O_{12}$, known as YIG. These are also electrical insulators and are used in magnetic resonance and spin wave studies.

14.7 SPIN WAVES

Individual elementary magnetic moments in a magnetic crystal are essentially completely ordered at $T = 0$ K. But, on increasing the temperature, the magnetization decreases towards zero at the critical temperature (T_c , T_N or T_f), since the atomic moments acquire enough thermal energy to turn against the effective molecular field. A deviation from the ordered state may be produced at $T = 0$ K as well by providing the spin system with an excitation, achieved with the energy from an external source. The excitations of a spin system are customarily described by treating the completely ordered (presumably at $T = 0$ K) as the ground state of the system. A state in which one or more spins are reversed relative to their orientation at absolute zero, then represents an excited state of the system.

Consider the simplest spin system with all its atomic magnetic moments in parallel alignment at absolute zero (i.e. a ferromagnet) with $S_i^z = S$, where S_i^z denotes the component of the spin vector state of a moment at site i along the magnetization direction (z-direction). An excitation of the spin at site i that may change the value of S_i^z from S to $(S - 1)$ against the effective molecular field or the exchange field B_{ex} would cost an energy $2\mu_B B_{ex}$. Because all the spins are coupled through the exchange interaction, the excitation does not remain localized at the site; it is in fact transferred to the neighbouring spin, setting its onward propagation in the crystal. Deviations in the spin direction at different sites follow a certain pattern such that the tips of the spin vectors convolute into a wave-like envelope (Fig. 14.19). The wave thus generated is called a *spin wave*. Discussions of ferromagnetism in terms of spin waves, however, became a practice only after the spin waves were observed* in the spin wave resonance of thin ferromagnetic films. On symmetry considerations, a spin representing a true excitation is expected to have the same amplitude at every site. The quantized unit of spin wave energy is called a *magnon*. The total magnetization decreases by one unit of spin with the excitation (or creation) of a magnon.

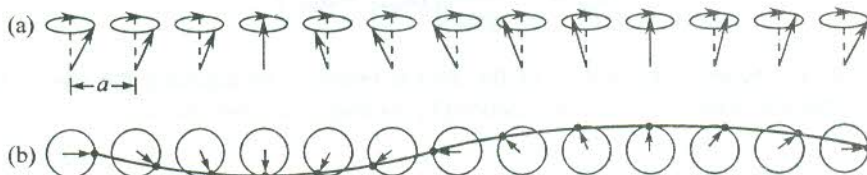


FIG. 14.19 Formation of a spin wave over a line of spins: (a) A perspective view of changing spin orientations. (b) Spin vectors as viewed from above. The curve joining the tips of spin vectors has a wave-like shape. A spin wave is shown here as an oscillation in the relative orientations of spins on a linear lattice.

* M.H. Seavey, Jr. and P.E. Tannenwald, *Phys. Rev. Letters*, **1**, 168 (1958).

We attempt in this section a classical treatment of magnons, also referred to as the elementary excitations of a spin system. It must, however, be observed that a quantum mechanical approach is the befitting way to deal with this problem, because spin is purely a quantum concept. Setting all reasons of simplicity and convenience aside, it must be emphasized at the same time that some of the results of a classical calculation are surprisingly the same as those given by a quantum mechanical method. The magnon dispersion relation for a model ferromagnet discussed below is one such example.

14.7.1 Magnons in Ferromagnets

Let us consider a one-dimensional ferromagnet consisting of a linear chain of identical magnetic ions. If there are in total N ions each of spin S , coupled by the exchange interaction with the nearest neighbour spins, the exchange energy of the spin system in the Heisenberg model is given by

$$U = -2J_{\text{ex}} \sum_{n=1}^N \mathbf{S}_n \cdot \mathbf{S}_{n+1} \quad (14.53)$$

with system in the ground state and spins treated as classical vectors, $\mathbf{S}_n \cdot \mathbf{S}_{n+1} = S^2$. Thus the ground state energy of the given ferromagnet is

$$U_0 = -2NJ_{\text{ex}}S^2 \quad (14.54)$$

The exchange energy contributed by the n th spin to (14.53) is

$$\begin{aligned} U_n &= -2J_{\text{ex}} \mathbf{S}_n \cdot (\mathbf{S}_{n+1} + \mathbf{S}_{n-1}) \\ &= -\mu_n \cdot \left(-\frac{2J_{\text{ex}}}{g\mu_B} \right) (\mathbf{S}_{n+1} + \mathbf{S}_{n-1}) \quad (\text{using } \mu_n = -g\mu_B \mathbf{S}) \end{aligned} \quad (14.55)$$

where μ_n is the magnetic moment associated with the n th spin.

The U_n can also be expressed as

$$U_n = -\mu_n \cdot \mathbf{B}_{\text{ex}} \quad (14.56)$$

where \mathbf{B}_{ex} is the effective molecular field.

Comparing (14.55) and (14.56), we have

$$\mathbf{B}_{\text{ex}} = \left(-\frac{2J_{\text{ex}}}{g\mu_B} \right) (\mathbf{S}_{n+1} + \mathbf{S}_{n-1}) \quad (14.57)$$

The gyroscopic equation of motion of the spin is obtained by equating the rate of change of its angular momentum with the torque experienced by its magnetic moment under the influence of the field \mathbf{B}_{ex} :

$$\hbar \frac{d\mathbf{S}_n}{dt} = 2J_{\text{ex}} \mathbf{S}_n \times (\mathbf{S}_{n+1} + \mathbf{S}_{n-1})$$

or

$$\frac{d\mathbf{S}_n}{dt} = \left(\frac{2J_{\text{ex}}}{\hbar} \right) [\mathbf{S}_n \times \mathbf{S}_{n+1} + \mathbf{S}_n \times \mathbf{S}_{n-1}] \quad (14.58)$$

This equation of motion is nonlinear. It can be linearized for small amplitudes by expressing S_n as

$$S_n = S + \sigma_n \quad (14.59)$$

where S denotes the component of S_n along the magnetization direction (z -direction) and σ_n is a small spin vector in the xy -plane.

The geometrical relationship between the three spin vectors of (14.59) is shown in Fig. 14.20. Note that S is a constant vector, i.e. $\frac{dS}{dt} = 0$. Placing the value of S_n from (14.59) in (14.58) and retaining only the first order terms in σ_n , we get

$$\frac{d\sigma_n}{dt} = \left(\frac{2J_{ex}}{\hbar} \right) S(\sigma_{n+1} + \sigma_{n-1} - 2\sigma_n) \quad \left(\text{enforcing } \frac{dS}{dt} = 0 \right) \quad (14.60)$$

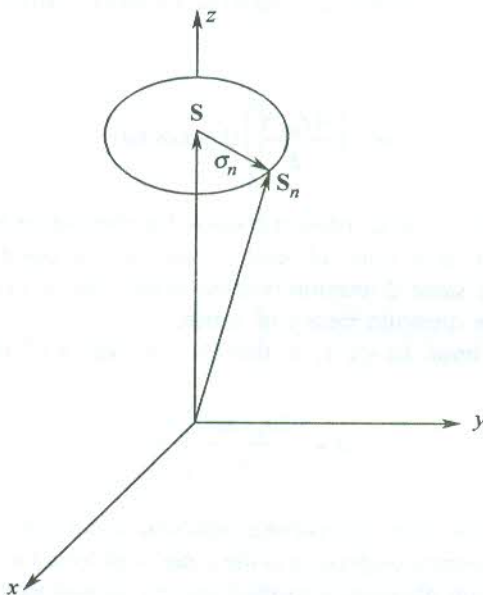


FIG. 14.20 Precession of spin vectors S_n in a classically interpreted spin wave.

From the above equation, the components of spin motion along the x and y directions may be written as

$$\left(\frac{d\sigma_n}{dt} \right)_x = \left(\frac{2J_{ex} S}{\hbar} \right) (2\sigma_n - \sigma_{n+1} - \sigma_{n-1})_y \quad (14.61)$$

$$\left(\frac{d\sigma_n}{dt} \right)_y = - \left(\frac{2J_{ex} S}{\hbar} \right) (2\sigma_n - \sigma_{n+1} - \sigma_{n-1})_x \quad (14.62)$$

If we construct a complex spin vector

$$\sigma^* = \sigma_x + i\sigma_y$$

relations (14.61) and (14.62) can be combined to yield

$$\frac{d\sigma_n^+}{dt} = \left(\frac{2J_{\text{ex}} S}{i\hbar} \right) (2\sigma_n^+ - \sigma_{n+1}^+ - \sigma_{n-1}^+) \quad (14.63)$$

By analogy with phonons we look for travelling wave solutions of (14.63) of the form

$$\sigma_n^+ = u \exp [i(kna - \omega t)] \quad (14.64)$$

where a is the interionic spacing in the chain.

Substituting the above solution in (14.63), we obtain

$$\omega = \left(\frac{2J_{\text{ex}} S}{\hbar} \right) \{2 - [\exp(ika) + \exp(-ika)]\}$$

or

$$\omega = \left(\frac{4J_{\text{ex}} S}{\hbar} \right) (1 - \cos ka) \quad (14.65)$$

Relation (14.65) is known as the dispersion relation for spin waves in a linear ferromagnet with nearest-neighbour interaction. It is quite pleasant to find that a quantum mechanical method of derivation gives precisely the same dispersion relation in this case as (14.65). This may be verified by looking into any book on quantum theory of solids.

In the long wavelength limit, $ka \ll 1$, so that $(1 - \cos ka) \approx 1/2(ka)^2$ and the frequency is

$$\omega \approx \left(\frac{2J_{\text{ex}} Sa^2}{\hbar} \right) \cdot k^2 \quad (14.66)$$

This shows that the magnon dispersion curve is parabolic in the long wavelength limit, contrasting the linear behaviour for the phonon dispersion in the same limit for a linear monatomic crystal lattice (see Fig. 4.4). By analogy with phonons, a method entirely similar to that described in Section 4.8 can be used for magnon creation and annihilation through the inelastic scattering of slow neutrons in a ferromagnetic solid. A dispersion curve obtained by this procedure is shown in Fig. 14.21.

The quantization of spin waves is carried out in a manner exactly similar to that for photons and phonons. If there are n_k magnons in a mode of frequency ω_k , the energy of the mode is expressed as

$$\varepsilon_k = \left(n_k + \frac{1}{2} \right) \hbar \omega_k \quad (14.67)$$

14.7.2 The Bloch $T^{3/2}$ Law

The concept of spin waves was introduced by Felix Bloch (1930) who correlated the thermal excitation of magnons with the decrease in spontaneous magnetization from its saturated value at absolute zero. He went on to set up a law that describes the temperature dependence of the decrease in magnetization.

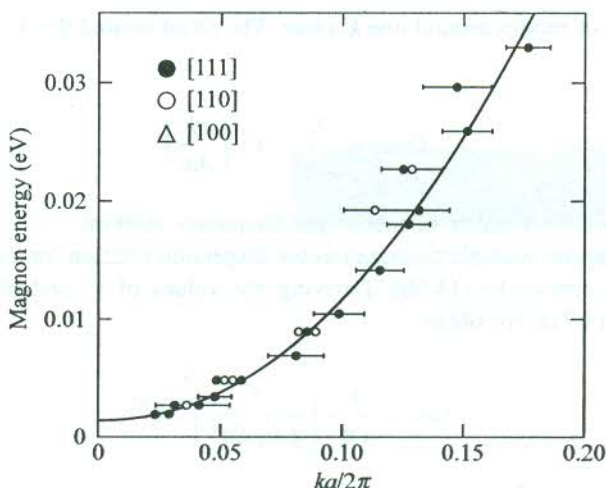


FIG. 14.21 Magnon dispersion relation in a ferromagnetic alloy (92% cobalt and 8% iron) determined from an inelastic neutron scattering experiment at room temperature. The energy is plotted against the dimensionless equivalent of wavevector. [After R.N. Sinclair and B.N. Brockhouse, *Phys. Rev.*, **120**, 1638 (1960).]

To derive the Bloch's law we essentially need to determine the average number of thermally excited magnons at thermal equilibrium. This number gives a measure of the decrease in magnetization, since with the excitation of each magnon there is a decrease in magnetization by one unit of spin moment.

It is evident from the form of (14.67) that the structure of energy levels of magnons is identical to those of a harmonic oscillator. This allows us to treat magnons in a manner similar to that in practice for the radiation oscillators of Planck. Thus the average number of magnons in the mode \mathbf{k} at thermal equilibrium is given by the Planck distribution function:

$$\langle n_{\mathbf{k}} \rangle = \frac{1}{\exp(\hbar\omega/k_B T) - 1} \quad (14.68)$$

Then, the total number of thermally excited magnons at temperature T is estimated to be equal to

$$\sum_{\mathbf{k}} n_{\mathbf{k}} = \int D(\omega) \langle n(\omega) \rangle d\omega \quad (14.69)$$

where $D(\omega)$ denotes the density of the magnon modes.

There is a single polarization for magnons for each value of \mathbf{k} and all the useful values of \mathbf{k} (the unique values) lie in the first Brillouin zone, as is the case with phonons. The integral in (14.69) is evaluated by emphasizing the analogy with phonons.

The periodic boundary condition gives the number of modes per unit volume in the \mathbf{k} -space as $V/(2\pi)^3$, where V is the volume of the crystal. Therefore, the number of modes of the wavevector measuring between k and $(k + dk)$ for a spherical distribution of momentum in the \mathbf{k} -space is equal to

$$\frac{V}{(2\pi)^3} \times \frac{d}{dk} \left(\frac{4\pi}{3} k^3 \right) = \frac{V}{2\pi^2} \cdot k^2 dk \quad (14.70)$$